The role of pulvinar-parietal circuitry in goal-directed saccades

Dissertation

for the award of the degree

“Doctor rerum naturalium”

of the Georg-August-Universität Göttingen

within the doctoral program systems neuroscience

of the Georg-August University School of Science (GAUSS)

submitted by

Mathieu Pachoud

from Manosque, France

Göttingen 2022

Thesis Committee

Dr. Igor Kagan, Decision and Awareness Group, Cognitive Neuroscience Laboratory, German Primate center (DPZ)

Prof. Dr. Melanie Wilke, Department of Cognitive Neurology, University Medical Center Göttingen (UMG)

Prof. Dr. Hansjörg Scherberger, Neurobiology Laboratory, German Primate Center (DPZ)

Members of the Examination Board

Referee: Dr. Igor Kagan, Decision and Awareness Group, Cognitive Neuroscience Laboratory, German Primate Center (DPZ)

2nd Referee: Prof. Dr. Melanie Wilke, Department of Cognitive Neurology, University Medical center Göttingen (UMG)

Further members of the Examination Board

Prof. Dr. Hansjörg Scherberger, Neurobiology Laboratory, German Primate Center (DPZ)

Prof. Dr. Alexander Gail, Sensorimotor Group, Cognitive Neuroscience Laboratory, German Primate Center (DPZ)

Prof. Dr. Andrea Antal, Department of Neurology University Medical Center Göttingen (UMG)

Prof. Dr. Michael Wibral, Department of Data-driven Analysis of Biological Networks, University of Göttingen

Date of oral examination: 29th of November 2022

Table of Contents

Abstract

The pulvinar, an important higher-order thalamic nucleus supporting many functions, is reciprocally connected with frontoparietal areas involved in sensorimotor transformations. Prior perturbation studies also revealed its role in spatial decision-making. In this thesis, we tried to get a better understanding on the role of pulvinar-parietal circuitry in visually-guided saccades and spatial decision-making, within one hemisphere and also in the context of inter-hemispheric interactions. To do so, in the first study we characterized neuronal activity and functional connectivity using local field potential (LFP) and spike-LFP synchronization within and between the dorsal pulvinar and area LIP. In the second study, we investigated the effect of reversible unilateral dorsal pulvinar inactivation on neuronal activity in area LIP in the inactivated and the opposite hemisphere. We showed the flexibility of functional interactions between the dorsal pulvinar and LIP with ongoing oscillations during the maintained fixation and movement preparation, and also in transient shifts upon visual processing and around saccade events. In addition, we reported that a stronger connectivity during free-choice trials led to a higher probability of selecting contralateral targets. We also showed that unilateral dorsal pulvinar inactivation led to an ipsilesional choice bias, a decreased cortical 'alert state' that might explain more general inactivation effects such as slight drowsiness, and an altered contralesional representation of visual goals as well as neuronal synchronization in area LIP in the same hemisphere. On the contrary, there was an upregulated neuronal activity in the opposite hemisphere. Finally, we found a decreased inter-hemispheric functional connectivity after the inactivation. Altogether, these studies shed light on a crucial role for pulvinar-parietal interactions in maintaining cortical alertness, the representation of contralateral visual goals and subsequent movement selection and planning. In a more general perspective, this work highlights the importance of thalamo-cortical loops in shaping the neuronal activity locally and inter-hemispheric ally across homotopic regions, as opposed to only relaying information across cortical regions within the same hemisphere. Finally, our results suggest push-pull interactions between the two hemispheres during spatial selection and oculomotor preparation.

1 General introduction

1.1 Visually guided behaviors

In order to interact with our environment, our brain has to gather, process and interpret different types of sensory information. Sensory inputs typically arise from sensory organs at the periphery and travel through afferent nerves to the central nervous system (CNS) where there are distributed, transformed and processed in various brain areas. As a result, we build a representation of our environment as well as our internal state from which we make decisions and plan actions.

In primates, as suggested by their evolution, among sensory systems the visual system arguably plays a crucial role in shaping behaviors. Indeed, vision allows not only to build an outside representation of the world but also to provide control on visually guided movements in order to interact with it. Another evidence of the importance of the visual system is the overwhelming number of studies focusing on various aspects of vision in non-human primates and humans.

1.2 The dorsal visual stream

Photoreceptors located in the retina are sensitive to light. We find two types of photoreceptors. Rods are located mainly at the periphery of the retina and are sensitive to low light levels while cones are located mainly in the center and are responsible for color vision. Cones and rods convert light energy into action potentials which travel to the lateral geniculate nucleus of the thalamus (LGN) through the optic tract. Signals from the left visual field arrive at the right LGN while signals from the right visual field arrive at the left LGN. The primary visual area (V1) then receives input coming from the LGN in the same hemisphere and is the starting route of two cortical pathways, ventral and dorsal (Mishkin et al., 1983). The dorsal visual stream or ‘where system’ also originates from V1 and projects to visual areas V2, V3, medial temporal area MT and several areas in the posterior parietal cortex such as area LIP that are reciprocally connected to the pulvinar. The dorsal pathway is involved in the localization of objects in space as well as their orientation and size. This information in turn is used to plan and perform goal-directed movements, in particular saccadic eye movements (Creem and Proffitt, 2001).

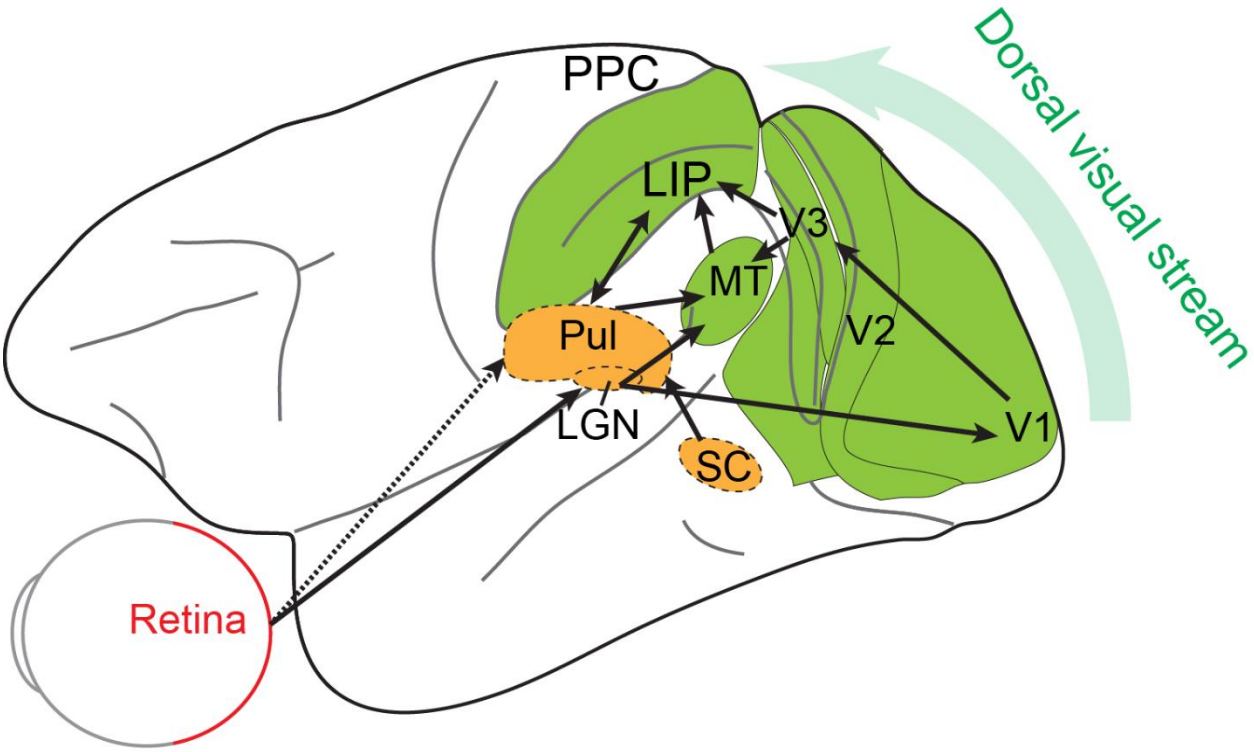

Figure 1.1: The dorsal visual pathway.

The visual system is very complex and is not exclusively located within the ventral or dorsal cortical pathways. For instance, in the midbrain, the superior colliculus (SC) receives direct input from the retina and is involved in the generation of fast saccadic eye movements (May, 2006). Additionally, the ventral part of the pulvinar, which is also interconnected with cortical areas involved in vision, has been proposed to play a role in selective visuospatial attention (Saalmann and Kastner, 2011). At the same time, the dorsal part of the pulvinar, the focus of this thesis, is also involved in visuospatial attention and a host of other functions related to perception and visually-guided action, including goal-directed eye movements.

1.3 The oculomotor system

The function of the oculomotor system is to plan and control the execution of eye movements. There are four main types of eye movements: saccades, smooth pursuit, vergence shifts and vestibulo-ocular movements. Saccades are fast eye movements that abruptly change the locus of fixation. Smooth pursuits are slower movements that are used to keep a moving target in the fovea. Vergence shifts are movements to align the fovea of each eye to the target distance. Finally, vestibulo-ocular movements are used to stabilize eyes relative to a target, for instance to compensate for head movements.

In this thesis, the focus will be on fast voluntary saccadic eye movements that are the main means of visual exploration in primates. Voluntary eye movements in primates involve several fronto-parietal areas such as the frontal eye field (FEF), the supplementary eye field (SEF) and area LIP. Area FEF contains visual, motor and visuomotor cells and participates in voluntary saccades (Bruce et al., 1985). Area SEF is more involved in complex movements involving gaze (Pierrot-Deseilligny et al., 2002). Area LIP, located in the lateral bank of the intraparietal sulcus, has long been shown to be involved in saccade intention. For example, in a memory-guided saccade task, some cells that are tuned for a specific direction and amplitude eye movement remained active during the memory period, suggesting the encoding of the upcoming saccade (Gnadt and Andersen, 1988). Similar activity was reported during delayed saccade task (Snyder et al., 1997). Additionally, in a double delayed saccade task, monkey had to remember the location of two stimuli before performing saccades in sequence. Most neurons' activity was encoded for the location of the first saccade and the firing changed after execution to encode the location of the second target (Mazzoni et al., 1996). Together, previous research on LIP provides strong evidence of its involvement in oculomotor preparation.

Voluntary eye movements also involve a subcortical region, the superior colliculus (SC). SC receives inputs from both area FEF and LIP. SC neurons in deep layers have a burst of activity before a contralateral saccade that corresponds to their movement field (direction and amplitude). The topographical organization is based on the center of each neuron movement field and microstimulation has been shown to elicit the corresponding saccade (Gandhi and Katnani, 2011). SC neurons in turn project to the paramedian pontine reticular formation (PPRF) which sends motor commands to seven extraocular muscles.

Finally, the pulvinar is interconnected with frontoparietal areas involved in sensory-motor and transformation and decision-making. Its contribution to visually-guided behaviors is the main focus of this thesis and will be discuss extensively in later sections.

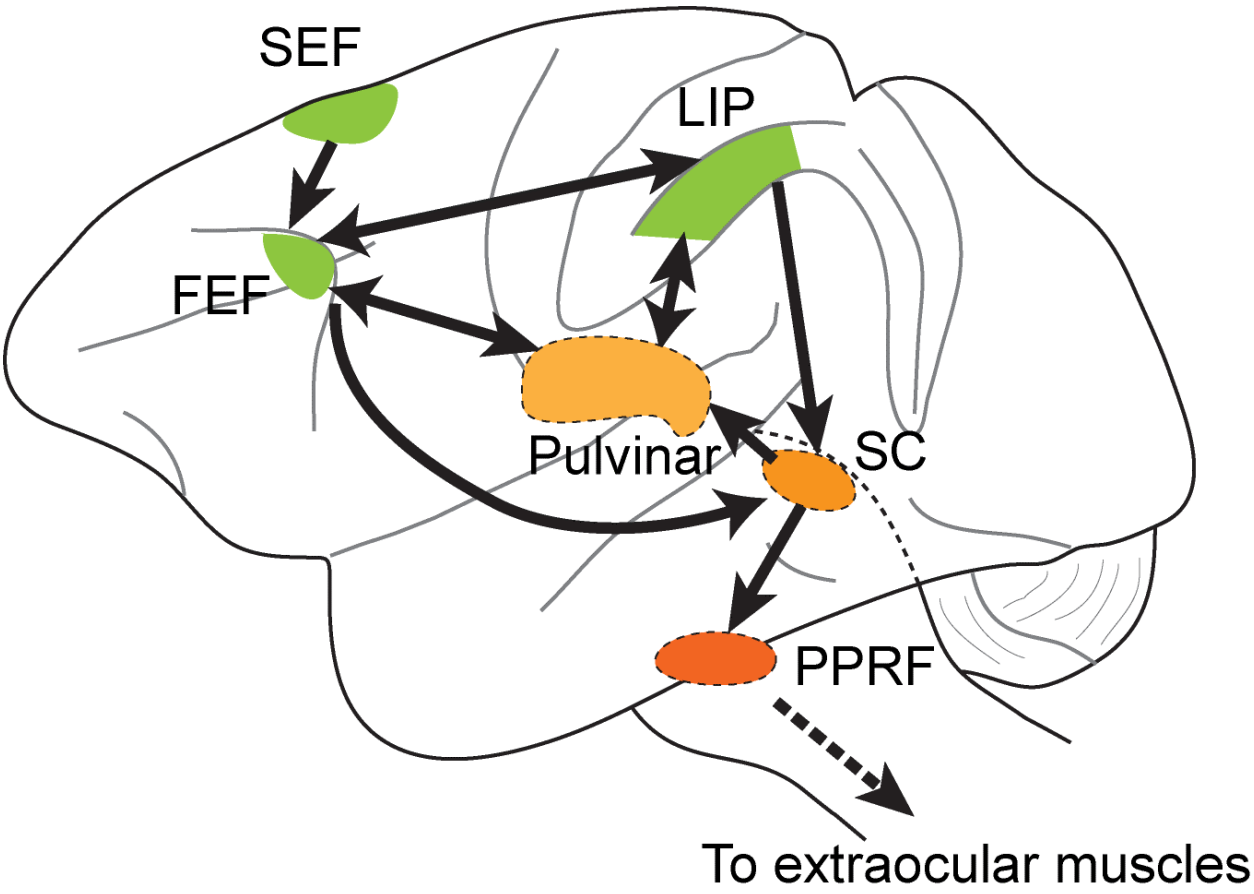

Figure 1.2: Voluntary eye movement network.

1.4 LIP and decision-making

Beyond visuomotor transformations and motor planning, electrophysiological studies in macaques revealed the role of area LIP in spatial decision-making. First, LIP has been proposed to play the role of salience map since neurons respond to flashed stimuli inside their receptive fields better than they do to static behaviorally irrelevant stimuli (Kusunoki et al., 2000). A few years later, it has been shown that individual neurons in LIP accumulate sensory evidence in a motion discrimination task in which monkeys communicate their choices through saccades to the corresponding target (Roitman and Shadlen, 2002; Huk and Shadlen, 2005). A similar task with reward contingencies showed that activity in LIP could be modulated by introducing a bias in the reward value associated with the decision (Rorie et al., 2010). Therefore, the neuronal activity in area LIP is modulated by sensory evidences and stimulus saliency, highlighting the role of LIP in oculomotor movement selection.

In addition to the its role in perceptual discrimination or reward-based decision, perturbation studies have highlighted the contribution of area LIP in spatial decision-making in the context of

free choices. Indeed, inactivation studies have shown that LIP inactivation leads to a choice bias toward ipsilesional hemifield in a free-choice saccade task (Balan and Gottlieb, 2009; Wilke et al., 2012) and is mostly specific to the oculomotor system since the choice bias was less pronounced when performing reaches (Christopoulos et al., 2018). However, the neuronal signature in area LIP in the context of free-choice saccade task remains to be investigated.

1.5 The thalamic pulvinar

The contribution of cortical areas involved in voluntary saccades and their direct interactions has been widely studied. However, an indirect route for cortical interactions involves higher-order thalamic nuclei such as the pulvinar (Pul). The functional significance of this indirect route through pulvinar and other higher-order thalamic nuclei has received greater attention over the last two decades but remains poorly understood. The pulvinar is the largest thalamic nucleus, located in the posterior part of the thalamus. In terms of phylogeny, the pulvinar can be considered a newly developed nucleus and has undergone a great expansion, in parallel to the expansion of the association cortex in primates (Kaas and Baldwin, 2019).

A major difference between first and higher-order nuclei is the origin of their driving inputs. Driving inputs are defined as the carrier of information and rely on ionotropic receptors to induce a fast post-synaptic response. On the other hand, modulator inputs affect certain aspects of the transmission and rely on metabotropic having a slow and prolonged effect. Unlike first-order thalamic nuclei such as LGN, which receive their driving inputs from peripheral nerves and subcortical regions and relay information to the cortex, the pulvinar receives driving inputs directly from cortical areas and sends projection back to the cortex (Guillery, 1995).

Furthermore, several combined perturbation-electrophysiological studies have provided evidence that pulvinar nuclei are involved in cortical processing. In cats, the inactivation of the lateral posterior-pulvinar complex of the thalamus decreased the strength of the synchronization and oscillations in the visual cortex, and the inactivation of the ventral lateral pulvinar in *Cebus* monkeys modulated the activity and directional selectivity tuning in area V2 (Shumikhina and Molotchnikoff, 1999; Soares et al., 2004). Naturally, the question of the functional contribution of this pathway to distributed information processing in the cortex rises.

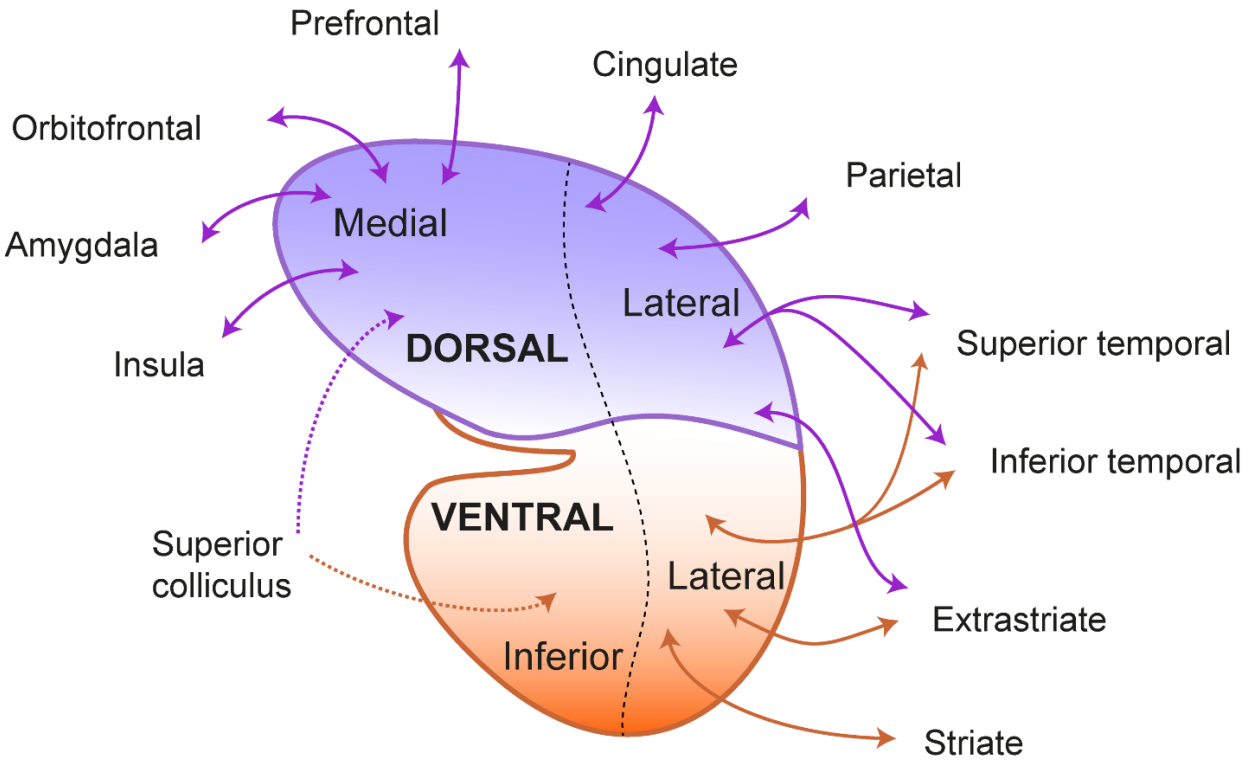

Figure 1.3: Pulvinar organization and connectivity. After Kaas and Lyon, 2007.

The view on the anatomical organization of the pulvinar may vary depending on the method used (cytoarchitecture, fMRI, electrophysiology) but generally, it can be traditionally divided into the anterior, medial, lateral and inferior parts. Each part can be further divided into different subnuclei based on their connectivity with multiple cortical areas. Despite this heterogeneity, recent anatomical and functional studies have differentiated between the dorsal pulvinar (dPul), composed of the medial part (PM) and the dorsal part of the lateral pulvinar (PLdm), and the ventral pulvinar (vPul), composed of the inferior pulvinar (PI) and ventral part of the lateral pulvinar (PLvl) (Kaas and Lyon, 2007; Arcaro et al., 2015; Dominguez-Vargas et al., 2017; Kagan et al., 2021).

The ventral part is often denoted as the visual pulvinar since it is strongly and bi-directionally connected to early cortical visual areas, such as V1, V2, V4 and IT, and has a high number of visually responsive neurons, follows the retinotopic organization and is mostly tuned to the contralateral hemifield (Bender, 1981; Petersen et al., 1985). Furthermore, some vPul neurons show saccade-related activity, mostly around and after the saccade (Robinson et al., 1986). The ventral pulvinar has been shown to be involved in visual attention since vPul neuronal activity is

modulated by attention (Saalmann et al., 2012) and vPul inactivation experiment showed altered attentional effects in visual area V4 (Zhou et al., 2016a).

Like the ventral pulvinar, the dorsal part of the pulvinar also shares connections with visual areas such as V4, but also with a variety of higher processing areas such as the dorsolateral prefrontal cortex (dlPFC), FEF, the insular cortex, the cingulate cortex, regions in the superior temporal sulcus (STS), superior temporal gyrus (STG), and the amygdala (Hardy and Lynch, 1992; Gutierrez et al., 2000). Importantly, the dorsal pulvinar also shares bi-directional functional connections with the PPC, including area LIP. Anatomical studies using tracers have shown that area LIP and the dorsal pulvinar share reciprocal projections (Hardy and Lynch, 1992; Romanski et al., 1997). This connectivity has also been described in humans using fMRI (Arcaro et al., 2018). Additionally, the use of microstimulation in combination with fMRI provides a tool to investigate functional or effective (stimulation-induced) connectivity *in vivo*. Using this technique, it has been shown that stimulating pulvinar increases activity in LIP (Kagan et al., 2021). Interestingly, unilateral pulvinar stimulation also elicited activation of cortical areas in the opposite hemisphere, including area LIP, suggesting polysynaptic transmission of the excitation. The extensive dorsal pulvinar connectivity suggests its implication in a wide range of functions that we will now discuss further.

Some neurons in the dorsal pulvinar are visually responsive and their receptive fields are mostly located in the contralateral hemifield (Mathers and Rapisardi, 1973; Schneider et al., 2020) but they do not follow a retinotopic organization. Their response is sometimes modulated by the shape and/or color of the visual stimuli with a shorter latency than the cortex (Benevento and Port, 1995). Therefore, the dorsal pulvinar encodes both location and features of an object and possibly provides such information to the cortex. Based on these properties, the dorsal pulvinar has also been proposed to play a role in visual attention. This hypothesis has been strengthened by the fact that dorsal pulvinar activity is modulated by attention (Bender and Youakim, 2001). Furthermore, Fiebelkorn and colleagues (Fiebelkorn et al., 2019) reported higher synchronization between the dorsal pulvinar and both FEF and LIP during visual attention. They reported in the same study an increased alpha/low-beta activity in mdPul in period of engagement (higher behavioral performance in attentional task) whereas an increased activity in the same frequency range in LIP was associated with disengagement (low behavioral performance). In addition, the direction of interactions also shifted from mdPul → LIP during period of engagement to LIP → mdPul during period of disengagement. Based on these findings, it has been proposed that the

differential activity and direction of interactions between the pulvinar and LIP promote either attentional sampling or shifting of attention.

Eye position signals have also been reported in the dorsal pulvinar (Robinson et al., 1990; Schneider et al., 2020). Indeed, the activity of some pulvinar neurons was modulated by the gaze direction in relation to the head position in two different ways. First, visual stimulation in the fovea showed modulation depending on the gaze in around 50% of the recorded units. Second, in a substantial number of neurons, the target position of an upcoming saccade was mainly under retinocentric reference frame after stimulus presentation and shifted to a body-centered reference frame around the saccade. Together, these results suggest a role for the dorsal pulvinar in reference frame transformation, from retinotopic to possibly head and/or body-centered (Grieve et al., 2000; Schneider et al., 2020).

Different studies showed that saccade-related activity in the dorsal pulvinar is heterogeneous. It was reported that some dPul neurons (65%) are responsive to saccades in an illuminated environment (Robinson et al., 1986). Interestingly, the response could be excitatory (46%), inhibitory (26%) or bi-phasic (28%). Another study showed directional pre- and post-saccadic response in visually- and memory-guided saccade tasks (Benevento and Port, 1995). Interestingly, same units also encoded stimuli feature such as color and their mean response latency was faster than in the parietal cortex, suggesting an earlier processing of both object feature and spatial position in dorsal pulvinar. Also, microstimulation of the dorsal pulvinar can elicit saccades in a fixation task. In a visually-guided saccade task, also shortened or delayed the reaction in a time-dependent manner. Similarly, microstimulation induced a selection bias in a visually-guided, but not memory, free-choice task, towards ipsiversive hemifield when the stimulation started before target onset and contraversive hemifield when it started after target onset (Dominguez-Vargas et al., 2017). In addition, unilateral dorsal pulvinar inactivation led to ipsilesional choice bias in an oculomotor memory-saccade task (Wilke et al., 2013) in a similar way to what has been described in LIP (Wardak et al., 2002; Christopoulos et al., 2018). In addition, microstimulation of dPul and LIP in combination with fMRI revealed that both regions belong to common circuitry involving several frontal and parietal areas supporting visually-guided movements (Kagan et al., 2021). The same study also reveals cue and saccadic activity modulation in both hemispheres with microstimulation. Specifically, ROIs showing contraversive selectivity showed a greater microstimulation effect when the monkey was instructed to saccade to the ipsiversive hemifield. Overall, there is a growing body of evidence suggesting a role for the dorsal pulvinar in saccades selection and execution.

The dorsal pulvinar role in visually-guided behavior is not limited to eye movements but also has been shown to be involved in reaching. Indeed, two separate studies have reported changes in dorsal pulvinar activity related to aimed arm movements (Cudeiro et al., 1989; Acuna et al., 1990). Furthermore, inactivation of the dorsal pulvinar leads to a constellation of deficits when performing visually-guided reaches, including target selection bias, optic ataxia and limb usage in a food retrieving task (Wilke et al., 2010).

Finally, studies of human patients with pulvinar lesions described both oculomotor and reach deficits, including spatial neglect in the contralesional field, partially consistent with causal perturbation in monkeys (Rafal et al., 2004; Arend et al., 2008; Van der Stigchel et al., 2010; Wilke et al., 2018), highlighting the fact that the dorsal pulvinar plays a crucial role in the selection and execution of visually-guided limb and eye movements. However, its functional contribution and underlying neuronal mechanisms remains poorly understood.

1.6 Functional connectivity measures

In order to study dynamic brain networks, different methods have been developed to assess functional connectivity. Those methods, such as coherence, phase synchronization and Granger causality can be applied to different types of signals, invasive and noninvasive neuronal recordings. In the scope of this thesis, we used invasive electrophysiological recordings from which we can derive two types of information: spikes and LFP. Spikes are rapid fluctuations of the neuronal membrane potential also called action potential that can be measured indirectly in extracellular recordings and are widely accepted. Unlike the spiking activity, the origin of LFP is more debated. However, it can be defined as low-frequency average voltage oscillations of a population of neurons surrounding (estimated between 200 and 400 µm) the electrode recording site (Pesaran, 2009). LFP is thought to primarily reflect synaptic currents, even though it is likely that other phenomenon such as intrinsic membrane oscillations and neuron glial interactions also contribute to the signal (Buzsáki et al., 2012). Since action potentials are the output of a neuron, measuring spiking activity is considered as measuring the output of one or a population of neurons. LFP however, is thought to represent the sum of the inputs received by the recorded population. Therefore, one can measure functional connectivity between or within regions by looking at both LFP-LFP and spikes-LFP synchronization. While both measures give indications about the strength of synchronization, spike-field analysis is also thought to include some directionality of interactions, with information flow from the site where spiking activity was recorded to the sites where LFP was recorded (Pesaran, 2010). There are different methods to calculate spikes-LFP synchronization such as Phase-Locking Value (PLV), Spike-Field

Coherence (SFC) and pairwise-phase consistency (PPC). To study both local (within each region, between sites) and inter-regional interactions, we utilized pairwise-phase consistency (PPC) since it avoids biases from the spike rate and the number of trials (Vinck et al., 2010; Fiebelkorn et al., 2019). Pairwise phase consistency estimates the LFP phase for each spike and then compares the similarities of spike phases pair-wise. Similarly, field-field PPC evaluates the similarities between different LFP phases of the two LFP signals at each time point for different frequencies separately.

1.7 Rationale of the thesis

The rationale of this thesis is driven by several open questions concerning: 1) the tuning properties of the dorsal pulvinar during instructed and choice oculomotor tasks, in comparison to oculomotor cortical area LIP; 2) the functional connectivity between these regions when their activity is recorded simultaneously; and 3) the electrophysiological signatures of cortical changes induced by pulvinar inactivation. These questions stem from the previous work in our lab as well as recent work on pulvinar-cortical interactions by other groups, in particular Kastner, Desimone, and Casanova labs. Furthermore, the third question is motivated by a more general inquiry into mechanisms of short-term plasticity and potential compensatory re-organization of remote cortical nodes during local lesions.

1) The tuning properties of dPul during instructed and choice task

To recap, there is little known about the basic oculomotor properties of dPul neurons during delayed response tasks. Contrary to one earlier study on a small subset of neurons with the memory guided task that did not find the cue responses (Benevento and Port, 1995), the recent work from our lab showed that many neurons are visually responsive to a short cue but most pulvinar neurons do not have a spatially-tuned enhancement during the memory delay, and do not signal an upcoming spatial target selection during the choice trials (Schneider et al., 2020, 2021). The latter finding is in line with absence of microstimulation-induced choice bias during the memory saccade delay (Dominguez-Vargas et al., 2017). However, it has been suggested that the prospective role of the pulvinar on spatial decision and motor planning might manifest more clearly when the visual target of the upcoming action is present (Dominguez-Vargas et al., 2017; Schneider et al., 2021). Therefore, here we utilize delayed but visually-guided saccade task, to investigate spiking and LFP tuning during the presence of a visual stimulus.

2) The functional connectivity between dPul and parietal cortex

The connectivity on the level of electrophysiological signals between the dorsal and the ventral pulvinar and cortical regions has been explored in the context of attentional tasks where the motor response was performed with hand button presses (Saalmann et al., 2012; Zhou et al., 2016a; Fiebelkorn et al., 2019), or during visual stimulation in anaesthetized cats (Cortes et al., 2020). However, such connectivity during the oculomotor behavior has not been yet investigated. Since the spike-field and field-field interactions might provide a crucial insight into the distributed processing, and since these measures have been previously demonstrated to be modulated by the choice context (Pesaran et al., 2008), we set out to investigate dPul-LIP interactions.

3) Cortical changes induced by pulvinar perturbation

Only very few studies in primates explored causal contribution of pulvinar or other higher-order thalamic nuclei to cortical activity underlying goal-directed behaviors (although considerably more work has been conducted in rodents, including optogenetic perturbations). Reversible inactivation of pulvinar in prosimian primate abolished visual responses in supragranular V1 layers (Purushothaman et al., 2012). The inactivation of the ventral pulvinar in macaques was shown to lead to attention deficits, a reduction of visual responses and overall gamma coherence within V4, and reduction of attentional effects on spiking rates and gamma synchrony in V4, as well as an increase in low-frequency cortical oscillations, often associated with low alertness or sleep. In contrast, the inactivation of the dorsal pulvinar during passive viewing condition (no task) was shown to cause reduction in LFP phase coherence between LIP and V4 in low frequencies (i.e. 4 – 15 Hz), but no significant changes in firing rates or LFP power. Synchronization between pulvinar spikes and cortical LFP phase also decreased in low frequencies, while the low frequency synchronization between LIP spikes and pulvinar LFP increased (Eradath et al., 2021). While there is currently no consistent picture of pulvinar influences on the cortex, in line with attentional effects of the thalamus, the electrical stimulation of the central thalamus was shown to lead to recruitment of large-scale fMRI-identified thalamocortical networks, restoring the signatures of arousal and awareness (Tasserie et al., 2022), and LFP-LFP coherence in FEF-LIP circuitry (Redinbaugh et al., 2020).

Most relevant for the present thesis, a not yet published study by Wilke, Kagan and Andersen found that after unilaterally inactivating the dPul during instructed (single target) and choice (two target) memory saccades, the contralesional single target BOLD fMRI cue/delay activity decreased in the LIP in the inactivated hemisphere (and in many other cortical regions), but

ipsilesional target activity increased in the opposite, intact LIP (Figure 1.4). Interestingly, during choice trials, the activity preceding contralesional selection did not change much, but was strongly reduced during the more frequent ipsilesional choices. However, since the BOLD fMRI signals are only an indirect measure of the neuronal activity and their relation to firing rates and different frequency bands of local LFP power or coherence are not yet clear, it is very important to assess these effects on the neuronal level.

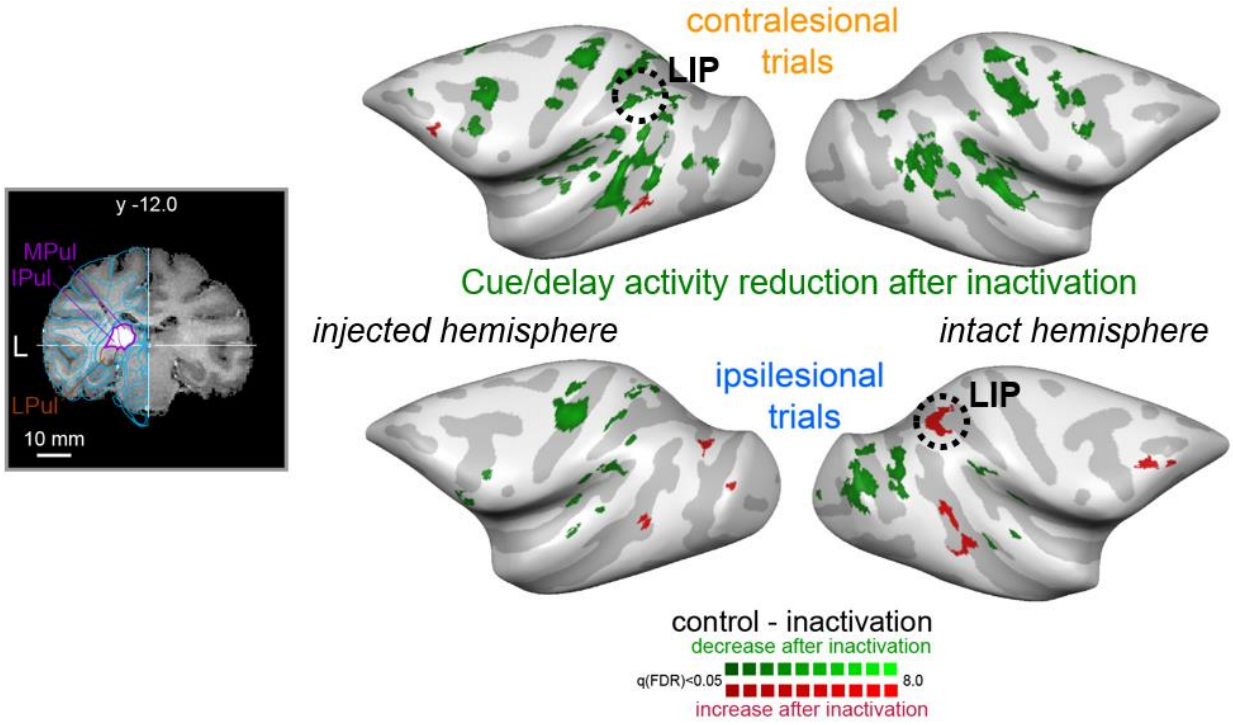

Figure 1.4: Cortical changes in contralesional and ipsilesional cue/delay representations after dorsal pulvinar inactivation. From Wilke*, Kagan*, Andersen, in preparation.

1.8 Specific aims of the thesis

To summarize, the role of cortical areas involved in visually-guided movements as well as their interactions through direct cortico-cortical projections, within one hemisphere, have been widely studied. But over the last few years, the indirect route for cortical communications passing through higher-order thalamic nuclei such as the pulvinar began receiving greater attention (Grieve et al., 2000; Saalmann et al., 2012; Zhou et al., 2016a; Fiebelkorn et al., 2019). Despite a growing body of evidence highlighting the role of the dorsal pulvinar in visually-guided behaviors, and presumed similarity of pulvinar saccade-related responses to that of area LIP - but see (Schneider et al., 2021) - the functional relationship between these two regions, and the contribution of the pulvinar to shaping of cortical response properties remains poorly understood. Furthermore, a potential

role for pulvinar-LIP interactions during spatial decisions (as opposed to simple instructed tasks) has not been investigated on the level of electrophysiological signals. The overall aim of this thesis is to use visually-guided saccade tasks with different levels of spatial choice, in combination with electrophysiological recordings and MRI-targeted pharmacological manipulation of the pulvinar, to get a better understanding of the role of pulvinar-parietal circuitry in decision-making and visually-guided behaviors. I pursued two related aims, in the two separate experiments, in the same animals:

1) In the first experiment, I utilized simultaneous multielectrode electrophysiological recordings in the two regions, the dorsal pulvinar (dPul) and LIP. This allowed to characterize similarities and differences in the neuronal tuning properties between the two regions, and to assess the functional connectivity between the dorsal pulvinar and LIP while monkeys performed instructed and free-choice delayed saccade movements, at the level of spike-LFP and LFP-LFP measures.

2) In the second experiment, I investigated the causal role of the dorsal pulvinar in oculomotor task performance and underlying modulation of the neuronal activity in area LIP, as well as interhemispheric cortico-cortical interactions. To do so, I recorded electrophysiological activity in both LIPs before and after reversible unilateral dorsal pulvinar inactivation.

* * *

The thesis is organized in 5 chapters. Chapter 1, this chapter, is a General introduction. Chapter 2 is General Materials and Methods applicable to both experimental chapters 3 and 4, written as stand-alone manuscripts. Chapter 5 is a General discussion.

2 Materials and Methods

All experimental procedures were conducted in accordance with the European Directive 2010/63/EU, the corresponding German law governing animal welfare, and German Primate Center institutional guidelines. The procedures were approved by the responsible government agency ("Niedersächsisches Landesamt für Verbraucherschutz und Lebensmittelsicherheit" - Lower Saxony State Office for Consumer Protection and Food Safety, LAVES, Oldenburg, Germany).

2.1 Animal preparation

Two adult male rhesus monkeys (*Macaca mulatta*) B and L weighing 9 and 10 kg respectively, were included in this project. Monkeys were implanted with a magnetic resonance imaging (MRI) compatible polyetheretherketone (PEEK) headpost embedded in a bone cement headcap (Palacos with Gentamicin, BioMet, USA) anchored by ceramic screws (Rogue Research, Canada), under general anesthesia and aseptic conditions. An MRI scan was made using a stereotaxic frame to plan, using Planner (Ohayon and Tsao, 2012), the implantation of PEEK MRI-compatible chambers (inside diameter 22 mm) on the top of each hemisphere allowing access to the pulvinar and the parietal cortex (Monkey B, - Left chamber: center at 6P, 16.5L, angle 19P, 26L - Right chamber: center at 3.5P, 16R, angle 15P, 3RL; Monkey L, - Left chamber: center at -3P, 19L, angle 20P, 36L – Right chamber: center at -4P, 18R, angle 20P, 38R). After confirming chambers position with a postsurgical MRI, partial craniotomies were made inside each chambers giving access to pulvinar and parietal cortex. The exposed dura was covered with a silicone elastomer (Kwik-sil, World Precision Instruments, USA) to reduce the granulation tissue growth and dura thickening.

2.2 Behavioral task

Monkeys were sitting in a dark room in a custom-made primate chair with the head restrained. Stimuli were presented on a 27" LED display (60 Hz refresh rate, model HN274H, Acer Inc. USA). The touchscreen was attached in front of the 27" stimuli display. The gaze position of the right eye was monitored at 220 Hz using an MCU02 ViewPoint infrared eyetracker (Arrington Research Inc. USA). Tasks were designed in MATLAB (version R2012b, The MathWorks, Inc., USA) using Psychophysics Toolbox.

2.3 Delay saccade task

Monkey started a trial by putting both hands on rest sensors mounted to the front part of the monkey chair and was required to keep this position for the entire trial. After a short time (500 ms), a dim fixation target for the eye (2° radius) appeared at the center of the screen (fixation acquisition). Monkey had to acquire fixation with the eye within the allowed time window (1500 ms) and maintain fixation for a variable time (700-1200 ms, fixation hold), within a radius of 8°. At the beginning of the fixation, the fixation target became bright as a visual feedback. At the end of the fixation, one (instructed) or two (free choice, opposite hemifields) dim red target appeared in the periphery (15°, Cue), with 6 potential angles from the horizontal line (40°, 0°, 320°, 220°, 180° and 140°). Monkey had to maintain fixation for a variable time (1000-1500 ms) until the disappearance of the fixation target (target acquisition) which was the “go signal” for the monkey to perform the saccade. After monkey stayed within the radius of 8° within for 400 ms (target hold), the trial was successfully completed and the animal received a drop of water/juice (~0.2 ml). In the case of choice trials, the unselected target disappeared when the eye position entered the radius of the selected target. All trials were randomly interleaved and recording block ended after 15 successful trials of each conditions for a total 180 trials (6 targets × 2 instructed/choice × 15 trials). Aborted trials were put back to the pool of upcoming trials in a randomized position.

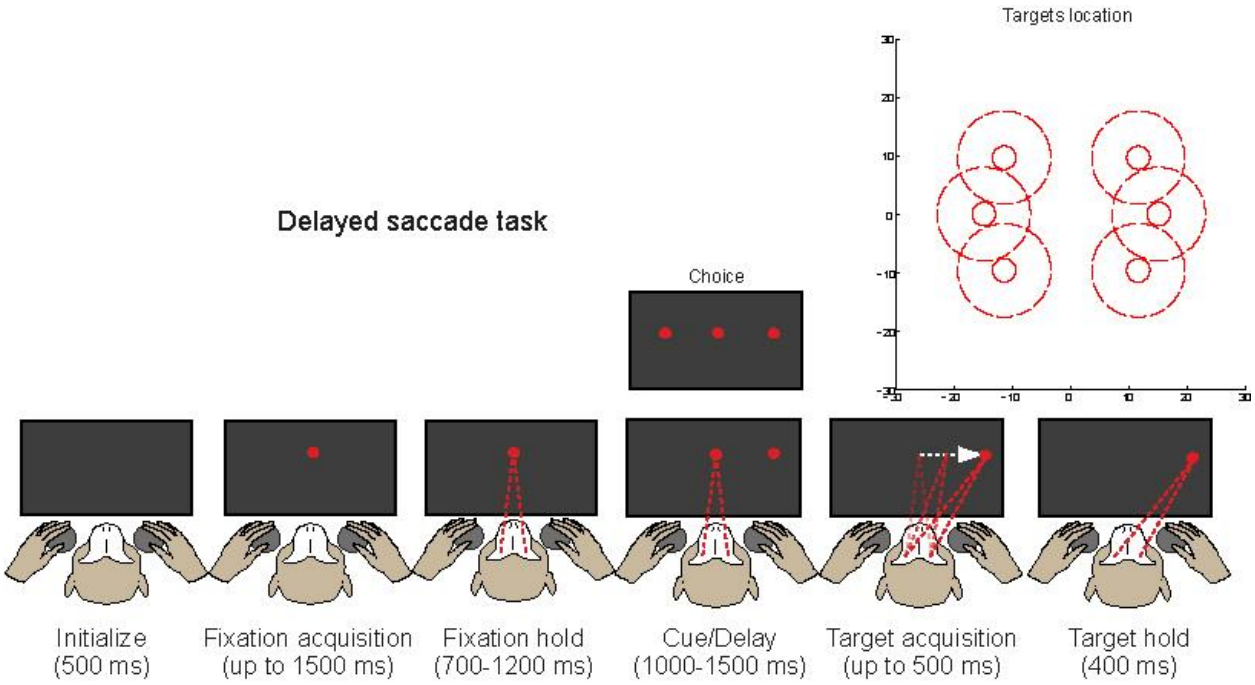

Figure 2.1: Delayed saccade task and target positions.

2.4 Dissociated delayed saccade task

All stimuli had circular shape with different size and color for different contingencies. Different colors served as signal for different effectors: red for eye, blue for left hand and green for the right hand. Red stimuli had lower luminance than blue and green stimuli. The luminance of blue and green stimuli were similar. Monkeys learned to associate red color with eye, green with right and blue with left hand movements. Monkey started a trial by putting both hands on rest sensors mounted to the front part of the monkey chair. After a short time (500 ms), dim fixation stimuli for hand (4° radius) and on top of it a dim fixation for the eye (2° radius) appeared at the center of the screen (fixation acquisition). Monkey had to acquire fixation with both effectors within the allowed time window (1500 ms and 1000 ms for eye and hand respectively) and allowed radius (hand: 6°, eye: 8°), and maintain fixation for a variable time (700-1200 ms, fixation hold). During this fixation time, stimuli became bright as a visual feedback. At the end of the fixation, one (instructed) or two (free choice, opposite hemifield) dim red target appeared in the periphery (15°, Cue, radius: 2°), with 6 potential angles from the horizontal line (40°, 0°, 320°, 220°, 180° and 140°). Monkey had to maintain fixation for a certain time (1000-1500ms) until the disappearance of the eye fixation stimuli (target acquisition) which was the “go signal” for the monkey to perform the saccade while maintaining fixation with the hand. After staying within the radius of 7° of the bright target for 150 ms (target hold), the trial was successful and the animal received a drop of water/juice (~250 µL). In the case of choice trials, the unselected target disappeared when the eye position entered the radius of the selected target. All trials were randomly interleaved and recording block ended after 10 successful trials of each conditions for a total 240 trials (6 targets*2 hands*2 instructed/choice*10 trials). Aborted trials were put back to the pool of upcoming trials in a randomized position in the remaining sequence.

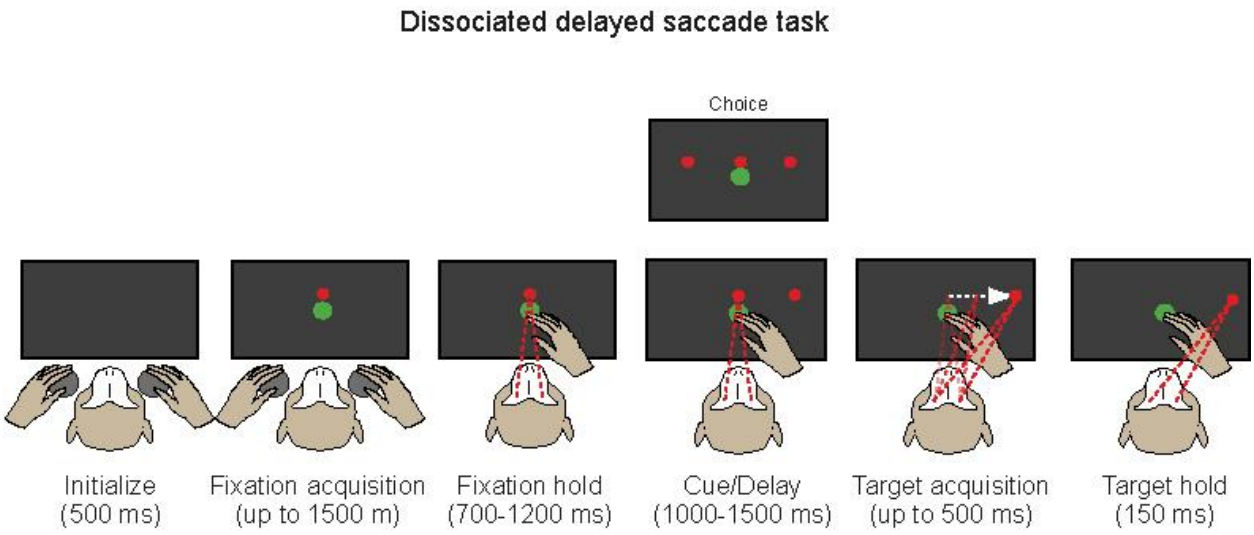

Figure 2.2: Delayed saccade task and target positions.

2.5 Saccade definition

Saccade velocity was calculated sample by sample as the square root of the sum of squared interpolated (220 Hz to 1 kHz) and smoothed (15 ms moving average rectangular window) horizontal and vertical eye position traces, and then smoothed again (15 ms moving average rectangular window). Saccade onset was defined as the first eye position change that exceeded a starting velocity threshold of 200°/s and ended when below velocity threshold of 50°/s.

2.6 Epoch definition and modulation

For a given trial, the following epochs were analyzed: Fixation hold, defined as -400 to -100 ms to target onset. Cue, defined as 50 to 150 ms after target onset. Delay, defined as the last 300 ms before the “Go” signal. Pre-saccade, defined as the last 200 ms before the saccade onset. Post-saccade, defined as the first 200 ms after the saccade end. Within each trial and each epoch, the average firing rate was computed by dividing the number of spikes by the duration. For analysis, we combined targets that were located in the same hemifield (3 left vs 3 right) and calculated the average firing rate as contralesional and ipsilesional space. To define the spatial tuning of each unit we used unpaired t-test between contralesional and ipsilesional targets and if there was a significant difference, the unit was classified as tuned to the hemifield associated with the highest firing rate. To define population of neurons such as visually responsive or motor responsive, we performed unpaired t-test between the firing rate of a specific epoch and the fixation hold epoch. For each unit, we also calculated the effect of inactivation using unpaired t-

test within epochs. In case of significant difference, unit was classified as being suppressed in that epoch if the firing rate was lower after inactivation and enhanced if higher.

2.7 Electrophysiological recordings

Dorsal pulvinar and LIP neuronal activity was recorded 16 or 32 channels linear V-probes (Plexon, Inc, USA) mounted on Motorized Electrode Manipulator (Thomas Recording, Germany). Single stainless steel guide tubes (27 gauge, Thomas Recording), filled with silicone oil (Thomas Recording), were used to protect electrodes during grid insertion and dura penetration. A reference tungsten rod was placed in the chamber filled with saline, and was connected to the electrode head stage. Neuronal signals were amplified (128 channels PZ2 preamplifier, Tucker-Davis Technologies, USA), digitized at 24 kHz and 16-bit resolution, and sent via fiber optics to an RZ2 BioAmp Processor (Tucker-Davis Technologies, USA) for online filtering (300 – 5000 Hz bandpass), display and storage on a hard drive together with behavioral and timing data streams.

2.8 Spike sorting

An offline procedure was used to obtain single/multi-unit spiking activity as follows: raw broadband data was filtered through high-pass (333Hz) and low-pass (5000Hz) Butterworth filter (MATLAB "butter" and "filtfilt" function). To detect individual spikes from single and multi-unit activity, we applied two different thresholds, 6*sigma and 3*sigma respectively, where sigma = median(abs(signal))/0.6745, to the filtered broadband data of each recording site individually. Before clustering, all spikes that were recorded in the inter-trial-interval were removed to avoid including in the analysis noise from monkey unspecific movements. Feature detection and the clustering of the spike waveforms were done by the modified version of the offline sorter Wave Clus (Quiroga et al., 2004; Kraskov et al., 2009; Michaels et al., 2016). The procedure includes computing multiple features by means of different methods including "wavelet decomposition", "Principle component analysis (PCA)", " raw spike waveforms" and "1st order derivative of the spike waveforms" and then select the first best 11 features with highest non-unimodality distribution using lillitest statistics. Then superparamagnetic clustering (SPC) was done on the selected features of a random sample of maximum 30000 spikes by applying Monte Carlo simulations with different starting values (Blatt et al., 1996). At this stage, temperatures used in SPC were manually selected independently for each channel and each unit, in a way that allows maximum separation between clusters (Figure 2.3). In case there were more than 30000 detected spikes, the remaining spikes were clustered by template matching with the mean features of each cluster. This procedure was done of for the all data recorded within one recording site/channel,

which could include several blocks of trials. This helped us to monitor the stability of spiking activity over time. Then the sorting and stability of each unit was assessed using the offline sorter (Plexon Inc, v3.0) for each block of the recording session separately. Plexon offline sorter allows to visualize all recorded waveforms within one block of trials, to visualize principal components and other features in 2D or 3D spaces, and to manually select waveforms if considered wrongly assigned or noise. Finally, waveform stability and firing rate over time were assessed using our visualization tools of the analysis pipeline. Both information from Waveclus and Plexon offline sorter were used to decide for final spike sorting in each recorded sites and each unit is graded in terms of signal to noise ratio, single or multi-unit and stability. Only unit that

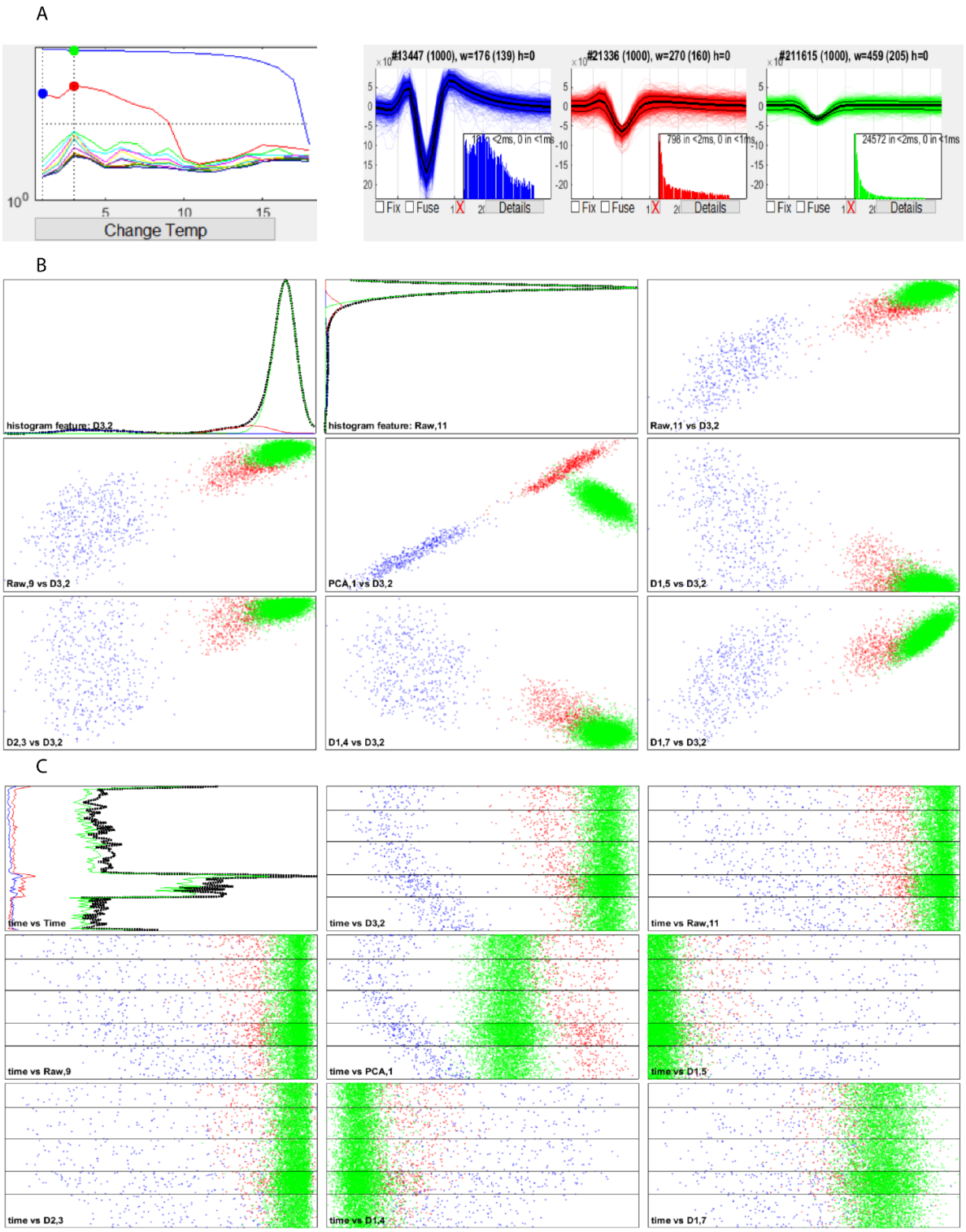

Figure 2.3: Waveclus offline sorting. *Selection of temperature for each cluster and stability assessment for an example recording site (20211208_ch44). A) Number of waveforms used as a template for each cluster in function of temperatures (left) and display of a subset of waveforms for each cluster. B) distribution of the two features that explain the maximum variance (top left and center) and scatter plot of features vs features. C) Scatter plots of features vs time.*

2.9 Local field potential

To obtain LFP signal, we applied a median filter on the broad band signal from each recording sites with the window size of 250 ms which reliably gave us LFP signal for the frequencies up to 150 Hz. To remove the 50 Hz AC line noise, band-stop Butterworth filter (Matlab "butter" and "filtfilt" functions) for the range of 49.9-50.1 Hz and also 99.9-100.1 Hz was applied. LFP signal power was computed using Fieldtrip toolbox (Oostenveld et al., 2011). LFP power was obtained for each of the frequency bins between 2 and 120 Hz in logarithmic steps ("logscale" function of MATLAB) by using Morlet wavelet convolution with a cycle-based time window for each frequency of n=6 cycles with a sliding window of 25 ms. This means for lower frequencies the time window was longer than higher frequencies. Since for a typical length of trial, the full power distribution for the whole trial in lower frequencies was not possible, zero-padding was done such that the length of a trial was enough for power calculations for all frequency bins. To detect noisy trials, we used different threshold based on amplitude (6*std for 10 consecutive samples), standard deviation (4*std of all trials), 1st derivative (6*std for 10 consecutive samples) and power (4*std of all trials). If in a specific trial, one of these thresholds were reached, the trial was considered as noisy and removed from further analysis. Normalization was performed as a relative change from baseline as follow: $P(rel) = \frac{P-\mu}{\mu}$ where P is the LFP power in a time-frequency bin and μ is the mean power of the baseline for that frequency. The time window used for baseline calculation was -500 to -50 ms from target onset. In difference plots, the statistical significance was calculated using a paired t-test on all recording site and Bonferroni correction was used to account for multiple comparison as follow: $\frac{\alpha}{Ntime*Nfrequency}$.

2.10 Peri-stimulus time histogram (PSTH)

Spike density functions were computed using a 10 ms bin size using a Gaussian kernel (20 ms). For each recorded unit, we either corrected the firing rate within each trial by subtracting the average ongoing firing rate in baseline or computed the relative change to baseline by the average firing rate across all trials within conditions as follow: $FR(rel) = \frac{FR-\mu}{\mu}$ where FR is the firing rate at a specific time point and μ is the mean firing rate in baseline. We used fixation hold epoch as baseline in both cases. Average responses for each unit were then derived by averaging the normalized spike density for each unit across all trials for the respective condition. Means and SE of these baseline-corrected and averaged spike densities across units of a given sub-population were calculated to display population responses.

2.11 Spike/LFP synchronization

To extract power and phase of LFP at each spike time a complex Morlet wavelet convolution was performed using Matlab R2011b function “cmorwavf”. We manually created a family of complex wavelets for logarithmically spaced frequencies from 4 to 100 Hz (covering 29 frequencies in total). We implemented a cycle-based approach, i.e. each complex wavelet contained 6 cycles for each frequency. The bin size of wavelets varied accordingly to make sure that the wavelet ends taper to zero. We did not address the issue of border spikes specifically because convolution was performed on concatenated trials and each trial has some extra time on the borders not included in the analysis. For spike-field coherence computation, we avoided using spikes and LFP from the same electrode because spike transients generated in the LFP signal typically inflate coherence measures. In Chapter 3 we calculated spike-field synchrony in all spike-LFP pairs (except same-electrode) within LIP area in both left and right hemisphere, but also across the hemispheres – using spikes from the left and LFP from the right hemisphere, and vice versa. In Chapter 4, we calculated spike-field synchrony within LIP and dPul of the recorded hemisphere and between the two regions. If spike-field synchrony is higher than zero, LFP activity at a particular frequency is correlated with the activity of neuron (Figure 2.4).

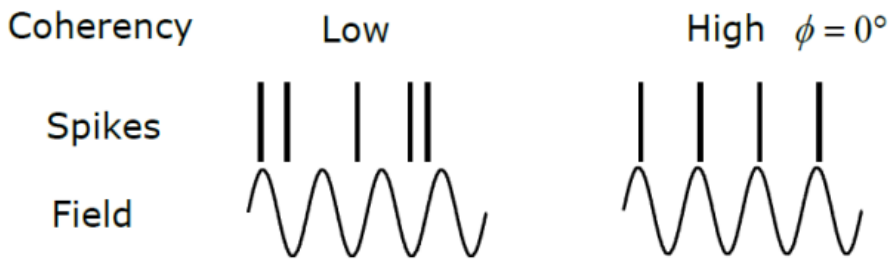

Figure 2.4. Example of spike-field synchrony of single spike-field pair. On the left spikes are distributed randomly resulting in the low coherence, while at the right spikes are clustered at the specific phase of sine wave resulting in high coherence (Singla, 2015).

We used pairwise phase consistency (ppc) (Vinck et al., 2010) because it is considered to be a bias-free (rate-independent) measure of rhythmic neuronal synchronization. For ppc calculation, LFP phases around each individual spike are found first and the pairs of observations are taken into consideration rather than all observations together (as it is the case in spectral coherence calculation). Then ppc is computed from the distribution of all pairwise differences (between pairs

of spikes) of the phases. The assumption is that the distribution of pairwise differences in the phases will be more strongly clustered around a specific value if phase synchronization is present.

In the paper of Vinck et al., 2010, ppc is calculated as follows:

$$PPC \equiv \frac{2}{N(N-1)} \sum_{j=1}^{N-1} \sum_{k=(j+1)}^{N} f\left(\theta_j, \theta_k\right),$$

where N is the number of observations (spikes), θj and θk are the relative phases from two observations, and j and k are indices of trials and spikes, correspondingly. The function f computes the dot product between two unit vectors and defined as:

$$f(\varphi, \omega) \equiv \cos(\varphi)\cos(\omega) + \sin(\varphi)\sin(\omega).$$

Ppc value is bound from -1 to 1, the value of 1 means absolute coherence, while 0 means no coherence. Negative values of ppc is a known shortcoming of ppc, they are not interpretable and usually happen due to the low number of observations.

The equation above calculates the average absolute angular distance between all observed relative phases. However, this is based on the assumption that spikes are generated as a Poissonian process (completely independent) and therefore all individual spike-LFP phases are statistically independent random variables. In reality, spikes are not independent – their occurrence might be affected by the refractory period, autorhythmicity, and burstiness. To address this problem improved ppc measure was suggested (Vinck et al., 2012): it considers pairs of spike-field phases obtained only from separate trials. Although in total fewer pairs of spike-field phase are included in ppc calculation, it helps to avoid artificially inflated or decreased ppc value. The price of it is the increased variance of improved ppc in comparison with previously described ppc.

2.12 LFP/LFP synchronization

To obtain LFP signal, we applied a median filter on the broad band signal from each recording sites with the window size of 250 ms which reliably gave us LFP signal for the frequencies up to 150 Hz. To remove the 50 Hz AC line noise, band-stop Butterworth filter (Matlab "butter" and

"filtfilt" functions) for the range of 49.9-50.1 Hz and also 99.9-100.1 Hz was applied. The LFP power and cross-spectrum was computed for each site pairs using the Fieldtrip toolbox (ft_freqanalysis) for each of the frequency bins between 2 and 120 Hz in logarithmic steps ("logscale" function of MATLAB) by using Morlet wavelet convolution with a cycle-based time window for each frequency of n=6 cycles with a sliding window of 25 ms. To detect noisy trials, we used different threshold based on amplitude (6*std for 10 consecutive samples), standard deviation (4*std of all trials), 1st derivative (6*std for 10 consecutive samples) and power (4*std of all trials). If in a specific trial, one of these thresholds were reached, the trial was considered as noisy and removed from further analysis. We then used the ft_connectivityanalysis function from FieldTrip toolbox to calculate the LFP-LFP phase synchronization spectrogram from the LFP-LFP cross power spectra for each site pairs recorded simultaneously. The LFP-LFP phase synchronization was computed using pair wise phase consistency method. Finally, LFP-LFP phase synchronization spectrogram of each site pairs were averaged.

3 Functional interactions between the dorsal pulvinar and LIP during spatial target selection and oculomotor planning

3.1 Abstract

The dorsal pulvinar is reciprocally connected to various cortical areas in the fronto-parietal network involved in sensory-motor transformation and decision-making. However, its functional contribution and underlying neuronal mechanisms remain poorly understood. In this study, we used simultaneous recordings in the dorsal pulvinar and in area LIP in macaques performing a delayed saccade task, to instructed targets and in the context of free choices, to characterize neuronal properties and functional connectivity within and between regions. We found contralateral tuning in the visual response to instructed targets in both regions but choice signals only in area LIP. Subpopulations of dorsal pulvinar neurons showed either increased or decreased activity without spatial tuning during movement preparation whereas in LIP, we observed an increased activity with a preference for contralateral targets. We observed ongoing synchronization within and between the two regions and transient shift in frequencies of interactions upon target presentation and saccades. In addition, inter-regions synchronization was stronger before contralateral choices. Finally, the spike-field synchronization profile suggested reciprocal interactions during visual processing and around saccades and directional connectivity from LIP to the dorsal pulvinar during fixation and movement preparation. Overall, results shed light on the role of pulvino-parietal circuitry, with strong flexible functional connectivity, in decision-making and oculomotor planning and execution.

3.2 Introduction

The process of flexible oculomotor target selection involves numerous cortical areas from visual areas V1/V2 to parietal area LIP, frontal area FEF and subcortical regions like the pulvinar and SC. The involvement of both cortical areas and the pulvinar implies a role for thalamocortical circuitry but the neural implementation of target selection has been mostly studied within separate regions areas/regions.

Electrophysiological studies in macaques revealed that individual neurons in area LIP accumulate sensory evidence in a motion discrimination task in which monkeys communicate their choices through saccades to the corresponding target (Roitman and Shadlen, 2002; Huk and Shadlen, 2005). A similar task with reward contingencies showed that activity in LIP could be modulated by introducing a bias in the reward value associated with the decision (Rorie et al., 2010). Therefore, neurons in area LIP reflect both the strength of sensory evidence and the value of the target inside and outside their corresponding response fields (Platt and Glimcher, 1999). However, pharmacological inactivation of LIP does not alter the decision in the motion discrimination task, questioning its role in perceptual decision-making (Katz et al., 2016). On the contrary, silencing LIP neurons leads to a reduction of contralesional choices in a free-choice task with equal reward (Wilke et al., 2012), highlighting the causal role of LIP in internally-generated, not stimulus-driven decisions. Furthermore, it has been shown that LIP role in free-choice decisions is mostly effector specific since LIP inactivation induced a greater choice bias when the decision was made with saccades rather than reaches (Christopoulos et al., 2018), opposite to the parietal reach area PRR (Christopoulos et al., 2015).

Similarly to LIP, the dorsal pulvinar (dPul) involvement in decision-making has been revealed by causal perturbation studies reporting choice bias in free-choice decisions after pharmacological inactivation or microstimulation (Wilke et al., 2010, 2013; Dominguez-Vargas et al., 2017). However, there is less information available on neuronal responses during oculomotor decision-making. Nevertheless, it has been shown that saccade-related activity in the dorsal pulvinar is heterogeneous since visually- and memory-guided saccade tasks can elicit directional enhancement and/or inhibition at different timing of the task, e.g. after stimuli presentation, during the memory period and in the pre- an/or post-saccadic window (Robinson et al., 1986; Benevento and Port, 1995). Current work in our lab has also systematically investigated dorsal pulvinar neuron tuning properties (L. Schneider, 2019, Perceptual and motor intentional processing in

dorsal pulvinar) (Schneider et al., 2021). At the population level, there was a clear contralateral preference for visual stimuli presentation. Surprisingly, the activity during the delay period was mostly suppressed and non-space specific. In addition, it did not reflect the upcoming saccade when two saccade options were available. These results suggest that the mechanism leading to choice bias after inactivation/microstimulation may not be explained only by looking at dorsal pulvinar neuron tuning properties.

Anatomical studies using tracers have shown that area LIP and the dorsal pulvinar share reciprocal projections (Hardy and Lynch, 1992; Romanski et al., 1997). This connectivity has also been described in humans using fMRI (Arcaro et al., 2018). Additionally, the use of microstimulation in combination with fMRI provided an additional tool to investigate functional connectivity. Using this technique, it has been shown that stimulating pulvinar increases activity in LIP (Kagan et al., 2021). Interestingly, it also elicited activation of cortical areas in the opposite hemisphere, including area LIP, suggesting polysynaptic transmission of the excitation.

In order to better understand the contribution of both LIP and the dorsal pulvinar to oculomotor decision-making it is important to consider not only their tuning properties but also their functional interactions. One way to assess such interactions is to look at the synchronization of neuronal activity. Indeed, synchronization of neuronal activity plays a crucial role in effective communication since neuronal populations tend to engage in rhythmic oscillations, creating fluctuations in their excitability and resulting in moments of excitation and inhibition. Because this is so, the timing to which an action potential is sent or received can dramatically affect its significance. Changes in neuronal synchronization then allow modulating communication without changing anatomical connections. This concept has been described by Pascal Fries under the term ‘Communication through coherence (CTC)’ (Fries, 2015). The communication through coherence hypothesis relies on three important concepts. First, the rhythmic fluctuation of postsynaptic excitability induces modulation in synaptic gain. In other words, inputs that arrive in a moment of high excitability will benefit from synaptic gain. Second, as a consequence of synaptic gain modulation, effective communication between population of neurons requires synchronization (or coherence) in their activity. Indeed, in the absence of coherence, inputs to a neuronal population will not benefit from synaptic gain since it arrives at random phases of the excitability cycle. Third, a specific neuronal population that receives different inputs will have a preferential response to synchronized ones. Therefore, synchronization allows selective communication between population of neurons.

Recently, Fiebelkorn and colleagues (Fiebelkorn et al., 2019) investigated neuronal interactions between the dorsal pulvinar and fronto-parietal network during a visual attention task. First of all, they report that the alpha/low beta activity in the dorsal pulvinar could be used as a prediction of behavioral performance. Second, by looking at spikes-LFP coherence, they show a significant coupling between pulvinar spikes and LIP LFP activity in the alpha/low beta range. With the idea of spikes reflecting the output of neuronal population and LFP the input, this result suggests that the dorsal pulvinar drives LIP alpha/low beta activity. Similar results were found when looking at spike-LFP coupling when using spikes from LIP and looking at alpha/low beta in the pulvinar. However, by looking at the same measure, in trials associated with a high level of attention versus low-level attention, they suggest that the dorsal pulvinar drives LIP alpha/low beta activity during high behavioral performance and vice versa.

Another recent study used pharmacological inactivation to investigate the role of the ventral lateral pulvinar in visual attention (Zhou et al., 2016). As has been described in the dorsal pulvinar, the activity of the ventral pulvinar was also modulated by attention, with higher activity in response to a stimulus that appeared in a cued location. Consequently, ventral pulvinar inactivation induced attentional behavioral deficits when relevant stimuli were located in the contralesional hemifield. By looking at spiking activity, they also showed that the inactivation reduced the evoked response to stimuli slight color change in area V4 as well as the attentional modulation index. In addition, inactivation had two distinct effects on neuronal synchronization within V4. First, it reduced spikes/LFP synchronization in gamma as well as its modulation by visual attention. Second, it also caused a large increase in LFP power below 20 Hz, suggesting a decreased “alert state” in area V4.

The goal of this experiment is to investigate the role of the pulvino-parietal circuitry during eye movement selection and execution. To do so, evaluated neuronal responses in each region as well as functional connectivity within and between the dorsal pulvinar and area LIP. We recorded simultaneously multichannel neuronal activity in the two regions while monkey performs instructed and free-choice oculomotor delayed response task, allowing us to evaluate synchronization in their activity during different cognitive demands and task epochs (i.e. instructed vs. free-choice, visual processing, movement planning, movement execution). From a more general perspective, this experiment sheds light on the crucial role of thalamocortical interactions in sensorimotor processing and transformation.

3.3 Material and methods

See **General Materials and Methods** for methodological aspects shared across Chapters 3 and 4. Here only specific aspects of this study are detailed.

3.3.1 Recording locations

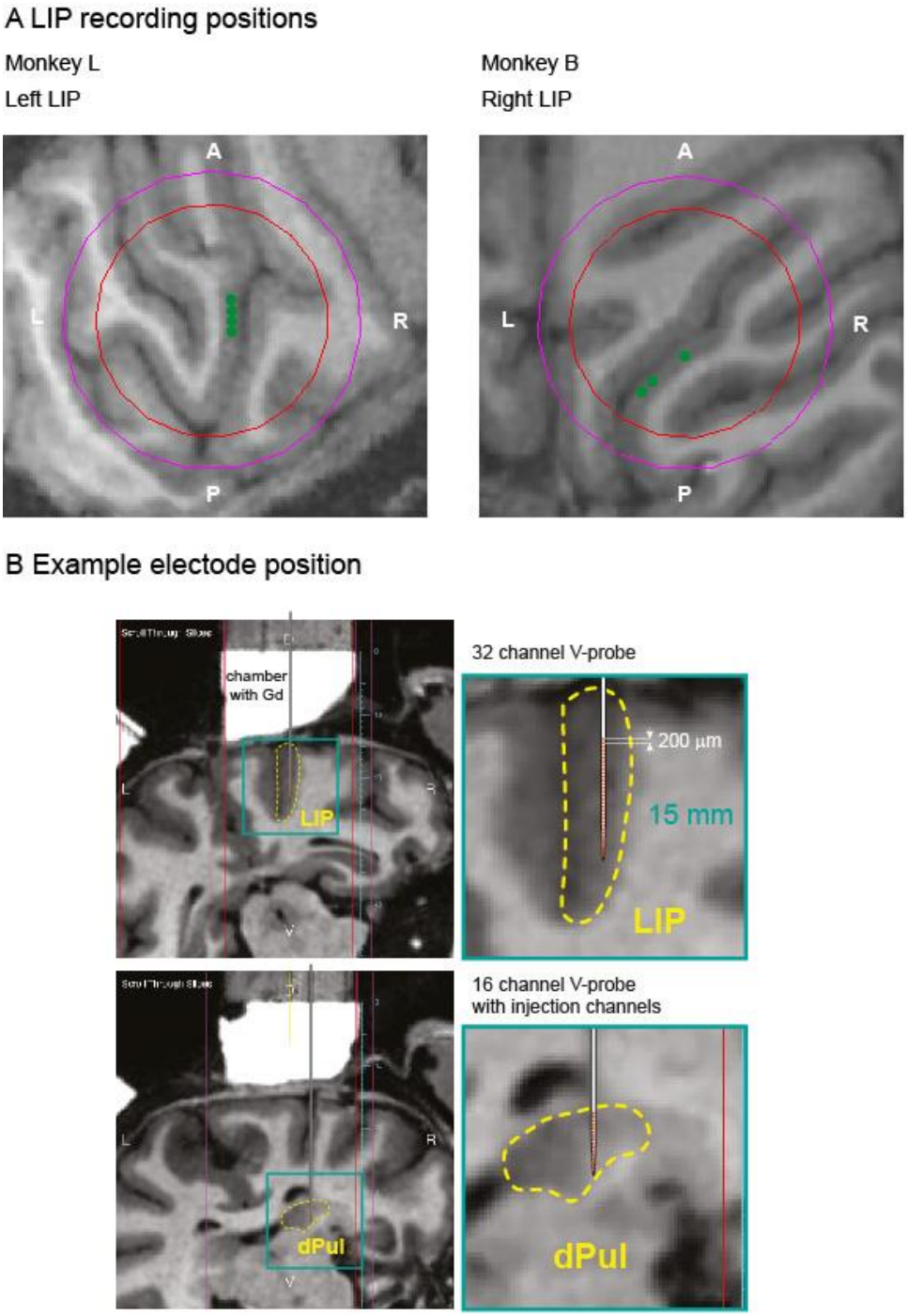

Figure 3.2.1 Simultaneous dPul/LIP recordings using multi-sites recording electrodes. A LIP recording locations in monkey L (left) and monkey B (right). **B** Example reconstruction of electrodes position in LIP (top) and the dorsal pulvinar (bottom).

We recorded simultaneously the activity in the dorsal pulvinar and LIP in two monkeys (Figure 3.2.1), monkey L and monkey B. In monkey L, we recorded 8 sessions (Table 3.2.1) in the left hemisphere during a delayed saccade task (see Materials and Methods for details). In Monkey B, we recorded 9 sessions (Table 3.2.2) in the right hemisphere during a delayed dissociated saccade task (see Materials and Methods for details).

Table 3.2.1 List of sessions and recording locations (x, y relative to grid center) for monkey L

Date	LIP recording location	dPul recording location	hemisphere
20211109	2;-1	1;8	left
20211110	2;0	1;9	left
20211111	2;0	1;9	left
20211112	2;0	1;9	left
20211117	2;0	1;9	left
20211118	2;1	1;9	left
20211119	2;1	1;9	left
20211124	2;2	1;8	left

Table 3.2.2 List of sessions and recording locations (x, y relative to grid center) for monkey B

Date	LIP recording location	dPul recording location	hemisphere
20200325	-4;-7	4;1	right
20200409	-4;-7	4;1	right
20200423	-4;-7	4;1	right
20200513	-4;-7	4;1	right
20200522	-5;-8	4;1	right
20200530	-5;-8	4;1	right
20200619	0;-4	4;3	right
20200624	0;-4	4;3	right
20200626	0;-4	4;3	right

3.3.2 Local field potential

To obtain LFP signal, we applied a median filter on the broad band signal from each recording site with the window size of 250 ms which reliably gave us LFP signal for frequencies up to 150 Hz. To remove the 50 Hz AC line noise, a band-stop Butterworth filter (MATLAB "butter" and "filtfilt" functions) for the range of 49.9-50.1 Hz and also 99.9-100.1 Hz was applied. LFP signal power was computed using the Fieldtrip toolbox (Oostenveld et al., 2011). LFP power was obtained for each of the frequency bins between 2 and 120 Hz in logarithmic steps ("logscale" function of MATLAB) by using Morlet wavelet convolution with a cycle-based time window for each frequency of n=6 cycles with a sliding window of 25 ms. This means for lower frequencies

the time window was longer than for higher frequencies. Since for a typical length of a trial, the full power distribution for the whole trial in lower frequencies was not possible, zero-padding was done such that the length of a trial was enough for power calculations for all frequency bins. To detect noisy trials, we used different thresholds based on amplitude (6*std for 10 consecutive samples), standard deviation (4*std of all trials), 1st derivative (6*std for 10 consecutive samples) and power (4*std of all trials). If in a specific trial, one of these thresholds was reached, the trial was considered noisy and removed from further analysis. Normalization was performed as a relative change from baseline as follows: $P(rel) = \frac{P-\mu}{\mu}$ where P is the LFP power in a time-frequency bin and μ is the mean power of the baseline for that frequency. We normalized LFP power in each frequency as a relative signal change to the baseline. The time window used for baseline calculation was -500 to -50 ms from target onset. In difference plots, the statistical significance was calculated using a paired t-test on all recording sites and Bonferroni correction was used to account for multiple comparisons as follows: $\frac{\alpha}{Ntime*Nfrequency}$.

3.3.3 Peri-stimulus time histogram (PSTH)

Spike density functions were computed using a 10 ms bin size using a Gaussian kernel (20 ms). Average responses for each unit were then derived by averaging the normalized spike density for each unit across all trials for the respective condition. Means and SE and averaged spike densities across units of a given sub-population were calculated to display population responses. Visually responsive neurons were defined as showing a significant increase in firing rate for at least one space condition in the cue epoch as compared to the fixation hold epoch. Motor responsive neurons were defined as showing a significant increase of firing rate for at least one space condition in the delay epoch as compared to the fixation hold epoch.

3.4 Results

3.4.1 Behavioral analysis

We analyzed the behavioral performance of monkey L who performed a delayed saccade task (8 sessions) and monkey B who performed a delayed dissociated saccade task (with central hand fixation, 9 sessions). We first looked at side selection in free-choice trials where two target options were available in the two hemifields. Monkey L showed a bias in selecting preferentially targets located in the ipsilateral to the recorded hemisphere hemifield (Figure 3.3.1, fraction of contra choices: 0.32 ± 0.03). Nevertheless, this choice bias does not prevent us from analyzing neuronal data from free-choice trials with an average of 116 contralateral choices (vs 250 ipsilateral choices) per session. We observed in monkey B slight bias toward the contralateral hemifield (Figure 3.3.1, contralateral choices: 0.62 ± 0.02). In the delayed saccade task (inactivation experiment), monkey B also had a choice bias towards this hemifield. Here again, the proportion of contralateral and ipsilateral choices allows the analysis of neuronal data during free-choice trials.

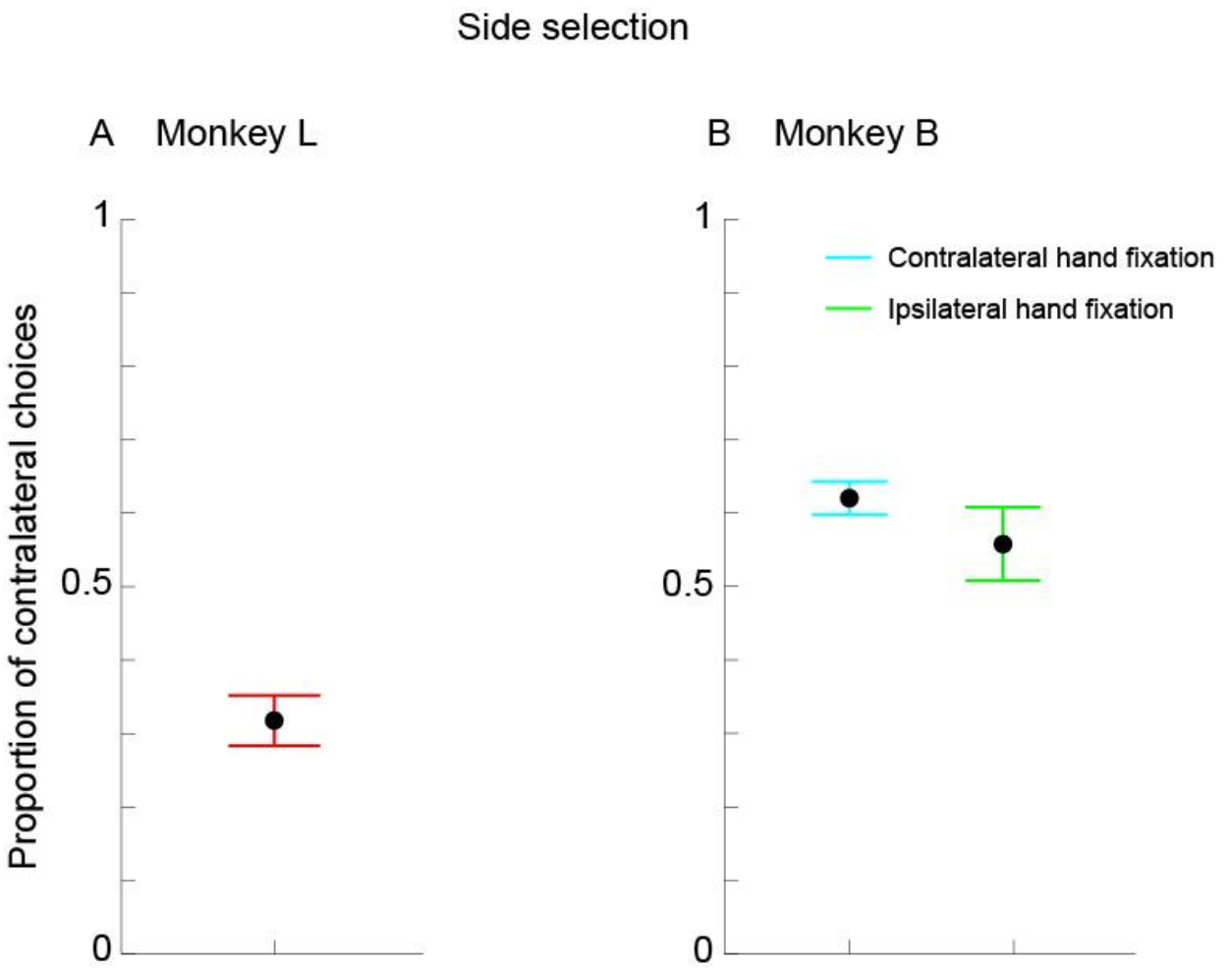

Figure 3.3.1 Side selection during free-choice trials for both monkeys. A Proportion of contralateral choices for monkey L (delayed saccade). **B** Proportion of contralateral choices for monkey B with contralateral and ipsilateral hand central fixation (dissociated delayed saccade) (Mean ± SEM).

Both monkeys could perform the task with a high performance (Figure 3.3.2: Monkey L: instructed contra: 0.92 ± 0.02; choice contra: 0.78 ± 0.03; instructed ipsi: 0.90 ± 0.02; choice ipsi: 0.96 ± 0.01; Monkey B: instructed contra: 0.96 ± 0.03 (contra hand), 0.95 ± 0.03 (ipsi hand); choice contra: 0.95 ± 0.04 (contra hand), 0.94 ± 0.03 (ipsi hand); instructed ipsi: 0.93 ± 0.02 (contra hand), 0.92 ± 0.03 (ipsi hand); choice ipsi: 0.93 ± 0.03 (contra hand), 0.95 ± 0.02 (ipsi hand). Surprisingly, monkey L showed a significantly lower success rate in free-choice trials when selecting contralateral targets. This lower success rate most likely explains the choice bias towards ipsilateral targets in monkey L.

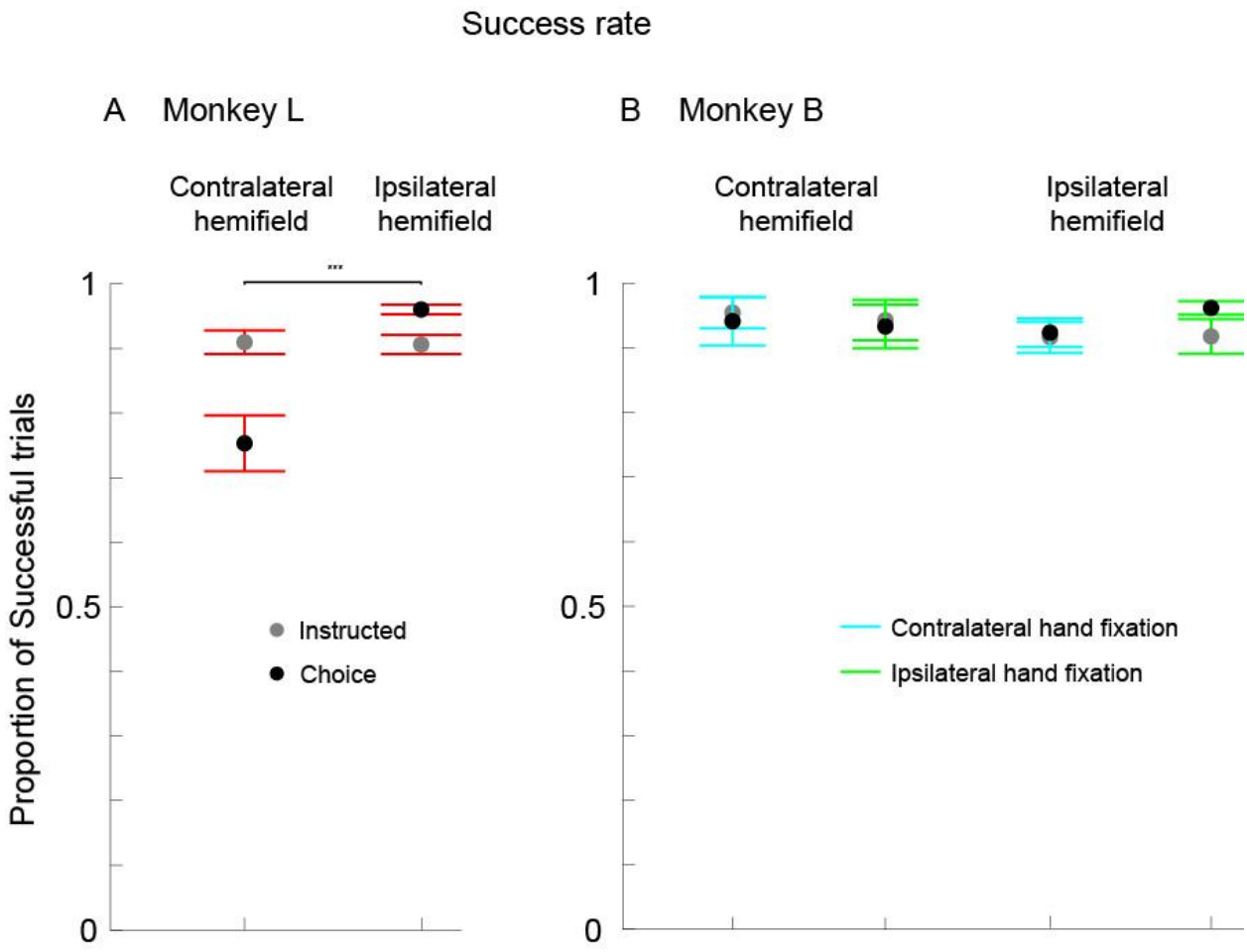

Figure 3.3.2 Performance during instructed and free-choice trials for both monkeys. A Proportion of successful trials for instructed and free-choice contralateral and ipsilateral targets for monkey L (delayed saccade). B Proportion of successful trials for instructed and free-choice contralateral and ipsilateral targets for monkey B with contralateral and ipsilateral hand central fixation (dissociated delayed saccade) (Mean ± SEM; * p<0.05, ** p<0.005, *** p<0.0005).

We also analyzed the saccadic reaction time, from the 'go signal' to the initiation of the saccade. Saccadic reaction times in both monkeys were comparable and we did not find any significant differences between space and/or hand conditions (Figure 3.3.3: Monkey L: instructed contra: 0.20 ± 0.03; choice contra: 0.19 ± 0.05; instructed ipsi: 0.20 ± 0.02; choice ipsi: 0.20 ± 0.03; Monkey B: instructed contra: 0.20 ± 0.07 (contra hand); 0.20 ± 0.04 (ipsi hand); choice contra: 0.18 ± 0.01 (contra hand); 0.18 ± 0.01 (ipsi hand); instructed ipsi 0.19 ± 0.01 (contra hand); 0.20 ± 0.01 (ipsi hand); choice contra: 0.18 ±0.08 (contra hand); 0.20 ± 0.02 (ipsi hand)).

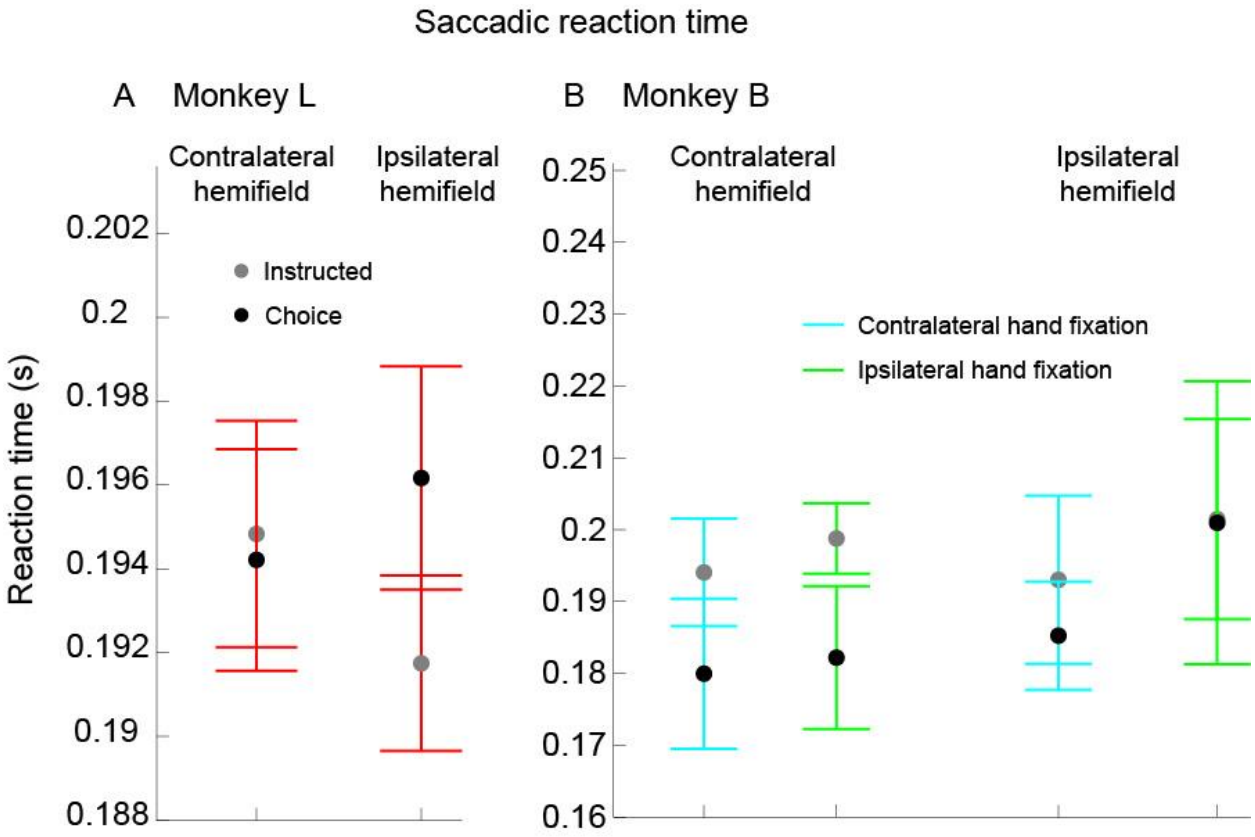

Figure 3.3.3 Saccadic reaction time during instructed and free-choice trials for both monkeys. A Reaction time for saccades to the contralateral and ipsilateral targets during instructed and free-choice trials for monkey L (delayed saccade). **B** Reaction time for saccades to the contralateral and ipsilateral targets during instructed and free-choice trials for monkey B with contralateral and ipsilateral hand central fixation (dissociated delayed saccade) (Mean ± SEM; * p<0.05, ** p<0.005, *** p<0.0005).

3.4.2 Spiking activity

In each session, we recorded single and multi-unit activity simultaneously in area LIP and the dorsal pulvinar (dPul) (Monkey L, LIP: n=278; dPul: n=297; monkey B, LIP: n=124, dPul: n=95) in two monkeys while they performed delayed saccade task (monkey L) or dissociated delay saccade task (monkey B). For comparison between monkeys, we will only show in monkey B conditions where the contralateral hand was used for central fixation.

3.4.2.1 Spiking activity within area LIP

We first looked at the neuronal spiking activity within the area LIP. As expected from previous work, we observed transient visual response to target presentation, in both monkeys (Figure 3.3.4). Indeed, 64% of recorded neurons in monkey L and 54% in monkey B showed a significant increase in activity after target presentation in at least one of the two hemifields. These visually responsive units showed a strong contralateral tuning in instructed trials where only one target was displayed (monkey L: contra: 83%, ipsi: 3%, not tuned: 14%; monkey B: contra: 68%, ipsi:

6%, not tuned: 26%). In free-choice trials where targets in both hemifields were presented, the contralateral tuning was less pronounced with a high proportion of units being not tuned to one hemifield. However, the tuned units were mostly tuned towards the contralateral hemifield (monkey L: contra: 34%, ipsi: 9%, not tuned: 57%; monkey B: contra: 35%, ipsi: 5%, not tuned: 60%). During two-target presentation, the visual scene that monkeys see were identical regardless of the upcoming choice. Therefore, differences in spiking activity in this time window might partially reflect the upcoming choice.

We also observed increased spiking activity during the late delay period (9% in monkey L, 28% in monkey B), relative to the initial fixation period. The different proportion of units showing delay activity in both monkeys suggests that recording locations in monkey L and monkey B targeted different subdivisions of area LIP, although this was not apparent from anatomical MRI. Nevertheless, in instructed trials, we found strong contralateral tuning before saccade onset, specifically in monkey L (monkey L: contra: 74%, ipsi: 3%, not tuned: 23%; monkey B: contra: 29%, ipsi: 16%, not tuned: 55%). Similarly, in free-choice trials most tuned units were tuned to upcoming saccades towards the contralateral hemifield (monkey L: contra: 43%, ipsi: 6%, not tuned: 51%; monkey B: contra: 27%, ipsi: 5%, not tuned: 68%). Therefore, choice signals were present in both monkeys in area LIP shortly before the saccade initiation.

Finally, we observed saccade-related activity. At the level of the population, the tuning was similarly biased towards the contralateral hemifield during both instructed and free-choice trials (instructed: monkey L: contra: 34%, ipsi: 6%, not tuned: 60%; monkey B: contra: 37%, ipsi: 18%, not tuned: 45%; free-choice: monkey L: contra: 36%, ipsi: 8%, not tuned: 56%; monkey B: contra: 32%, ipsi: 25%, not tuned: 42%). Interestingly, when looking at delay responsive units, we observed differences between monkeys. Namely, in monkey L, the post-saccadic activity was tuned to the contralateral space whereas in monkey B, it was tuned to the ipsilateral space (instructed: monkey L: contra: 46%, ipsi: 3%, not tuned: 51%; monkey B: contra: 24%, ipsi: 39%, not tuned: 37%; free-choice: monkey L: contra: 37%, ipsi: 26%, not tuned: 37%; monkey B: contra: 24%, ipsi: 46%, not tuned: 30%). This different activity profile might reflect the analysis of different subpopulations in the two monkeys. It is possible that in monkey L, recording sites were located in a more visual subdivision of LIP and that the activity during delay and before the saccade onset was not related to movement selection and preparation but was instead sustained visual activity in the presence of visible targets.

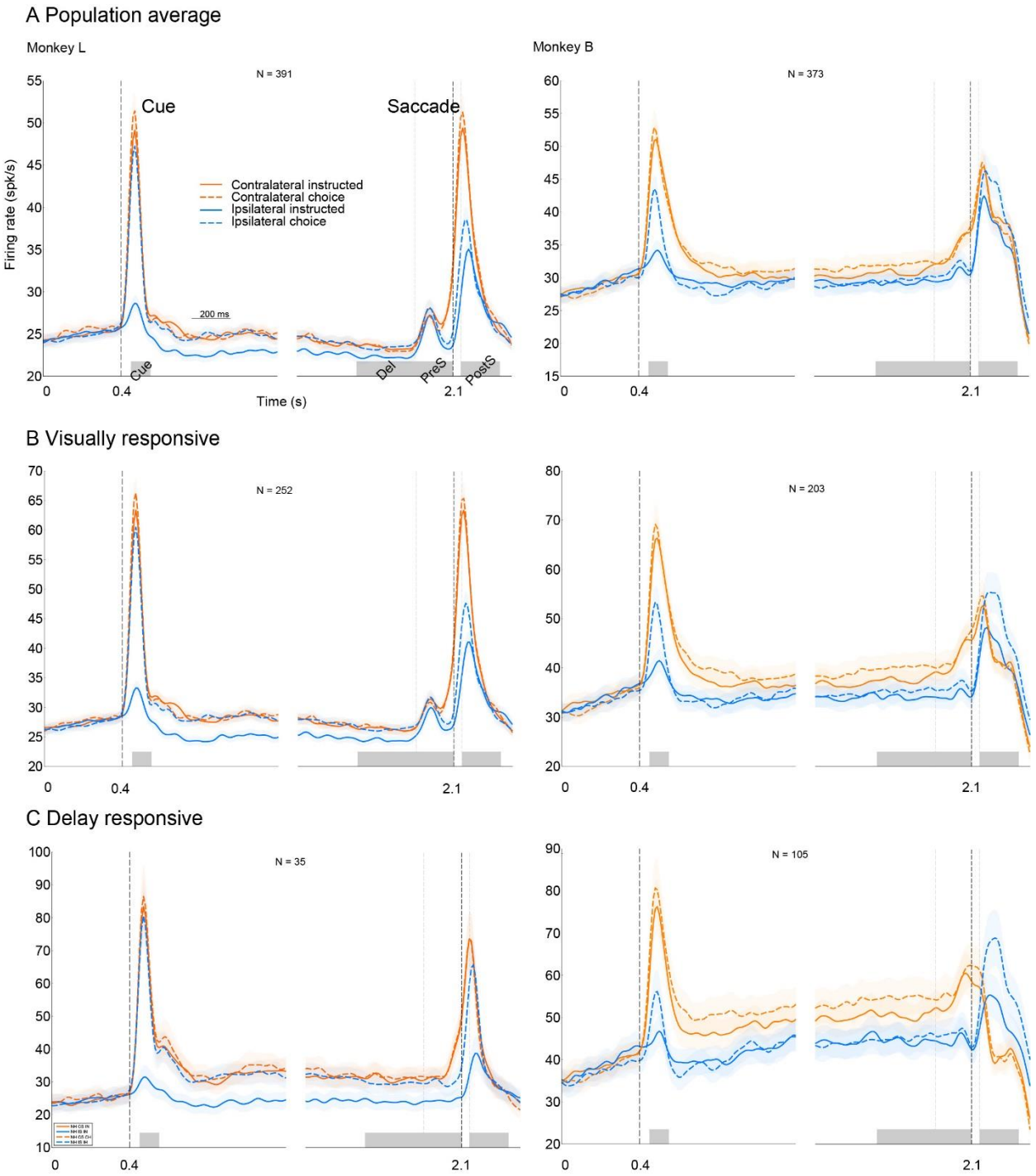

Figure 3.3.4. Spiking activity in area LIP in both monkeys. A Spike density average of all recorded neurons. **B** Spike density average for visually responsive neurons. **C** Spike density average for delay responsive neurons. The spike density average (mean ± SEM) is shown independently for instructed/choice (solid/dotted) and contralesional/ipsilesional space (orange/blue)

3.4.2.2 Spiking activity within dorsal pulvinar

We found in the dorsal pulvinar a high heterogeneity in terms of spiking activity during delayed saccade task (Figure 3.3.5). For example, some units showed a transient visual response to target presentation on the contralateral hemifield. We also found units with activity gradually increasing or increasing after target presentation in both hemifields. We also observed units with ipsilateral cue and saccade-related activity as well as contralateral post-saccadic response. Finally, some units showed decreased activity after target presentation and before saccades towards the ipsilateral hemifield. Such variability reflects the wide anatomical and functional connectivity of the pulvinar.

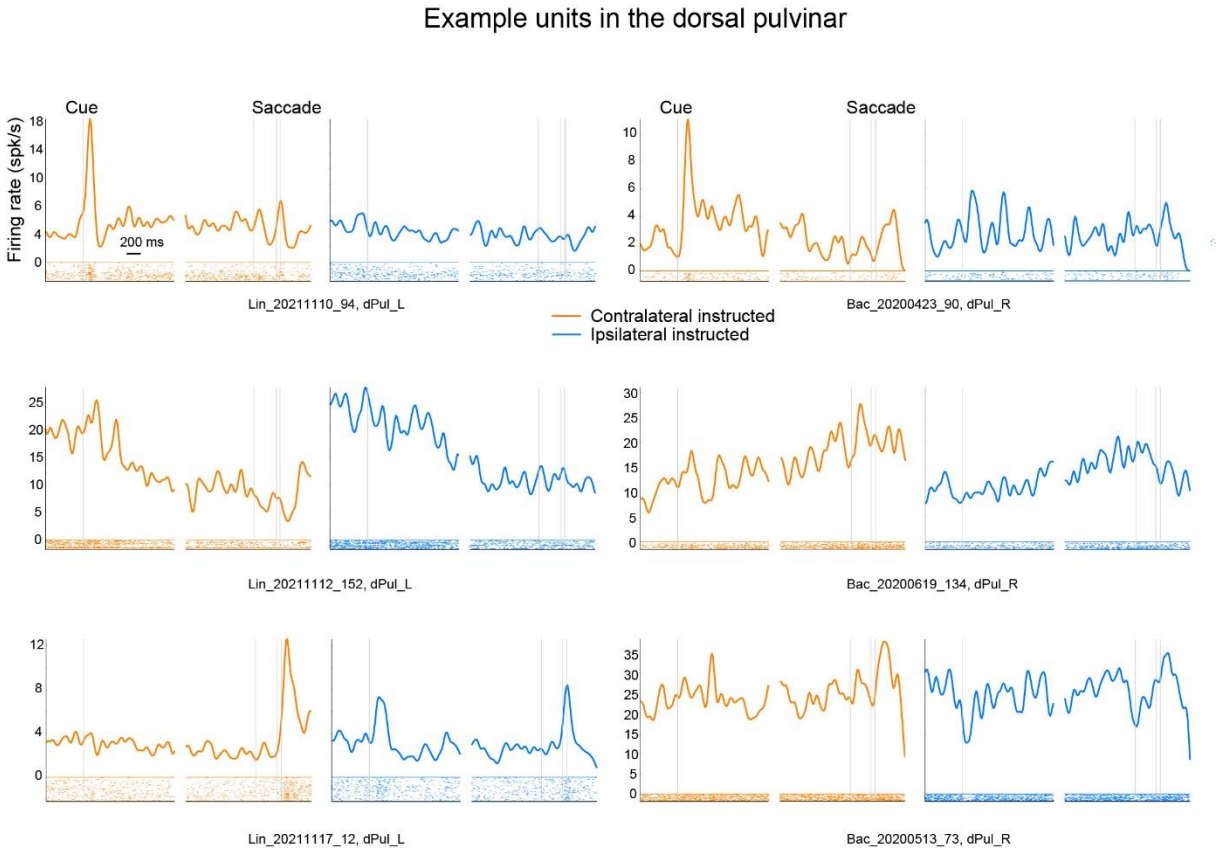

Figure 3.3.5. Example units spiking activity in the dorsal pulvinar. Average spike density across trials and raster plots for single trials. Only instructed trials are shown (blue: ipsilateral, orange: contralateral).

Despite the variability in the dorsal pulvinar neuronal responses, we could observe a transient increase in activity at the population level after target presentation to the contralateral hemifield and during free-choice trials. Consistently with what was previously described in our lab (Schneider et al., 2021) using memory saccades, we found around 27% (12% in monkey L, 42% in monkey B) units showing a significantly enhanced (relative to the fixation baseline) visual

response (Figure 3.3.6). Visually responsive units were mostly tuned to the contralateral hemifield during instructed trials (monkey L: contra: 37%, ipsi: 11%, not tuned: 52%; monkey B: contra: 36%, ipsi: 3%, not tuned: 61%) and were mostly not tuned during free-choice trials (monkey L: contra: 8%, ipsi: 4%, not tuned: 88%; monkey B: contra: 4%, ipsi: 3%, not tuned: 93%).

Some units showed a significant increase in activity during the delay period (Figure 3.3.7), associated with motor preparation (11% in monkey L, 27% in monkey B). But despite the continuous presence of a visual target, this subpopulation did not show strong contralateral tuning even during instructed trials (monkey L: contra: 14%, ipsi: 6%, not tuned: 80%; monkey B: contra: 4%, ipsi: 7%, not tuned: 89%), and even less so during the choice trials (**). The lack of contralateral tuning during movement preparation is in contrast with what we observed in area LIP, but matches previous findings from our lab with the memory saccades (Schneider et al., 2021).

Interestingly, we found a comparable proportion of units showing a decreased activity during the delay period (19% in monkey L, 21% in monkey B). Suppressed activity in the dorsal pulvinar during movement preparation was also observed in a memory saccade task (Schneider et al., 2021). As we described for the subpopulation showing enhanced activity during delay, we did not find a strong tuning towards one hemifield, neither during instructed nor free-choice trials (instructed: monkey L: contra: 10%, ipsi: 13%, not tuned: 77%; monkey B: contra: 14%, ipsi: 5%, not tuned: 81%; free-choice: monkey L: contra: 14%, ipsi: 5%, not tuned: 81%; monkey B: contra: 3%, ipsi: 6%, not tuned: 91%). Together, the fact that dorsal pulvinar activity is modulated during the delay period highlights its role in movement preparation. However, the lack of spatial tuning, both in subpopulation being enhanced or suppressed, questions the dorsal pulvinar implication in prospective spatial target selection during the delay period.

Finally, we also observed in the dorsal pulvinar saccade-related activity. More precisely, 17% of units in monkey L and 34% in monkey B showed a significant post-saccadic increase in firing rate. In this subpopulation, the tuning was bias towards the contralateral hemifield in both instructed in free-choice trials (instructed: monkey L: contra: 23%, ipsi: 3%, not tuned: 74%; monkey B: contra: 28%, ipsi: 19%, not tuned: 53%; free-choice: monkey L: contra: 16%, ipsi: 2%, not tuned: 82%; monkey B: contra: 22%, ipsi: 17%, not tuned: 60%).

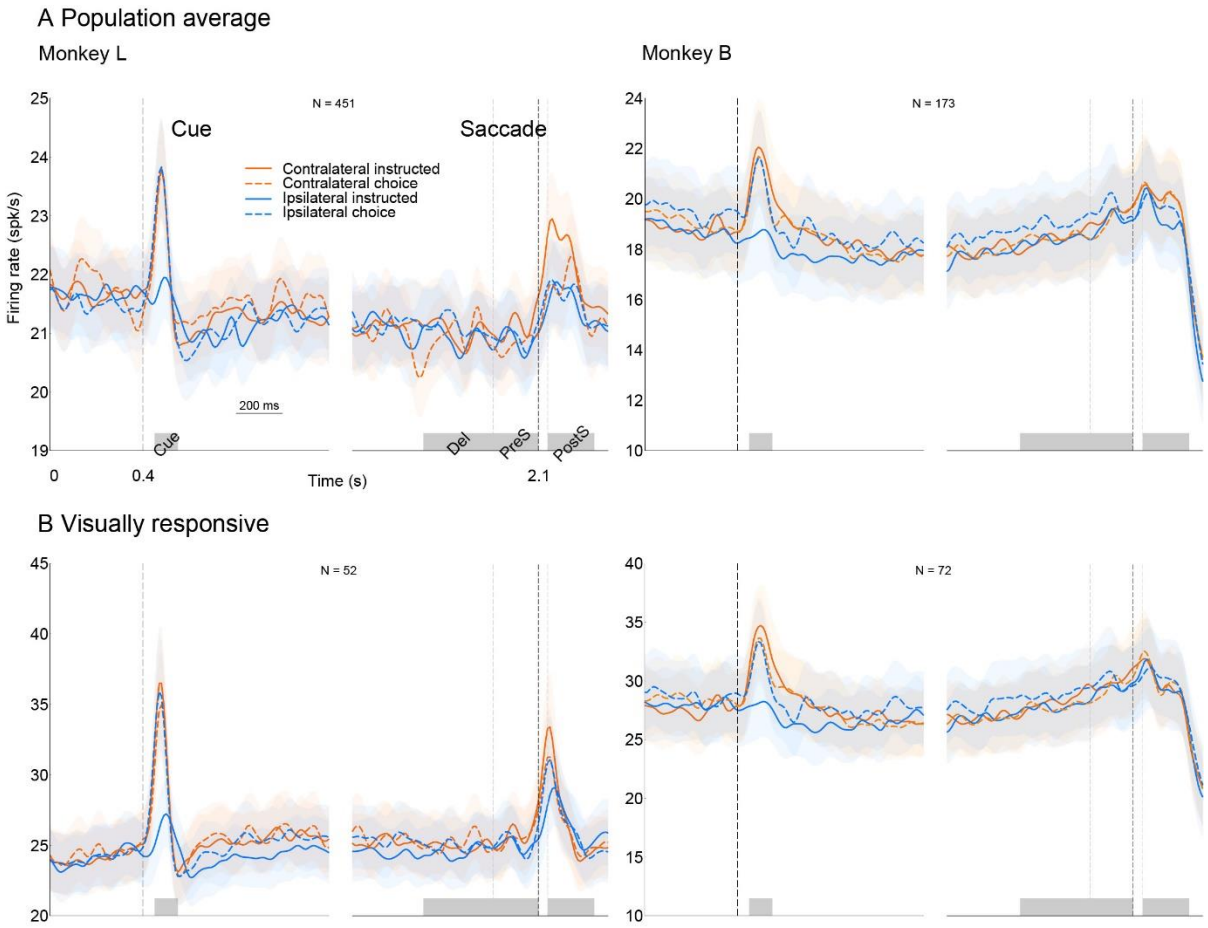

Figure 3.3.6. Spiking activity in the dorsal pulvinar in both monkeys. A Spike density average of all recorded neurons. **B** Spike density average for visually responsive neurons. The spike density average (mean ± SEM) is shown independently for instructed/free-choice (solid/dotted) and contralesional/ipsilesional space (orange/blue)

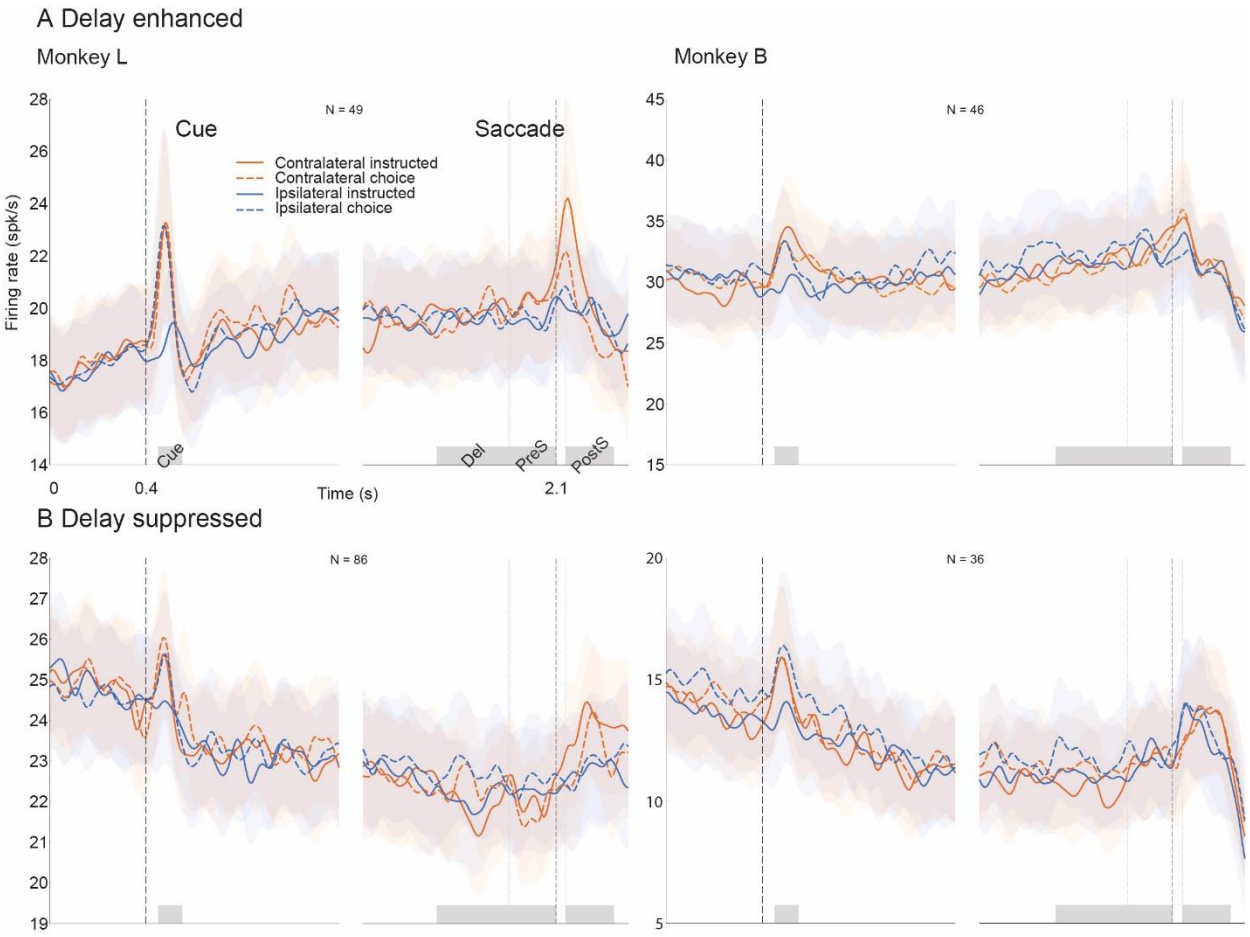

Figure 3.3.7. Spiking activity in the dorsal pulvinar in both monkeys. A Spike density average for delay-enhanced neurons. **B** Spike density average for delay suppressed neurons. The spike density average (mean ± SEM) is shown independently for instructed/free-choice (solid/dotted) and contralesional/ipsilesional space (orange/blue)

To summarize, we found both similarities and differences between the activity of the dorsal pulvinar and area LIP. First, we found in both regions transient visual response to contralateral stimuli representing the goal of an upcoming saccade. However, we found a different profile during movement selection and preparation. While we found enhanced activity in area LIP during movement preparation with a tuning bias towards the contralateral hemifield, the activity in the dorsal pulvinar was either enhanced or suppressed without apparent tuning towards the contralateral hemifield. Such contrast between the two regions suggests a different role during movement selection and preparation. Finally, we found saccadic-related activity, mostly when the direction of the saccade was toward the contralateral hemifield. The post-saccadic activity in the dorsal pulvinar, like in area LIP, might be related to the saccadic inhibition and/or saccadic error processing (Zhou et al., 2016b).

3.4.3 Local field potentials

We recorded local field potentials within the lateral bank of IPS (putative LIP, spanning the depth of the sulcus) and in the dorsal part of the pulvinar in the same hemisphere (monkey L LIP: 248, dPul: 232; monkey B, LIP: 279, dPul: 288) while monkey performed delayed saccade task (monkey L) or dissociated delayed saccade task (monkey B).

3.4.3.1 LFP response profile in area LIP

Consistently with the spiking activity and with previous knowledge of area LIP, we observed transient visual response to contralateral target presentation (Figure 3.3.8). The contralateral transient visual response was seen in gamma frequencies in both monkeys. It was also seen in lower frequencies but with slight differences between the two monkeys. In monkey L, we saw transient increase in power from theta to low-beta (4-18 Hz) whereas, in monkey B, the power increase was limited to delta and theta frequencies (2-4 Hz). Interestingly, this increase was significantly stronger in free-choice trials before contralateral choices in both monkeys in respective frequencies.

During the delay period, there was a decreased power in beta (12-32 Hz) typically associated with movement preparation. Surprisingly, in monkey B, the decreased power was weaker before contralateral choices. In addition, we also observed increased power in theta, which was tuned to the contralateral hemifield in monkey L but not in monkey B. In monkey L, the power in the gamma range was also higher before instructed contralateral saccades.

In addition, there was saccade-related activity in both monkeys at different frequencies. First, we observed an increased power in the gamma range around the saccade onset, more strongly for contralateral saccades. At the same time, there was also a power increase in the theta range without significant tuning. Finally, there was a post-saccadic decreased power in alpha and beta independently of the target position.

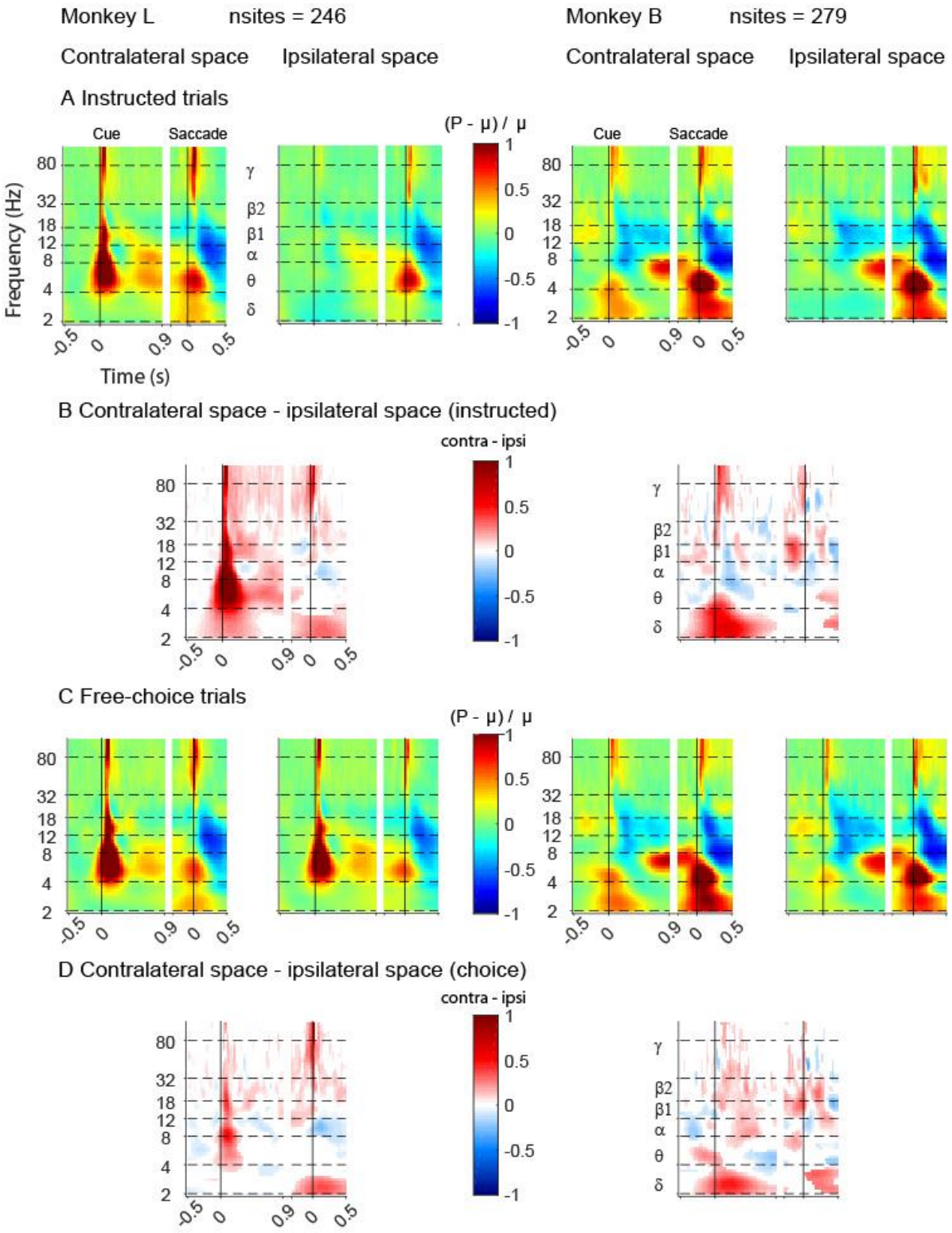

Figure 3.3.8 LFP time-frequency spectrogram in area LIP. A Time-frequency spectrogram in instructed trials. **B** Difference between contralesional and ipsilesional instructed targets (only significant bins are shown, paired t-test with Bonferroni correction). **C** Time-frequency spectrogram in free-choice trials. **D** Difference between contralesional and ipsilesional choices (only significant bins are shown, paired t-test with Bonferroni correction).

3.4.3.2 LFP response profile in the dorsal pulvinar

Unlike area LIP, there was no or weak increase in power in the gamma range in response to visual stimulation (Figure 3.3.9). However, we did observe strong increased power in low frequencies (~8 Hz in monkey L and ~6 Hz in monkey B) after target presentation in the contralateral hemifield. Surprisingly, this increase was stronger in monkey L before contralateral choices but weaker in monkey B.

During the delay, the LFP power was modulated differently in the two monkeys. In monkey L, we observed an increased power in the beta band which was stronger before upcoming contralateral saccades, in instructed and free-choice trials. Conversely, in monkey B, the power was decreased in the same frequency range and it was stronger decreased before instructed contralateral saccades whereas it was weaker before contralateral choices. Despite inconsistent observations between the two monkeys, the presence of choice signals within the dorsal pulvinar suggests a role in target selection and saccade preparation, which is in contrast with what we observed in the spiking activity.

We also observed saccade-related activity in both monkeys. First, there was a transient increase in gamma power (80-120 Hz) shortly before saccades onset. Interestingly, the power was also increased in low gamma (32-80 Hz) shortly after saccades onset, independently of their direction since we did not observe differences in the power modulation between saccades towards contralateral and ipsilateral hemifield. Secondly, the power in theta increased around the saccade with a strong bias towards the contralateral hemifield, both in instructed and free-choice trials. Finally, we observed two distinct post-saccadic power modulations. In alpha/low-beta (8-18 Hz), the power decreased independently of the saccade direction. At the same time, we observed an increased activity in high-beta (18-32 Hz) after contralateral saccades, in both instructed and free-choice trials.

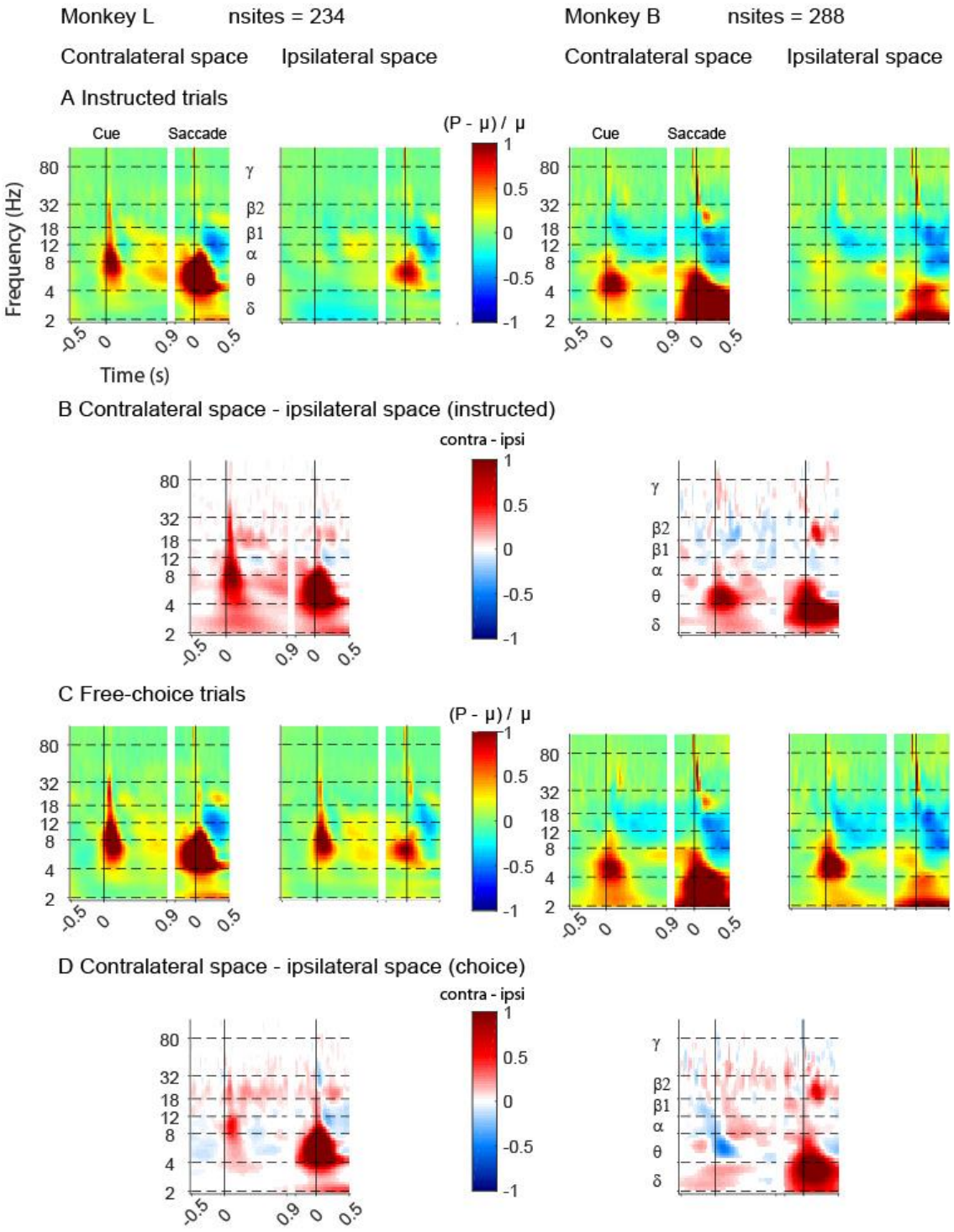

Figure 3.3.9 LFP time-frequency spectrogram in the dorsal pulvinar. A Time-frequency spectrogram in instructed trials. **B** Difference between contralesional and ipsilesional instructed targets (only significant bins are shown, paired t-test with Bonferroni correction). **C** Time-frequency spectrogram in free-choice trials. **D** Difference between contralesional and ipsilesional choices (only significant bins are shown, paired t-test with Bonferroni correction).

In summary, we found in both regions, consistently with spiking activity, shared features and dissimilarities in LFP modulation. First, we observed visual responses to stimuli presentation with a strong bias towards the contralateral hemifield in low frequencies but only in area LIP in higher frequencies. During movement selection and preparation, the activity was mostly modulated in the beta range and despite some differences between monkeys, we found choice signals in both regions. Around the saccade, we found increased power in high frequencies. However, in the dorsal pulvinar, there was two distinct transient increase, shortly before and after saccade onset, which were not tuned to a particular saccade direction. We also found around saccades an increased power in lower frequencies with a strong bias towards the contralateral hemifield in the dorsal pulvinar but not in LIP. Finally, there was a post-saccadic decrease in alpha/low-beta power, independently of the saccade direction in both regions.

3.4.4 Spike-field synchronization within and between regions

3.4.4.1 Spike-field synchronization within area LIP

After the cue onset, spike-field synchronization in theta (4-8Hz) and alpha (8-12 Hz) increased when the target was located in the contralateral hemifield (Figure 3.3.10), reflecting the evoked LFP and spiking cue responses observed in the same condition. Surprisingly, there was no synchronization in the gamma range despite the transient power increase observed on LFP signals in this frequency range.

The synchronization during the delay period in beta (12-30 Hz) was stronger before ipsilateral than contralateral saccades during instructed trials. This is in agreement with lower beta LFP power and spike-LFP coherence during the planning of movements into the receptive field (typically contralateral), as compared to the fixation baseline and movements out of the receptive field, observed in LIP. (Dean et al., 2012; Hawellek et al., 2016). Surprisingly, the beta synchronization was stronger before contralateral choices in monkey L. We also observed during the delay an increased coherence in theta.

Around the saccade onset, there was an increased synchronization in theta (4-8Hz) and alpha (8-12 Hz). Interestingly, the post-saccadic increase in spike-field synchronization was stronger in monkey L for contralateral saccades, which was in the contrast with the LFP power but was consistent with the spiking activity.

Throughout the trial, we did not observe spike-field synchronization in the gamma range (30-100 Hz), even after target presentation where we observed a transient increase in gamma power and spiking activity.

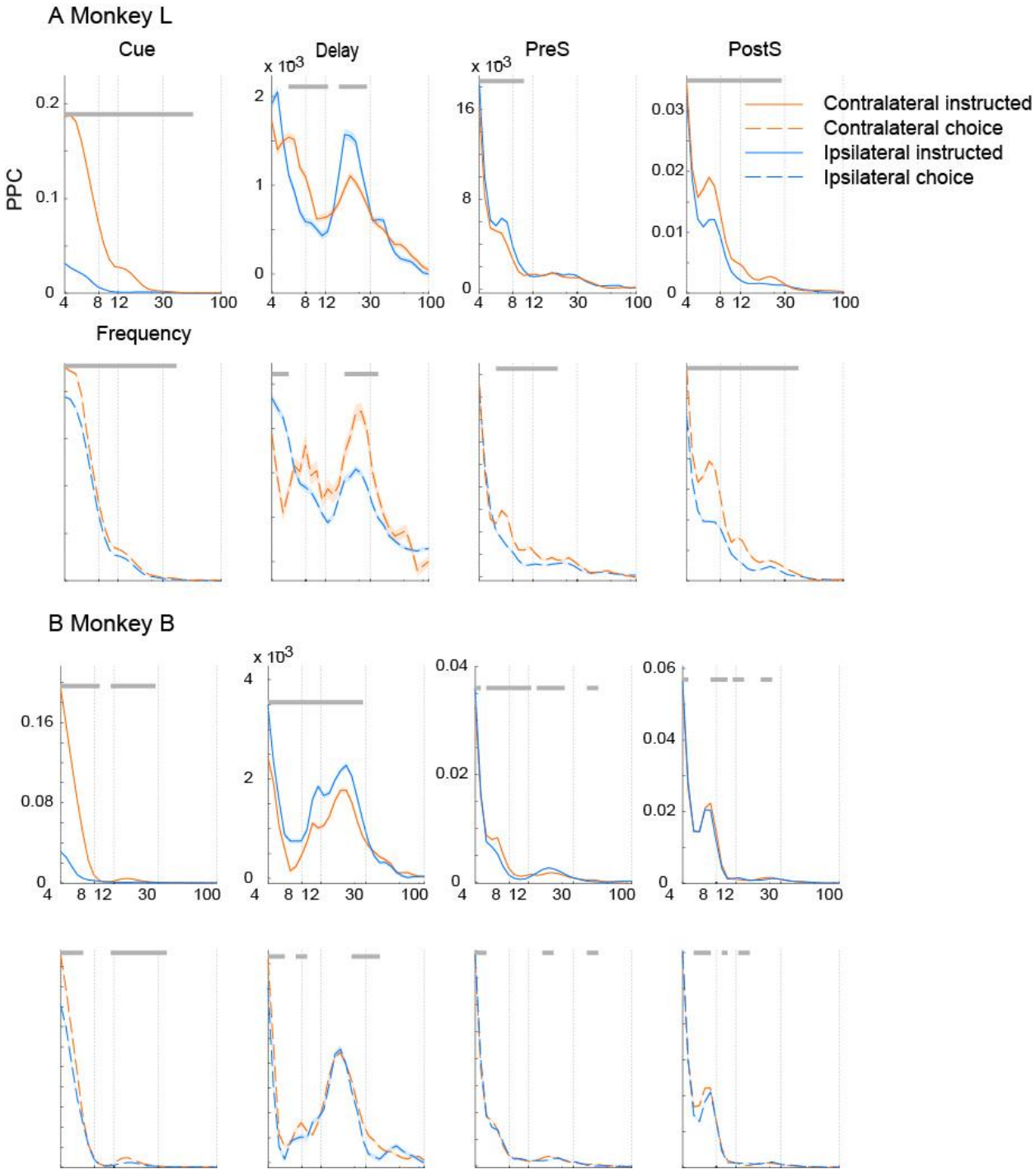

Figure 3.3.10 Spike-field pairwise phase consistency within area LIP. A PPC value across frequencies averaged in different epochs in monkey L. **B** PPC value across frequencies averaged in different epochs in monkey B. Mean ± SEM are shown independently for instructed/free-choice (solid/dotted) and contralesional/ipsilesional space (orange/blue). Grey shaded area shows significant difference (cluster-based adjusted p-value < 0.05, t-test)

3.4.4.2 Spike-field synchronization within dorsal pulvinar

Like area LIP, there was an increased, spike-field synchronization in theta (4-8Hz) and alpha (8-12 Hz) as a transient visual response when the target was located in the contralateral hemifield (Figure 3.3.11), reflecting the evoked LFP and spiking cue responses observed in the same condition.

Interestingly, we observed different synchronization within the two regions during the delay period. In the dorsal pulvinar, there was no increase in the beta (12-30 Hz) range. We observed coherent activity in theta, but unlike area LIP, the synchronization was stronger before upcoming saccades towards the contralateral hemifield.

Around saccades, spike-field synchronization increased in theta (4-8Hz) and alpha (8-12 Hz). Like during delay period activity, we observed stronger spike-field coherence during contralateral saccades, reflecting the space tuning observed in LFP signals.

Both regions showed increased spike-field synchronization in low frequencies upon presentation of contralateral visual stimuli. During movement selection preparation, we observed synchronization in theta in both regions, which was stronger for contralateral targets in the dorsal pulvinar but not in LIP. In addition, we only observed beta synchronization in area LIP which was lower for contralateral targets. Finally, the saccade-related spike-field coherence was comparable between the two regions with an increase in theta and alpha, particularly around contralateral saccades.

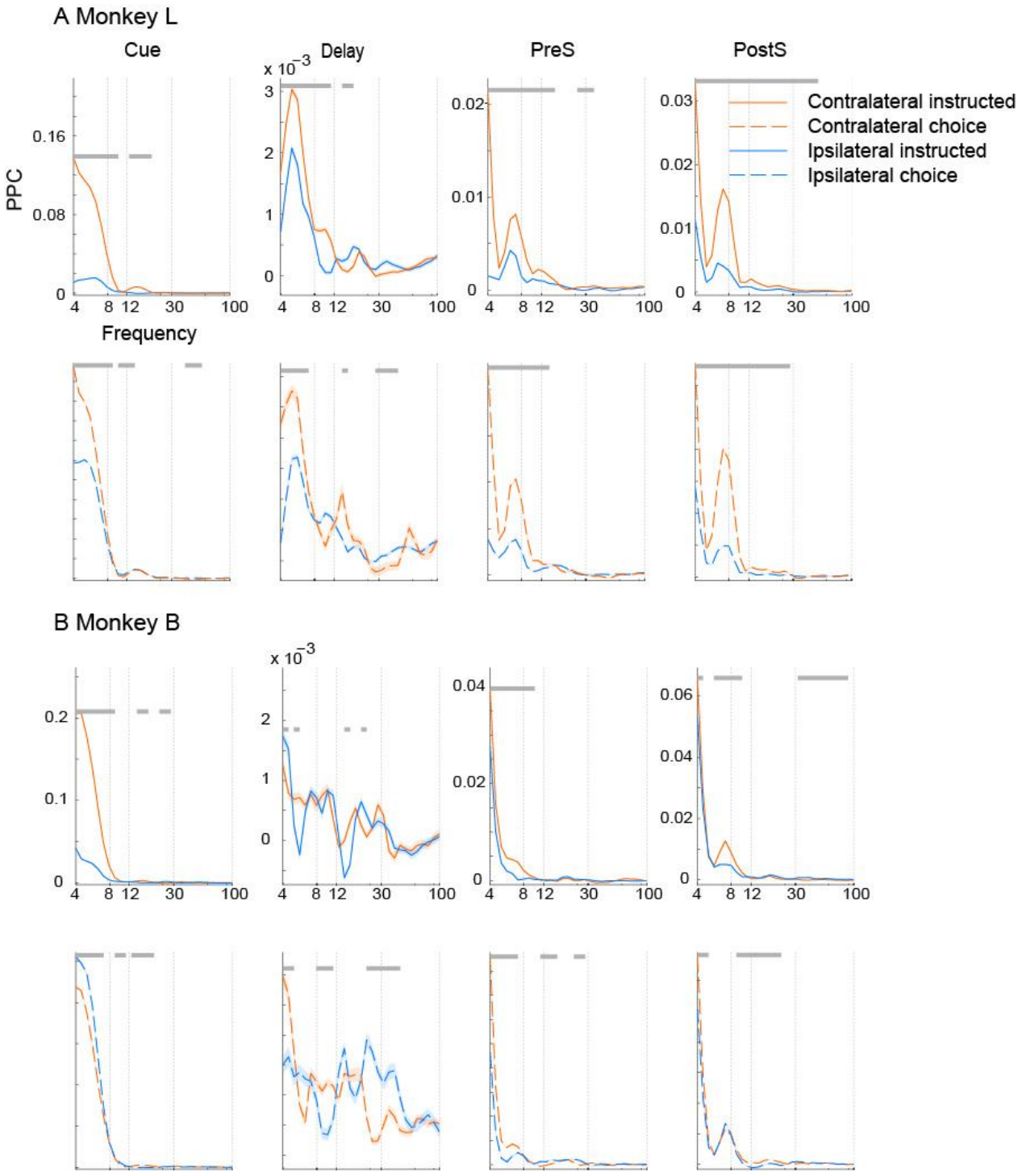

Figure 3.3.11 Spike-field pairwise phase consistency within dorsal pulvinar. A PPC value across frequencies averaged in different epochs in monkey L. **B** PPC value across frequencies averaged in different epochs in monkey B. Mean ± SEM are shown independently for instructed/free-choice (solid/dotted) and contralesional/ipsilesional space (orange/blue). Grey shaded area shows significant difference (cluster-based adjusted p-value < 0.05, t-test)

3.4.4.3 Spike-field synchronization from LIP to the dorsal pulvinar

First of all, the transient visual response to contralateral stimuli in spiking activity in LIP and low frequencies LFP in the dorsal pulvinar resulted in an increased spike-LFP synchronization (Figure 3.3.12) between the two regions (LIP → dPul) in theta (4-8Hz) and alpha (8-12 Hz).

During the delay period, we observed spike-field coherence in theta (4-8Hz) in both monkeys. Like within area LIP, there was spike field coherence in beta (12-30 Hz). Consistently, the synchronization was weaker before ipsilateral saccades. In monkey L, there was also synchronization in alpha, which was stronger before contralateral saccades and probably reflects increased alpha power observed on the time-frequency spectrogram suggesting directional communication from LIP to the dorsal pulvinar during movement planning. This interaction relies on alpha (8-12Hz) and beta (12-30 Hz) oscillations. Together with the LFP profile in the dorsal pulvinar, results suggest that alpha and beta oscillations in the dorsal pulvinar during movement preparation are driven by the spiking activity of area LIP. Interactions between LIP and the dorsal pulvinar during saccades planning may play an inhibitory role on the visual processing of potential stimuli.

We observed around the saccade a comparable spike-field coherence profile as within regions. There was strong spike-field synchronization in theta (4-8 Hz) and alpha (8-12 Hz) with a bias towards the contralateral hemifield. The common spike-field synchronization pattern within and between regions suggests strong functional connectivity around contralateral saccades.

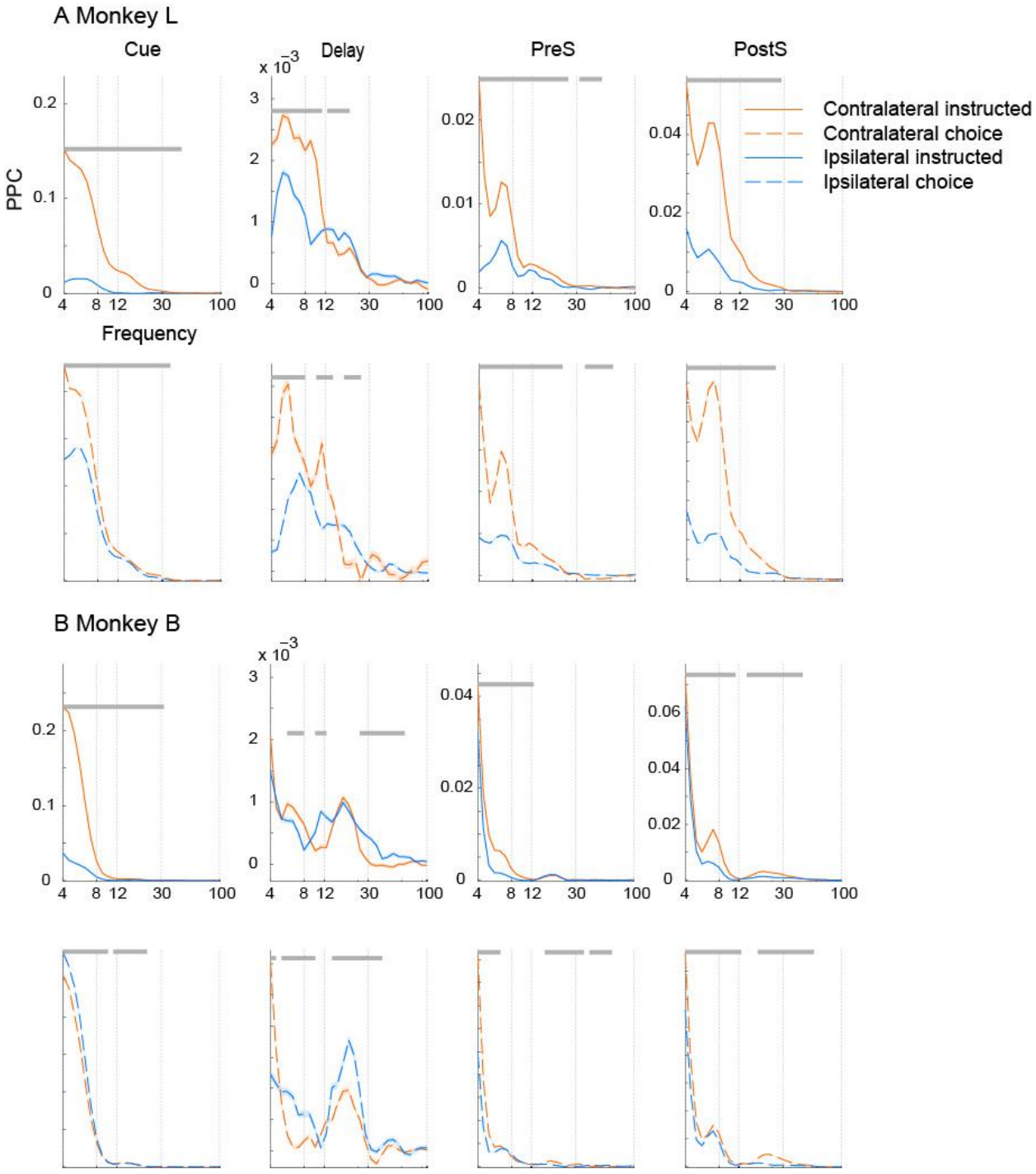

Figure 3.3.12 Spike-field pairwise phase consistency from LIP to the dorsal pulvinar (LIP → dPul). A PPC value across frequencies averaged in different epochs in monkey L. **B** PPC value across frequencies averaged in different epochs in monkey B. Mean ± SEM are shown independently for instructed/free-choice (solid/dotted) and contralesional/ipsilesional space (orange/blue). Grey shaded area shows significant difference (cluster-based adjusted p-value < 0.05, t-test)

3.4.4.4 Spike-field synchronization from the dorsal pulvinar to area LIP

Upon target presentation in the contralateral hemifield, we observed an increased spike-field coherence in theta (4-8 Hz) and alpha (8-12 Hz; Figure 3.3.13). Like within regions and between LIP and the dorsal pulvinar (LIP → dPul), the synchronization reflects the transient increase in power and spiking activity.

During the delay period, we only observed spike-field synchronization in theta (4-8 Hz). Interestingly, there was low coherence in alpha (8-12 Hz) and beta (12-30 Hz). This result is in agreement with the idea that during movement preparation, interactions between the dorsal pulvinar and area LIP are mostly driven by the spiking activity in area LIP and may play the role of functional inhibition.

Finally, around saccades, we observed spike-field synchronization in theta (4-8 Hz) and alpha (8-12 Hz). However, unlike the coherence within regions and from LIP to the dorsal pulvinar, it was not stronger for contralateral saccades. The lack of contralateral bias in spike field synchronization could reflect the visual processing of a target in the fovea or in a more general scope, the processing of visual information after the scene change elicited by the saccade.

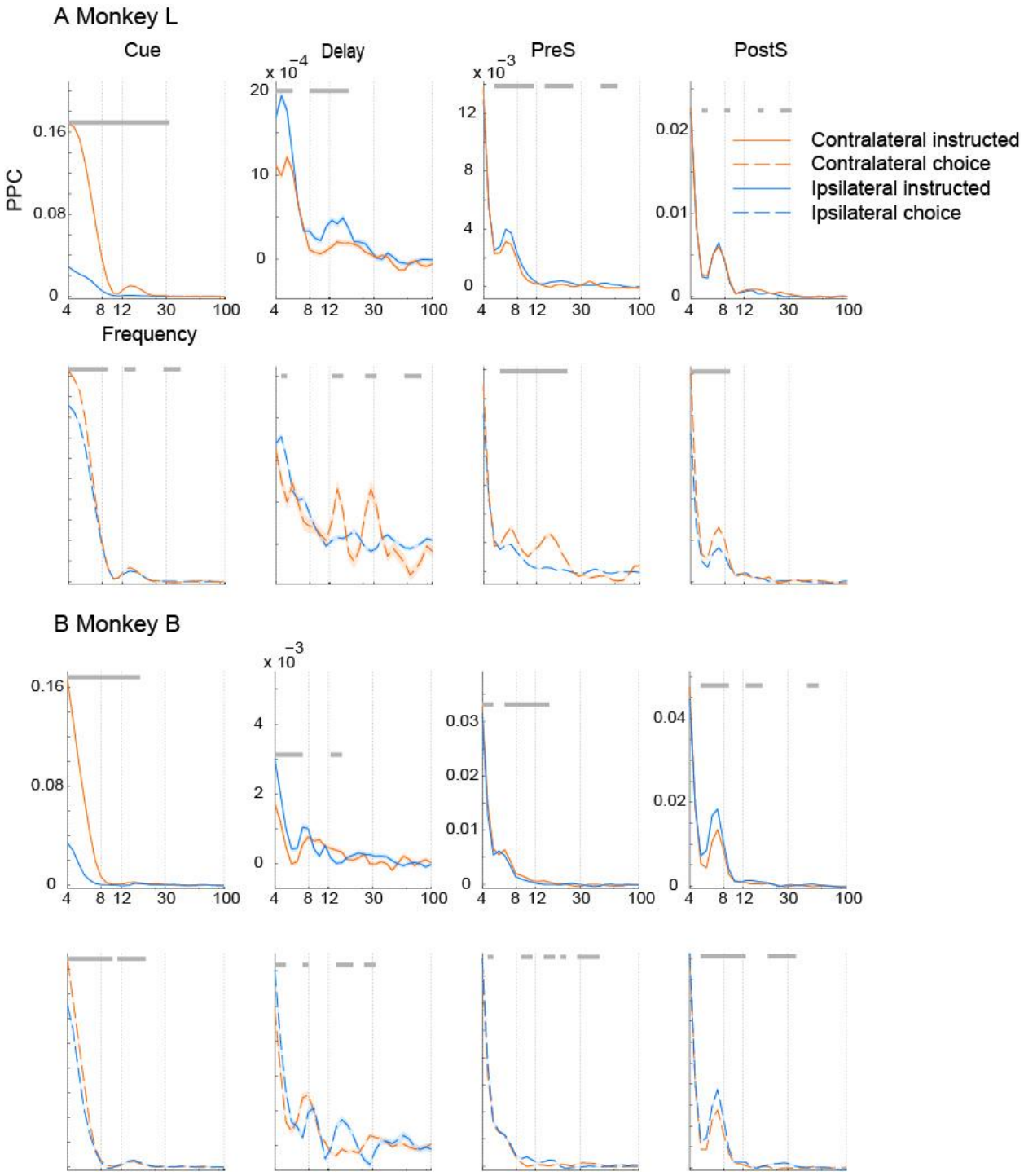

Figure 3.3.13 Spike-field pairwise phase consistency from the dorsal pulvinar to LIP (dPul → LIP). A PPC value across frequencies averaged in different epochs in monkey L. **B** PPC value across frequencies averaged in different epochs in monkey B. Mean ± SEM are shown independently for instructed/free-choice (solid/dotted) and contralesional/ipsilesional space (orange/blue). Grey shaded area shows significant difference (cluster-based adjusted p-value < 0.05, t-test)

To summarize, we found after contralateral stimuli presentation strong spike-field synchronization in low frequencies (theta and alpha) within and between regions in both directions (LIP → dPul and dPul → LIP). The increase in coherence reflects the transient response observed in spiking activity and LFP signals in both regions and a strong bidirectional functional connectivity, relying of low frequencies, upon the processing of visual information. We did not observe synchronization in the gamma range, which was expected based on the distance between the two regions but was surprising within LIP where we observed a transient increase in power in the gamma range on LFP signals.

During the delay period, we only observed spike-field coherence in the beta range within area LIP and between LIP and the dorsal pulvinar (LIP → dPul). In area LIP, the decreased synchronization before contralateral saccades is in accordance with lower beta LFP power and spike-LFP coherence during the planning of movements towards preferred directions which is mostly contralateral (Dean et al., 2012; Hawellek et al., 2016). Between the two regions, it implies that LIP drives interactions during movement preparation and together with the common suppression of dorsal pulvinar spiking activity, suggest a functional inhibitory role, relying on beta oscillations.

Finally, spike-field coherence was increased in low frequencies before the saccade initiation as well as after the saccade end. Like after stimuli presentation, it reflects transient responses on LFP and spiking activity in both regions. However, we found a stronger coherence around contralateral saccades within the dorsal pulvinar and from LIP to the dorsal pulvinar (LIP → dPul) but not within LIP and from the dorsal pulvinar to LIP (dPul → LIP). The saccade-related activity has been related to several functions such as saccade inhibition, error processing and saccade update (Bisley and Goldberg, 2010; Mirpour and Bisley, 2016; Zhou et al., 2016b). Interactions between the two regions are in agreement with the idea that the dorsal pulvinar plays a role in mediating processes linking visual processing and eye movements (Grieve et al., 2000; Berman, 2005; Sherman, 2007; Saalmann, 2014).

3.4.5 Field-Field synchronization within and between regions

3.4.5.1 Field-Field synchronization within area LIP

We analyzed the pairwise phase consistency between 3660 LFP site pairs in monkey L (8 sessions) and 4189 in monkey B (9 sessions) within area LIP (Figure 3.3.14).

During central fixation, we observed in both monkey field-field synchronizations in alpha (8-12Hz) in monkey B and low-beta in monkey L (12-18Hz). After the appearance of a target in the contralateral (to recording sites) hemifield, there was an increased coherence in alpha in monkey

L and delta (2-4Hz) in monkey B. The different frequencies between the two monkeys correspond to the evoked response described on respective time-frequency spectrograms. During the delay period, we observed a stronger synchronization in beta and weaker in theta (4-8Hz) before contralateral saccades in both monkeys. In addition, in monkey B, coherence in alpha increased until the saccade onset independently of the target position. Around ipsilateral saccades, we observed a transient increase in theta. Interestingly, there was no space specificity in this frequency range on time-frequency spectrograms. Finally, in monkey L, field-field synchronization increased in delta around contralateral saccades.

Overall, the pairwise phase consistency between LFP sites within area LIP revealed interactions from delta to beta frequencies. Despite increased oscillations in gamma during visual processing and saccades in area LIP, we did not observe field-field coherence in this frequency range. Nevertheless, interactions in lower frequencies were modulated during visual stimuli processing, target selection and movement execution. In addition, the synchronization was differentially modulated both in instructed and free-choice trials between contralateral and ipsilateral saccades.

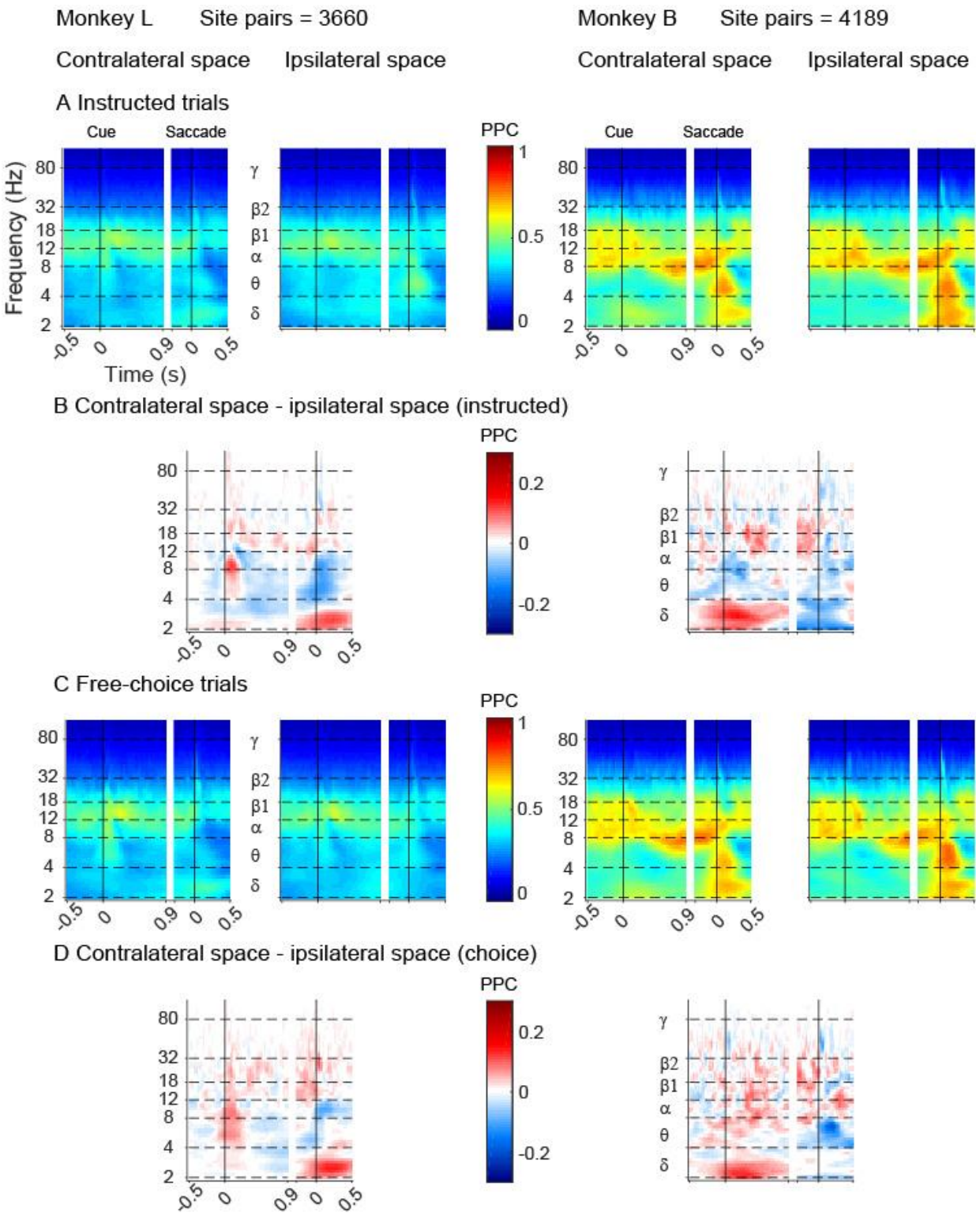

Figure 3.3.14 Field-field pairwise phase consistency within area LIP. A LFP-LFP PPC in instructed trials. **B** Difference between contralesional and ipsilesional instructed targets (only significant bins are shown, paired t-test with Bonferroni correction). **C** LFP-LFP PPC in free-choice trials. **D** Difference between contralesional and ipsilesional choices (only significant bins are shown, paired t-test with Bonferroni correction).

3.4.5.2 Field-field synchronization within dorsal pulvinar

We analyzed the pairwise phase consistency between 3306 LFP site pairs in monkey L (8 sessions) and 4464 in monkey B (9 sessions) within area LIP (Figure 3.3.15).

Throughout the entire trial (except after saccade onset), there was strong synchronization in the beta range (12-32Hz). Interestingly, there were no or weak differences between task epochs and targets position in these frequencies. Therefore, the local synchronization in beta might be an intrinsic property of the pulvinar nucleus. After contralateral targets presentation, we observed an increased field-field coherence in theta (4-8Hz) in both monkeys. In monkey L, this transient increase in coherence was also spanning alpha and beta frequencies. Surprisingly, in free-choice trials, the synchronization was stronger in monkey L before contralateral choices whereas it was weaker in monkey B. Nonetheless, the field-field coherence in both monkeys was differentially modulated before contralateral and ipsilateral choices. Around saccades, there was an increased synchronization in theta in both monkeys. In both instructed and free-choices trials, the field-field coherence was stronger around contralateral saccades.

The field-field synchronization profile within the dorsal pulvinar was different from what we observed in area LIP. First, there were strong interactions in the beta range independently of the task demand. We did not find synchronization changes during the delay period in any of the analyzed frequencies. The lack of modulation during delay is consistent with the idea of functional inhibition within the dorsal pulvinar during movement preparation. On the contrary, we found modulation in theta during stimuli presentation and around saccades, more strongly when targets were located in the contralateral hemifield and free-choice trials before contralateral saccades. Together, it highlights the role of the dorsal pulvinar during visual processing and saccades execution.

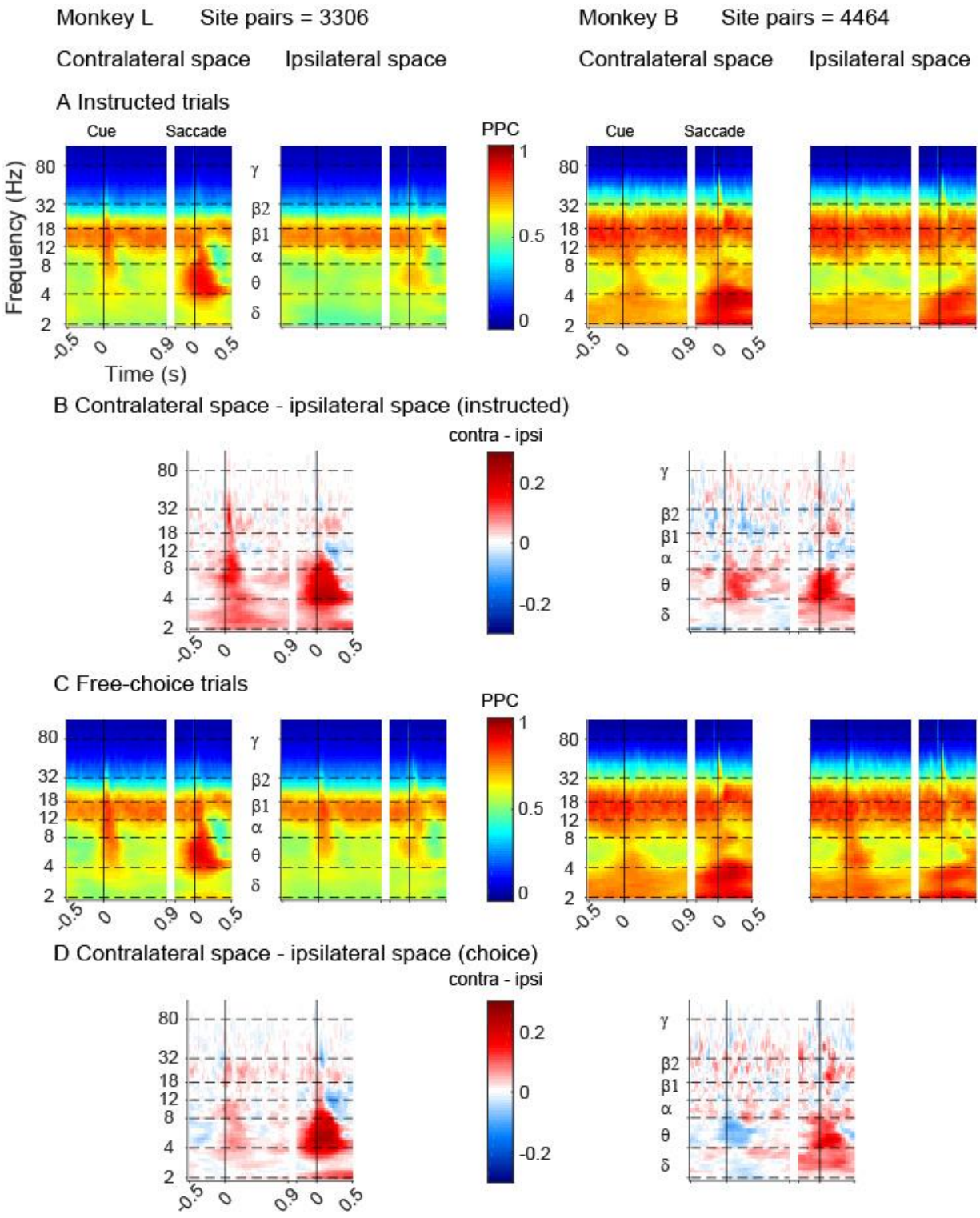

Figure 3.3.15 Field-field pairwise phase consistency within dPul. A LFP-LFP PPC in instructed trials. **B** Difference between contralesional and ipsilesional instructed targets (only significant bins are shown, paired t-test with Bonferroni correction). **C** LFP-LFP PPC in free-choice trials. **D** Difference between contralesional and ipsilesional choices (only significant bins are shown, paired t-test with Bonferroni correction).

3.4.5.3 Field-Field synchronization between the dorsal pulvinar and area LIP

We analyzed the pairwise phase consistency between dPul and LIP LFP site pairs (7194 in monkey L (8 sessions) and 8928 in monkey B (9 sessions)) (Figure 3.3.16).

During central fixation, there was field-field synchronization in low-beta in monkey L and alpha in monkey B. After target presentation in the contralateral hemifield, there was a transient synchronization shift from low-beta to alpha in monkey L and from alpha to delta in monkey B. Interestingly, in free-choice trials, we found stronger synchronization when the upcoming choice was towards the contralateral hemifield. After this transient shift during visual processing, we observed synchronized activity back to low-beta in monkey L and alpha in monkey B during delay, like during central fixation. Both during central fixation and delay, monkeys had to maintain central fixation and therefore inhibit eye movement initiation. It is therefore likely that interactions in these frequencies between the two regions play a functional inhibitory role. This result is consistent with our interpretation of the spike-field analysis. Together, results suggest that LIP drives inter-region interactions during periods of sensory processing (fixation and idling) functional inhibition, relying on alpha and low-beta oscillations. On the contrary, upon presentation of visual stimuli in the contralateral hemifield, we observed bi-directional interactions between the two regions relying on theta/alpha oscillations in monkey L and delta/theta in monkey B. Around saccades, we also observed a transient decrease in alpha/low-beta synchronization. In addition, there was an increased coherence in theta, more strongly before contralateral saccades, both in instructed and free-choice trials. Surprisingly, there was also a sharp increase in low-gamma synchronization (32-80Hz) in monkey B.

Together, the field-field synchronization profile between LIP and the dorsal pulvinar revealed interactions in alpha/low-beta during periods when the task demands inhibition of movement initiation, even during delay when movement planning occurs in parallel. These interactions were disrupted during visual processing and saccades-related processes in favor of synchronization in lower frequencies (delta, theta and/or alpha), more strongly when visual stimuli in contralateral hemifield were the target of an upcoming saccade.

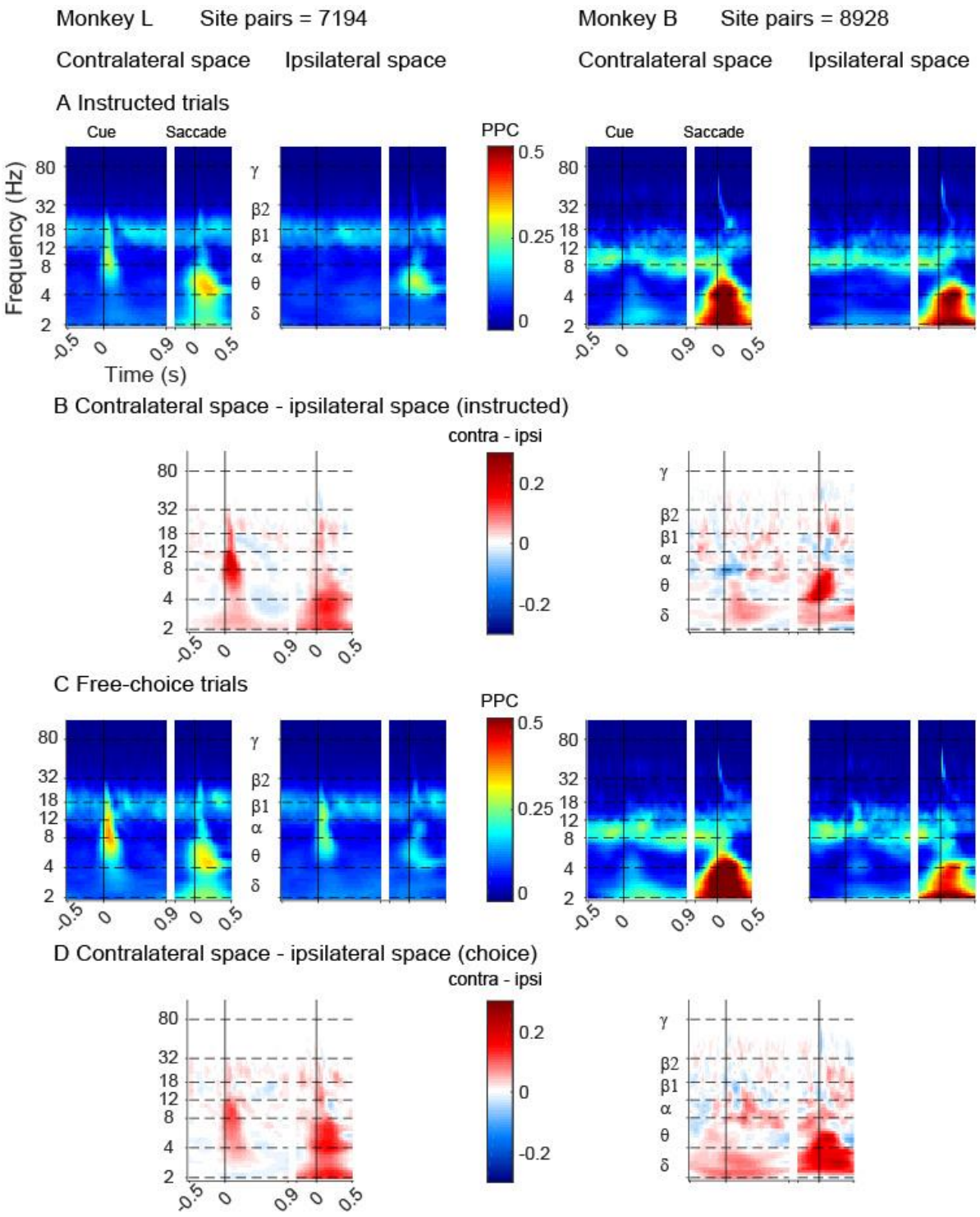

Figure 3.3.16 Field-field pairwise phase consistency between dPul and LIP. A LFP-LFP PPC in instructed trials. **B** Difference between contralesional and ipsilesional instructed targets (only significant bins are shown, paired t-test with Bonferroni correction). **C** LFP-LFP PPC in free-choice trials. **D** Difference between contralesional and ipsilesional choices (only significant bins are shown, paired t-test with Bonferroni correction).

To summarize, we found mostly found field-field synchronization within and between regions in low frequencies, from delta to low-beta. Within regions, the field-field coherence was modulated depending on the task demand, reflecting flexible neuronal interactions during fixation, visual processing, movement preparation and execution. In addition, we found stronger modulation when targets were located in the contralateral hemifield or before contralateral choices, both during visual processing and around saccades highlighting the role of dPul and LIP in target selection. However, we did not find modulation during the delay period within the dorsal pulvinar, consistent with the idea of functional inhibition within the dorsal pulvinar during fixation and movement preparation. Field-field synchronization profile between LIP and the dorsal pulvinar revealed different interactions during period of fixation and visual processing and saccades-related processes. More precisely, there was a switch in frequency synchronization, from low-beta to alpha/theta and from alpha to delta in monkey L and B respectively. This synchronization frequency switch reflects rapid functional connectivity changes between the dorsal pulvinar and area LIP upon different cognitive processes. The functional connectivity was also stronger for instructed contralateral targets or contralateral choices, highlighting the role of thalamocortical interactions during oculomotor movement selection and execution.

3.5 Discussion

3.5.1 Similarities and differences between dorsal pulvinar and LIP neuronal activity

In this study, we simultaneously recorded from dorsal pulvinar and LIP in the same hemisphere while monkeys performed instructed and choice delayed saccades. As previously reported, the neuronal activity in area LIP and in the dorsal pulvinar transiently increased due to a visual response to a target presentation, with a strong contralateral preference in spiking activity, LFP signals and local synchronization (Barash et al., 1991; Schneider et al., 2021). When two targets were presented in opposite, we found contralateral tuning in area LIP but not in the pulvinar. Therefore, only visual responses in area LIP could be predictive of the upcoming choice. This spatial tuning in LIP upon targets presentation might be due to previous experiences and/or the locus of attention at target onset and drives the eventual decision. During the delay, we found similar contralateral tuning during free choices in LIP but not in the pulvinar. In addition, a subpopulation of neurons in the dorsal pulvinar showed a suppressed activity during movement preparation, as reported in a recent study using memory saccades (Schneider et al., 2021), Despite a the activity modulation, the suppressed activity together with the lack of spatial tuning question the functional role of the pulvinar during the delay period. Finally, we found similar saccades-related activity with contralateral preference in both regions. Saccades-related activity in the pulvinar was consistent with what has been previously reported (Benevento and Port, 1995) is likely related to error processing (Zhou et al., 2016b) and visual stabilization related to eye movements (Robinson et al., 1986).

3.5.2 Functional connectivity within and between regions

By looking at the field-field synchronization, a common pattern appeared within LIP, within the dorsal pulvinar and between the two regions throughout the trial. Namely, there was an ongoing synchronization during central fixation and the delay period that was disrupted in favor of synchronization in lower frequencies upon target presentation and around saccades. This phenomenon revealed the flexibility of pulvino-parietal functional connectivity, according to the cognitive demand. This flexibility of pulvino-parietal interactions has been demonstrated in the context of attentional selection (Saalmann et al., 2012; Fiebelkorn et al., 2019). Therefore, this result brings additional evidences for a role of the pulvinar in modulating information transmission across cortical neuronal populations. In the same line, spike-field connectivity suggests bi-directional interactions during visual processing and saccades and directional interactions from

LIP to dPul in moments of fixation and movement planning. Interestingly, LFP-LFP synchronization was stronger between the two regions after bilateral target presentation before upcoming contralateral choices. Therefore, a stronger functional connectivity between the dorsal pulvinar and area LIP when two targets are presented in opposite hemifield led to a higher probability to select the contralateral target, highlighting the role of the pulvino-parietal circuitry in decision-making despite the lack of choice signals in dorsal pulvinar neuronal activity. Around saccades, there was overall a strong synchronization in lower frequencies. Interestingly, the field-field synchronization, both within and between regions was stronger around instructed contralateral saccades and contralateral choices, emphasizing the role of pulvino-parietal circuitry in saccades related processes as discussed previously.

3.5.3 Conclusions and future directions

Together, results shed light on shared neuronal responses as well as dissimilarities in the pulvinar and the parietal cortex during the processing of visual information, movement preparation and saccades. Both regions showed contralateral tuning to instructed targets but we only found choice signals during bilateral targets presentation in the parietal cortex. During movement preparation, the activity was strikingly different between the two regions, with a suppressed activity and a lack of spatial tuning in the pulvinar. Around saccades, we found similar neuronal responses in the two regions, with a stronger response to contralateral saccades. In addition, the functional connectivity profile within and between the two regions, with ongoing synchronization and transient shift in frequencies of interactions upon target presentation and saccades revealed strong flexibility of the pulvino-parietal network according to cognitive demands. It also suggests strong bi-directional interactions during visual processing and saccades-related processes while during movement preparation, data suggest a directional functional inhibition from the parietal cortex to the pulvinar. The stronger connectivity between the two regions during bilateral target presentation when the upcoming choice was towards the contralateral hemifield highlighted their role in decision-making. Overall, this experiment gave more insight into reciprocal and directional interactions between the dorsal pulvinar and area LIP, and more generally between higher order nuclei and the cortex, during oculomotor decision-making, planning and execution. Simultaneous recordings also offer the possibility to further investigate pulvino-parietal circuitry by looking for example at the correlation in activity between the two regions at the trial by trial level. Finally, in order to get a better picture on the function of thalamo-cortical circuitry, it would be interesting to record simultaneously from the pulvinar, LIP and a frontal area like FEF, to explore the pulvinar

role in cortico-cortical communication (Grieve et al., 2000; Zhou et al., 2016a; Fiebelkorn et al., 2019).

4 The effect of unilateral dorsal pulvinar inactivation on bi-hemispheric LIP activity

4.1 Abstract

The dorsal pulvinar is reciprocally connected to the posterior parietal cortex and perturbation studies revealed its involvement in oculomotor decision-making. In order to understand how dorsal pulvinar leads to a choice bias towards the ipsilesional hemifield, we recorded simultaneously the neuronal activity in area LIP in both hemispheres, before and after unilateral dorsal pulvinar inactivation. In the inactivated hemisphere, we observed increased low-frequency oscillations, highlighting the role of the dorsal pulvinar in maintaining an alert cortical state. We also showed an altered local neuronal synchronization, bringing additional evidence for a modulation of coherent activity. Finally, there was a deficit in the representation of visual stimuli located in the contralesional hemifield and subsequent movement preparation. In the intact hemisphere, the upregulation of neuronal activity highlighted push-pull interactions between the two hemispheres during target selection. In addition, the ipsilesional representation of visual stimuli was reinforced. Finally, we showed that interactions between the two hemispheres were reduced after inactivation throughout the trial and that during the processing of visual stimuli, it was altered more strongly when the target was located in the contralesional hemifield. Altogether, this study shed light on the role of the dorsal pulvinar in spatial decision-making through its modulation of neuronal activity in area LIP and the regulation of information transmission between the two hemispheres, bringing new insight into inter-hemispheric communication.

4.2 Introduction

The dorsal pulvinar involvement in visually-guided movements has been revealed by evaluating behavioral deficits after perturbation in animal models and human patient studies. First, inactivation of the dorsal pulvinar led to increased reaction time in an attentional task when stimuli were located in the contralesional hemifield (Petersen et al., 1987). Later, it was shown that inactivation of the dorsal pulvinar leads to a constellation of deficits when performing visually-guided reaches, including target selection bias, optic ataxia, and limb usage in a retrieving task (Wilke et al., 2010). Dorsal pulvinar inactivation also led to ipsilesional choice bias in an oculomotor memory-saccade task as well as an increased reaction time when the saccade was towards the contralesional space (Wilke et al., 2013). Dorsal pulvinar microstimulation also shortened or delayed the reaction in a time-dependent manner during the visually-guided saccade task. Similarly, microstimulation induced a selection bias in a free-choice task, towards ipsiversive hemifield when the stimulation started before target onset and contraversive hemifield when it started after target onset (Dominguez-Vargas et al., 2017). Finally, studies of human patients with pulvinar lesions described both oculomotor and reach deficits, including spatial neglect in the contralesional field, partially consistent with causal perturbation in monkeys (Rafal et al., 2004; Arend et al., 2008; Van der Stigchel et al., 2010; Wilke et al., 2018). However, the neuronal mechanisms leading to behavioral deficits remains poorly understood.

Different studies showed that saccade-related activity in the dorsal pulvinar is heterogeneous. Indeed, visually and memory-guided saccade tasks can elicit directional enhancement and/or inhibition at different timing of the task, e.g. after stimuli presentation, during the memory period, and in the pre- and/or post-saccadic window (Robinson et al., 1986; Benevento and Port, 1995). Previous work in our lab has also highlighted the heterogeneity of responses in the dorsal pulvinar (L.Schneider, 2019, Perceptual and motor intentional processing in the dorsal pulvinar). Nevertheless, at the population level, there was a clear contralateral preference for visual stimuli presentation. Surprisingly, the activity during the delay period was mostly suppressed and non-space-specific. In addition, it did not reflect the upcoming saccade when two saccade options were available, challenging the idea that dorsal pulvinar is involved in target selection. These results suggest that the mechanism leading to choice bias after inactivation may not be explained only by looking at dorsal pulvinar neurons tuning properties.

Alternatively, it is likely that dorsal pulvinar inactivation also induces specific and/or non-specific changes in the frontoparietal network involved in saccades selection and execution. In line with this idea, LIP inactivation leads to similar behavioral deficits, including choice bias (Wardak et al., 2002; Christopoulos et al., 2018), prompting us to investigate the effect of dorsal pulvinar inactivation on LIP neuronal activity. The activity in area LIP may be altered in different ways. First, the strong response to the contralateral presentation of visual stimuli might be decreased, leading to a weaker contralateral tuning. We might observe a similar phenomenon during movement preparation, in which we also observe strong contralateral tuning (Gnadt and Andersen, 1988; Barash et al., 1991). Therefore, the firing rate and by extension the tuning might also be altered before the saccade onset to contralateral targets. The activity in area LIP also reflects choice selectivity when two saccades options are available with equal reward probability (Wilke et al., 2012; Kagan et al., 2021). Since inactivation induces a choice bias towards the ipsilesional space, we expect to see a weaker activity in the inactivated hemisphere before ipsilesional choices. Another aspect of neuronal communication relies on the synchronization of neuronal assemblies. It is likely that the inactivation also alters the synchronization within LIP, which would be reflected in spike-LFP and LFP-LFP connectivity measures (Zhou et al., 2016a; Fiebelkorn et al., 2019). Finally, the pulvinar, like other thalamic nuclei, has been shown to play a role in maintaining cortical alertness through low-frequency activity (Zhou et al., 2016a). Therefore, we expect a general increase in low-frequency oscillations, that are typically associated with inattention and sleep.

Inter-hemispheric projections are crucial in order to integrate many lateralized sensory, motor and association processes in the brain. Those projections are mostly going through the corpus callosum (CC) and the anterior commissure (AC) (Suárez et al., 2014). Interestingly, the anatomical connectivity between the two hemispheres did not increase proportionally to increased brain size through evolution. Moreover, it has been shown that the spatial representation in the parietal cortex in humans is less contralateral than in monkeys (Kagan et al., 2010). Asymmetry between hemispheres was also stronger in humans compared to monkeys. Together, these results suggest that the evolution of the complex brain favored a decreased contralaterality in favor of hemisphere specialization or lateralization of information processing. Nevertheless, inter-hemispheric functional connectivity has been shown to be stronger between homotopic areas than heterotopic connections (Shen et al., 2015). This stronger connectivity has also been reported to be more stable over time and to depend on the conductivity of callosal axons, highlighting the role of the corpus callosum in maintaining stable functional connections between the two hemispheres. In line with this idea, developmental failure of the corpus callosum has been

associated with several behavioral and social deficits in humans (Paul et al., 2007). It is clear that inter-hemispheric communication is crucial for brain development and many sensory-motor processing. For instance, a complex unimanual movement elicits stronger ipsilateral motor cortex activity than a less complex task (Verstynen et al., 2005). This study describes an example of inter-hemispheric collaboration, which has also been reported in motor learning (Hordacre and Goldsworthy, 2018). However, choice bias towards ipsilesional targets after LIP or dorsal pulvinar inactivation also raises the question of inter-hemispheric competition during decision-making. Inter-hemispheric competition (IHC) model proposes that the contralateral hemisphere inhibits the ipsilateral hemisphere during ipsilateral limb movement preparation. Collaboration and competition between the two hemispheres are not necessarily exclusive hypotheses but might depend on the context and the behavioral demand. Therefore, looking at the effect of unilateral dorsal pulvinar inactivation on both hemispheres might contribute to a better understanding of inter-hemispheric communications.

The goal of this experiment is to find neuronal correlates of the behavioral deficits observed after unilateral dorsal pulvinar inactivation, in the parietal area LIP. More precisely, we aim to demonstrate the causal role of the dorsal pulvinar in modulating neuronal activity in the parietal cortex during visual processing, movement selection and execution. In order to better understand the neuronal mechanism leading to the deficit, we also assess the neuronal changes in the intact hemisphere. To do so, we recorded activity in bi-hemispheric LIP while monkey performs delayed saccade task to instructed targets and free-choices between targets located in opposite hemifield, before and after unilateral dorsal pulvinar inactivation.

4.3 Material and methods

See General Materials and Methods for aspects shared across Chapters 3 and 4. Here only specific aspects of the study are detailed.

4.3.1 Experimental timeline

In every inactivation session (10 sessions for monkey L, 8 sessions for monkey B), we first recorded the activity in LIP in both hemispheres while monkeys performed a delayed saccade task (pre-injection block, 180 successful trials). At the end of the pre-injection block, we injected THIP (~12 min) and waited for 15 min. Monkey then performed one or more post-injection blocks until the end of the session (Figure 4.2.1). For analyses, we compared the pre-injection block with the first post-injection block (except for 2 sessions in Monkey L in which we used the 2nd post-injection block because we observed stronger choice bias). We also performed control or "sham" sessions (8 sessions monkey L, 7 sessions monkey B, in which we followed the same experimental timeline but we did not inject THIP.

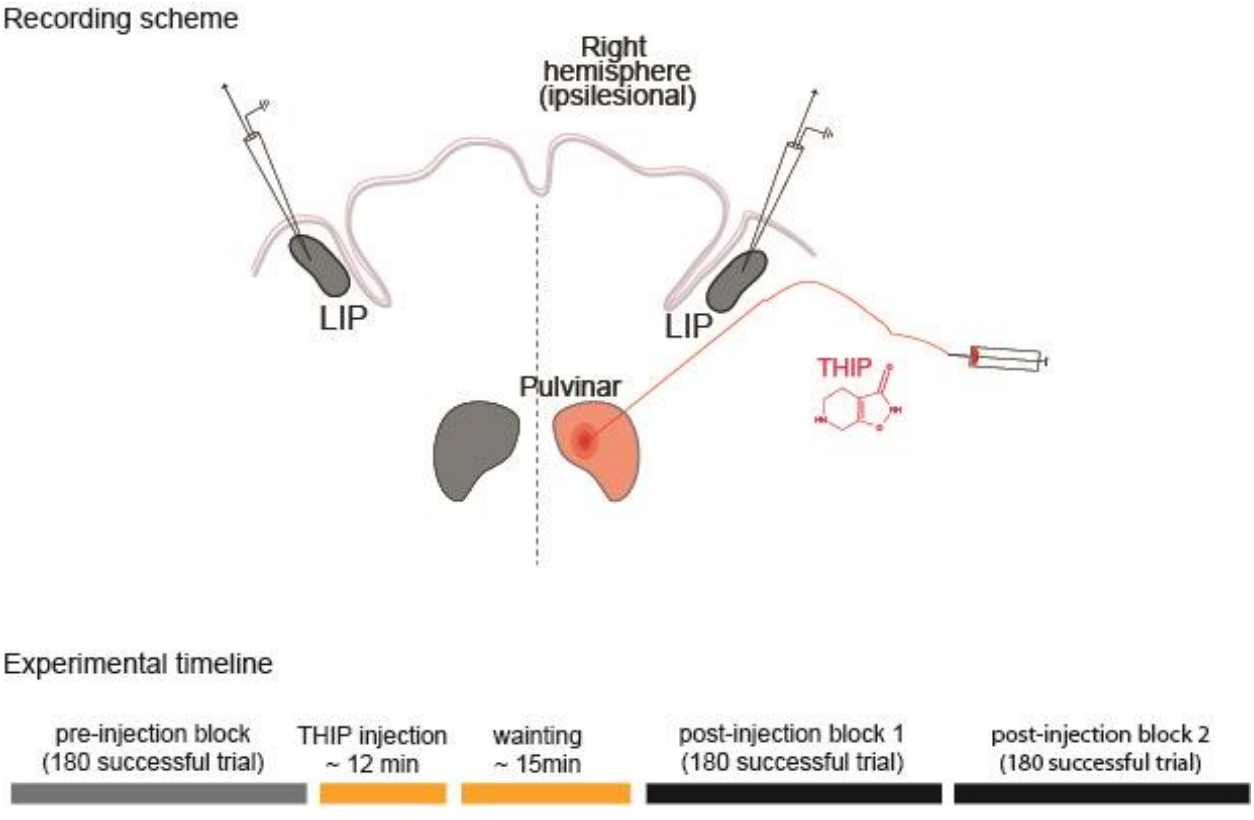

Figure 4.2.1 Recording scheme and experimental timeline

4.3.2 Dorsal pulvinar inactivation

To suppress neuronal activity in the dorsal pulvinar, we used THIP, which is a less potent derivative of Muscimol and an agonist of GABA-A receptors. THIP injections were performed while the animals were awake and sitting in their primate chair, with their heads restrained via implanted head posts. The injection was done with a high precision microinjection syringe pump (Harvard Apparatus, USA). A microinjection sharp-tip steel cannula (28 gauge; 50mm length) was sitting inside the custom-made guide-tube such that the tip of the cannula landed in the target location within the dorsal pulvinar (Figure 4.2.2). The target location was calculated on MRI images using Planner. The injection volume across sessions was in the range of 2.25-3 µL and the injection rate was 0.25 µL/min for all sessions. In total, we collected 10 inactivation sessions in monkey L and 8 in monkey B (see tables 4.2.1 and 4.2.2 for details).

Monkey L

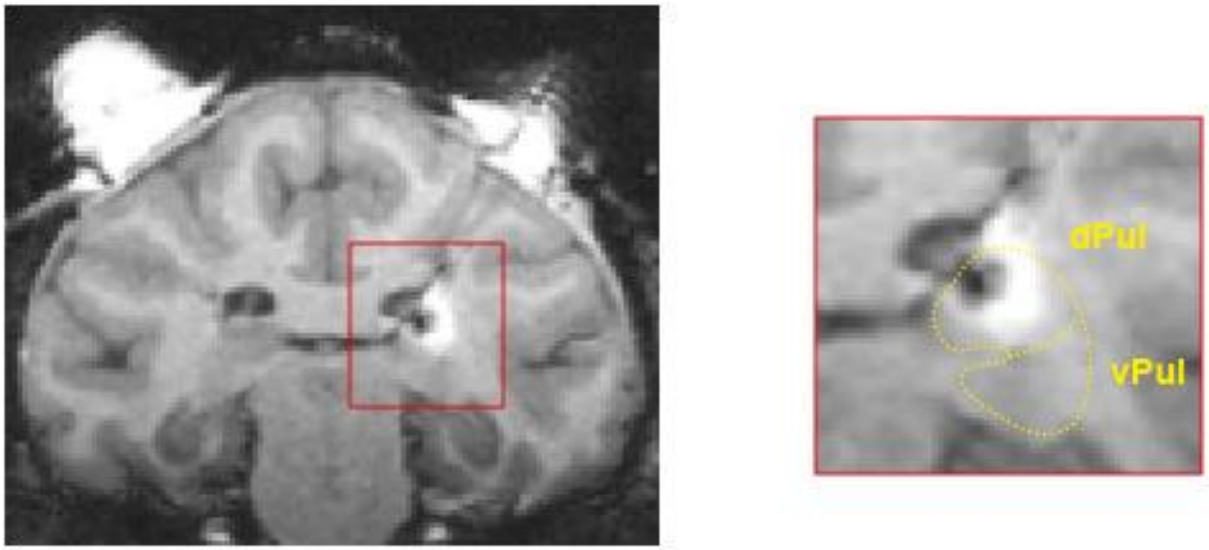

Monkey B

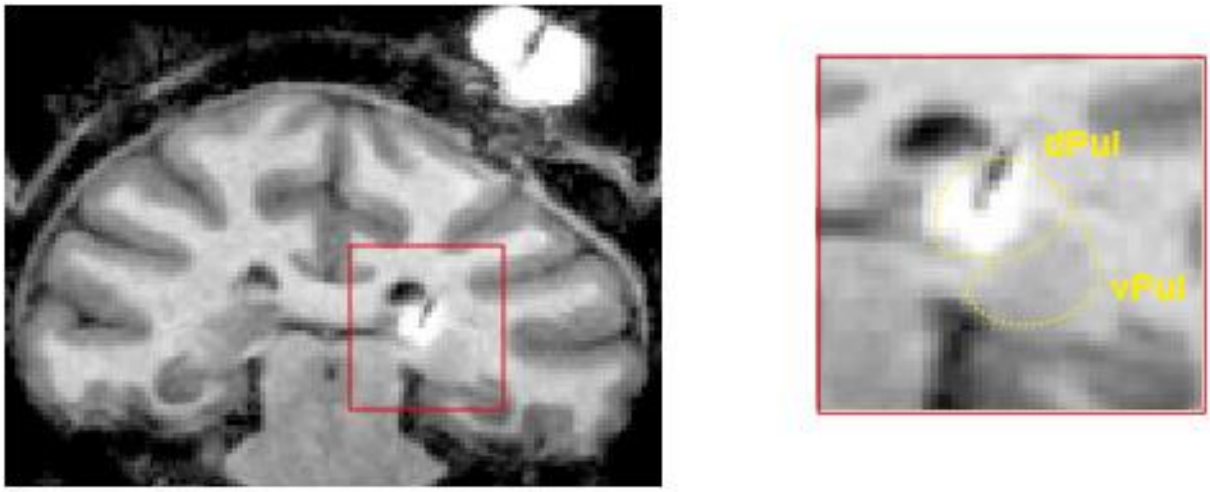

Figure 4.2.2: Inactivation locations. Localization of inactivation region in both monkeys on a coronal slice visualized after gadolinium injection (1.5 µL, 1/200).

4.3.3 Recording locations

We recorded the activity in area LIP in both hemispheres (Table 4.2.1-4). Recording locations were calculated from MRI images using Planner (Figure 4.2.3).

Table 4.2.1: List of inactivation sessions for monkey L

Date	right LIP recording location	left LIP recording location	injection location	injection volume (µL)
20210520	-5;3	0;3	3;7 (right)	3

20210610	-6;1	2;-2	3;7 (right)	2.5
20210616	-6;1	2;-2	3;7 (right)	2.5
20210709	-6;1	2;-2	3;7 (right)	2.5
20210901	-3;3	2;-3	3;7 (right)	2.5
20211006	-3;3	2;-4	3;7 (right)	3
20211021	-3;3	2;-4	3;7 (right)	3
20211126	-4;5	1;2	1;8 (left)	2.5
20211201	-4;5	2;-1	1;8 (left)	3
20211208	-4;5	2;-1	1;8 (left)	3

Table 4.2.2: List of inactivation sessions for monkey B

Date	right LIP recording location	left LIP recording location	injection location	injection volume (μL)
20201112	0;-4	NA	4;1 (right)	2.5
20201119	0;-4	0;1	4;1 (right)	2.5
20201126	-2,-5	0;1	4;1 (right)	2.5
20201203	-1;-5	0;1	4;1 (right)	2.5
20201217	0;-4	0;1	4;1 (right)	2.5
20210225	1;-3	0;1	4;1 (right)	2.25
20210304	1;-3	0;1	4;1 (right)	2.25
20210311	1;-3	0;1	4;1 (right)	2.25

Table 4.4.3: List of control sessions for monkey L

Date	right LIP recording location	left LIP recording location
20210623	-6;1	2;-2
20210729	-5;2	2;-3
20210910	-3;3	2;-3
20211013	-3;3	2;-4
20211028	-3;4	2;-3
20211029	-2;4	2;-1
20211203	-4;5	2;-1
20211210	-4;5	2;-1

Table 4.4.4: List of control sessions for monkey B

Date	right LIP recording location	left LIP recording location
20201209	1;-3	0;1
20210127	1;-3	0;1

20210203	1;-3	0;1
20210205	1;-3	0;1
20210317	1;-3	0;1
20210325	1;-3	0;1
20210401	1;-3	0;1

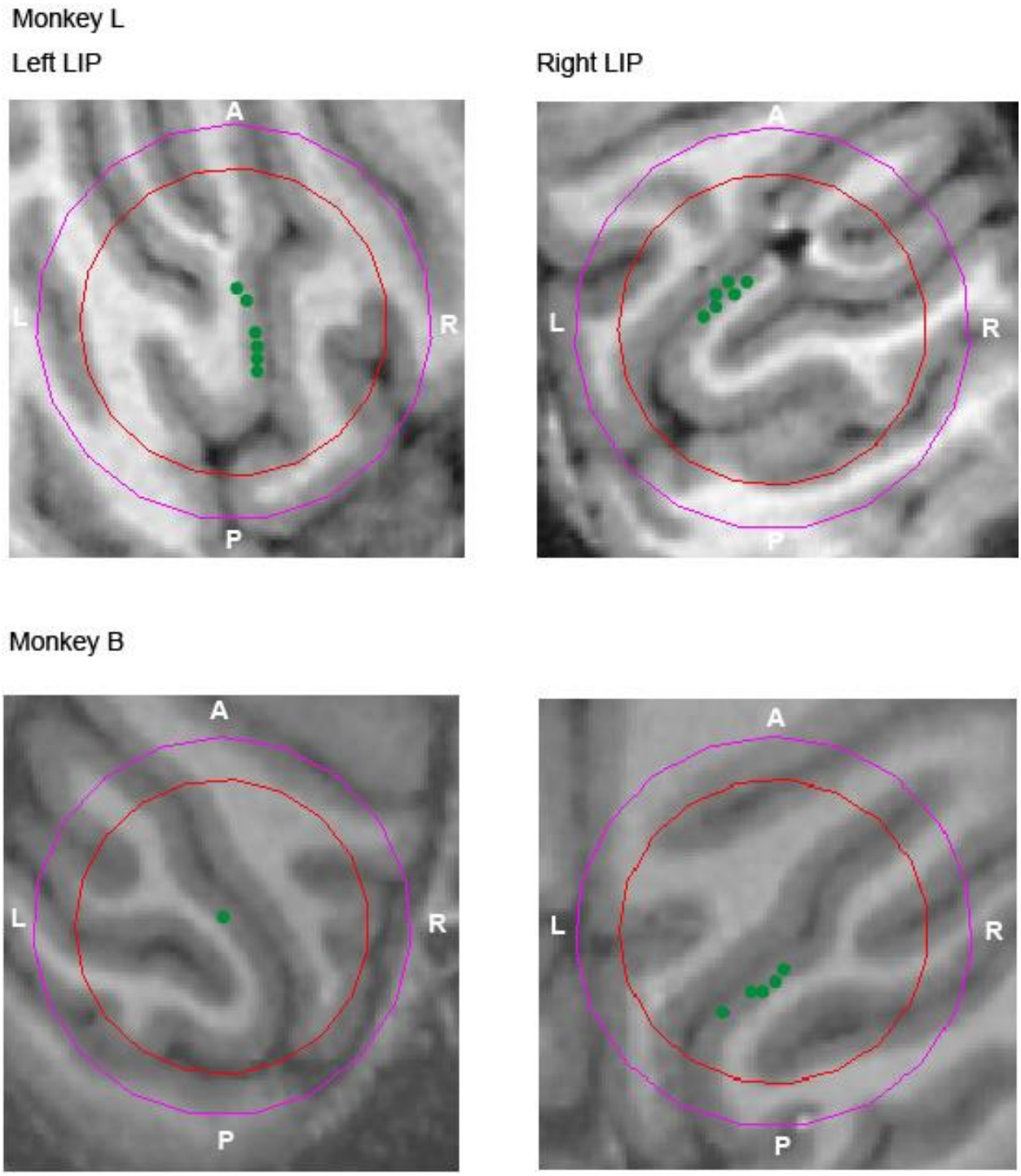

Figure 4.2.3: Recording locations in both monkeys and both hemispheres. Monkey L on top and monkey B below. Left LIP on left side and right LIP on right side.

4.3.4 Local field potential

To obtain LFP signal, we applied a median filter on the broadband signal from each recording site with the window size of 250 ms which reliably gave us LFP signal for frequencies up to 150 Hz.

To remove the 50 Hz AC line noise, a band-stop Butterworth filter (Matlab "butter" and "filtfilt" functions) for the range of 49.9-50.1 Hz and also 99.9-100.1 Hz was applied. LFP signal power was computed using the Fieldtrip toolbox (Oostenveld et al., 2011). LFP power was obtained for each of the frequency bins between 2 and 120 Hz in logarithmic steps ("logscale" function of MATLAB) by using Morlet wavelet convolution with a cycle-based time window for each frequency of n=6 cycles with a sliding window of 25 ms. This means for lower frequencies the time window was longer than for higher frequencies. Since for a typical length of a trial, the full power distribution for the whole trial in lower frequencies was not possible, zero-padding was done such that the length of a trial was enough for power calculations for all frequency bins. To detect noisy trials, we used different thresholds based on amplitude (6*std for 10 consecutive samples), standard deviation (4*std of all trials), 1st derivative (6*std for 10 consecutive samples) and power (4*std of all trials). If in a specific trial, one of these thresholds was reached, the trial was considered noisy and removed from further analysis. Normalization was performed as a relative change from baseline as follows: $P(rel) = \frac{P-\mu}{\mu}$ where P is the LFP power in a time-frequency bin and μ is the mean power of the baseline for that frequency. The normalization was done in two different ways. First, in order to visualize global changes, we normalized pre- and post-injection (post- 'sham injection for control session) blocks using the baseline calculated in the pre-injection block. In order to evaluate task-specific changes, we also normalized both blocks to their own baseline. The time window used for baseline calculation was -500 to -50 ms from target onset. In difference plots, the statistical significance was calculated using a paired t-test on all recording sites and Bonferroni correction was used to account for multiple comparisons as follows: $\frac{\alpha}{Ntime*Nfrequency}$.

4.3.5 Peri-stimulus time histogram (PSTH)

Spike density functions were computed using a 10 ms bin size using a Gaussian kernel (20 ms). For each recorded unit, we either corrected the firing rate within each trial by subtracting the average ongoing firing rate in baseline or computed the relative change to baseline by the average firing rate across all trials within conditions as follows: $FR(rel) = \frac{FR-\mu}{\mu}$ where FR is the firing rate at a specific time point and μ is the mean firing rate in baseline. Consistently with the LFP analysis, we also normalized pre- and post- injection blocks either using the baseline of the pre-injection block or the respective baseline. We used fixation hold epoch as baseline in both cases. Average responses for each unit were then derived by averaging the normalized spike density for each unit across all trials for the respective condition. Means and SE of these baseline-corrected and

averaged spike densities across units of a given sub-population were calculated to display population responses. Visually responsive neurons were defined as showing a significant increase in firing rate for at least one space condition in the cue epoch as compared to the fixation hold epoch. Motor responsive neurons were defined as showing a significant increase of firing rate for at least one space condition in the delay epoch as compared to the fixation hold epoch.

4.4 Results

4.4.1 Behavioral deficits after dorsal pulvinar inactivation

In control trials, before inactivation, both monkeys had a choice bias towards one hemifield. monkey L had a choice bias towards ipsilesional space (35% of contralesional choices) whereas monkey B had a choice bias towards contralesional space (65% of contralesional choices). After unilateral dorsal pulvinar inactivation, in most sessions (Table 4.3.1 and 4.3.2) both monkeys decreased their proportion of contralesional targets selection in favor of ipsilesional targets in free-choice trials. Indeed, we observed a significant decrease of contralesional choices after inactivation (Figure 4.3.1: monkey L: from 0.35 ± 0.04 to 0.24 ± 0.04; monkey B: from 0.65 ± 0.05 to 0.46 ± 0.06). This result was expected from human patient studies as well as perturbation studies in monkeys (Arend et al., 2008; Van der Stigchel et al., 2010; Wilke et al., 2013; Dominguez-Vargas et al., 2017). In addition to the gadolinium injection and its visualization in the MRI scan, the ipsilesional choice bias after pulvinar inactivation is therefore an indication that the location and the volume of the injection certainly match our planning.

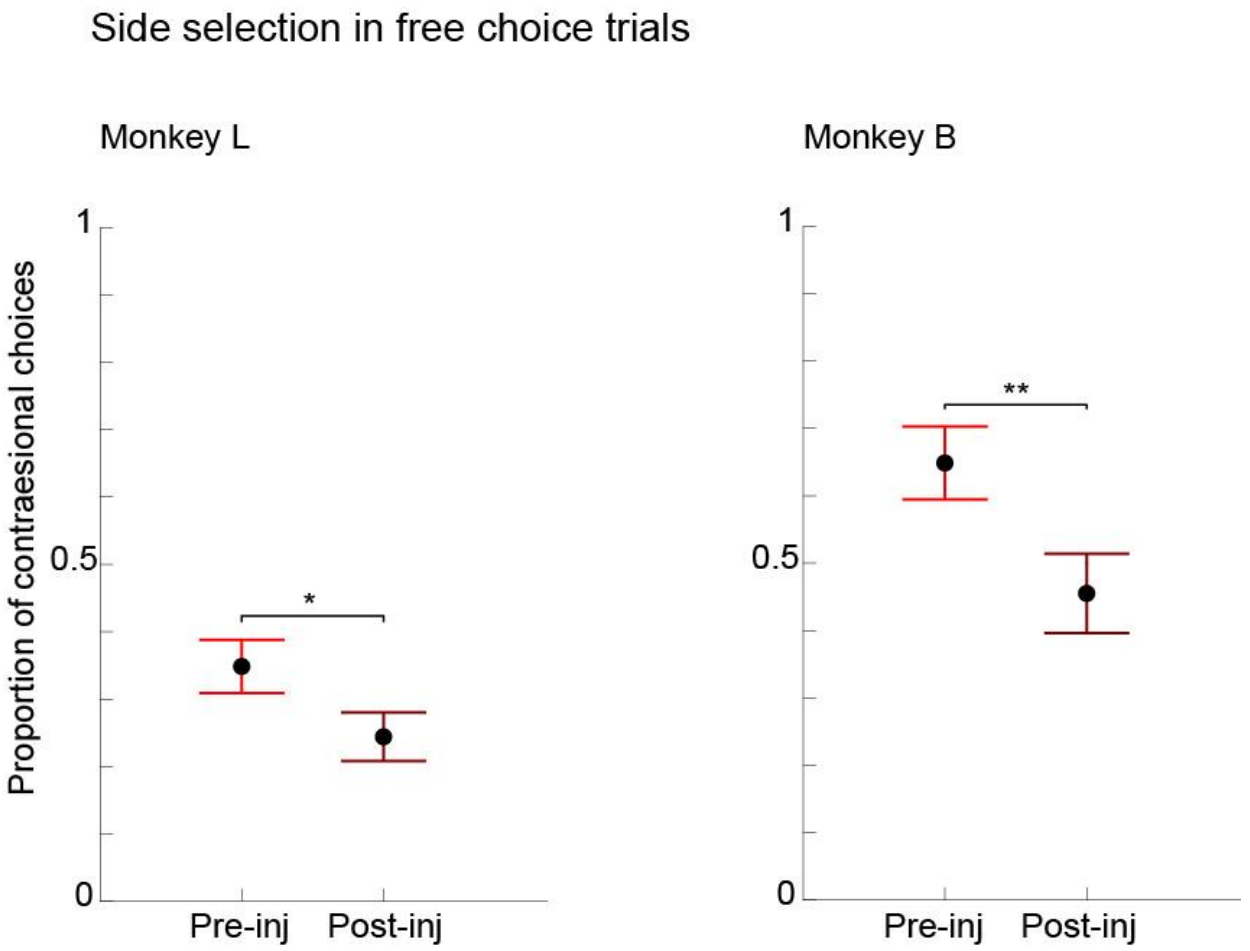

Figure 4.3.1. Contralesional selection in free-choice trials. Proportion of contralesional choices before and after inactivation in monkey L (left) and monkey B (right) across sessions (Mean ± SEM; * p<0.05, ** p<0.005, *** p<0.0005).

Table 4.3.1: Proportion of contralesional choices in pre- and post-injection blocks in monkey L

session	Contralesional choices pre-injection	Contralesional choices post-injection
20210520	0.144	0.100
20210610	0.333	0.178
20210616	0.258	0.236
20210709	0.444	0.133
20210901	0.300	0.411
20211006	0.438	0.289
20211021	0.211	0.267
20211126	0.400	0.178
20211201	0.389	0.200
20211208	0.567	0.449

Table 4.3.2: Proportion of contralesional choices in pre- and post-injection blocks in monkey B

session	Contralesional choices pre-injection	Contralesional choices post-injection
20201112	0.722	0.667
20201119	0.389	0.233
20201126	0.767	0.539
20201203	0.422	0.311
20201217	0.733	0.256
20210225	0.722	0.611
20210304	0.678	0.533
20210311	0.756	0.489

Saccadic reaction times (RT) in monkey L before inactivation were comparable in instructed and free-choice trials for both sides of space (Figure 4.3.2: in seconds: instructed contra: 0.193 ± 0.003, instructed ipsi: 0.195 ± 0.005, choice contra: 0.197 ± 0.004, choice ipsi: 0.189 ± 0.005). The lack of difference between instructed and free-choice RTs implies that in both trial types, the target selection was made before the go signal. Unexpectedly, in monkey B, saccadic reaction times before inactivation were higher for instructed trials than for free-choice (instructed contra: 0.185 ± 0.008, instructed ipsi: 0.203 ± 0.007, choice contra: 0.168 ± 0.004, choice ipsi: 0.181 ± 0.005). Monkey B's reaction times were also lower for contralesional targets (preferred before inactivation). After inactivation, there were no significant inactivation-induced differences for monkey L (Figure 4.3.2 instructed contra: 0.194 ± 0.002, instructed ipsi: 0.191 ± 0.003, choice contra: 0.199 ± 0.003, choice ipsi: 0.193 ± 0.004). However, monkey B showed a significant increase in saccadic reaction times for ipsilesional choices (Figure 4.3.2 'pre-inj' ipsi choice: 0.181 ± 0.005; 'post-inj' ipsi choice: 0.195 ± 0.006). Interestingly, the saccadic reaction time was also higher for ipsilesional than contralesional choices after inactivation ('post-inj' ipsi choice: 0.173 ± 0.005; 'post-inj' contra choice: 0.195 ± 0.006). This increase, in combination with the ipsilesional choice bias, likely reflects alterations during target selection.

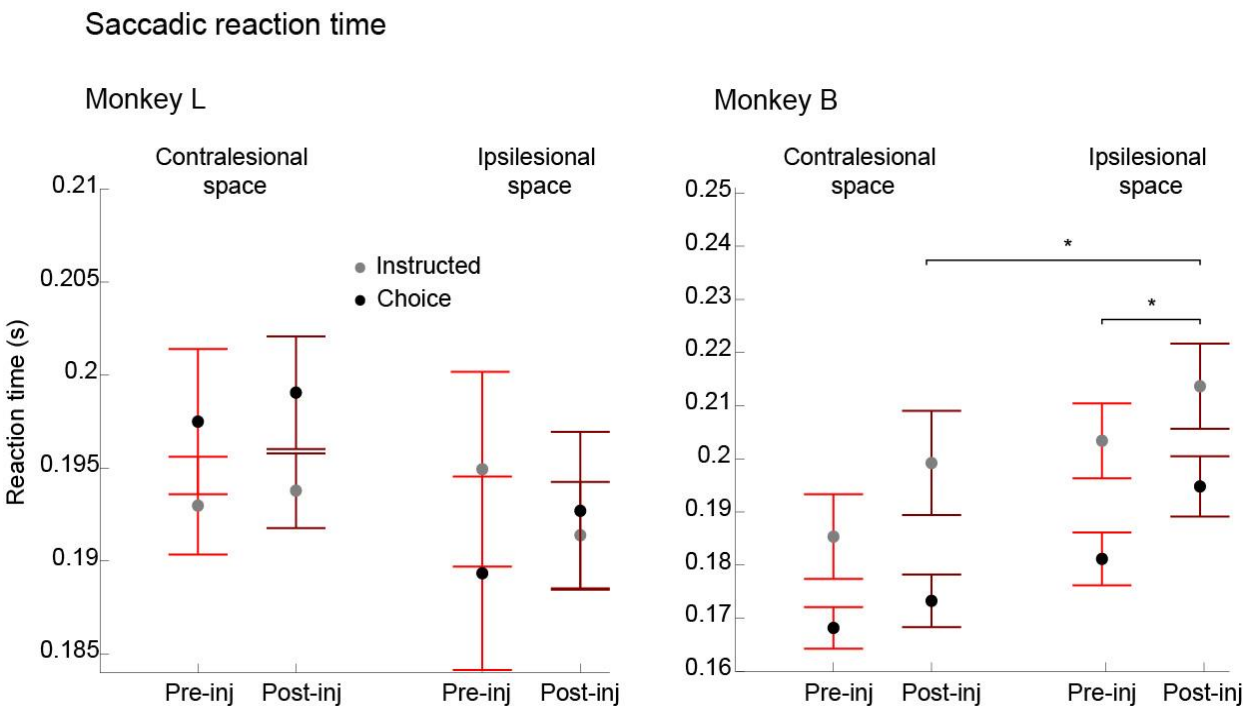

Figure 4.3.2: Saccadic reaction time to target acquisition. Reaction times before and after inactivation in monkey L (left) and monkey B (right) across sessions (Mean ± SEM; * p<0.05, ** p<0.005).

In control condition, both monkeys were performing the task with a high success rate (Figure 4.3.3: monkey L: instructed contra: 0.91 ± 0.014, instructed ipsi: 0.94 ± 0.01, choice contra: 0.87 ± 0.02, choice ipsi: 0.93 ± 0.01; monkey B: instructed contra: 0.99 ± 0.006, instructed ipsi: 0.97 ± 0.01, choice contra: 0.97 ± 0.01, choice ipsi: 0.96 ± 0.01). Despite a slight decrease in monkey L to contralesional choices, there was no significant performance decrease in both animals after inactivation (Monkey L: instructed contra: 0.93 ± 0.02, instructed ipsi: 0.95 ± 0.01, choice contra: 0.83 ± 0.04, choice ipsi: 0.92 ± 0.02; monkey B: instructed contra: 0.97 ± 0.01, instructed ipsi: 0.98 ± 0.01, choice contra: 0.96 ± 0.01, choice ipsi: 0.94 ± 0.02). However, the success rate for ipsilesional choices was significantly higher than contralesional choices after inactivation in monkey L ('post-inj' choice contra: 0.82 ±0.04; 'post-inj' choice ipsi: 0.92 ± 0.02). These results suggest that the inactivation induced oculomotor deficits when selecting targets located in the contralesional hemifield.

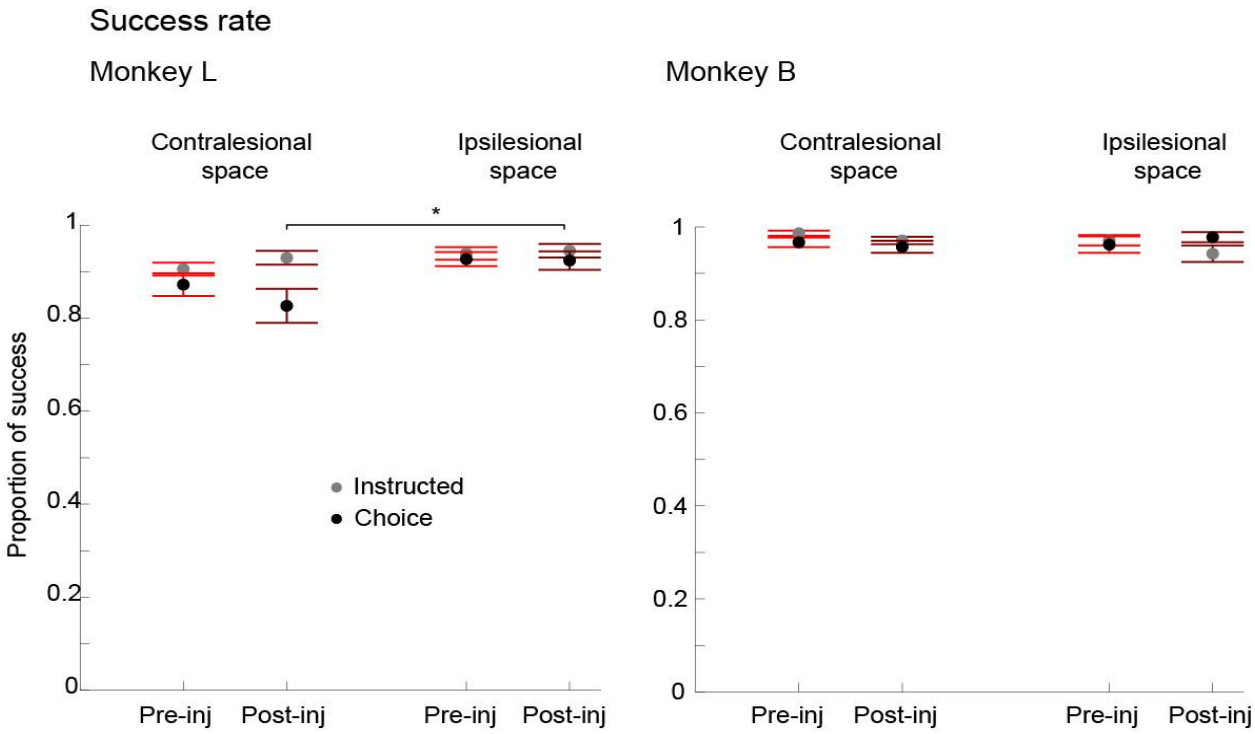

Figure 4.3.3 Success rates. Success rates before and after inactivation in monkey L (left) and monkey B (right) across sessions (Mean ± SEM; * p<0.05, ** p<0.005)

Globally, we observed an ipsilesional choice bias after dorsal pulvinar inactivation, confirming previous results in our lab. Monkey B also showed a higher reaction time when selecting targets located in the ipsilesional hemifield. In addition, we observed in monkey L a decreased performance after inactivation when selecting contralesional targets in comparison with ipsilesional targets. Together, results suggest alterations in movement selection and execution after dorsal pulvinar inactivation.

4.4.2 Local field potentials

We recorded local field potentials within the lateral bank of IPS (putative LIP, spanning the depth of the sulcus) in both hemispheres before and after unilateral dorsal pulvinar inactivation (monkey L, inactivated: 307, intact: 303; monkey B, inactivated: 233, intact: 210) and in control sessions where we did not perform inactivation (monkey L, inactivated: 247, intact: 238; monkey B, inactivated: 205, intact: 211).

4.4.2.1 LFP power response profile and tuning in control condition

As expected from area LIP, we observed a strong contralateral tuning to cue presentation, during movement preparation and execution. First, there was a transient increase in LFP power as a visual response to contralateral targets presentation (Figures 4.3.4 and 4.3.5). This transient response was comparable between the two monkeys in higher frequencies (gamma, 32-120 Hz). The visual response is also seen in lower frequency bands like delta (4-8 Hz), alpha (8-12 Hz) and beta (12-32 Hz), with some differences between monkeys. During delay, there was an increased power in higher frequencies and a decreased power in beta (18-32 Hz) in instructed trials towards the contralateral space. Both observations are typically associated with motor preparation. Finally, we observed a transient increase in gamma and theta around the saccade as well as a post-saccadic decrease in alpha/low-beta. Unexpectedly, in free-choice trials, we did not observe differences in the cue and delay response between contralateral and ipsilateral choices, indicating a lack of choice signal at these stages. This result may reflect that both monkeys did not commit to a target selection until the “go” signal. Around the saccade, there was a higher gamma power before contralateral choices as well as a lower power in theta (apart from the inactivated hemisphere in monkey B).

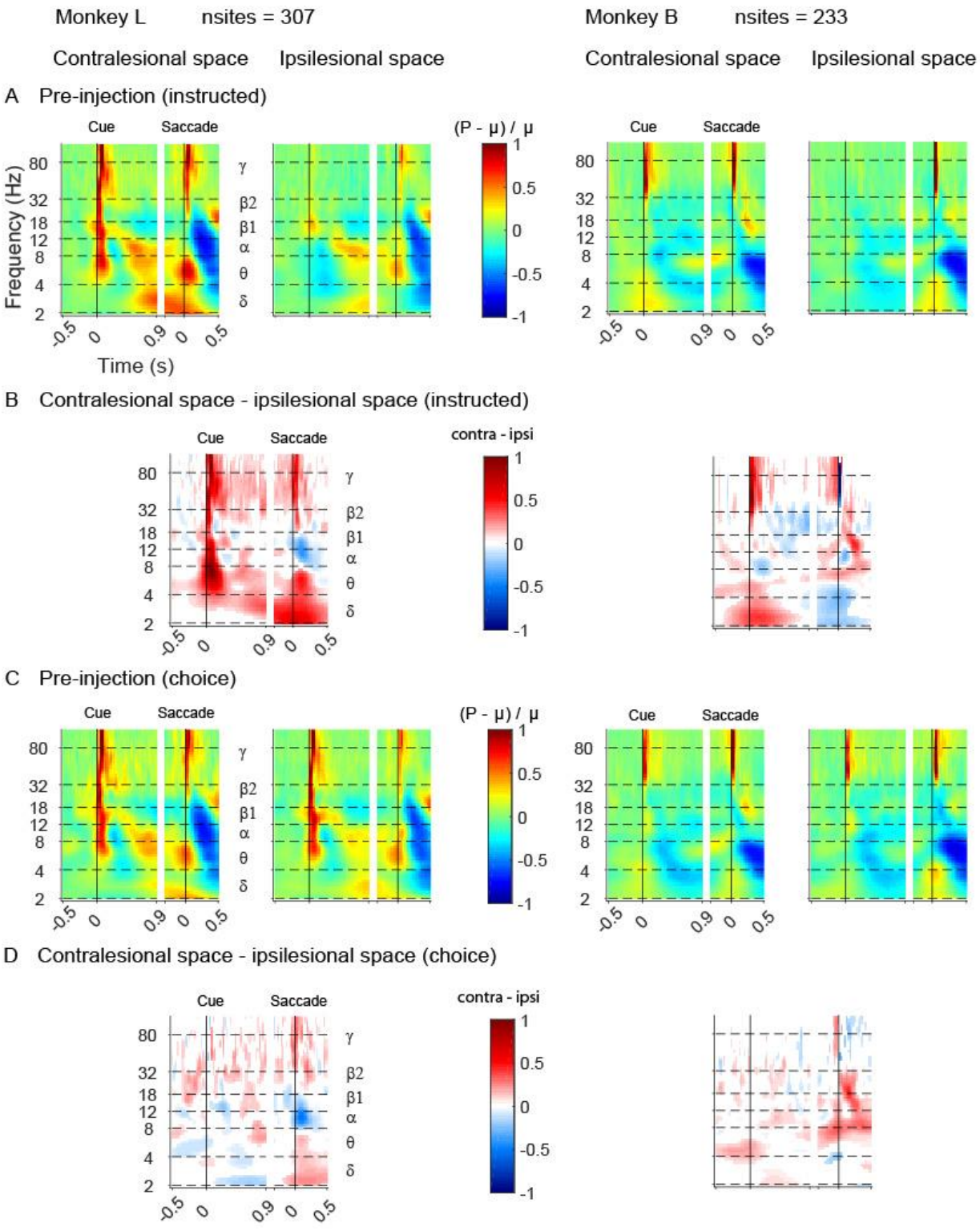

Figure 4.3.4. LFP space tuning in the inactivated hemisphere in pre-injection block. A Time-frequency spectrogram in instructed trials in pre-injection block. **B** Difference between contralesional and ipsilesional instructed targets (only significant bins are shown, paired t-test with Bonferroni correction). **C** Time-frequency spectrogram in free-choice trials before in pre-injection block. **D** Difference between contralesional and ipsilesional choices (only significant bins are shown, paired t-test with Bonferroni correction).

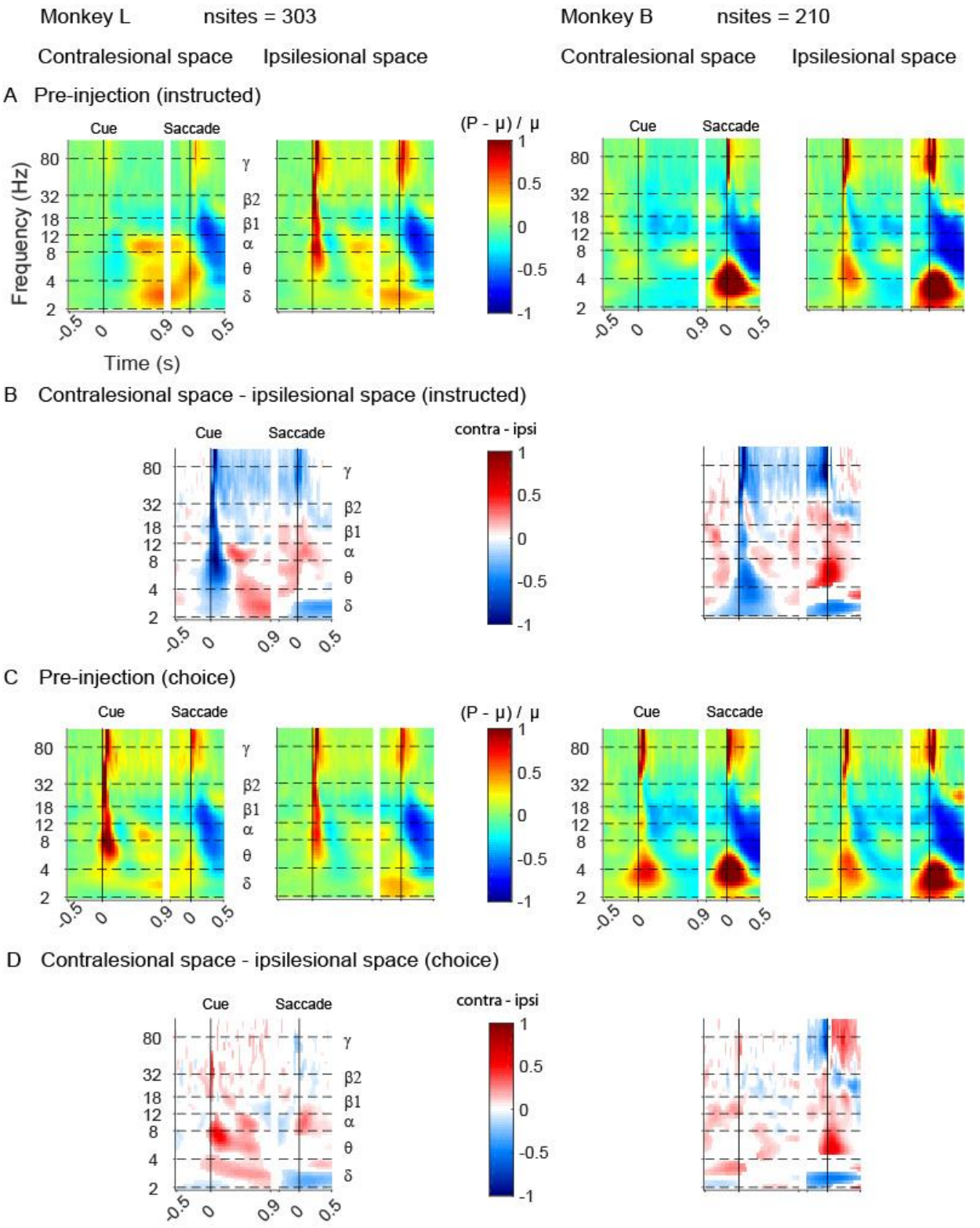

Figure 4.3.5 LFP space tuning in the intact hemisphere in pre-injection block. A Time-frequency spectrogram in instructed trials in pre-injection block. **B** Difference between contralesional and ipsilesional instructed targets (only significant bins are shown, paired t-test with Bonferroni correction). **C** Time-frequency spectrogram in free-choice trials before in pre-injection block. **D** Difference between contralesional and ipsilesional choices (only significant bins are shown, paired t-test with Bonferroni correction).

4.4.2.2 Effects of dorsal pulvinar inactivation on LFP in the inactivated hemisphere

In order to assess the global effect of inactivation, we first normalized the pre-injection and post-injection blocks in inactivation sessions to the pre-injection block and looked at the difference in time-frequency spectrograms (post-injection – post-injection). We observed in both monkeys an increased power in low frequencies (delta, theta and alpha). The power in those frequencies has been typically associated with the level of alertness (Brüers and VanRullen, 2018). Particularly alpha oscillations are seen as a mechanism to suppress sensory processing during selective attention (Foxe and Snyder, 2011). Therefore, this result suggests that the dorsal pulvinar inactivation leads to decreased cortical alertness and is in line with the idea that the pulvinar plays a role in maintaining cortical alertness. Coherently, we observed this effect in both instructed and free-choice trials.

We also observed a decreased power in beta, particularly in monkey L. A decrease in beta power in the parietal cortex is often associated with movement preparation and was observed in our recordings during the delay and before the saccade onset in both monkeys, more strongly for the contralateral space (Figure 4.3.4 and 4.3.5). However, the inactivation-induced beta decrease was seen throughout the entire trial, including epochs of the task where there is no motor preparation involved such as during fixation hold (Figures 4.3.6 and 4.3.7). This suggests an alteration of the synchronization in beta, independent of the task demand. Therefore, this general decrease most likely does not reflect increased movement preparation. On the contrary, when looking at the difference in beta power when each block was normalized to its own baseline, we saw a relative increase of beta power specifically during the delay period (Figures 4.3.8 and 4.3.9), suggesting a decreased movement preparation after inactivation and matching our expectations.

Finally, we observed differences across monkeys regarding the power in high frequencies. In monkey L, there was no change after inactivation, with both types of normalization. In monkey B, there was a global increase throughout the entire trial when both blocks were normalized by the pre-injection block. This increase was not task-specific since there was no relative change when the power was normalized within each block. Also, we observed a similar increase in high frequencies in monkey B when looking at the difference between pre-injection and post-injection sham sessions in which there was no injection. We conclude the effect on high frequencies in monkey B was not related to inactivation but rather to the instability of the signal over time.

We were also expecting to see some contralesional-specific alterations in the inactivated hemisphere. In other words, we asked whether the effect of inactivation was different for contralesional and ipsilesional targets. In order to evaluate such dissimilarities, we looked at the

difference of the difference. In other words, we first subtracted the pre-injection to the post-injection block and then we subtracted the ipsilesional space to the contralesional space. As a result, an observed higher power could be due to a stronger increase for contralesional targets or a stronger decrease for ipsilesional targets. Similarly, an observed lower power could be due to a weaker increase for contralesional targets or a weaker decrease for ipsilesional targets. First, in monkey L, there was a higher power in delta after instructed contralesional target presentation and during the delay period (Figure 4.3.6 and 4.3.8) Surprisingly, we observed the opposite effect in monkey B. However, we observed higher delta power in both monkeys around saccades to instructed contralesional targets. We also observed in both monkeys a higher power in alpha and beta shortly after contralesional cue presentation, which was not seen in sham sessions (Figure 4.3.10). We made the same observation in free-choice trials in monkey L, but not in monkey B (Figures 4.3.7 and 4.3.9). The time and frequency of space-specific effects did not overlap with the transient visual response observed in the pre-injection block. Therefore, it should not be interpreted as an increased visual response. On the contrary, we observed in control condition in this time and frequency range, a decreased power. This higher power after inactivation then suggests a deleterious effect of inactivation on sensory processing, particularly when targets were located in the contralesional hemifield.

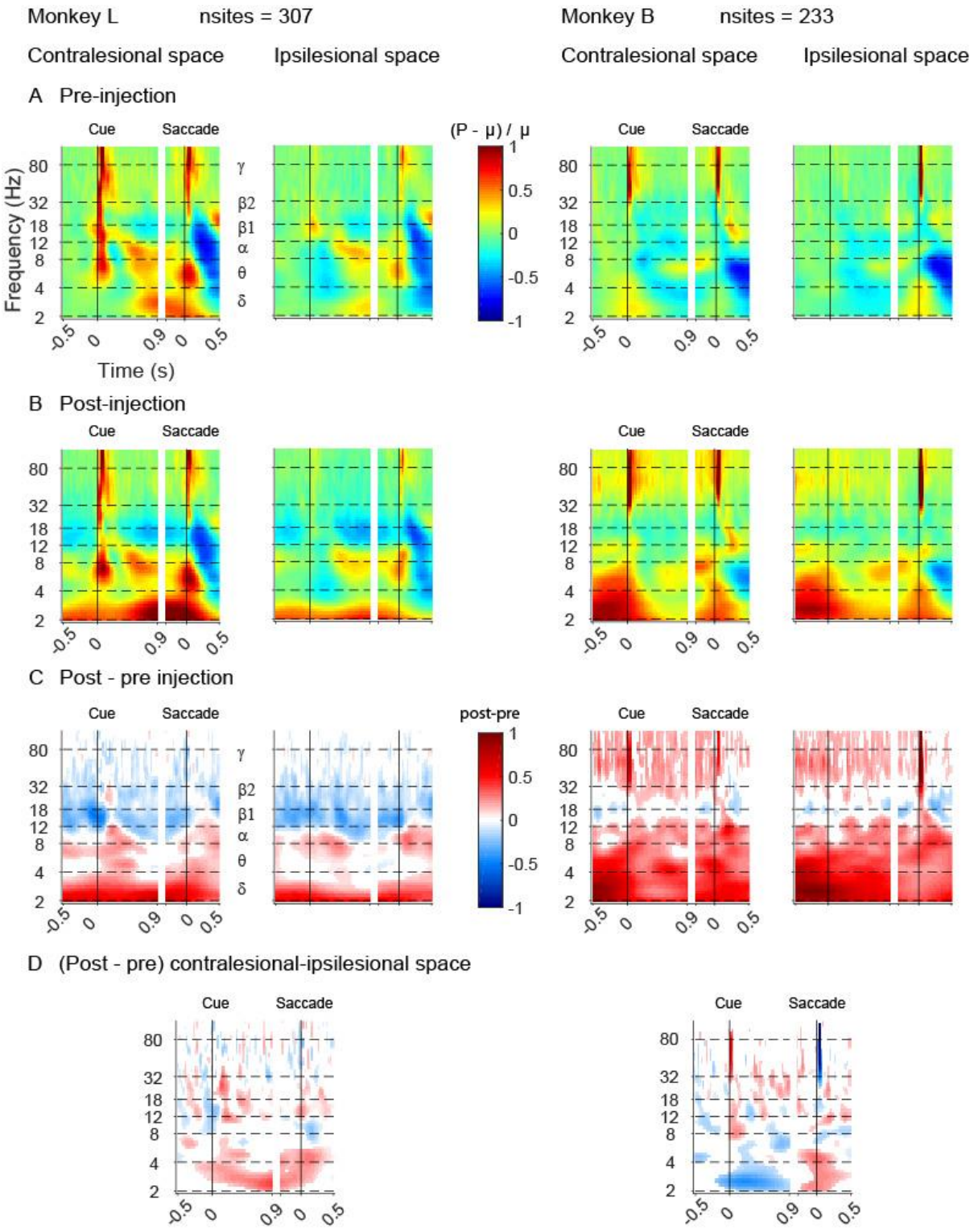

Figure 4.3.6. Effect of inactivation on LFP in the inactivated hemisphere in instructed trials (normalized by pre-injection block). A Time-frequency spectrogram in the pre-injection block. **B** Time-frequency spectrogram post-injection. **C** Difference time-frequency spectrogram between pre- and post-injection. Only significant bins are shown (paired t-test with Bonferroni correction). **D** Difference time-frequency spectrogram between contralesional and ipsilesional of the difference between pre- and post-injection (C). Only significant bins are shown (paired t-test with Bonferroni correction).

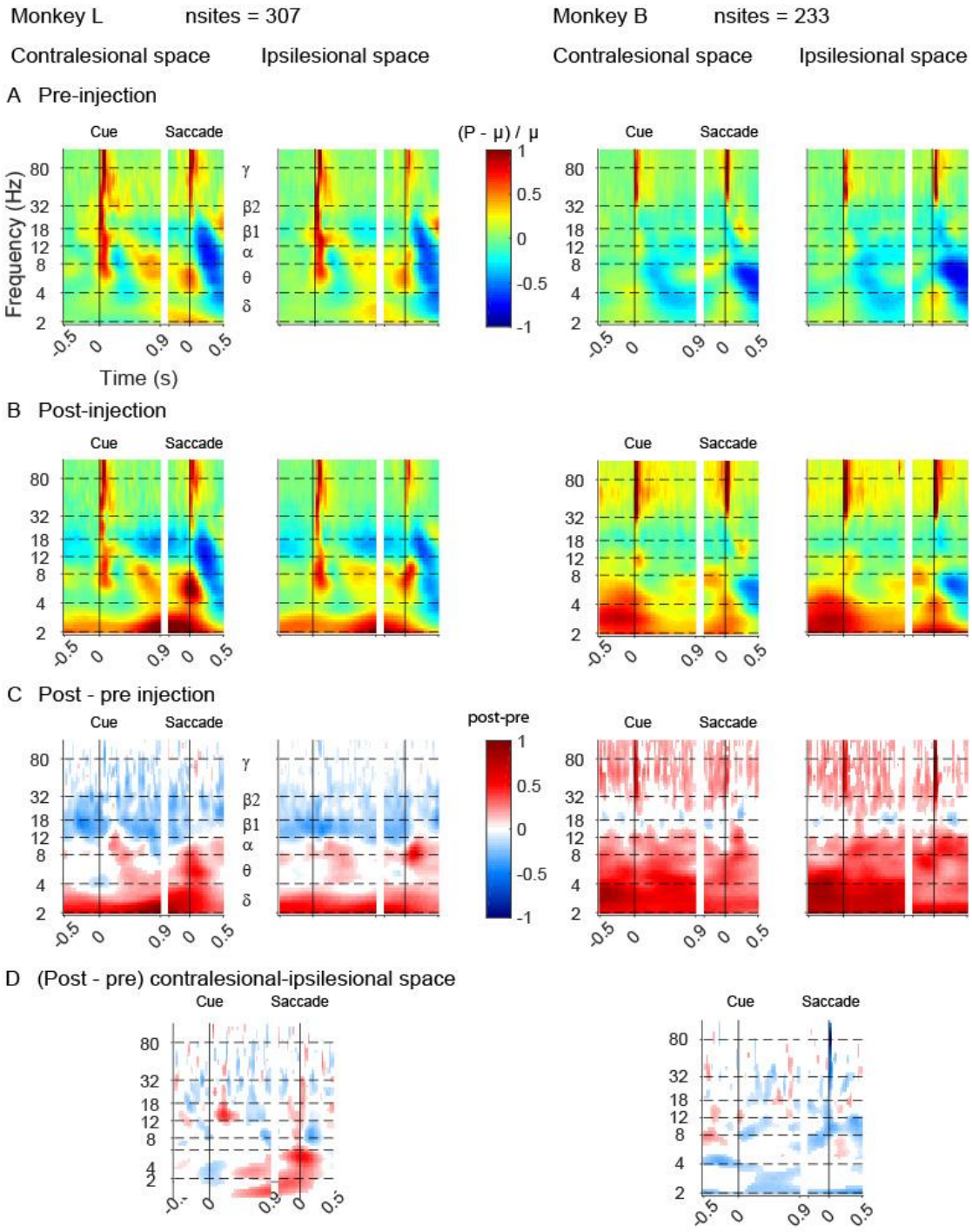

Figure 4.3.7. Effect of inactivation on LFP in the inactivated hemisphere in free-choice trials (normalized by pre-injection block). A Time-frequency spectrogram in the pre-injection block. **B** Time-frequency spectrogram post-injection. **C** Difference time-frequency spectrogram between pre- and post-injection. Only significant bins are shown (paired t-test with Bonferroni correction). **D** Difference time-frequency spectrogram between contralesional and ipsilesional of the difference between pre- and post-injection (C). Only significant bins are shown (paired t-test with Bonferroni correction).

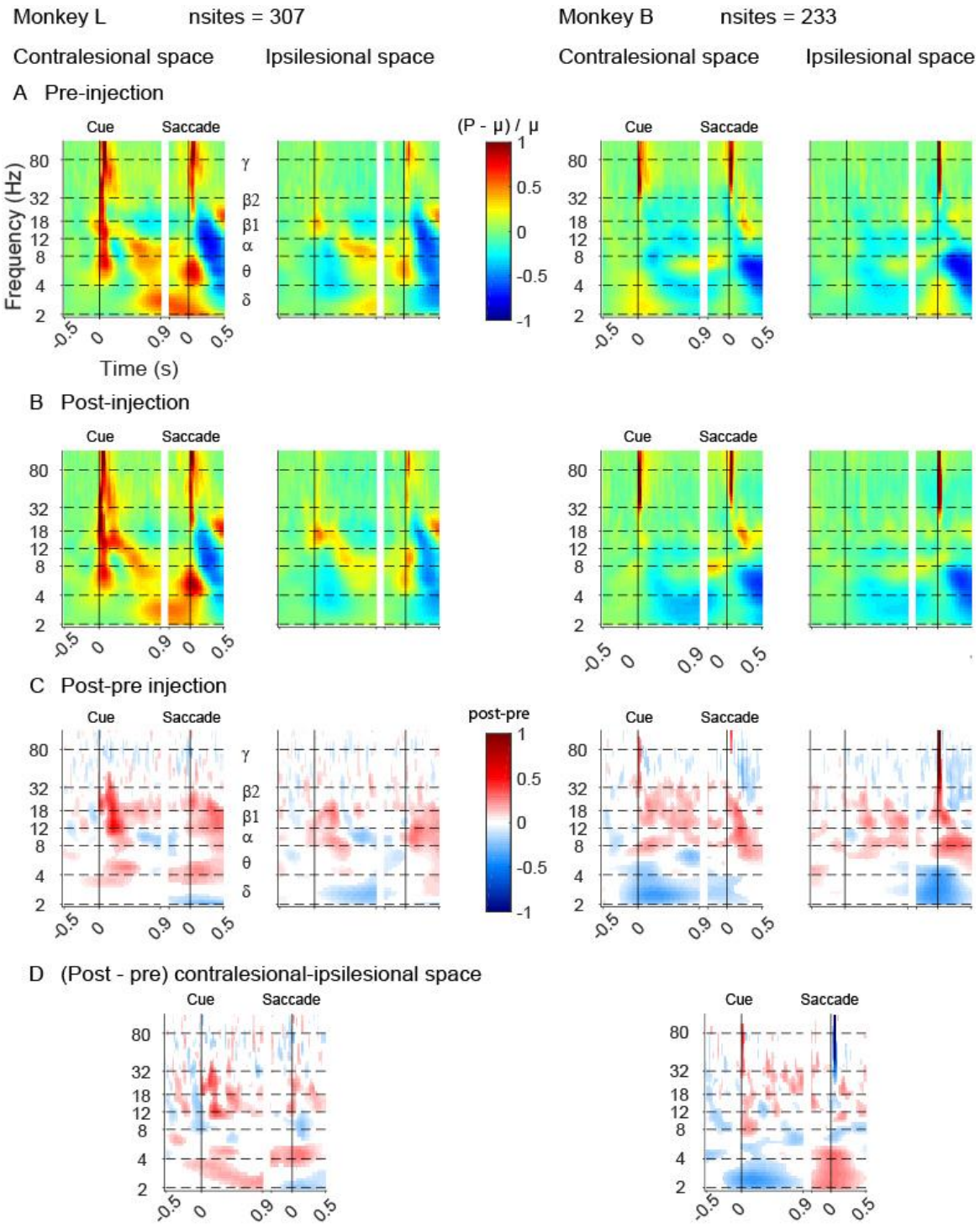

Figure 4.3.8 Effect of inactivation on LFP in the inactivated hemisphere in instructed trials (normalized within each block). A Time-frequency spectrogram in the pre-injection block. **B** Time-frequency spectrogram post-injection. **C** Difference time-frequency spectrogram between pre- and post-injection. Only significant bins are shown (paired t-test with Bonferroni correction). **D** Difference time-frequency spectrogram between contralesional and ipsilesional of the difference between pre- and post-injection (C). Only significant bins are shown (paired t-test with Bonferroni correction).

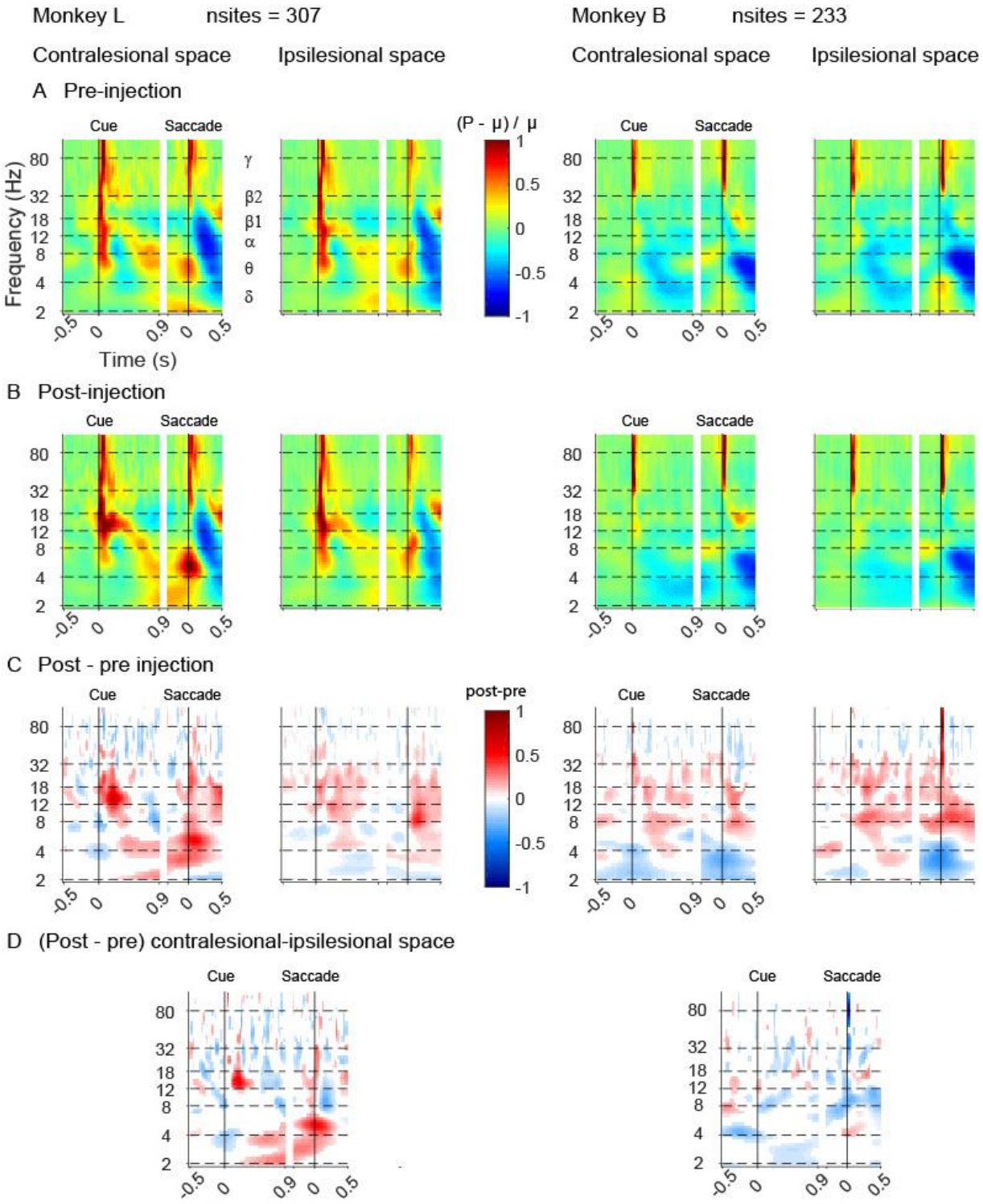

Figure 4.3.9 Effect of inactivation on LFP in the inactivated hemisphere in free-choice trials (normalized within each block). A Time-frequency spectrogram in the pre-injection block. **B** Time-frequency spectrogram post-injection. **C** Difference time-frequency spectrogram between pre- and post-injection. Only significant bins are shown (paired t-test with Bonferroni correction). **D** Difference time-frequency spectrogram between contralesional and ipsilesional of the difference between pre- and post-injection (C). Only significant bins are shown (paired t-test with Bonferroni correction).

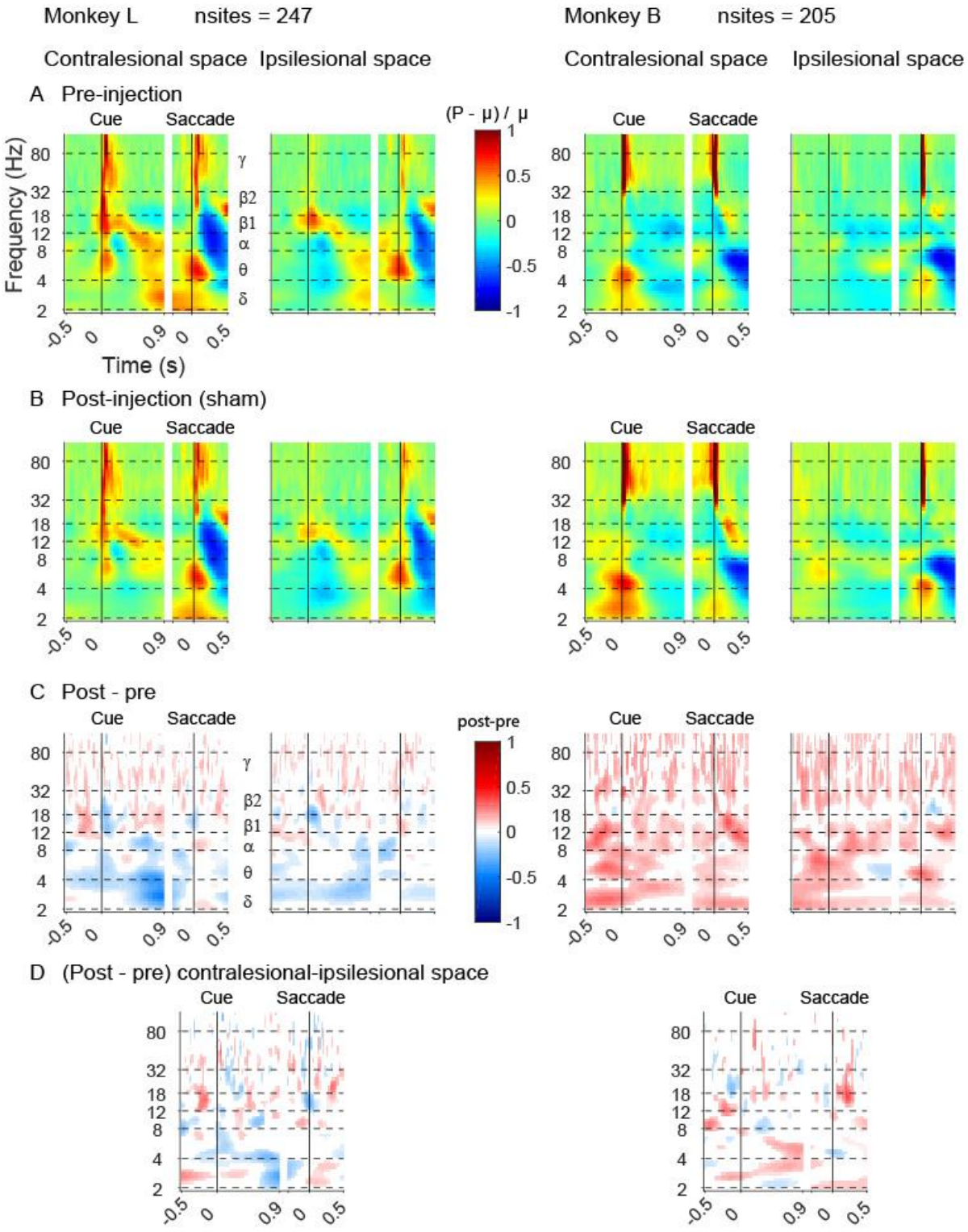

Figure 4.3.10. Control sessions: LFP in the 'inactivated' hemisphere in instructed trials (normalized by "pre-'sham' injection" block). A Time-frequency spectrogram in the control condition. **B** Time-frequency spectrogram after inactivation. **C** Difference time-frequency spectrogram between pre- and post- 'sham' injection. Only significant bins are shown (paired t-test with Bonferroni correction). **D** Difference time-frequency spectrogram between contralesional and ipsilesional of the difference between pre- and post- 'sham' injection (C). Only significant bins are shown (paired t-test with Bonferroni correction).

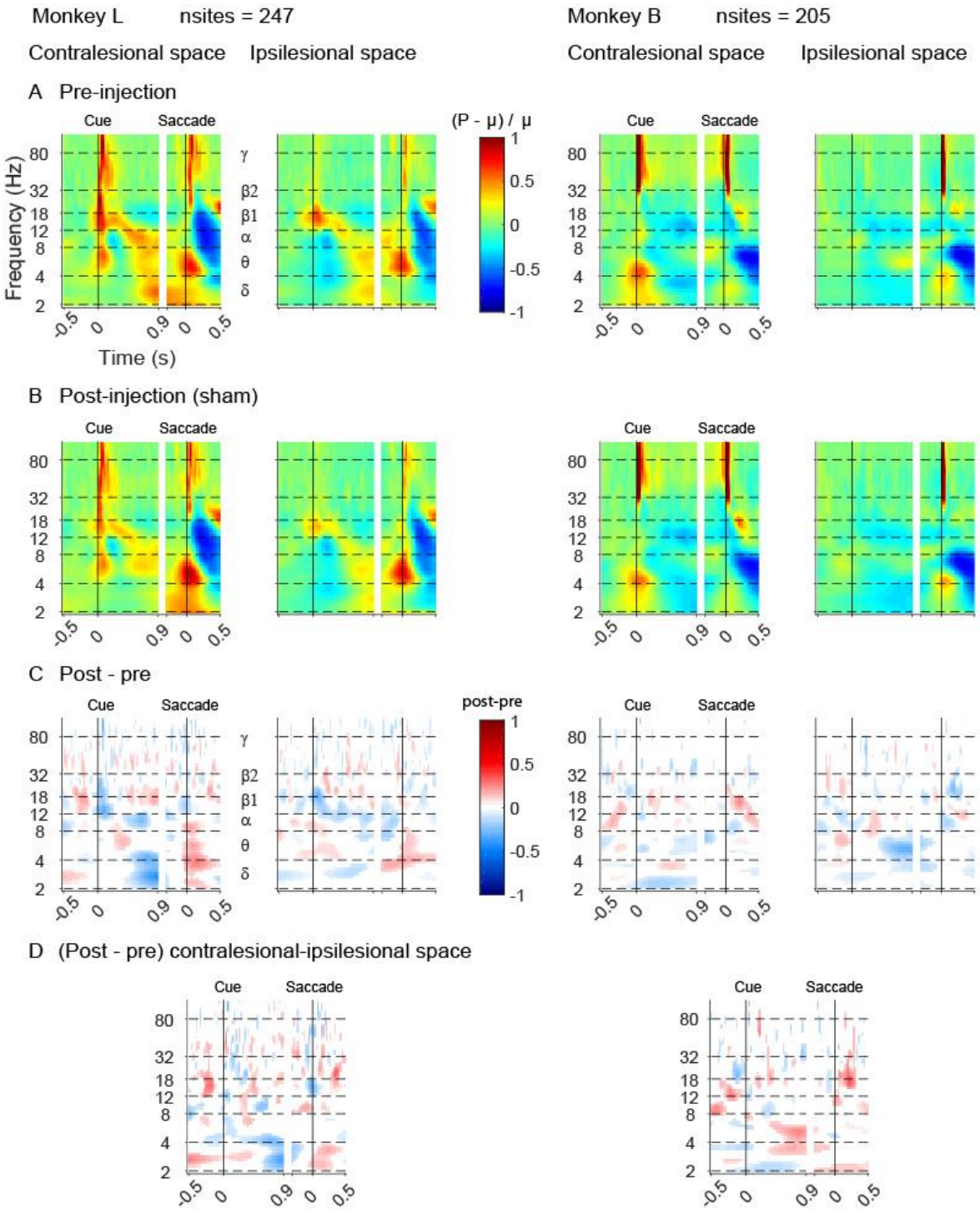

Figure 4.3.11. Control sessions: LFP in the 'inactivated' hemisphere in instructed trials (normalized within blocks). A Time-frequency spectrogram in the control condition. **B** Time-frequency spectrogram after inactivation. **C** Difference time-frequency spectrogram between control and 'fake-inactivation'. Only significant bins are shown (paired t-test with Bonferroni correction). **D** Difference time-frequency spectrogram between contralesional and ipsilesional of the difference between 'fake-inactivation' and control (C). Only significant bins are shown (paired t-test with Bonferroni correction).

4.4.2.3 Effect of dorsal pulvinar inactivation on LFP in the intact hemisphere

We first normalized both recording blocks to the control block in order to visualize the global effect of inactivation. We first observed in both monkeys a general increased power in the gamma range (32-120 Hz). This increase was seen in both instructed and free-choice trials (Figures 4.3.12 and 4.3.13). This increase in gamma power seems to be unspecific to targets location since we did not see significant differences between contralesional and ipsilesional trials, either instructed or free-choices. In addition, we did not see changes in the gamma power when both pre-injection and post-injection blocks were normalized to their own baseline (Figure 4.3.14 and 4.3.15), indicating the lack of task specificity in this effect. We did observe some slight increase in gamma power in 'sham' sessions, where there was no inactivation, likely due to instability of the signal. Altogether, this indicates a global increase of high-frequency power after inactivation, independent of the target location and the behavioral demand (i.e. visual processing or motor preparation). This general increase of activity in the intact hemisphere might reflect the lack of inhibition from the opposite hemisphere after inactivation and is in line with the idea of push-pull interactions between hemispheres during target selection.

In monkey L, the LFP power in theta (4-8 Hz), alpha (8-12 Hz) and beta (12-32 Hz) was mostly unaltered (Figure 4.3.12). Nevertheless, we did see a decreased power in theta during the delay and before the saccade onset during instructed trials. However, we also observed the same phenomenon in 'sham' sessions (Figure 3.4.16 and 3.4.17), suggesting neurophysiological variability over time or variability in the stability of the signal. In monkey B, we observed an unexpected increase in alpha and theta power when both blocks were normalized on pre-injection block (Figures 4.3.12 and 4.3.13). However, we observed similar changes in 'sham' sessions, here again suggesting some variability in the signal and/or in the neurophysiological responses over the time of the experiment.

When looking at the difference between pre- and post-injection normalized within each block, we observed a decreased power in delta and theta range (Figures 4.3.14 and 4.3.15). We observed this decrease during the delay period until the saccade onset in both monkeys but in monkey B, it was also seen from the cue onset. However, by looking at the LFP profile in the pre- and post-injection block, it seems that this effect is driven by different phenomenon in both monkeys. In monkey L, the power in this frequency range was increasing during the delay period and this increase was weaker after inactivation. In monkey B, we observed the opposite phenomenon. The power was decreasing during the same epoch and this decrease was more pronounced after

inactivation. Therefore, the functional significance of this effect might be different across the two monkeys.

Finally, we observed an increased beta power during the delay period after instructed contralesional cue presentation in both monkeys with both normalization (Figure 4.3.14). This result suggests an altered movement preparation towards contralesional targets, in a similar way to what we described in the inactivated hemisphere. The fact that we also observe this effect in the inactivated hemisphere is an argument against the hypothesis that we might observe some compensation mechanisms in the intact hemisphere after pulvinar inactivation.

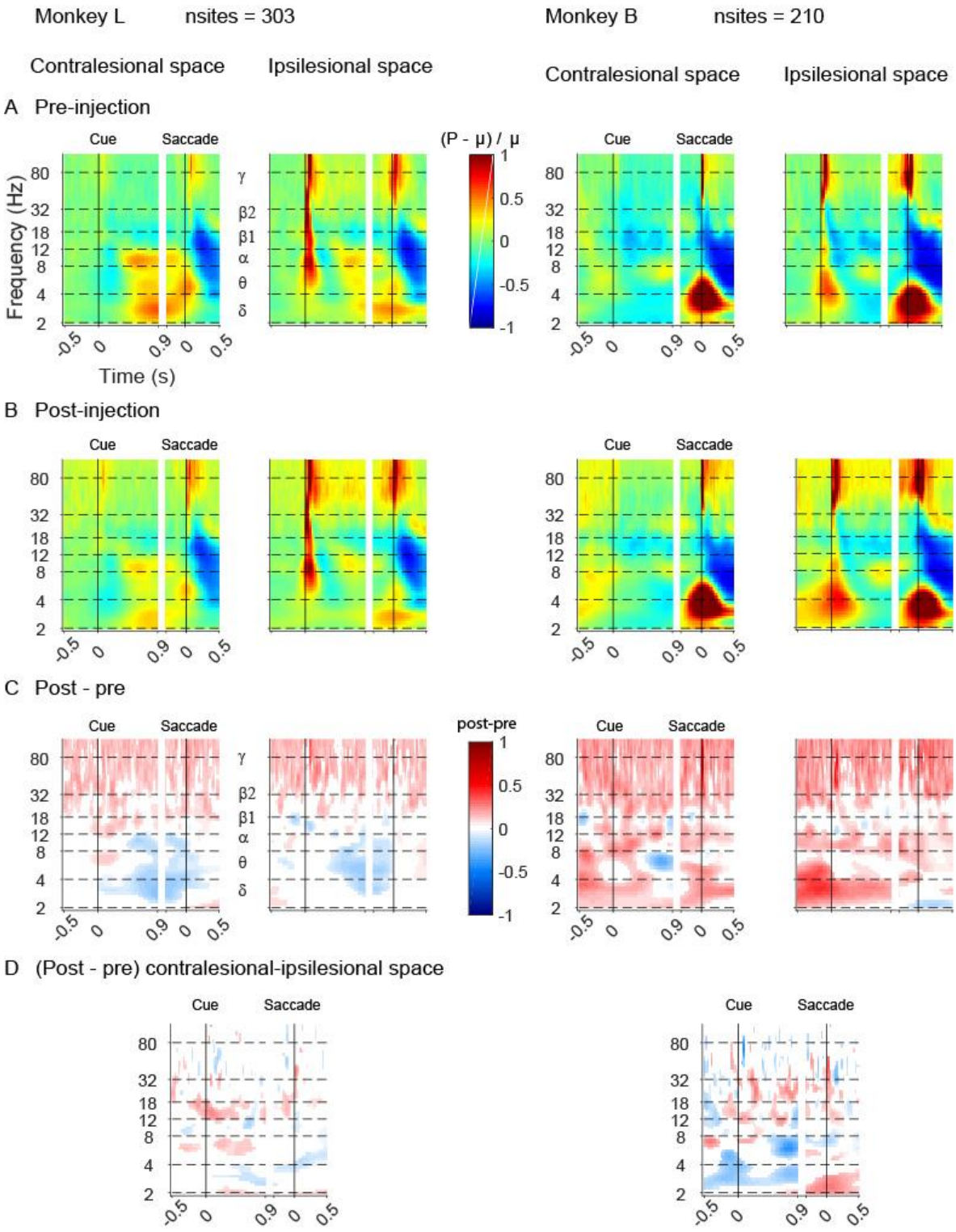

Figure 4.3.12. Effect of inactivation on LFP in the intact hemisphere during instructed trials (normalized by "pre-injection" block). A Time-frequency spectrogram in the pre-injection block. **B** Time-frequency spectrogram in the post-injection block. **C** Difference time-frequency spectrogram between pre- and post-injection. Only significant bins are shown (paired t-test with Bonferroni correction). **D** Difference time-frequency spectrogram between contralesional and ipsilesional of the difference between pre- and post-injection (C). Only significant bins are shown (paired t-test with Bonferroni correction).

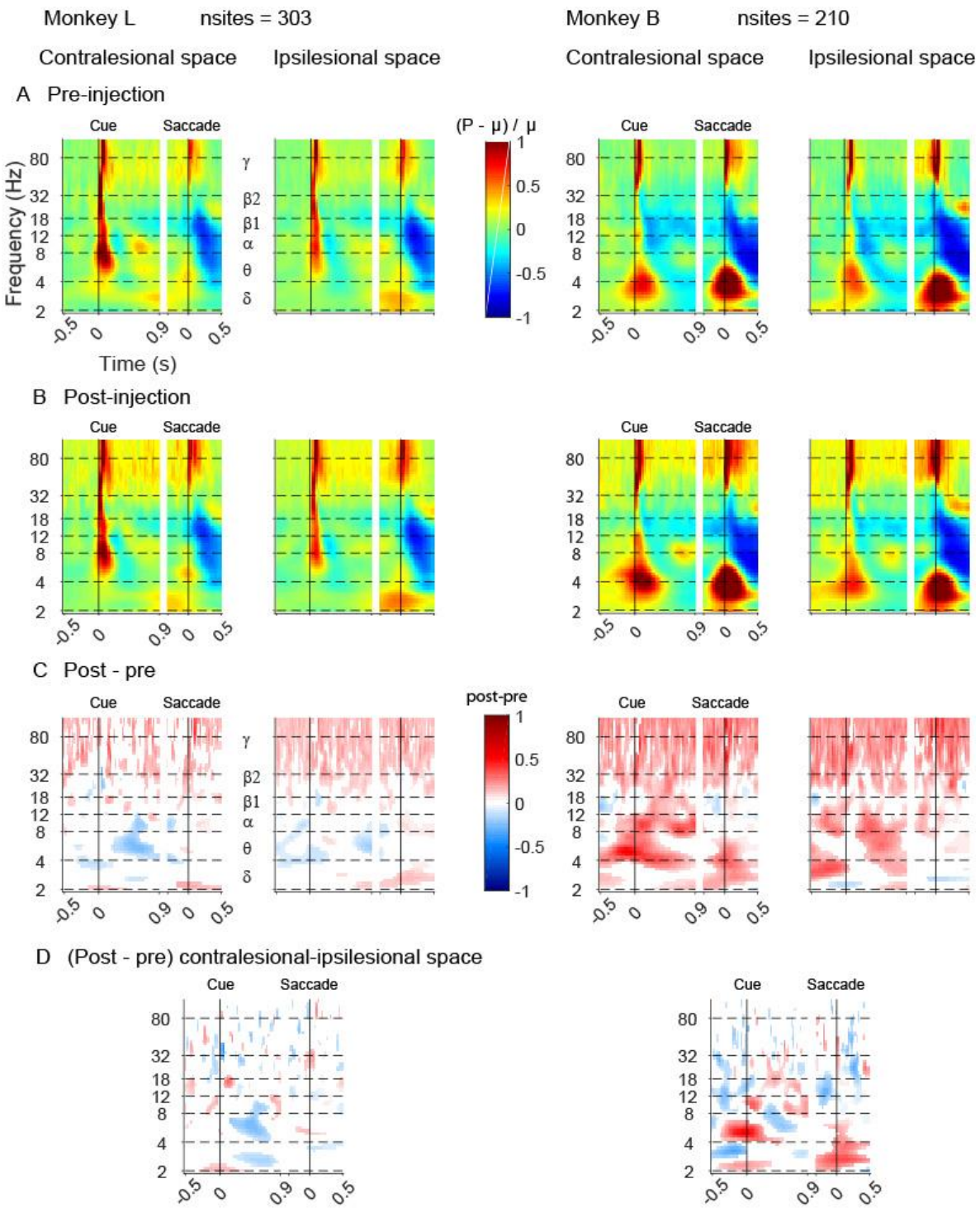

Figure 4.3.13. Effect of inactivation on LFP in the intact hemisphere during free-choice trials (normalized by "pre-injection" block). A Time-frequency spectrogram in pre-injection block. **B** Time-frequency spectrogram in post-injection block. **C** Difference time-frequency spectrogram between pre- and post-injection. Only significant bins are shown (paired t-test with Bonferroni correction). **D** Difference time-frequency spectrogram between contralesional and ipsilesional of the difference between pre- and post-injection (C). Only significant bins are shown (paired t-test with Bonferroni correction).

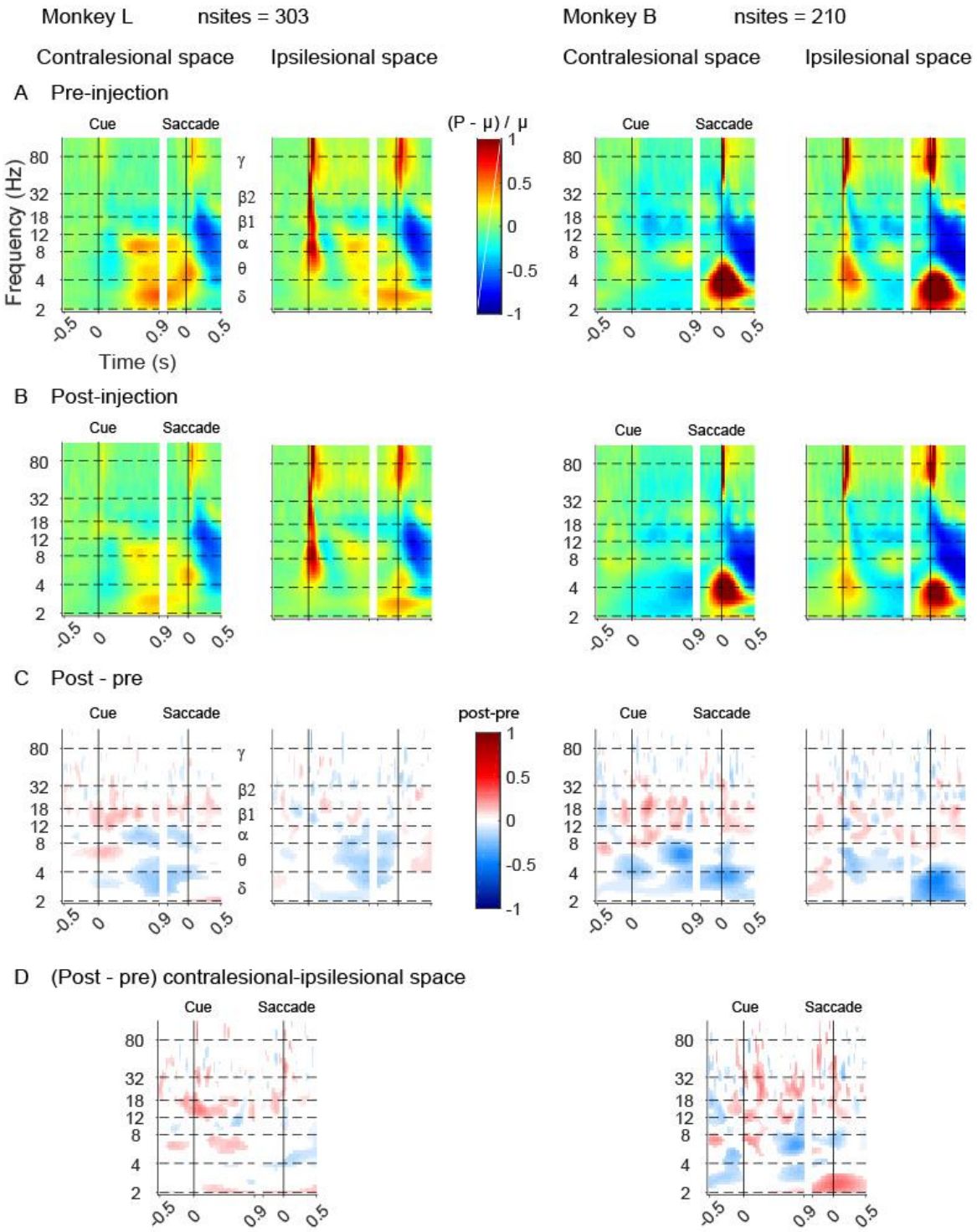

Figure 4.3.14. Effect of inactivation on LFP in the intact hemisphere during instructed trials (normalized within blocks). A Time-frequency spectrogram in the pre-injection block. **B** Time-frequency spectrogram in the post-injection block. **C** Difference time-frequency spectrogram between pre- and post-injection. Only significant bins are shown (paired t-test with Bonferroni correction). **D** Difference time-frequency spectrogram between contralesional and ipsilesional of the difference between pre- and post-injection (C). Only significant bins are shown (paired t-test with Bonferroni correction).

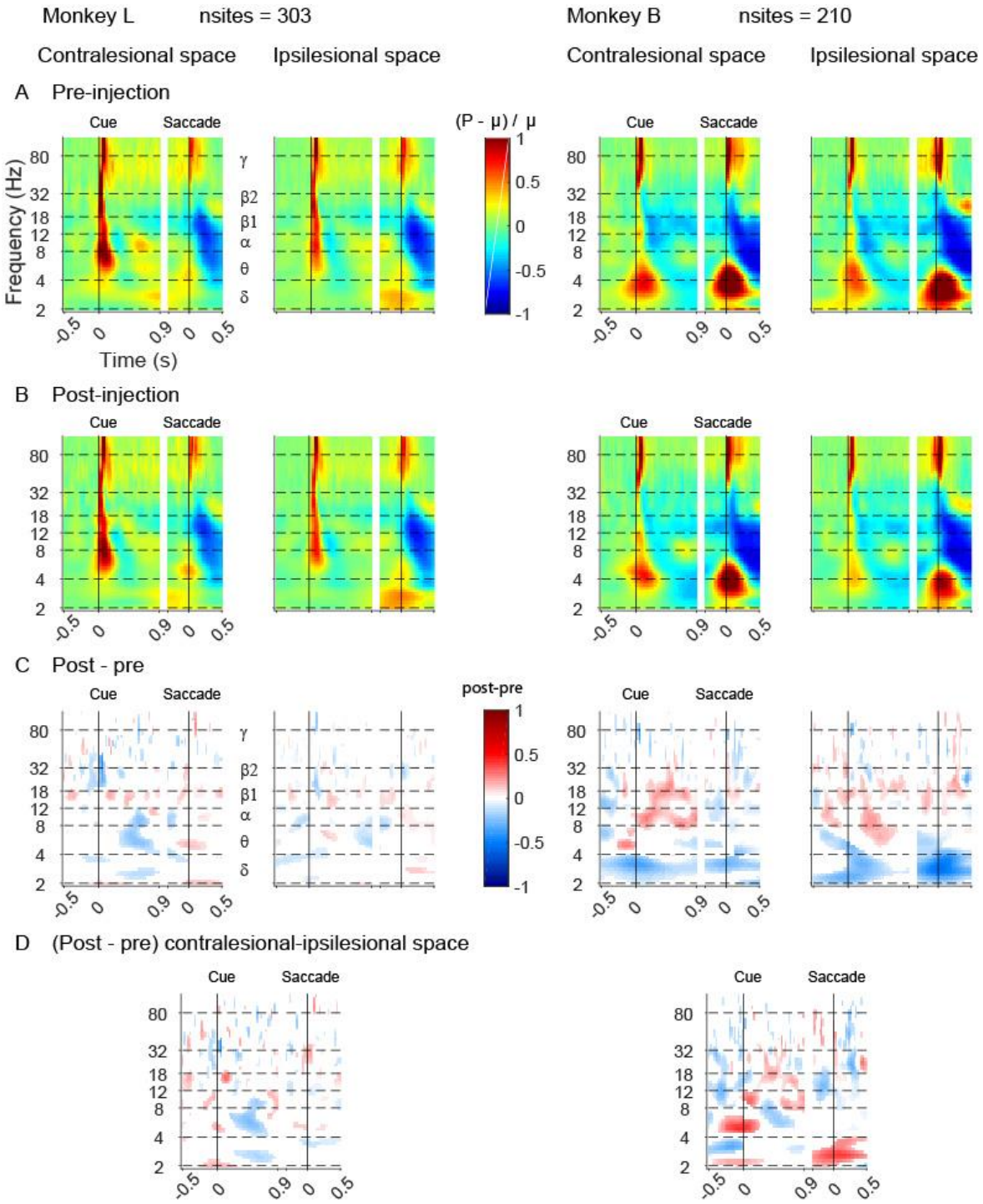

Figure 4.3.15. Effect of inactivation on LFP in the intact hemisphere during free-choice trials (normalized within blocks). A Time-frequency spectrogram in the pre-injection block. **B** Time-frequency spectrogram in the post-injection block. **C** Difference time-frequency spectrogram between pre- and post-injection. Only significant bins are shown (paired t-test with Bonferroni correction). **D** Difference time-frequency spectrogram between contralesional and ipsilesional of the difference between pre- and post-injection (C). Only significant bins are shown (paired t-test with Bonferroni correction).

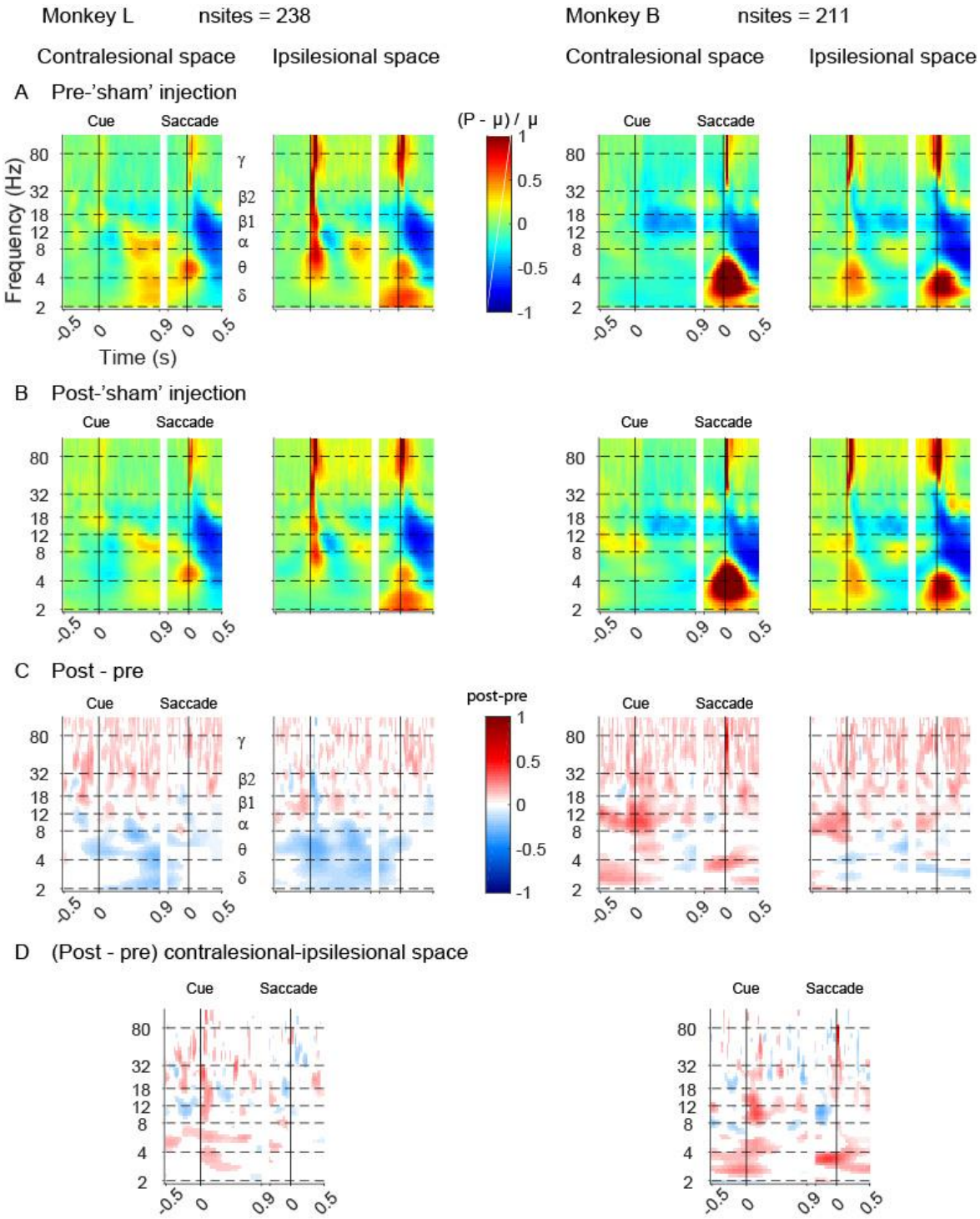

Figure 4.3.16. Control sessions: LFP in the 'intact' hemisphere in instructed trials (normalized on pre- 'sham' injection). A Time-frequency spectrogram in the pre- 'sham' injection block. **B** Time-frequency spectrogram in the post- 'sham' injection block. **C** Difference time-frequency spectrogram between pre- and post- 'sham' injection. Only significant bins are shown (paired t-test with Bonferroni correction). **D** Difference time-frequency spectrogram between contralesional and ipsilesional of the difference between pre- and post- 'sham' injection (C). Only significant bins are shown (paired t-test with Bonferroni correction).

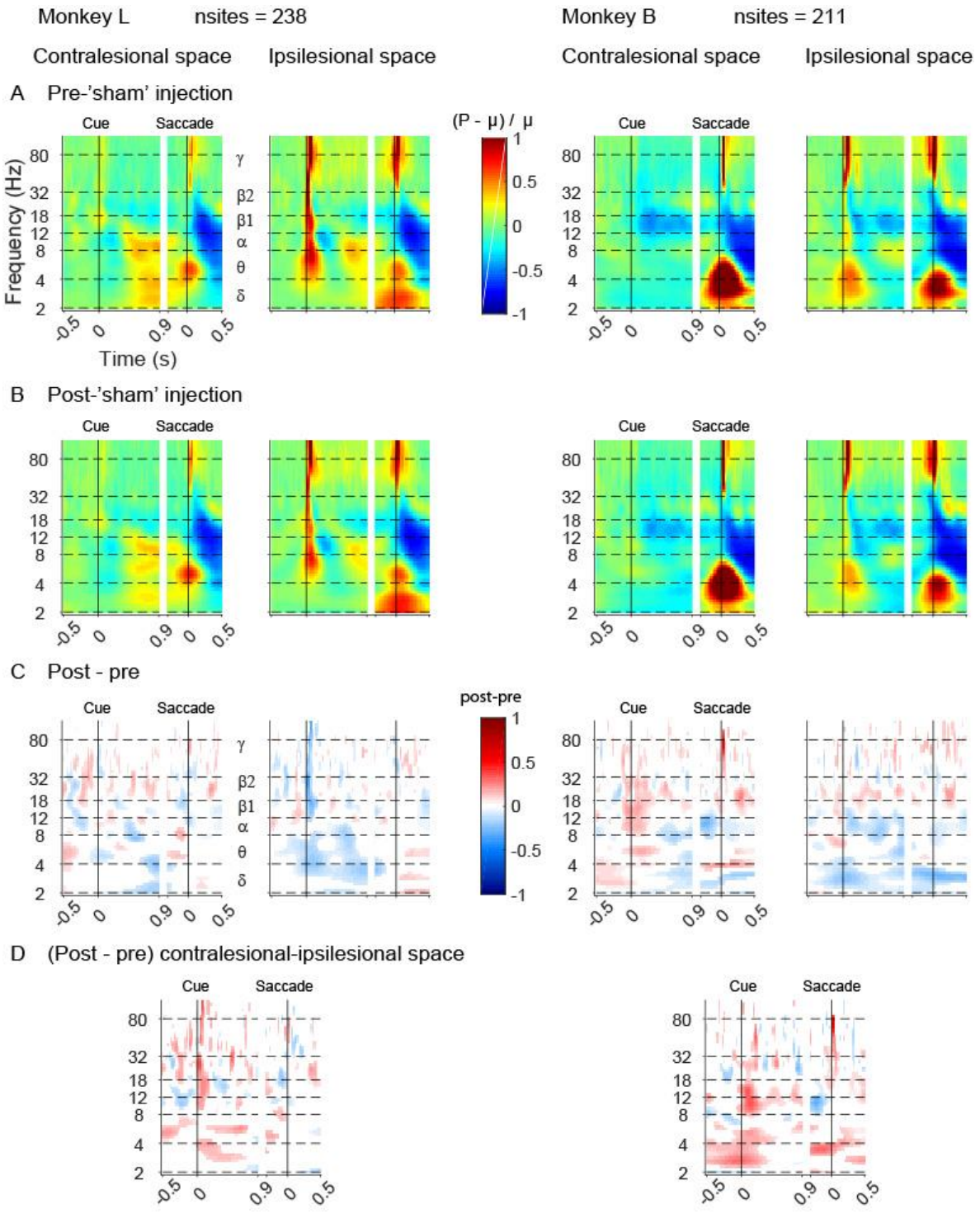

Figure 4.3.17. Control sessions: LFP in the 'intact' hemisphere in instructed trials (normalized within blocks). **A** Time-frequency spectrogram in the pre- 'sham' injection block. **B** Time-frequency spectrogram in the post- 'sham' injection block. **C** Difference time-frequency spectrogram between pre- and post- 'sham' injection. Only significant bins are shown (paired t-test with Bonferroni correction). **D** Difference time-frequency spectrogram between contralesional and ipsilesional of the difference between pre- and post- 'sham' injection (C). Only significant bins are shown (paired t-test with Bonferroni correction).

4.4.2.4 Summary of inactivation effects on LFP signals in both hemispheres

By looking at changes in power normalized by the baseline of the pre-injection block, we first observed in the inactivated hemisphere a general increase in low frequencies (delta, theta and alpha) in both monkeys, suggesting a decreased 'alert state' in the ipsilesional hemisphere after pulvinar inactivation. This effect was stronger (delta and theta) around saccades towards the contralesional space. However, we observed discrepancies between monkeys after cue presentation and during the delay period. Indeed, in monkey B, the increase was weaker when the upcoming saccade was towards the contralesional space. Nevertheless, this result is consistent with the idea that the pulvinar plays a role in maintaining cortical alertness. Secondly, we observed in both monkeys a decrease in beta power throughout the entire trial. Therefore, pulvinar inactivation induces synchronization alteration in the beta band, typically associated with movement preparation, independently of the task demand. However, we did observe a weaker decrease in monkey L shortly after contralesional cue presentation and in monkey B during delay before contralesional saccades, possibly reflecting space-specific alterations in the beta band. In the gamma band, we did not observe significant changes in monkey L. In monkey B, there was a general increased power but this was also the case in control session where we did not perform inactivation, suggesting signal instability rather than an inactivation effect. Consistently, there were no differences between contralesional and ipsilesional targets. Together, results suggest that the local processing reflected in gamma activity was not altered after inactivation.

We also looked at changes in power when both pre- and post-injection blocks were normalized to their own baseline. In delta/theta, we observed the opposite effect in both monkeys with an increased (monkey L) or decreased (monkey B) power after the cue and around the saccade. In alpha and beta, we observed an increased power shortly after cue presentation and during the delay period. Interestingly, this increase was stronger for instructed contralesional saccades, suggesting a space-specific alteration in movement preparation. Finally, the power in the gamma band was not altered in both monkeys. This result is consistent with findings using pre-injection baseline for normalization showing no alterations in higher frequencies.

Altogether, results show that dorsal pulvinar inactivation induces both global and space/task alterations in LFP synchronization. Indeed, we observed an increased delta, theta and alpha power as well as decreased beta power, suggesting a decreased cortical alertness and altered movement preparation respectively. In addition, we also observed stronger alterations in the beta band during the delay period before contralesional saccades, indicating some space-specific alterations in movement preparation.

In the intact hemisphere, we first observed a global increase of activity in the gamma band, independently of the target location or the task demand. This increase in activity might be due to the lack of inhibition from the inactivated hemisphere in the context of 'push-pull' interactions. Unlike the inactivated hemisphere, we did not see changes in the beta range when both blocks were normalized to the 'pre-injection' block and only a slight increase in monkey L after contralesional cue presentation. Therefore, movement preparation was mostly not altered in the intact hemisphere. Regarding the power in the alpha range, we did not see differences in monkey L and increased power in monkey B with no space-specificity. However, we also observed an alpha increase in control sessions, suggesting here again signal instability rather than activity alteration. Finally, in low frequencies (delta and theta), the power was decreased in monkey L and increased in monkey B when both blocks were normalized to the 'pre-injection' block. However, when each block was normalized to its own baseline, we observed a decreased power from target presentation to saccade onset. This result might reflect an opposite effect in the intact hemisphere with an increased level of cortical alertness during visuomotor transformation after inactivation. Together, the activity in the intact hemisphere was upregulated after pulvinar inactivation. Interestingly, we did not find any signs of compensation mechanisms in neuronal activity.

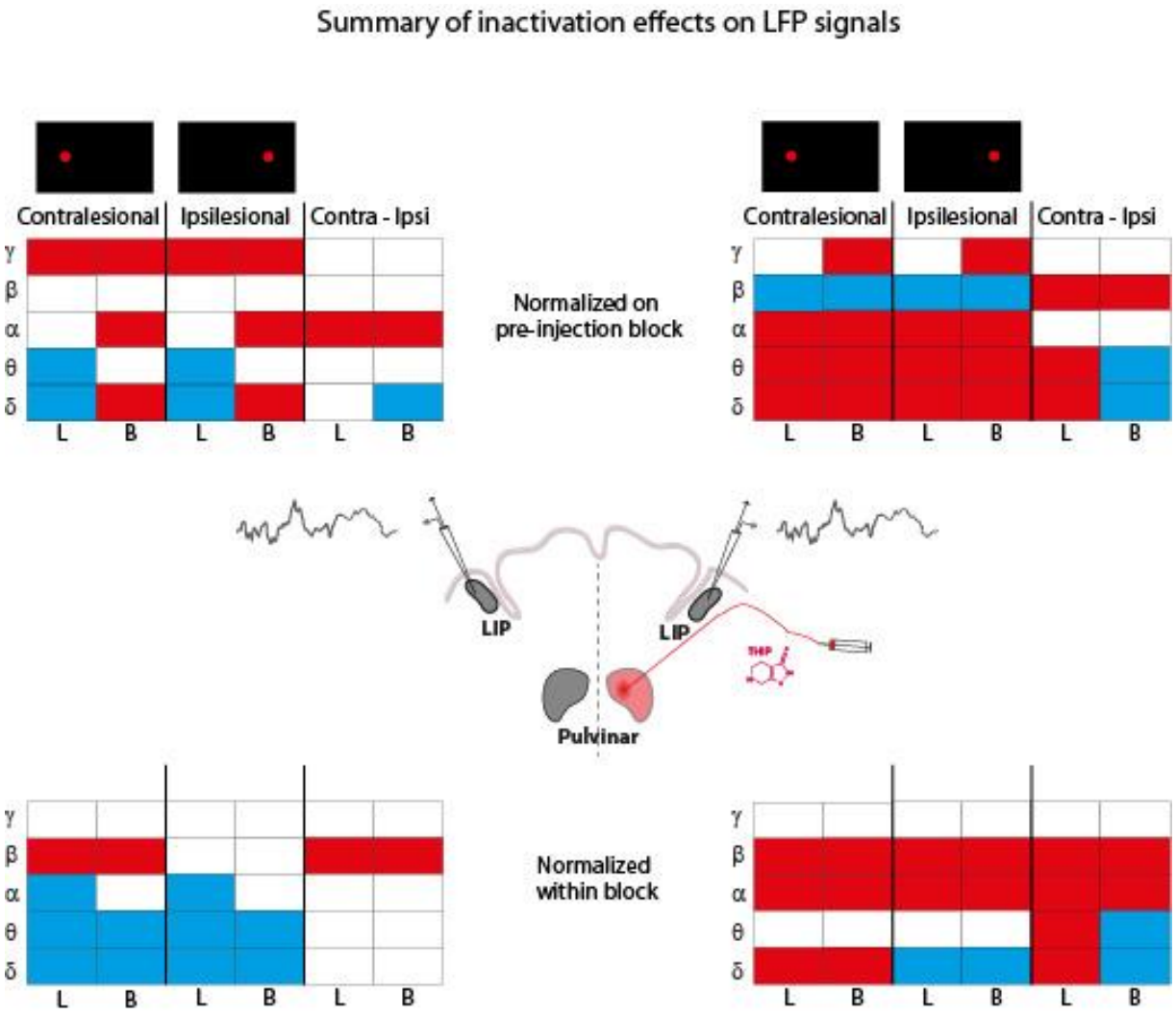

Figure 4.3.18. Summary of inactivation effects on LFP signals. Summarized inactivation effects in the contralesional (left panel) and ipsilesional (right panel) hemisphere with normalization based on the pre-injection block (top panel) and within blocks (bottom panel). Tables represent the inactivation effect for contralesional and ipsilesional targets as well as the differential effect between targets for both monkeys (L = Monkey L, B = monkey B). Red = increase, blue = decrease, white = no change.

4.4.3 Effect of inactivation on spiking activity in LIP

We recorded single and multi-unit activity in LIP in both hemispheres (Monkey L, intact: n=278; inactivated: n=297; monkey B, intact: n=124, inactivated: n=95) before and after unilateral dorsal pulvinar inactivation during delayed saccade task.

4.4.3.1 Example units

We observed in the inactivated hemisphere a variety of effects on spiking activity. First of all, some units (19% in monkey L and 7% in monkey B). did not show any changes in their firing rate after injection (Figure 4.4.1: top left and right). Therefore, the vast majority of recorded units (81%

in monkey L and 93% in monkey B) showed modulation of their spiking activity after dPul inactivation. Interestingly, we observed both increased (middle right and bottom left) and decreased (middle left and right bottom) either throughout the trial or at specific epoch(s). As an example, 28% of units in monkey L and 44% in monkey B showed a significant modulation of their spiking activity in free-choice trials during the cue epoch after baseline subtraction, indicating modulation going beyond baseline shift. Interestingly, in the same condition, we found more frequently a decreased (17% in monkey L and 35% in monkey B) rather than increased activity (11% and 9%).

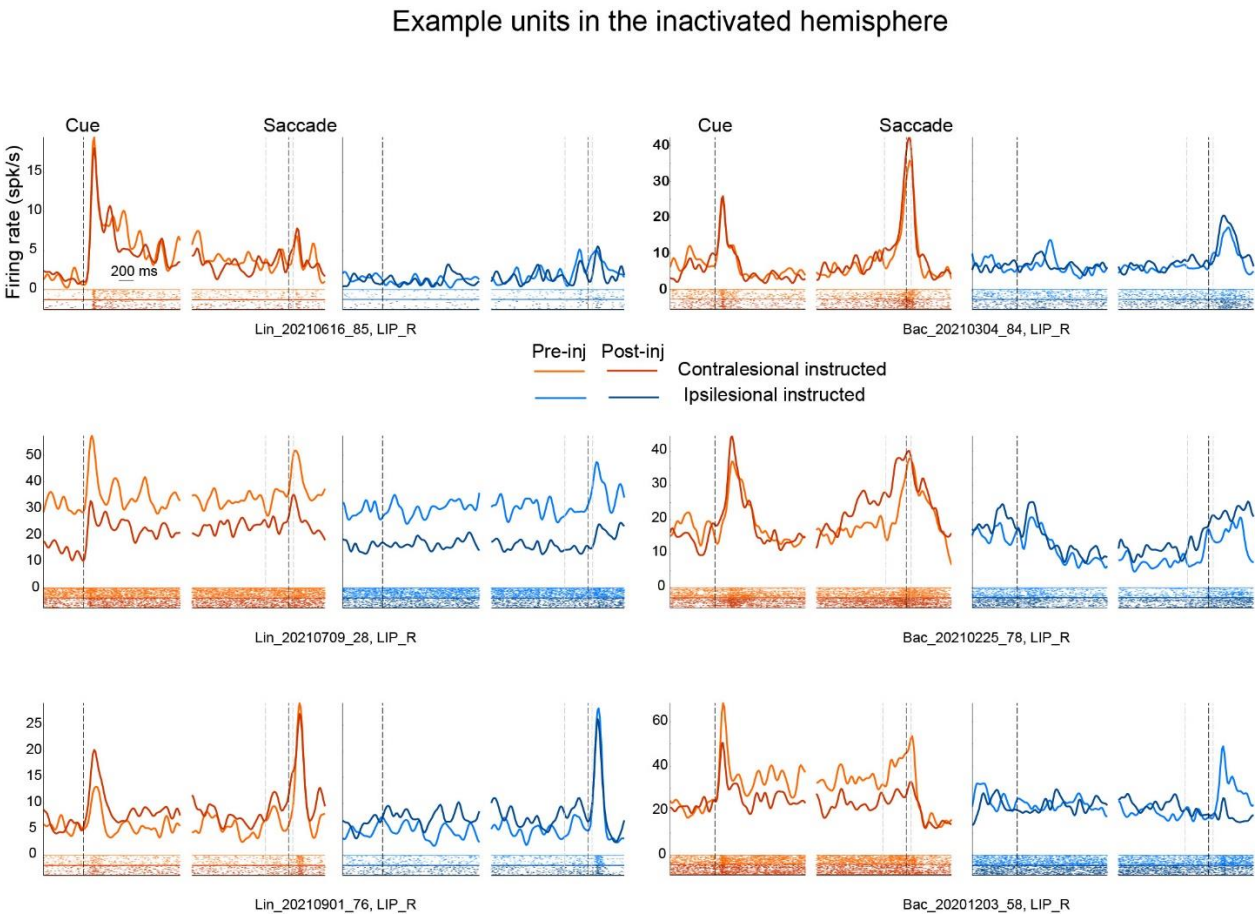

Figure 4.4.1. Example units spiking activity in the inactivated hemisphere in both monkeys, pre- and post-injection. Average spike density across trials and raster plots for single trials. Only instructed trials are shown (blue: ipsilateral, orange: contralateral, bright: pre-injection, dark: post-injection).

Interestingly, in the opposite hemisphere from inactivation, most units also showed modulation of their firing rate (79% in monkey L and 81% in monkey B). Like in the inactivated hemisphere, we observed heterogeneity in inactivation effects. For example, some units spiking activity was increased (Figure 4.4.2: top left) or decreased (middle left) after contralesional cue presentation. Some units showed a basal increase, either to both sides of space (top right) or specifically to

ipsilesional space (middle right). In addition, some units' activity was increased (bottom left) or decreased (bottom right) after stimuli onset and during the delay period when the target was located in the ipsilesional hemifield. In this line, 39% of units in monkey L and 60% in monkey B showed significant modulation in free-choice trials after baseline subtraction.

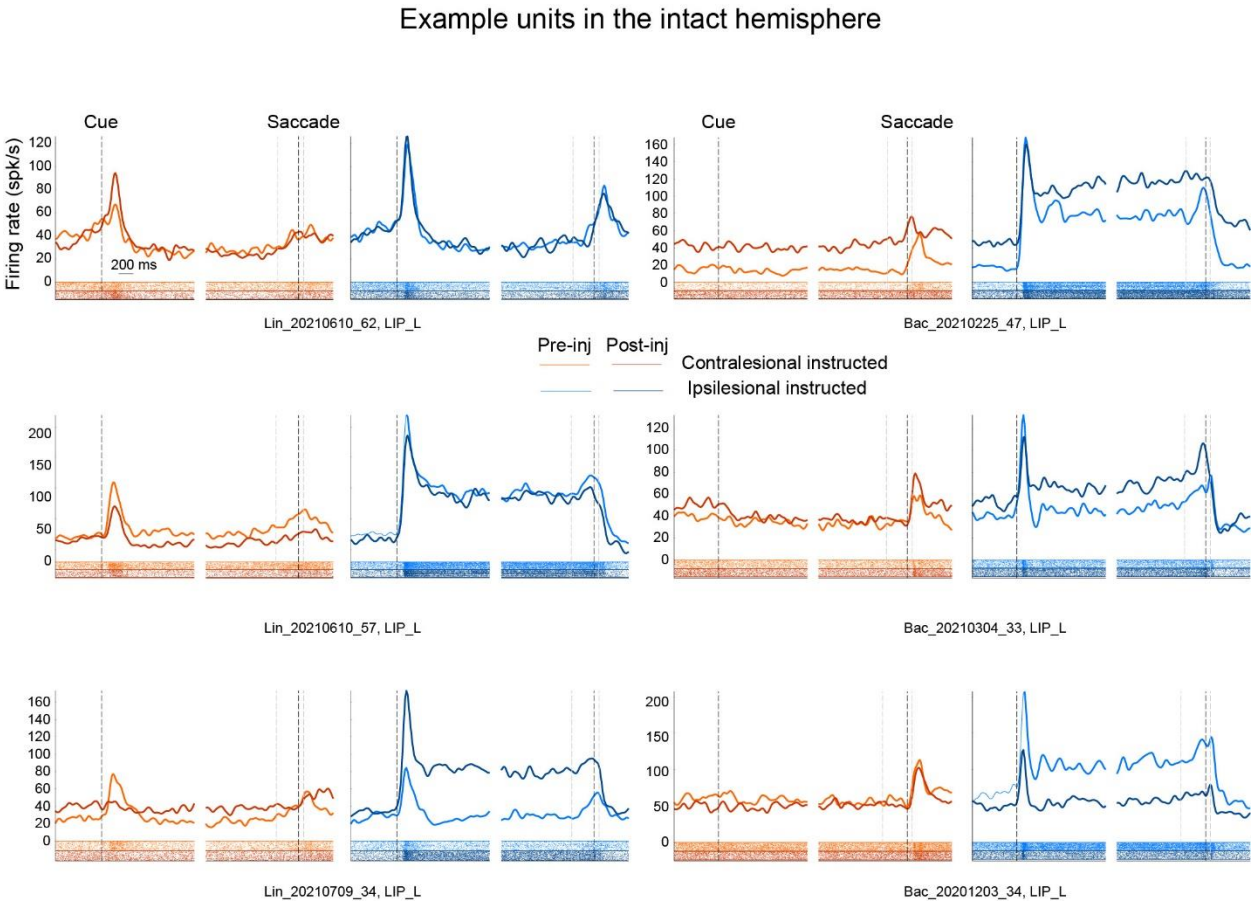

Figure 4.4.2. Example units spiking activity in the intact hemisphere in both monkeys, pre- and post-injection. Average spike density across trials and raster plots for single trials. Only instructed trials are shown (blue: ipsilateral, orange: contralateral, bright: pre-injection, dark: post-injection).

4.4.3.2 Entire population

After inactivation, we observed at the population level different effects in the inactivated hemisphere in both monkeys. In monkey L, the firing rate slightly increased (Figure 4.4.3) during instructed trials towards both sides of spaces. The firing rate was also increased in free-choice trials except in the cue and the pre-saccadic epoch when the upcoming saccade was toward contralesional space. After subtractive fixation baseline normalization (Figure 4.4.4), an increased firing rate was observed during cue, delay and post-saccadic epoch in instructed trials. Interestingly, there was a pre-saccadic decrease in normalized firing rate in ipsilesional instructed and free-choice trials ($p = 0.067$) trials. In monkey B, we observed a decreased firing rate in the

cue response to contralesional targets in instructed trials and during free-choice trials, independently of the upcoming choice. The spiking activity was also decreased before ipsilesional choices. Overall, in both monkeys, 10-30% of units showed task-related spiking activity modulation.

In the intact hemisphere, we observed an increased firing rate in both monkeys (Figure 4.4.4). The increased spiking activity was observed in instructed and free-choice trials in all epochs (apart from cue in monkey B). The global increase of spiking activity in the intact hemisphere is in line with the idea of push-pull interactions between the two hemispheres, at least in monkey B. On top of the global increase of activity, around half of recorded units showed modulation after baseline subtraction (Figure 4.4.6), either increased or decreased. For example, in free-choices trials, we found an equal proportion (around 20% in monkey L and 30% in monkey B) of units showing significantly increased or decreased activity after bilateral cue presentation.

Next, we evaluated the consequences of spiking activity alterations on the tuning index. In inactivated hemisphere, the tuning index in instructed trials was decreased (corresponding to decreased contralesional tuning) in cue and pre-saccadic epoch in monkey L but not in monkey B (Figure 4.4.7). In both monkeys, there were no tuning index alterations in free-choice trials. We also looked at the tuning index separately for units having a contralesional and ipsilesional preference. Interestingly, in both monkeys and both instructed and choice trials, we observed a decreased preferred tuning. In addition, the proportion of units tuned to contralesional and ipsilesional targets was altered after inactivation. For instance, during the delay period, 32% of units were tuned to instructed contralateral targets pre-injection versus 10% post-injection in monkey L and 24% versus 13% in monkey B. We observed comparable results for instructed ipsilesional targets and during free-choice trials. Together, the results suggest a loss of spatial tuning in the inactivated hemisphere.

In the intact hemisphere, we observed an increased tuning index (corresponding to decreased ipsilesional tuning) in monkey L in the cue and delay epoch during instructed trials (Figure 4.4.8). In monkey B, we did not see tuning index alterations. However, there was 41% of units tuned to ipsilateral instructed targets pre-injection versus 49% post-injection in monkey L and 35% versus 55% in monkey B. Therefore, results suggest an increased ipsilesional tuning in both monkeys after inactivation. It is possible that the lack of effect (or increase) on the tuning index resulted from the global increase of the firing rate (TI = (contra-ipsi)/(contra+ipsi)).

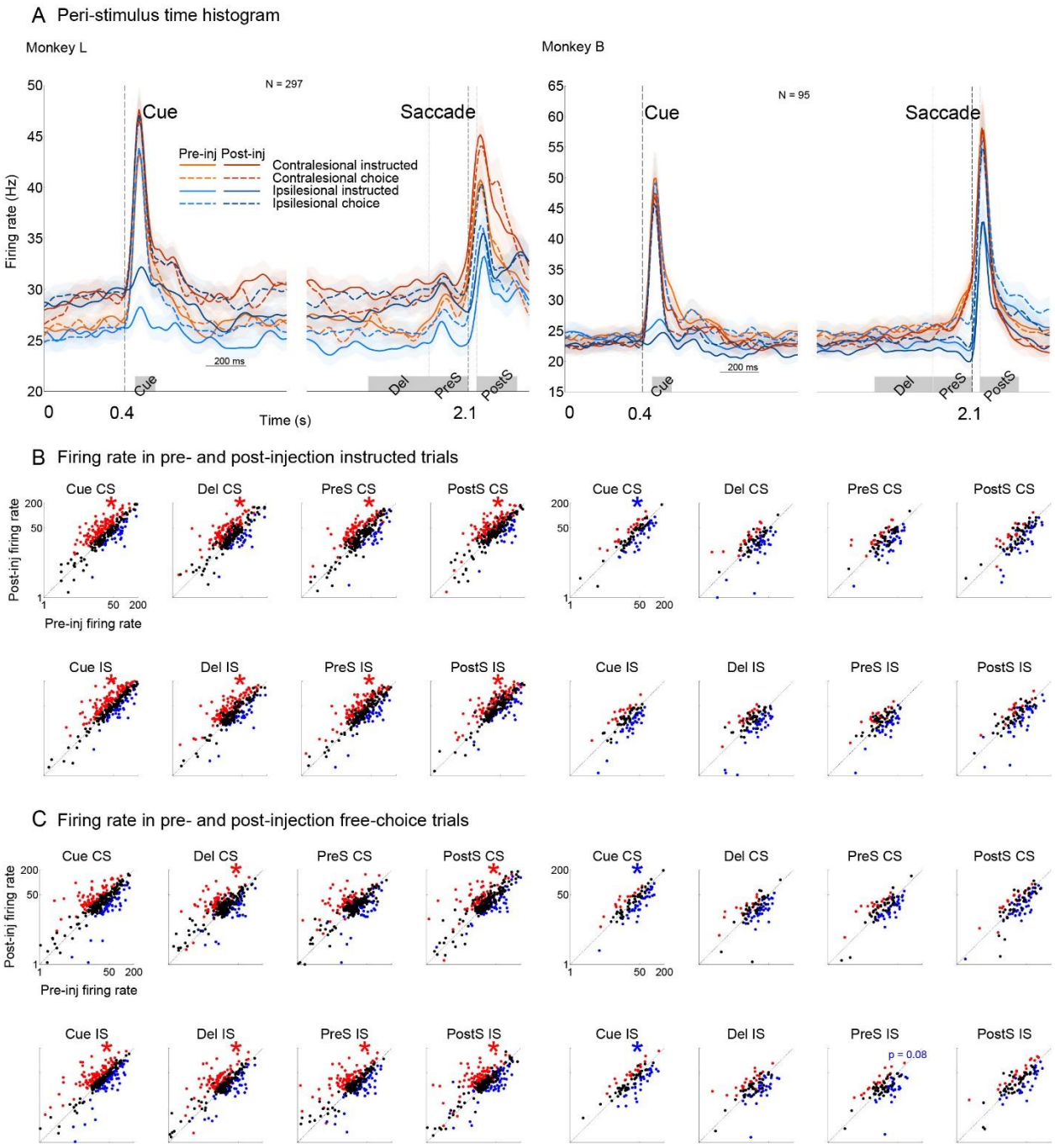

Figure 4.4.3. Effect of inactivation on spiking activity in the inactivated hemisphere. A Spike density average shown independently for instructed/free-choice (solid/dotted), contralesional/ipsilesional space (orange/blue) and pre-/post-injection (bright/dark). **B** Scatter plots comparing the firing rate in pre- and post-injection in analyzed epochs for instructed contralesional (top) and ipsilesional (bottom) targets. Per unit significance was calculated in the cue epoch (unpaired t-test, red: increase, blue: decrease). Population significance was calculated within each epoch (red: increase, blue: decrease, *: $p<0.05$). **C** Scatter plots comparing the firing rate in pre- and post-injection in analyzed epochs for choices towards contralesional (top) and ipsilesional (bottom) targets. Per unit significance was calculated in the cue epoch (unpaired t-test, red: increase, blue: decrease). Population significance was calculated within each epoch (red: increase, blue: decrease, *: $p<0.05$).

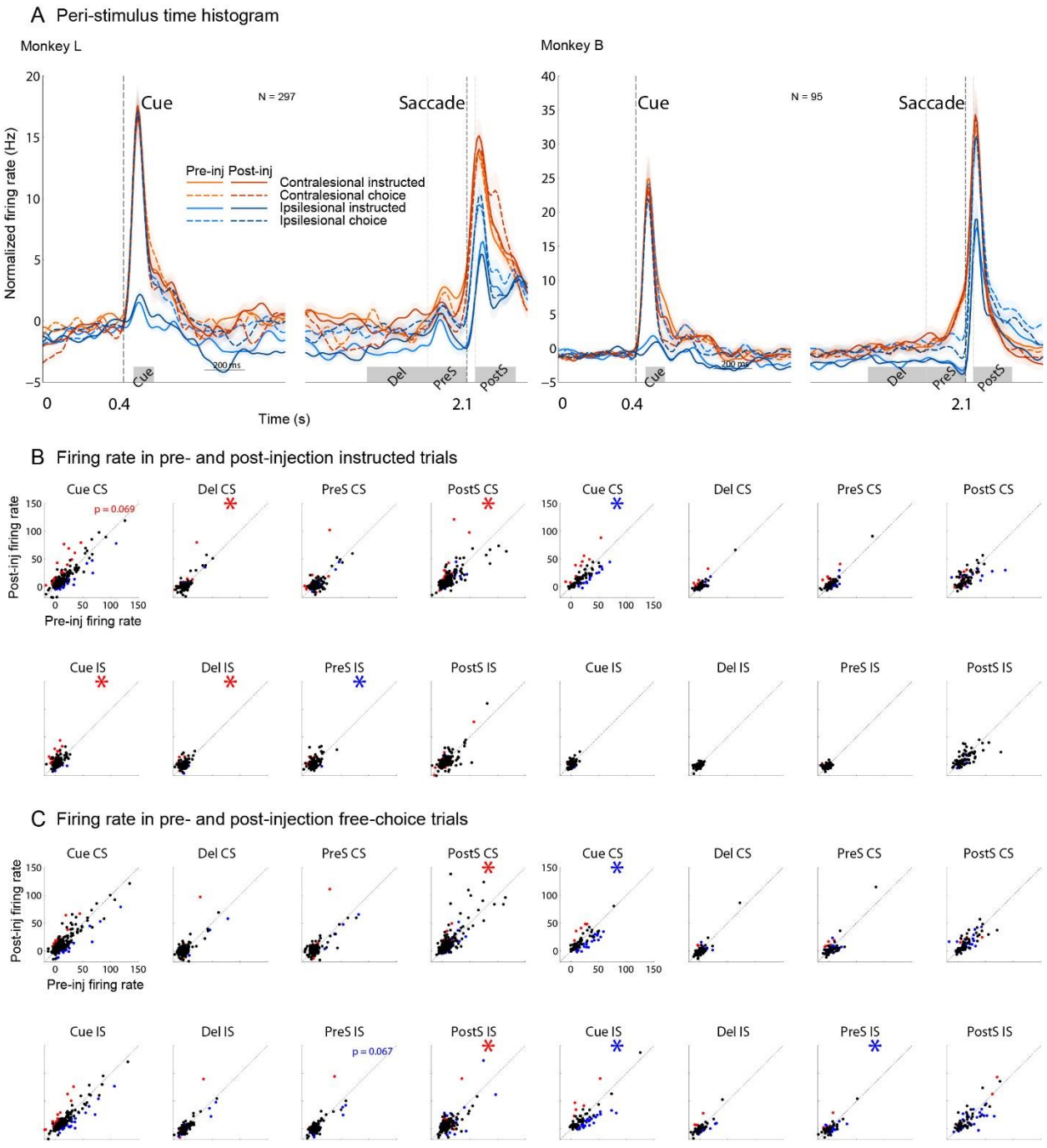

Figure 4.4.4. Effect of inactivation on normalized spiking activity in the inactivated hemisphere. A Spike density average shown independently for instructed/choice (solid/dotted), contralesional/ipsilesional space (orange/blue) and pre-/post-injection (bright/dark). **B** Scatter plots comparing the firing rate in pre- and post-injection in analyzed epochs for instructed contralesional (top) and ipsilesional (bottom) targets. Per unit significance was calculated in the cue epoch (unpaired t-test, red: increase, blue: decrease). Population significance was calculated within each epoch (red: increase, blue: decrease, *: $p<0.05$). **C** Scatter plots comparing the firing rate in pre- and post-injection in analyzed epochs for choices towards contralesional (top) and ipsilesional (bottom) targets. Per unit significance was calculated in the cue epoch (unpaired t-test, red: increase, blue: decrease). Population significance was calculated within each epoch (red: increase, blue: decrease, *: $p<0.05$).

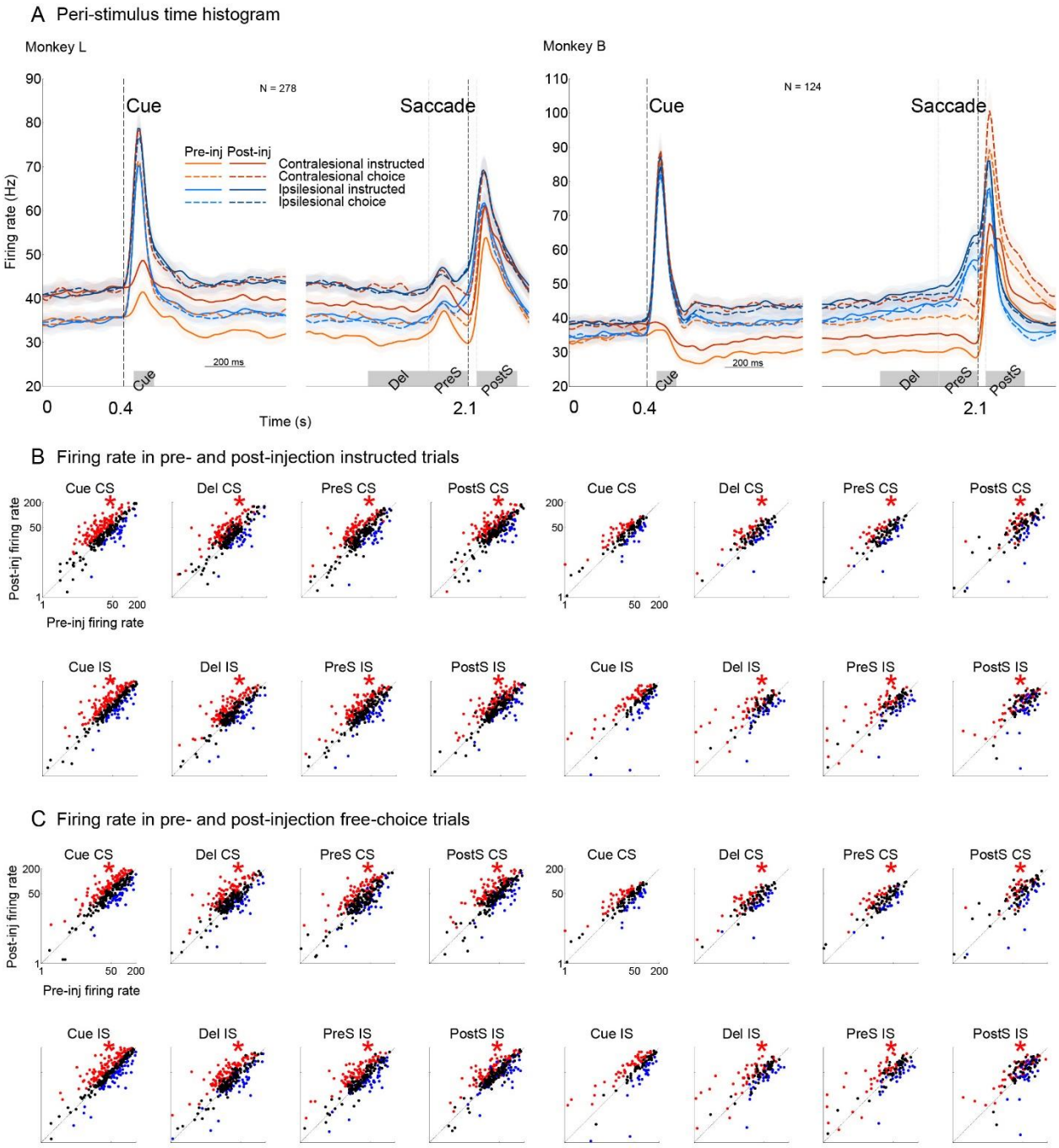

Figure 4.4.5. Effect of inactivation on spiking activity in the intact hemisphere. A Spike density average shown independently for instructed/free-choice (solid/dotted), contralesional/ipsilesional space (orange/blue) and pre-/post-injection (bright/dark). **B** Scatter plots comparing the firing rate in pre- and post-injection in analyzed epochs for instructed contralesional (top) and ipsilesional (bottom) targets. Per unit significance was calculated in the cue epoch (unpaired t-test, red: increase, blue: decrease). Population significance was calculated within each epoch (red: increase, blue: decrease, *: $p<0.05$). **C** Scatter plots comparing the firing rate in pre- and post-injection in analyzed epochs for choices towards contralesional (top) and ipsilesional (bottom) targets. Per unit significance was calculated in the cue epoch (unpaired t-test, red: increase, blue: decrease). Population significance was calculated within each epoch (red: increase, blue: decrease, *: $p<0.05$).

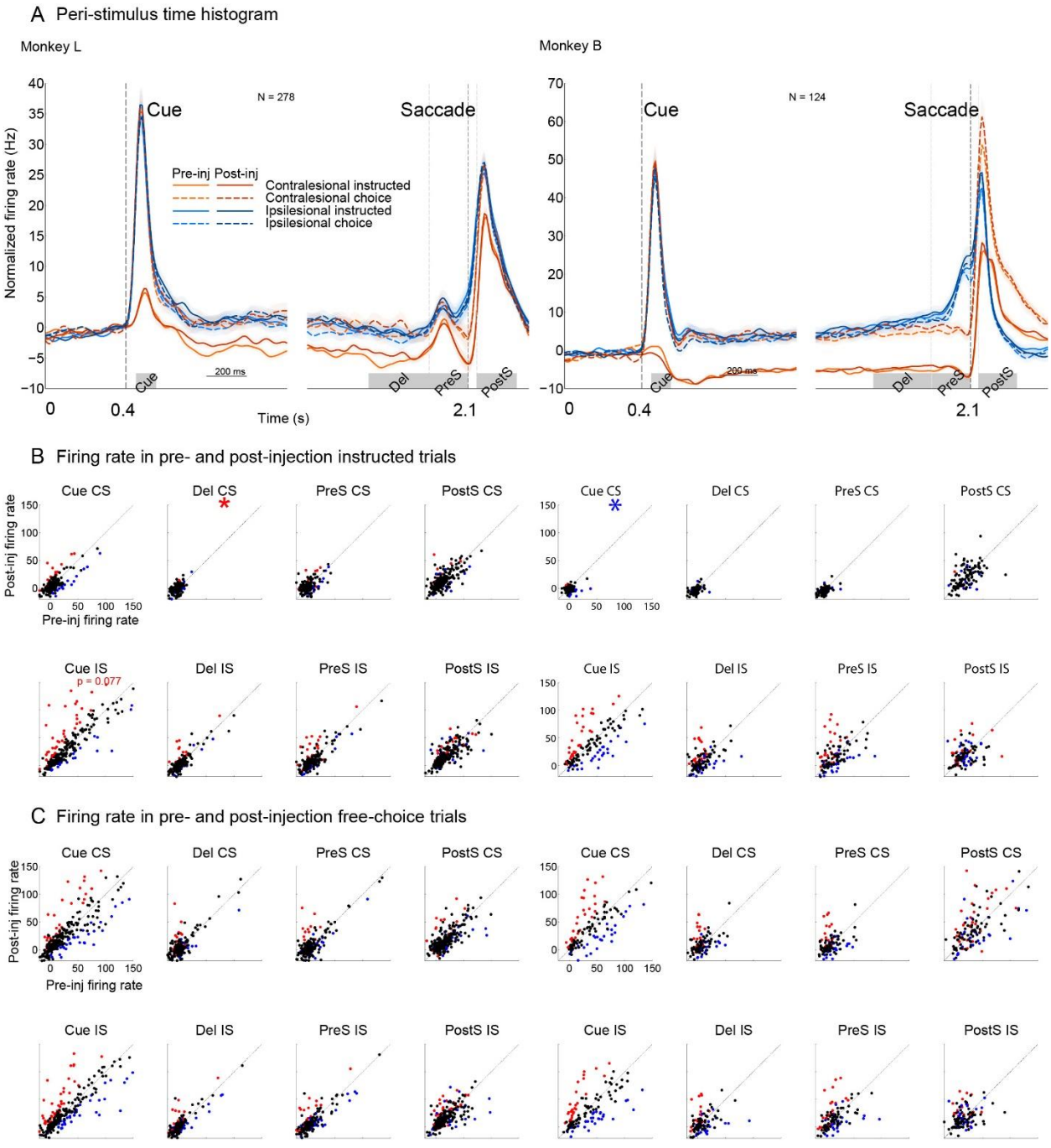

Figure 4.4.6. Effect of inactivation on normalized spiking activity in the intact hemisphere. A Spike density average shown independently for instructed/choice (solid/dotted), contralesional/ipsilesional space (orange/blue) and pre-/post-injection (bright/dark). **B** Scatter plots comparing the firing rate in pre- and post-injection in analyzed epochs for instructed contralesional (top) and ipsilesional (bottom) targets. Per unit significance was calculated in the cue epoch (unpaired t-test, red: increase, blue: decrease). Population significance was calculated within each epoch (red: increase, blue: decrease, *: $p<0.05$). **C** Scatter plots comparing the firing rate in pre- and post-injection in analyzed epochs for choices towards contralesional (top) and ipsilesional (bottom) targets. Per unit significance was calculated in the cue epoch (unpaired t-test, red: increase, blue: decrease). Population significance was calculated within each epoch (red: increase, blue: decrease, *: $p<0.05$).

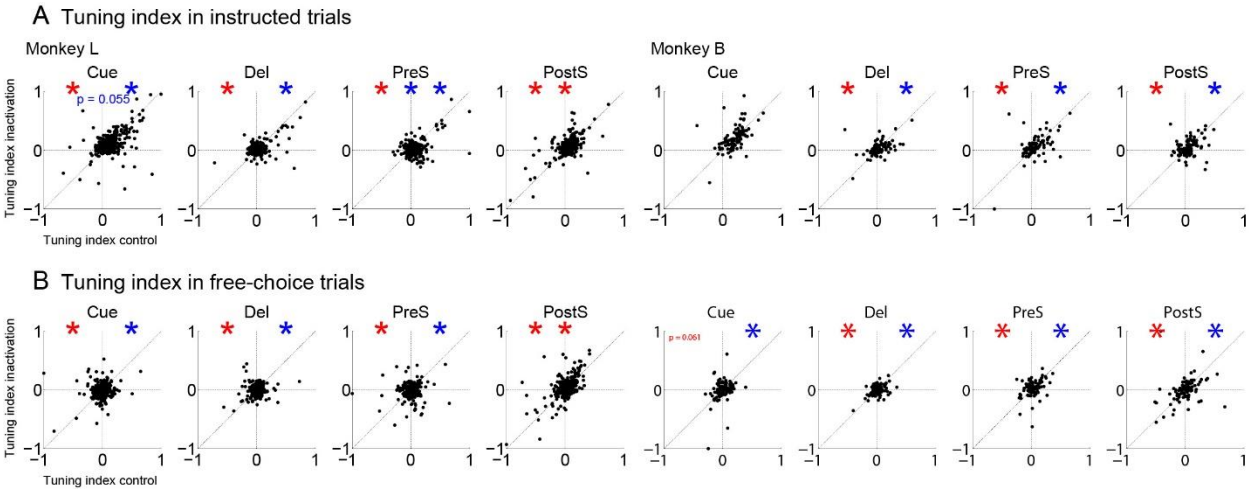

Figure 4.4.7. Effect of inactivation on the tuning index in the inactivated hemisphere. A Scatter plots comparing the tuning index pre- and post-injection during instructed trials. Statistics are shown for the population (center), for positive (right) and negative indices (left) (red: increase, blue: decrease, *: p<0.05). **B** Scatter plots comparing the tuning index pre- and post-injection during free-choice trials. Statistics are shown for the population (center), for positive (right) and negative indices (left) (red: increase, blue: decrease, *: p<0.05).

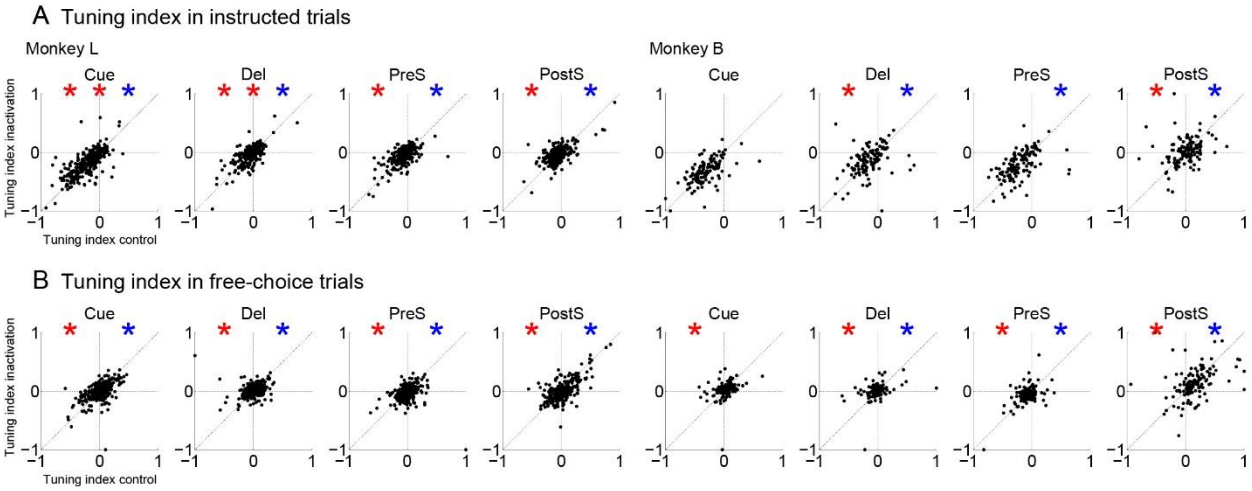

Figure 4.4.8. Effect of inactivation on the tuning index in the intact hemisphere. A Scatter plots comparing the tuning index pre- and post-injection during instructed trials. Statistics are shown for the population (center), for positive (right) and negative indices (left) (red: increase, blue: decrease, *: p<0.05). **B** Scatter plots comparing the tuning index pre- and post-injection during free-choice trials. Statistics are shown for the population (center), for positive (right) and negative indices (left) (red: increase, blue: decrease, *: p<0.05).

4.4.3.3 Visually responsive subpopulation

We then tried to assess how different subpopulations of neurons might be affected by the dorsal pulvinar inactivation. At first, we looked at visually responsive neurons in both hemispheres (Monkey L, intact: n=193 (69%); inactivated: n=166 (56%); monkey B, intact: n=101 (81%), inactivated: n=73 (77%)).

In the inactivated hemisphere (Figure4.4.9), the normalized firing rate was slightly increased during the delay for instructed trials in monkey L. In monkey B, the cue response to contralesional instructed targets was reduced. This was also the case for choice trials independently of the upcoming choice and before contralesional choices in monkey L (p-value = 0.06) Interestingly, we also observed a decreased activity in both monkeys during the pre-saccadic epoch before upcoming ipsilesional choices (p-value = 0.06 in monkey L). In the inactivated hemisphere, it is likely that a decreased activity in free-choice trials before the saccade onset leads to higher probability to select ipsilesional targets.

In the intact hemisphere (Figure 4.4.10), we did not see differences between pre-and post-injection blocks on the normalized activity averaged across visually responsive neurons apart from a decreased contralesional cue response during instructed trials in monkey B. However, many units showed a significant modulation of their activity after inactivation (~40%) either increased or decreased.

The tuning index of visually responsive neurons was also altered. In the inactivated (Figure 4.4.11), matching our expectations, we observed in monkey L a decreased tuning index (reflecting a decreased contralesional tuning) in both instructed and choice trials. In monkey B, this was only the case when looking specifically at units having a contralesional preference in the pre-injection block. In addition, and like at the level of the population, we found a lower fraction of tuned units (to either side of space) after inactivation.

In the intact hemisphere (Figure 4.4.12), we observed an increased tuning index (reflecting a decreased ipsilesional tuning) in instructed cue in monkey L as well as in delay in monkey B. In addition, the tuning index was also increased in monkey B during the delay before ipsilesional choices. However, we also found a higher fraction of units tuned to ipsilesional hemifield in instructed trials (47% versus 69% in monkey L and 39% vs 62% in monkey B).

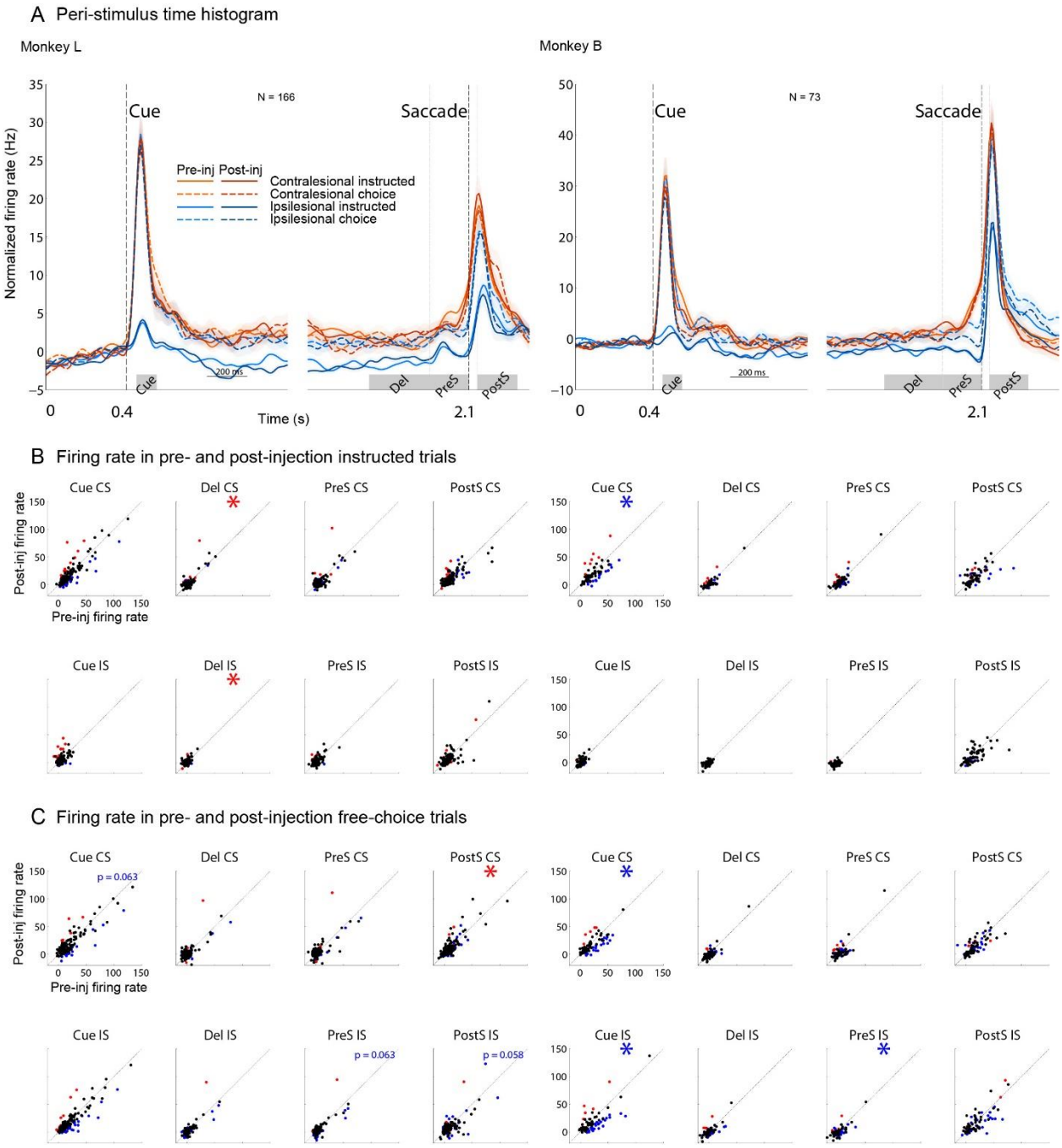

Figure 4.4.9. Effect of inactivation on visually responsive neurons normalized spiking activity in the inactivated hemisphere. **A** Spike density average shown independently for instructed/choice (solid/dotted), contralesional/ipsilesional space (orange/blue) and pre-/post-injection (bright/dark). **B** Scatter plots comparing the firing rate in pre- and post-injection in analyzed epochs for instructed contralesional (top) and ipsilesional (bottom) targets. Per unit significance was calculated in the cue epoch (unpaired t-test, red: increase, blue: decrease). Population significance was calculated within each epoch (red: increase, blue: decrease, *: p<0.05). **C** Scatter plots comparing the firing rate in pre- and post-injection in analyzed epochs for choices towards contralesional (top) and ipsilesional (bottom) targets. Per unit significance was calculated in the cue epoch (unpaired t-test, red: increase, blue: decrease). Population significance was calculated within each epoch (red: increase, blue: decrease, *: p<0.05).

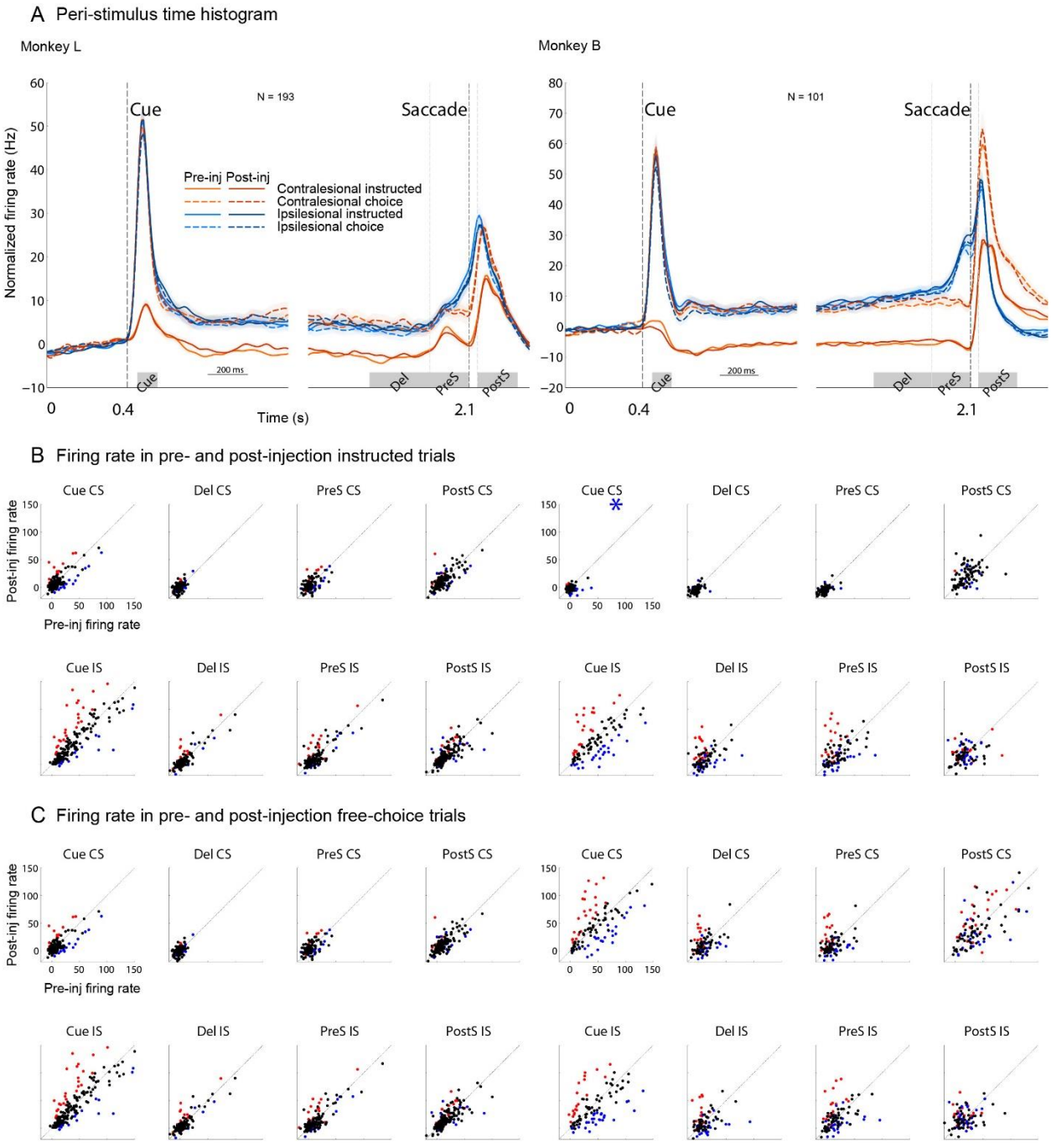

Figure 4.4.10. Effect of inactivation on visually responsive neurons normalized spiking activity in the intact hemisphere. A Spike density average shown independently for instructed/choice (solid/dotted), contralesional/ipsilesional space (orange/blue) and pre-/post-injection (bright/dark). **B** Scatter plots comparing the firing rate in pre- and post-injection in analyzed epochs for instructed contralesional (top) and ipsilesional (bottom) targets. Per unit significance was calculated in the cue epoch (unpaired t-test, red: increase, blue: decrease). Population significance was calculated within each epoch (red: increase, blue: decrease, *: $p<0.05$). **C** Scatter plots comparing the firing rate in pre- and post-injection in analyzed epochs for choices towards contralesional (top) and ipsilesional (bottom) targets. Per unit significance was calculated in the cue epoch (unpaired t-test, red: increase, blue: decrease). Population significance was calculated within each epoch (red: increase, blue: decrease, *: $p<0.05$).

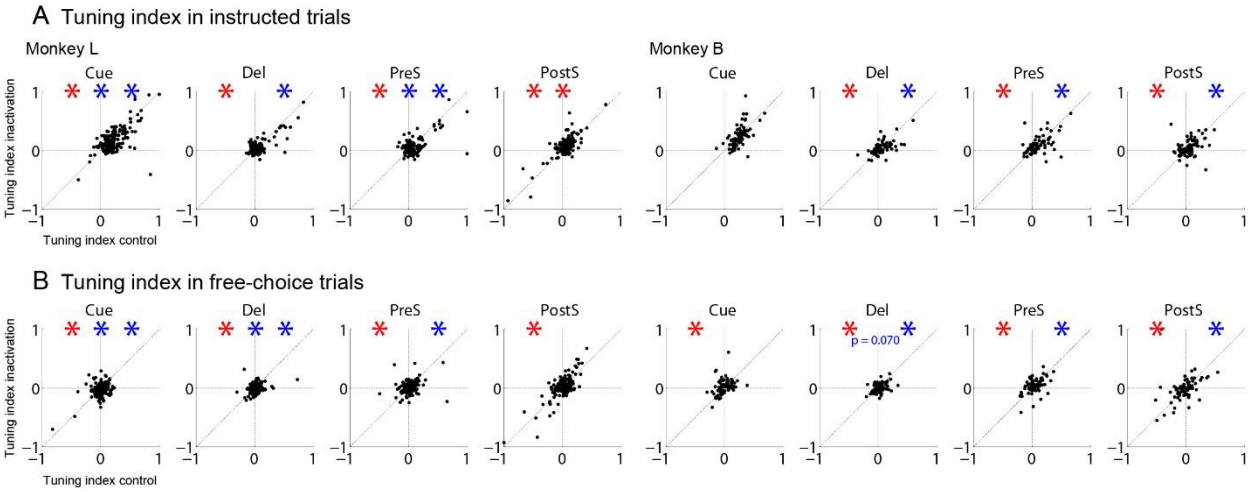

Figure 4.4.11. Effect of inactivation on the tuning index of visually responsive neurons in the inactivated hemisphere. A Scatter plots comparing the tuning index pre- and post-injection during instructed trials. Statistics are shown for the population (center), for positive (right) and negative indices (left) (red: increase, blue: decrease, *: p<0.05). **B** Scatter plots comparing the tuning index pre- and post-injection during free-choice trials. Statistics are shown for the population (center), for positive (right) and negative indices (left) (red: increase, blue: decrease, *: p<0.05).

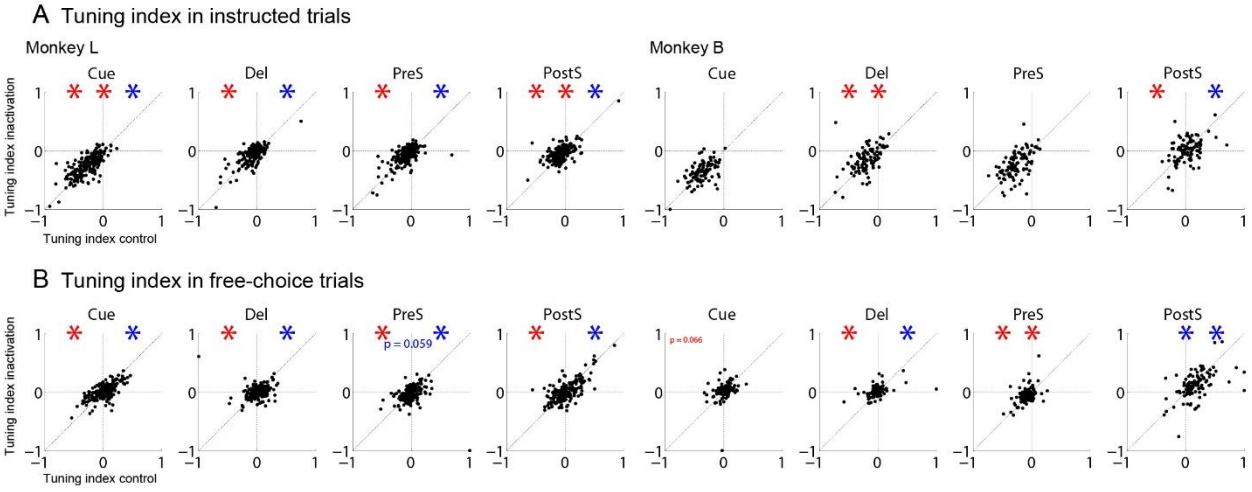

Figure 4.4.12. Effect of inactivation on the tuning index of visually responsive neurons in the inactivated hemisphere. A Scatter plots comparing the tuning index pre- and post-injection during instructed trials. Statistics are shown for the population (center), for positive (right) and negative indices (left) (red: increase, blue: decrease, *: p<0.05). **B** Scatter plots comparing the tuning index pre- and post-injection during free-choice trials. Statistics are shown for the population (center), for positive (right) and negative indices (left) (red: increase, blue: decrease, *: p<0.05).

4.4.3.4 Delay enhanced subpopulation

Finally, we evaluated the effect of inactivation on a subpopulation that showed enhanced activity during the delay period (monkey L, intact: n=64 (23%); inactivated: n=35 (12%); monkey B, intact: n=57(46%), inactivated: n=25 (26%)).

In the inactivated hemisphere, we observed a slight decrease in spiking activity during delay in instructed trials towards contralesional space in monkey B. Interestingly, we observed a decreased cue response as well as during delay and pre-saccadic epoch in choice trials before ipsilesional choices. In monkey L, we did not see changes apart from an increased response to instructed ipsilesional cue. The effect of inactivation on spiking activity in the inactivated hemisphere was mostly consistent across subpopulations analyzed.

In the intact hemisphere, we observed in both monkeys a decreased evoked response to instructed ipsilesional targets. We observed the same effect in choice trials, independently of the upcoming choice. In addition, we also observed in monkey B a decreased spiking activity during the pre-saccadic epoch, in both instructed ipsilesional targets and before ipsilesional choices. Interestingly, this effect was only observed in the subpopulation showing enhanced activity during the delay.

The tuning index was decreased (corresponding to a decreased contralesional tuning) in the inactivated hemisphere in both monkeys during instructed trials. More precisely, we saw an effect in the cue ($p=0.05$), in the pre-saccadic epoch in monkey L and during delay ($p=0.07$) as well as in the pre-saccadic epoch in monkey B. Consistently, the proportion of units tuned to instructed contralateral targets during the delay was 40% pre-injection versus 29% post-injection in monkey L and 50% versus 31% in monkey B. Like in the whole population and visually-responsive subpopulation, we also observe a decreased preferred tuning in choice trials.

In the intact hemisphere, the tuning was also altered with an increased tuning index (corresponding to decreased ipsilesional tuning) in instructed trials in both monkeys. In monkey L, the decreased ipsilesional tuning was observed in the cue, delay and pre-saccadic epoch. In monkey B, there was a significant ipsilesional tuning decrease in the delay and pre-saccadic epoch. Interestingly, we observed a comparable proportion of units tuned to ipsilesional targets during delay in monkey B (50% pre-injection versus 49% post-injection) and an increased proportion in monkey L (38% pre-injection versus 52% post-injection).

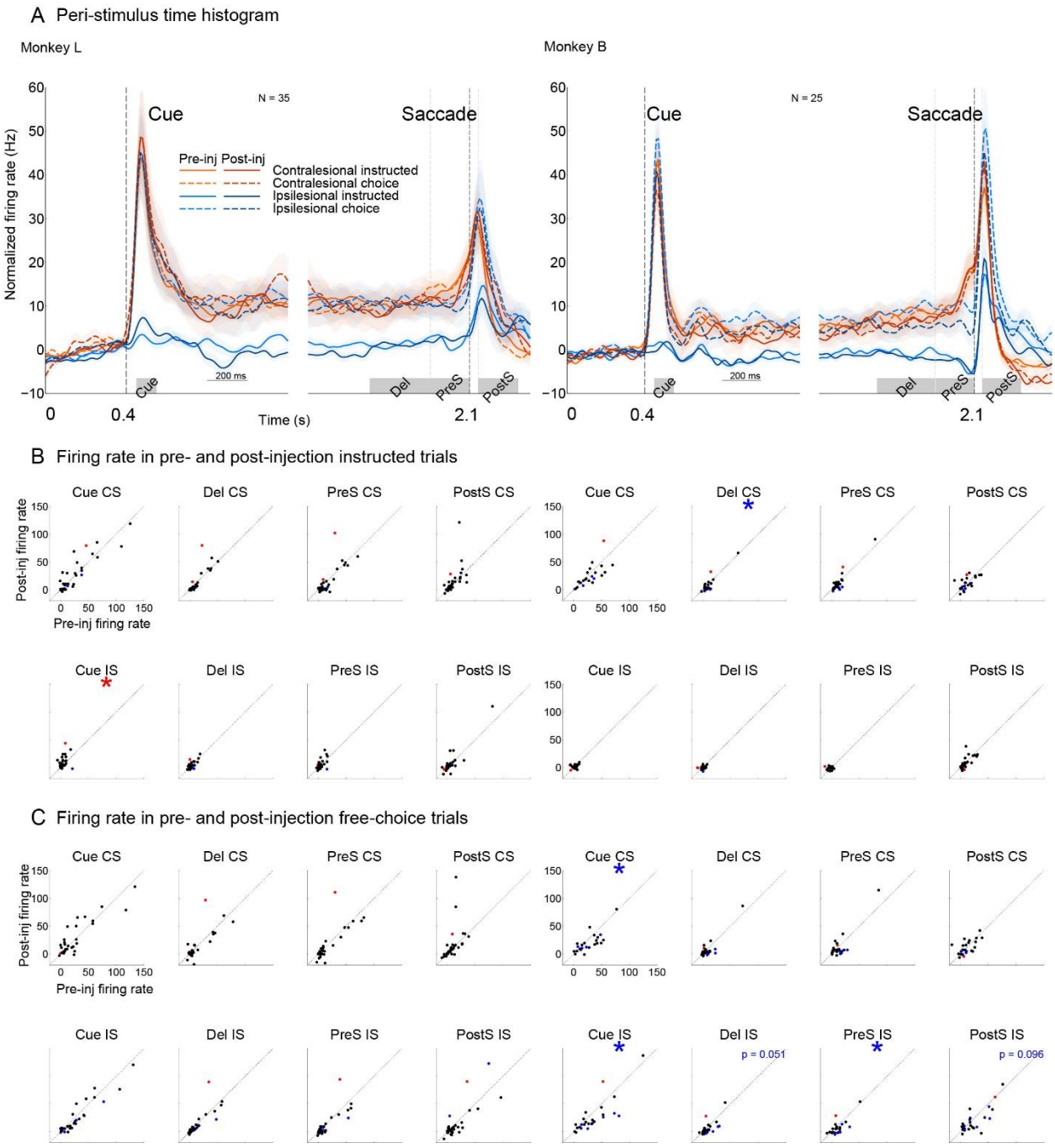

Figure 4.4.13. Effect of inactivation on delay enhanced neurons normalized spiking activity in the inactivated hemisphere. A Spike density average shown independently for instructed/choice (solid/dotted), contralesional/ipsilesional space (orange/blue) and pre-/post-injection (bright/dark). **B** Scatter plots comparing the firing rate in pre- and post-injection in analyzed epochs for instructed contralesional (top) and ipsilesional (bottom) targets. Per unit significance was calculated in the cue epoch (unpaired t-test, red: increase, blue: decrease). Population significance was calculated within each epoch (red: increase, blue: decrease, *: p<0.05). **C** Scatter plots comparing the firing rate in pre- and post-injection in analyzed epochs for choices towards contralesional (top) and ipsilesional (bottom) targets. Per unit significance was calculated in the cue epoch (unpaired t-test, red: increase, blue: decrease). Population significance was calculated within each epoch (red: increase, blue: decrease, *: p<0.05).

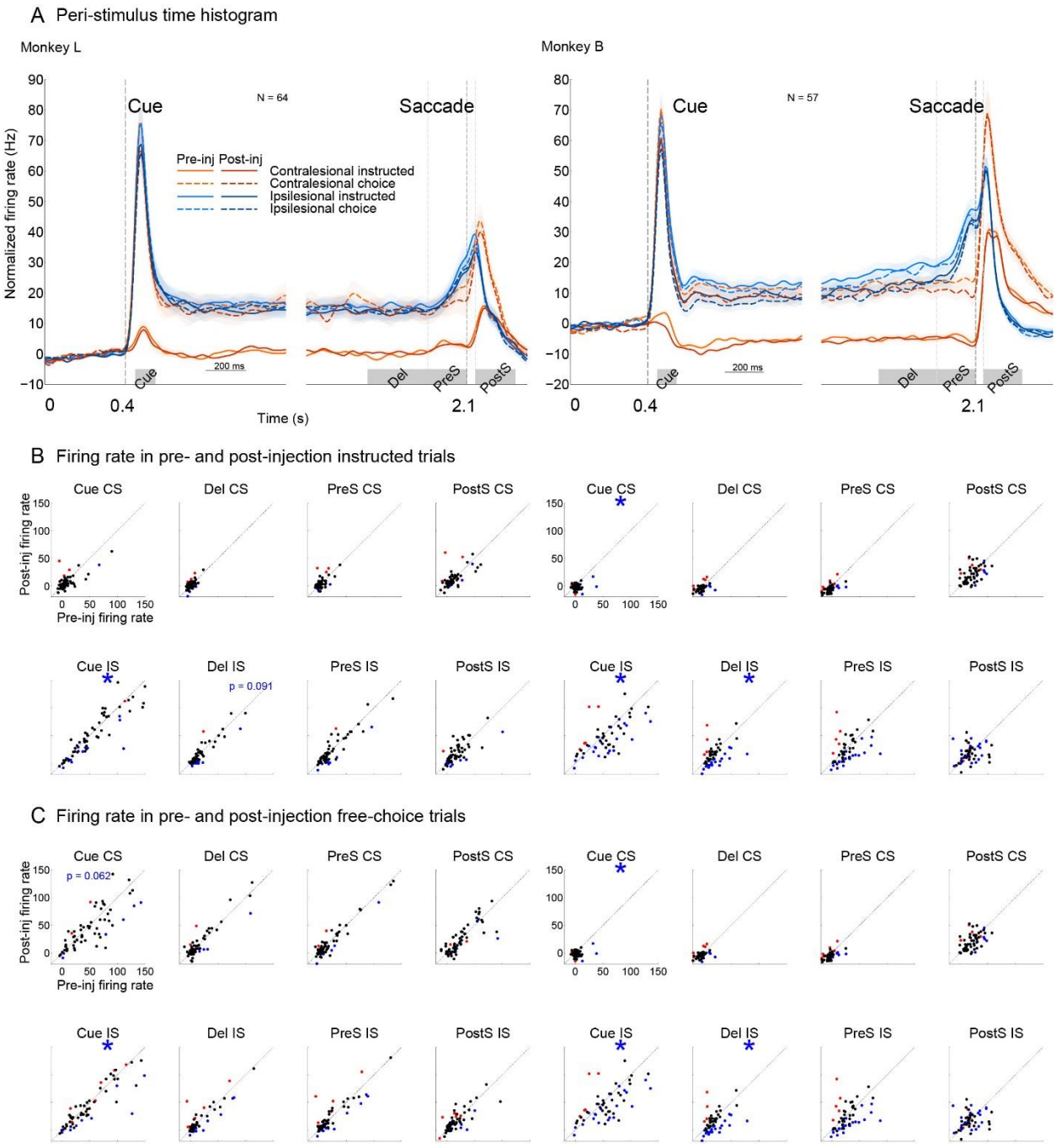

Figure 4.4.14. Effect of inactivation on delay enhanced neurons normalized spiking activity in the intact hemisphere. A Spike density average shown independently for instructed/choice (solid/dotted), contralesional/ipsilesional space (orange/blue) and pre-/post-injection (bright/dark). **B** Scatter plots comparing the firing rate in pre- and post-injection in analyzed epochs for instructed contralesional (top) and ipsilesional (bottom) targets. Per unit significance was calculated in the cue epoch (unpaired t-test, red: increase, blue: decrease). Population significance was calculated within each epoch (red: increase, blue: decrease, *: p<0.05). **C** Scatter plots comparing the firing rate in pre- and post-injection in analyzed epochs for choices towards contralesional (top) and ipsilesional (bottom) targets. Per unit significance was calculated in the cue epoch (unpaired t-test, red: increase, blue: decrease). Population significance was calculated within each epoch (red: increase, blue: decrease, *: p<0.05).

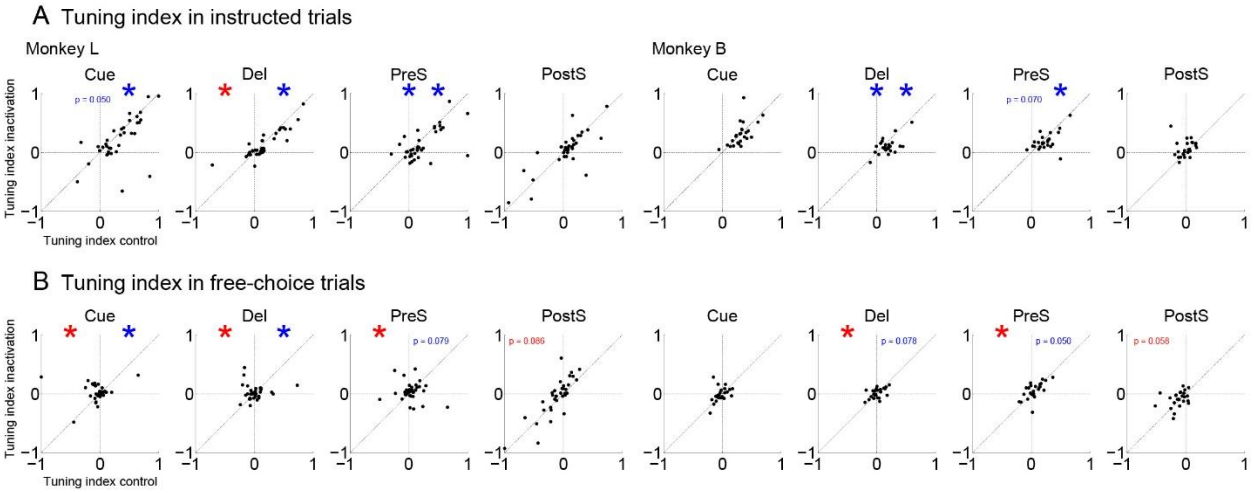

Figure 4.4.15. Effect of inactivation on the tuning index of delay enhanced neurons in the inactivated hemisphere. A Scatter plots comparing the tuning index pre- and post-injection during instructed trials. Statistics are shown for the population (center), for positive (right) and negative indices (left) (red: increase, blue: decrease, *: p<0.05). **B** Scatter plots comparing the tuning index pre- and post-injection during free-choice trials. Statistics are shown for the population (center), for positive (right) and negative indices (left) (red: increase, blue: decrease, *: p<0.05).

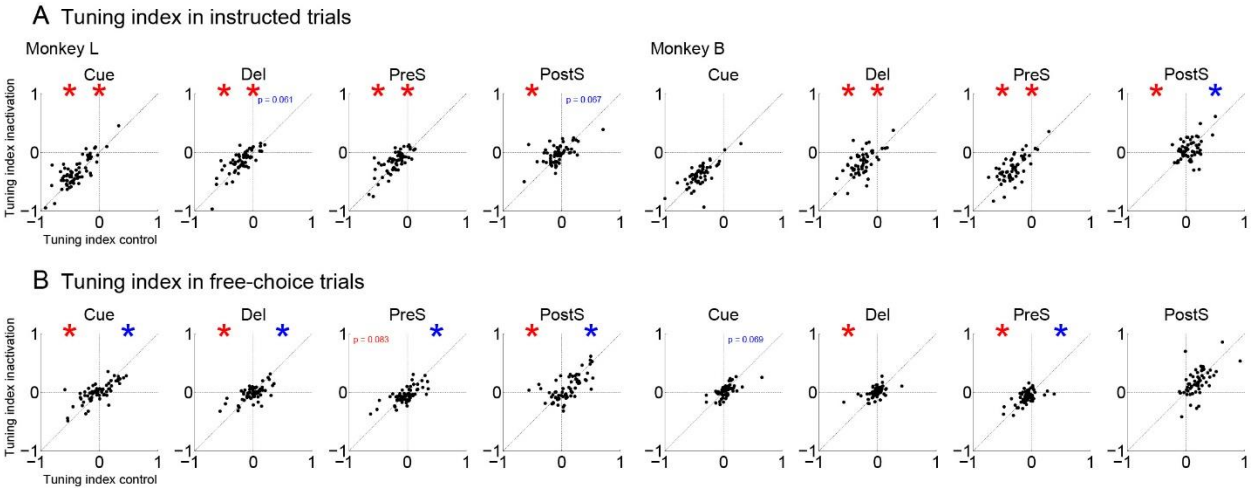

Figure 4.4.16. Effect of inactivation on the tuning index of delay enhanced neurons in the intact hemisphere. A Scatter plots comparing the tuning index pre- and post-injection during instructed trials. Statistics are shown for the population (center), for positive (right) and negative indices (left) (red: increase, blue: decrease, *: p<0.05). **B** Scatter plots comparing the tuning index pre- and post-injection during free-choice trials. Statistics are shown for the population (center), for positive (right) and negative indices (left) (red: increase, blue: decrease, *: p<0.05).

4.4.3.5 Summary of dPul inactivation on LIP spiking activity in both hemispheres

In the inactivated, we observed a differential effect of dPul inactivation on spiking activity in both monkeys (Figure 4.4.17). In monkey L, the raw firing rate was mostly increased with some units (~20%) showing additional task-specific modulation, leading to increased or decreased activity. In monkey B, we observed a specific decreased evoked response to contralateral targets

presentation. In addition, the firing rate was also decreased during the delay before ipsilesional free-choices. In contrast with the differential effect on the firing rate, we observed in both monkeys a loss of space tuning, for both hemifield during both instructed and free-choice trials. Firing rates and space tuning alterations were comparable between neuronal subpopulations, visually responsive, or showing increased activity during delay.

In the intact hemisphere, we observed in both monkeys an increased raw firing rate. The increase was mostly global but around 30% of units also showed some task-specific modulation. Interestingly, we found a higher proportion of neurons tuned to ipsilesional targets during the cue after inactivation in both monkeys. Surprisingly, this was not the case during free-choice trials where we saw decreased proportion before both contralesional and ipsilesional saccades.

Dorsal pulvinar inactivation led to neuronal activity modulation in both hemispheres. In the inactivated hemisphere, the specific contralesional decrease in monkey B and the loss of spatial tuning in both monkeys reflect deficits in sensory-motor processing of visual stimuli that are targets of an upcoming saccade when located in the contralesional hemifield. In the intact hemisphere, the global increase of spiking activity together with the increased ipsilesional tuning suggests disinhibition from the inactivated hemisphere during spatial target selection and is in line with the idea of push-pull interactions between the two hemispheres.

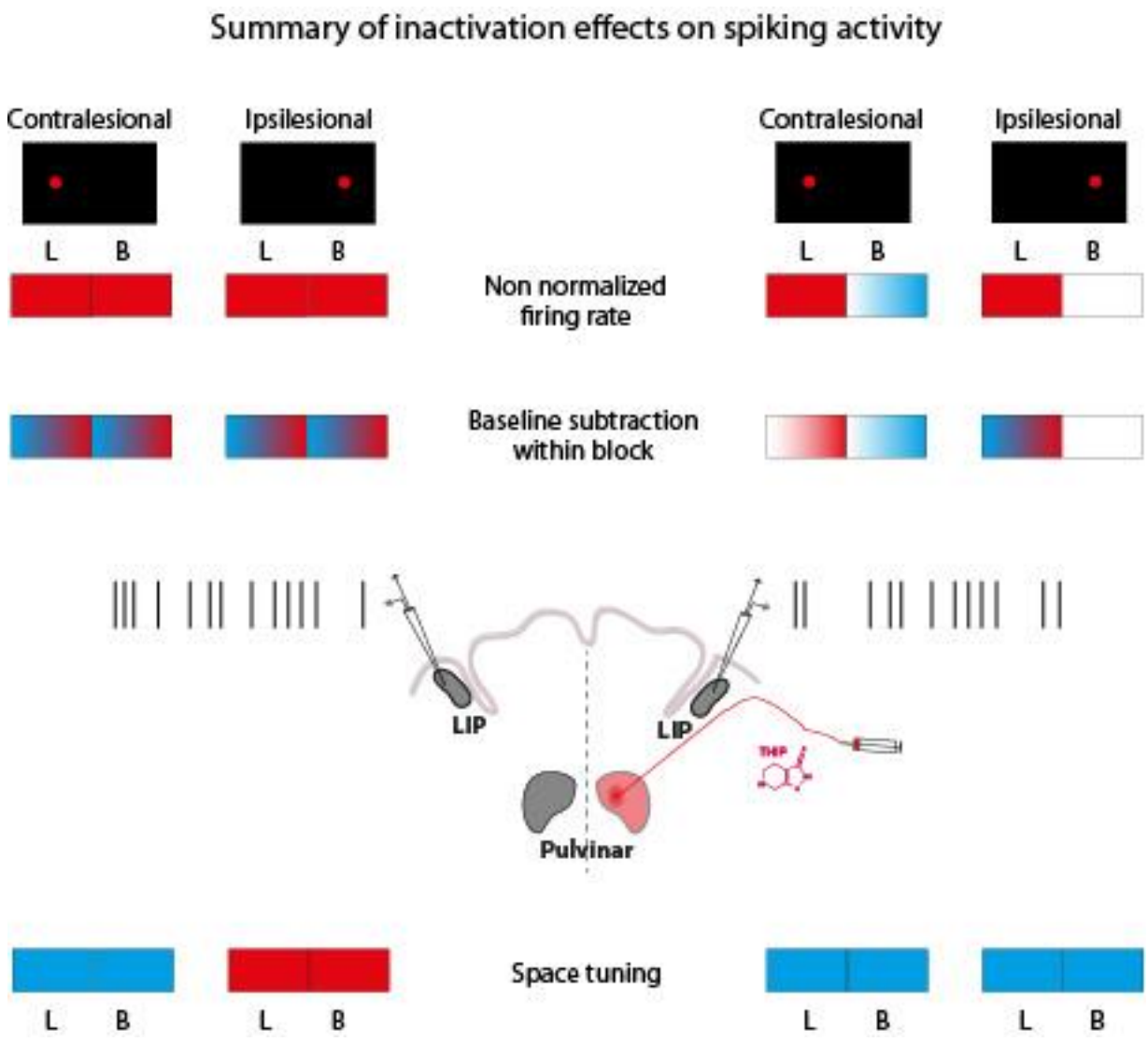

Figure 4.4.17. Summary of inactivation effects on spiking activity. Summarized effects in the contralesional (left panel) and ipsilesional (right panel) hemisphere on raw firing rate (top panel) and baseline subtraction within block (middle panel) as well as space tuning (bottom panel). Tables represent changes in firing rate (top and middle) or space tuning (bottom) for both monkeys (L = Monkey L, B = monkey B). Red = increase, blue = decrease, white = no change.

4.4.4 Inactivation effect on spike-field synchronization within and between hemispheres

4.4.4.1 Spike-field connectivity within the inactivated hemisphere

We calculated spike-field pairwise phase consistency within the inactivated hemisphere between 8759 pairs in monkey L and 2634 in monkey B both in instructed (Figure 4.4.18) and in free-choice trials (Figure 4.4.19).

We observed in both monkeys, spike-field synchronization in theta and alpha after contralateral target presentation. After inactivation, the synchronization was weaker in the theta range,

suggesting alterations in contralesional visual stimuli processing. At the same time, we observed an increased pairwise phase consistency in alpha/low-beta in monkey L whereas it decreased in monkey B.

During the delay period, we observed mostly coherence in the alpha and beta range, with beta synchronization being lower before contralesional saccades. After inactivation, there was a decreased synchronization in alpha before contralesional saccades in both monkeys. In addition, there was an increased pairwise phase consistency in beta before contralesional saccades, particularly in monkey B. We observed the opposite effect before ipsilesional saccades. Together, it suggests alterations of contralesional saccades preparation and ipsilesional facilitation in the inactivated hemisphere.

Consistently with the LFP profile, we observed around saccades synchronization mostly in the theta and alpha range. Before saccades onset, there were no striking differences after inactivation. In monkey L, the synchronization in alpha was higher shortly after contralesional saccades as compared with ipsilesional saccades. Interestingly, after inactivation, the synchronization in alpha increased for ipsilesional saccades.

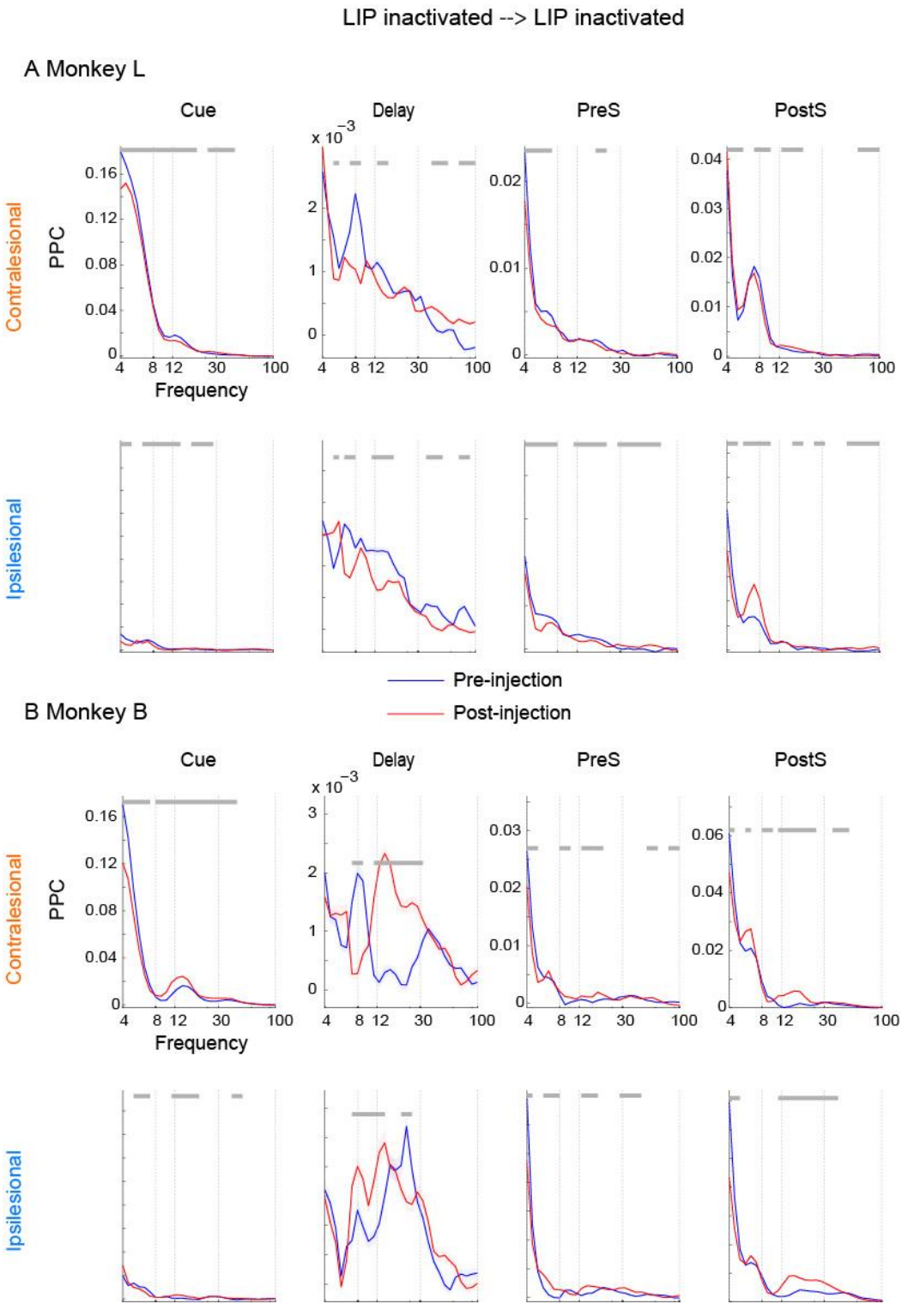

Figure 4.4.18 Spike-field pairwise phase consistency within inactivated hemisphere (instructed trials). A PPC value across frequencies averaged in different epochs pre- and post-injection in monkey L. **B** PPC value across frequencies averaged in different epochs pre- and post-injection in monkey B. Mean ± SEM are shown independently for pre- and post-injection blue/red) and contralesional/ipsilesional space (top/bottom row). Grey shaded area shows significant differences (cluster-based adjusted p-value < 0.05, t-test)

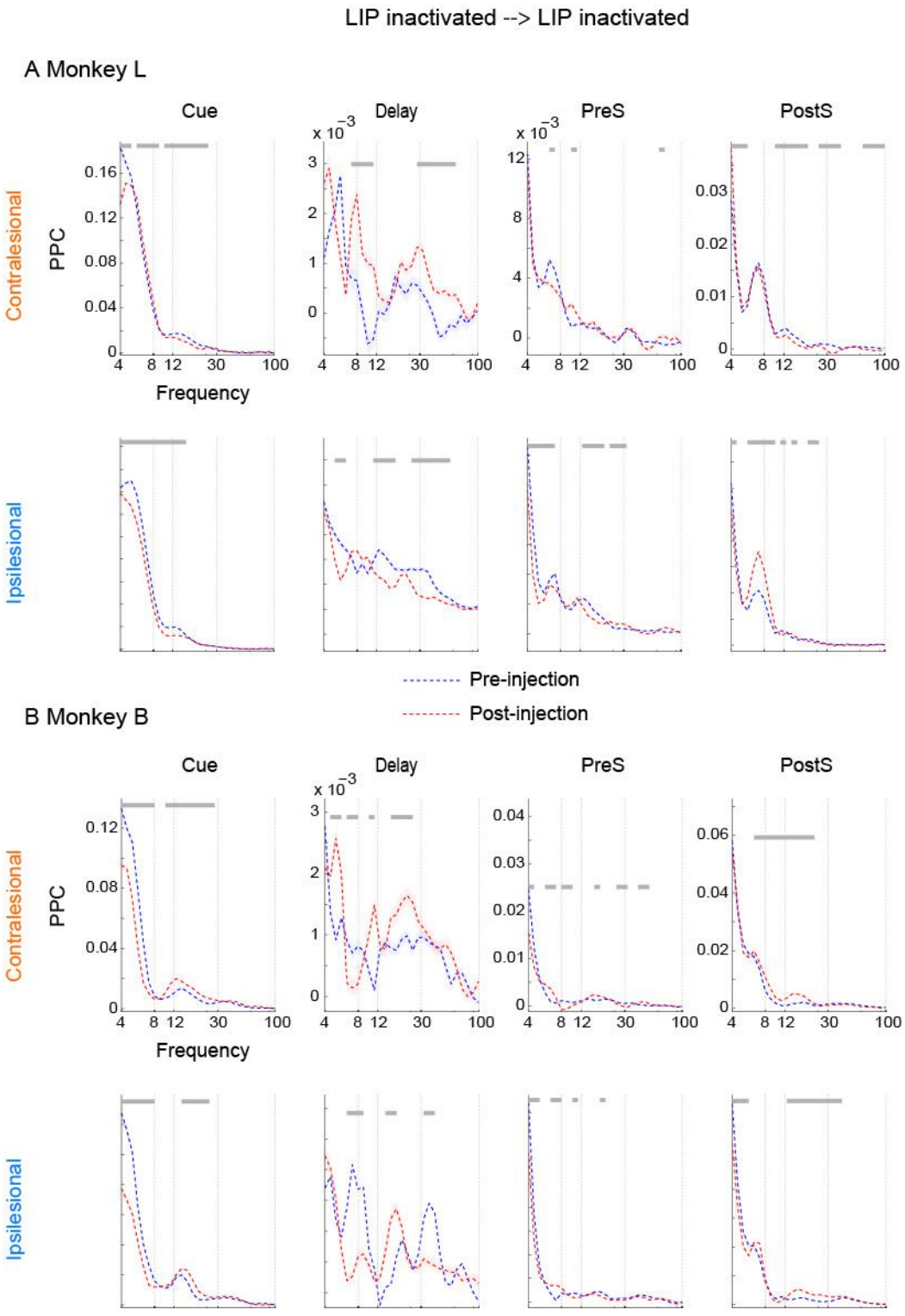

Figure 4.4.19 Spike-field pairwise phase consistency within inactivated hemisphere (free-choice trials). A PPC value across frequencies averaged in different epochs pre- and post-injection in monkey L. **B** PPC value across frequencies averaged in different epochs pre- and post-injection in monkey B. Mean ± SEM are shown independently for pre- and post-injection blue/red) and contralesional/ipsilesional space (top/bottom row). Grey shaded area shows significant differences (cluster-based adjusted p-value < 0.05, t-test)

4.4.4.2 Spike-field connectivity within intact the hemisphere

We calculated spike-field pairwise phase consistency within the inactivated hemisphere between 8164 pairs in monkey L and 3573 in monkey B both in instructed (Figure 4.4.20) and in free-choice trials (Figure 4.4.21).

We observed spike-field synchronization in theta and alpha after target presentation in the ipsilesional (contralateral) hemifield. After inactivation, there were no major alterations when targets were located in the ipsilesional hemifield. Interestingly, pairwise phase consistency after inactivation was lower in theta when instructed targets were located in the contralesional hemifield. Therefore, the visual processing of stimuli located in the contralesional hemisphere might be altered, even in the intact hemisphere.

During the delay, the spike-field synchronization in beta was lower before ipsilesional (contralateral) saccades, associated with movement preparation. After inactivation, we observed a decreased pairwise phase consistency before instructed ipsilesional saccades that might reflect facilitation of movement preparation. In monkey B, we observed the opposite effect before instructed contralesional saccades. However, this was not the case in monkey L where synchronization in beta was lower after inactivation.

Around saccades, there was spike-field synchronization in the theta and alpha range. After inactivation, we saw no or little changes in the coherence profile. During instructed trials, we only observed a decreased pairwise phase consistency in alpha after contralesional saccades. In free-choice trials, it was also lower before contralesional saccades but only in monkey L.

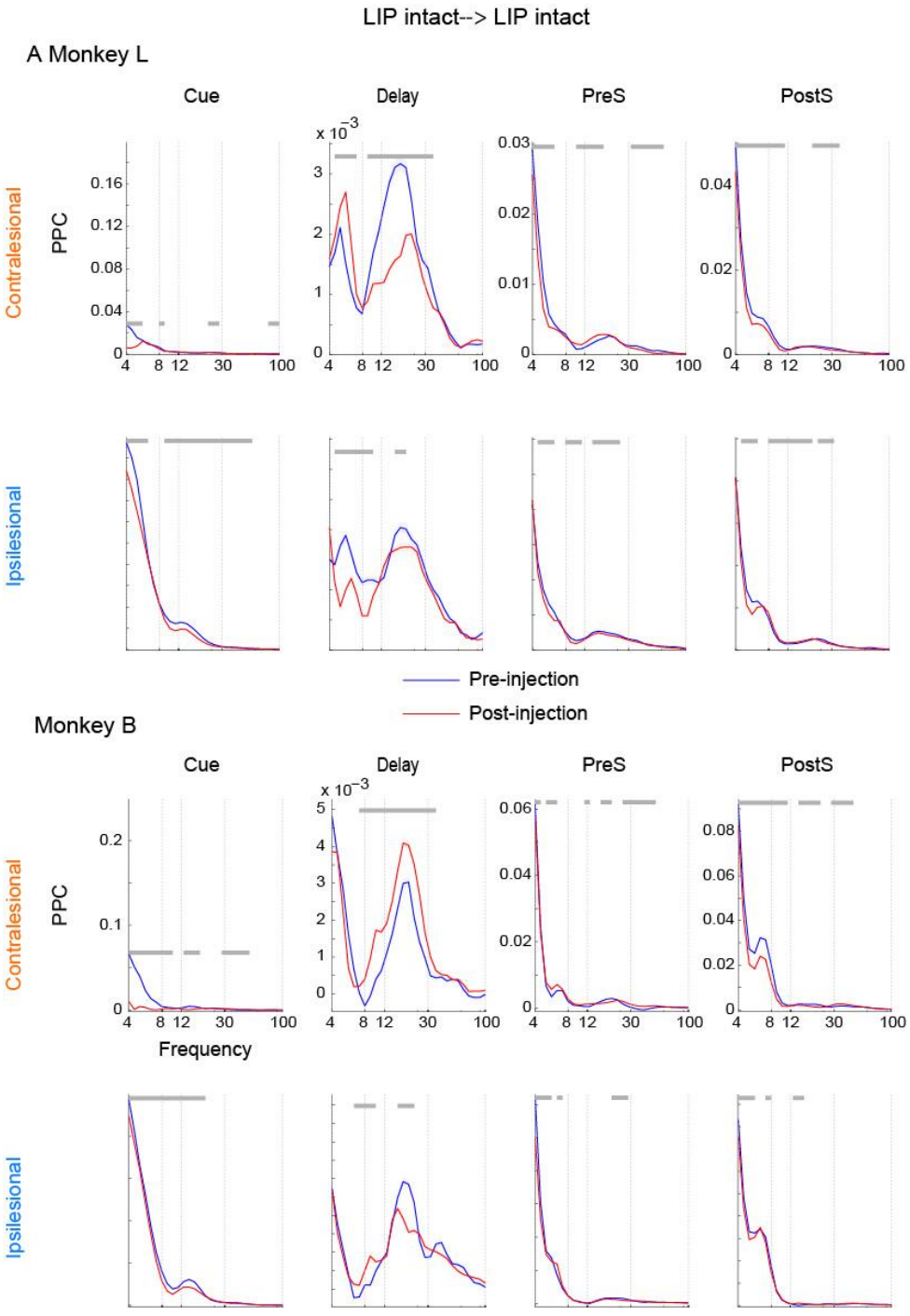

Figure 4.4.20 Spike-field pairwise phase consistency within intact hemisphere (instructed trials). A PPC value across frequencies averaged in different epochs pre- and post-injection in monkey L. **B** PPC value across frequencies averaged in different epochs pre- and post-injection in monkey B. Mean ± SEM are shown independently for pre- and post-injection blue/red) and contralesional/ipsilesional space (top/bottom row). Grey shaded area shows significant differences (cluster-based adjusted p-value < 0.05, t-test)

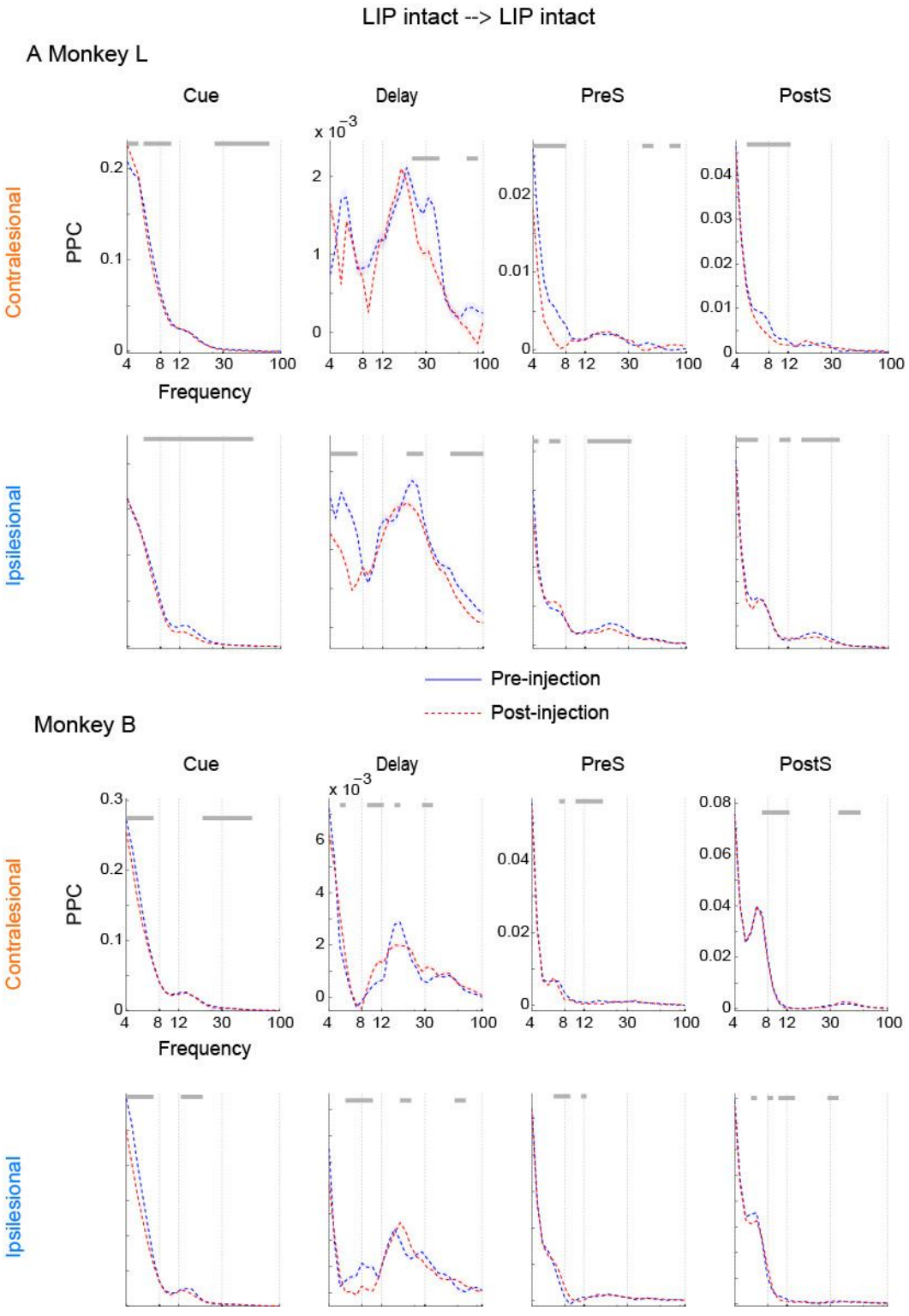

Figure 4.4.21 Spike-field pairwise phase consistency within intact hemisphere (free-choice trials). A PPC value across frequencies averaged in different epochs pre- and post-injection in monkey L. **B** PPC value across frequencies averaged in different epochs pre- and post-injection in monkey B. Mean ± SEM are shown independently for pre- and post-injection blue/red) and contralesional/ipsilesional space (top/bottom row). Grey shaded area shows significant differences (cluster-based adjusted p-value < 0.05, t-test)

4.4.4.3 Spike-field connectivity between spikes from the inactivated hemisphere and LFP signals from the intact hemisphere

We calculated spike-field pairwise phase consistency between spikes from the inactivated hemisphere and LFP signals from the intact hemisphere (9021 pairs in monkey L and 2538 in monkey B) both in instructed (Figure 4.4.24) and in free-choice trials (Figure 4.4.25).

After ipsilesional (to the inactivated hemisphere) cue presentation, we observed spike-field synchronization in the theta and alpha range that was not altered after dPul inactivation. It likely reflects the transient evoked response on the LFP signal in the intact hemisphere. To some extent, there was also some synchronization in theta after contralesional targets presentation. Interestingly, the synchronization was weaker after dPul inactivation. Therefore, the directional connectivity from the inactivated to intact hemisphere was decreased after target presentation, only when targets were located in the contralesional hemifield.

During the delay period, we observed stronger spike-field synchronization in theta when targets were located in the contralesional hemifield and it was not altered after dPul inactivation. Interestingly, there was in monkey B synchronization in the beta range, more strongly before saccades towards the contralesional hemifield. After dPul inactivation, the pairwise phase consistency decreased before both contralesional and ipsilesional saccades. This result suggests a decreased functional connectivity from the inactivated to intact hemisphere during movement preparation.

Around saccades, we found spike-field coherence in the theta and alpha range. In monkey L, the synchronization was weaker after inactivation shortly before saccades onset towards the contralesional hemifield, both in instructed and free-choice trials. Shortly after saccades end, there was a slight increase in alpha pairwise phase consistency.

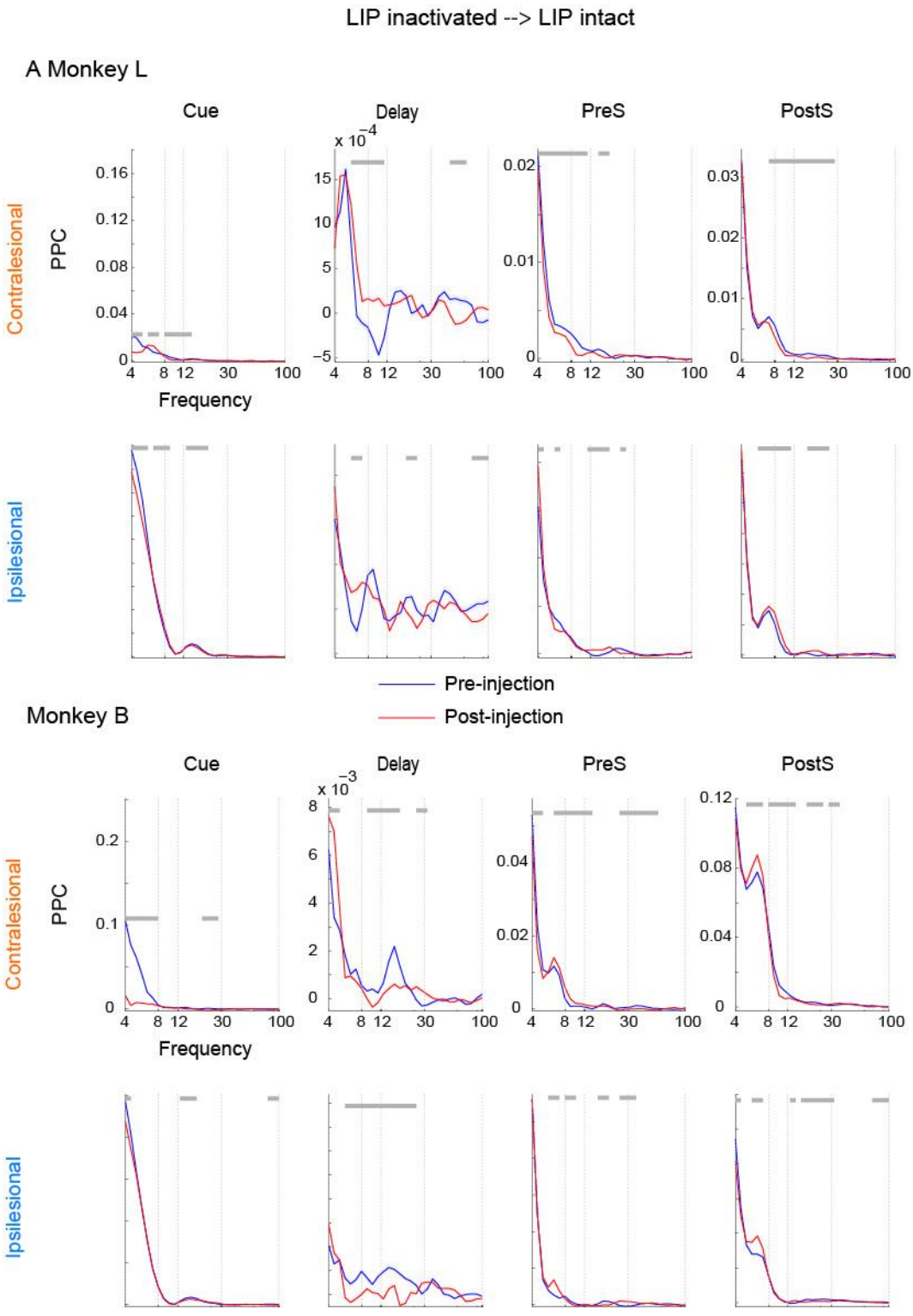

Figure 4.4.24 Spike-field pairwise phase consistency between spikes from inactivated hemisphere and LFP from intact hemisphere (instructed trials). A PPC value across frequencies averaged in different epochs pre- and post-injection in monkey L. **B** PPC value across frequencies averaged in different epochs pre- and post-injection in monkey B. Mean ± SEM are shown independently for pre- and post-injection blue/red) and contralesional/ipsilesional space (top/bottom row). Grey shaded area shows significant differences (cluster-based adjusted p-value < 0.05, t-test)

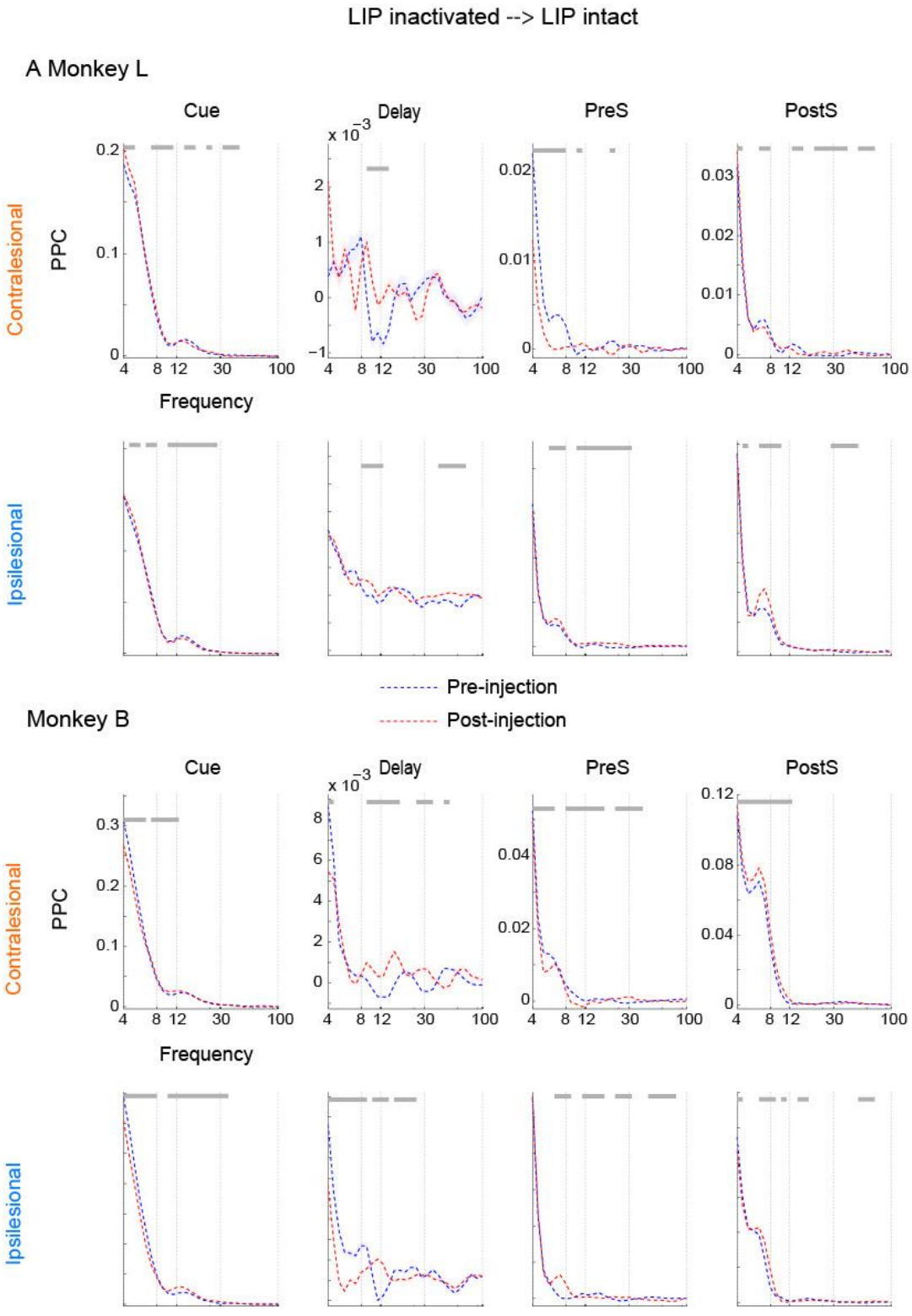

Figure 4.4.25 Spike-field pairwise phase consistency between spikes from inactivated hemisphere and LFP from intact hemisphere (free-choice trials). A PPC value across frequencies averaged in different epochs pre- and post-injection in monkey L. **B** PPC value across frequencies averaged in different epochs pre- and post-injection in monkey B. Mean ± SEM are shown independently for pre- and post-injection blue/red) and contralesional/ipsilesional space (top/bottom row). Grey shaded area shows significant differences (cluster-based adjusted p-value < 0.05, t-test)

4.4.4.4 Spike-field connectivity between spikes from the intact hemisphere and LFP signals from the inactivated hemisphere

We calculated spike-field pairwise phase consistency between spikes from the intact hemisphere and LFP signals from inactivated hemisphere (8437 pairs in monkey L and 3682 in monkey B) both in instructed (Figure 4.4.26) and in free-choice trials (Figure 4.4.27).

After contralesional (to the inactivated hemisphere) cue presentation, we observed spike-field synchronization in theta and alpha range. Interestingly, the pairwise phase consistency in theta was decreased after dPul inactivation, both in instructed and free-choice trials. Therefore, the directional connectivity from the intact to inactivated hemisphere was decreased after target presentation when at least one of them was located in the contralesional hemifield.

During the delay period, we found spike-field synchronization in theta in both monkeys as well as in beta in monkey B. In monkey L, the synchronization was decreased in theta/alpha after dPul inactivation before contralesional instructed saccades. In free-choice trials, we found in both monkeys an increased theta/alpha before contralesional choices and decreased before ipsilesional choices. In monkey B, there was a lower pairwise phase consistency in beta before contralesional saccades and it was increased before ipsilesional saccades. During free-choice trials, we found a decreased synchronization both before contralesional and ipsilesional saccades.

Around saccades, there was mostly spike-field synchronization in the theta and alpha range. In monkey L, there was a slight decrease after dPul inactivation in theta synchronization shortly before ipsilesional instructed saccades or before ipsilesional choices. In monkey B, the spike-field pairwise phase consistency was mostly unaltered around saccades after dPul inactivation.

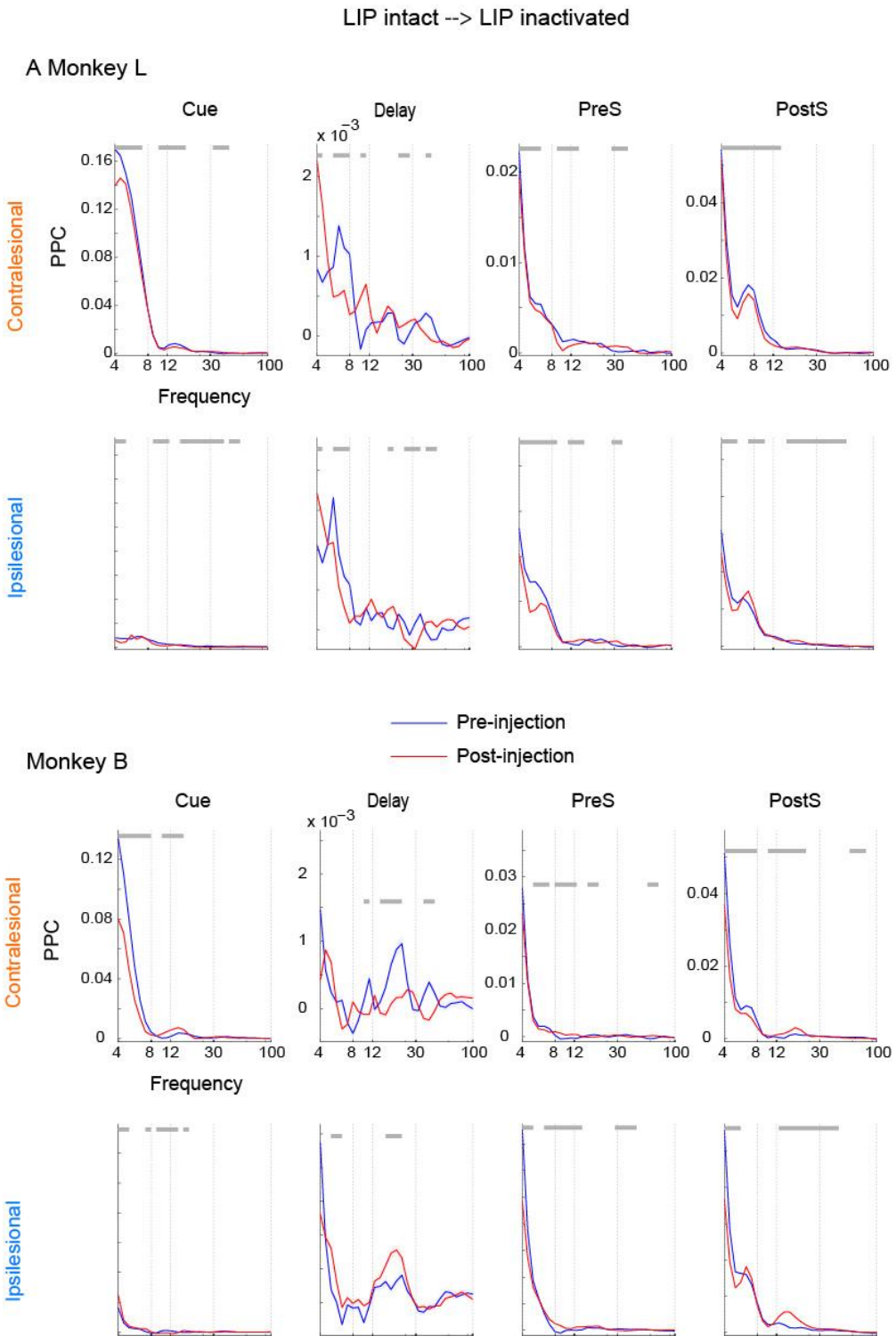

Figure 4.4.26 Spike-field pairwise phase consistency between spikes from intact hemisphere and LFP from inactivated hemisphere (instructed trials). A PPC value across frequencies averaged in different epochs pre- and post-injection in monkey L. **B** PPC value across frequencies averaged in different epochs pre- and post-injection in monkey B. Mean ± SEM are shown independently for pre- and post-injection blue/red) and contralesional/ipsilesional space (top/bottom row). Grey shaded area shows significant differences (cluster-based adjusted p-value < 0.05, t-test)

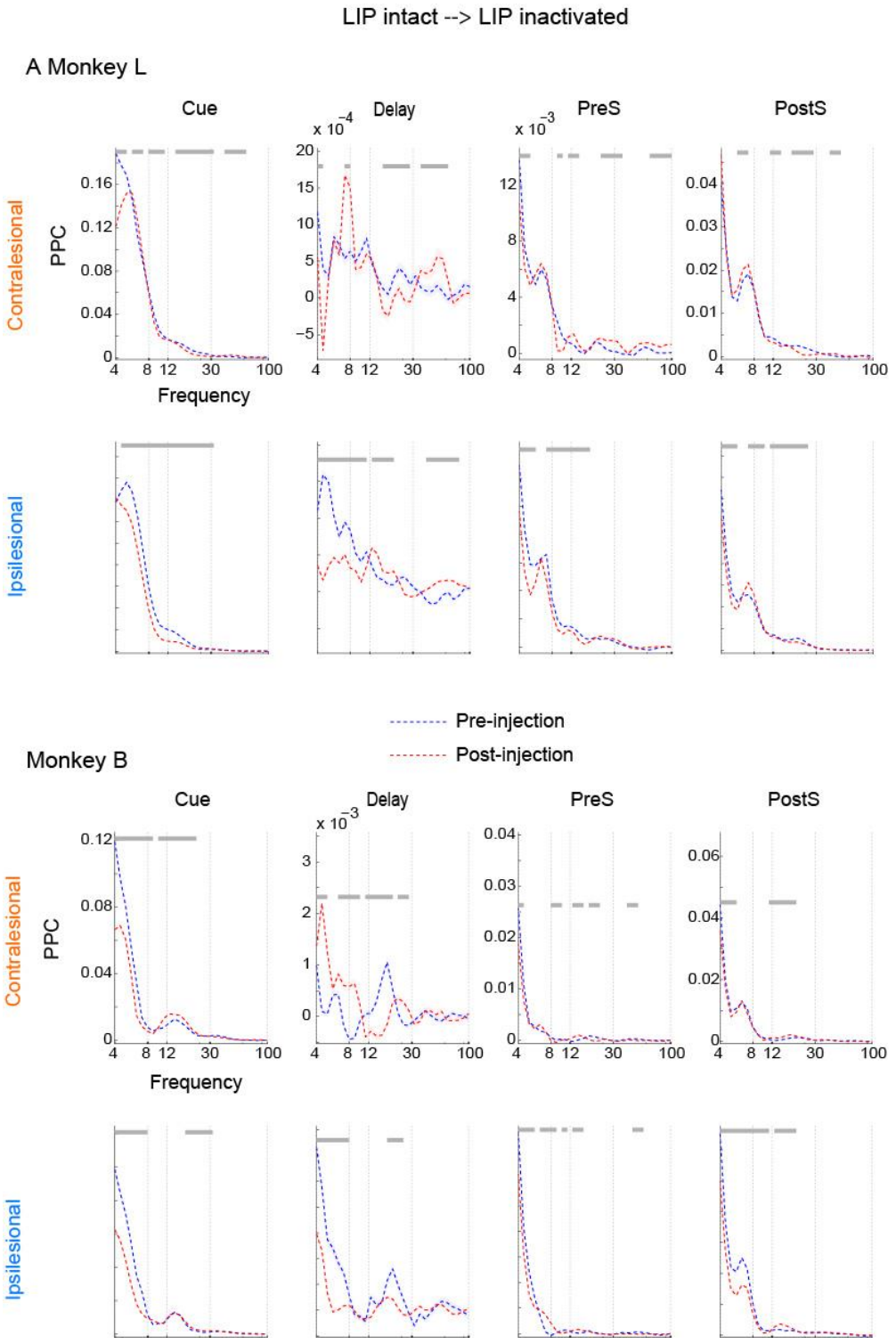

Figure 4.4.27 Spike-field pairwise phase consistency between spikes from intact hemisphere and LFP from inactivated hemisphere (free-choice trials). A PPC value across frequencies averaged in different epochs pre- and post-injection in monkey L. **B** PPC value across frequencies averaged in different epochs pre- and post-injection in monkey B. Mean ± SEM are shown independently for pre- and post-injection blue/red) and contralesional/ipsilesional space (top/bottom row). Grey shaded area shows significant differences (cluster-based adjusted p-value < 0.05, t-test)

4.4.4.5 Summary of dorsal pulvinar inactivation effect on spike-field synchronization within and between LIP from inactivated and intact hemisphere

After dorsal pulvinar inactivation, the spike-field synchronization after contralesional target presentation within LIP of the inactivated hemisphere, the intact hemisphere and between both hemispheres, suggesting an alteration of visual stimuli processing, both within and between hemispheres, when the target was located in the contralesional hemifield.

During the delay period, we also found alterations in spike-field synchronization. Within LIP, we found in both hemispheres a decreased beta pairwise phase consistency before ipsilesional saccades, suggesting facilitation in ipsilesional movement preparation. On the contrary, we found an increased synchronization before contralesional saccades in the inactivated hemisphere as well as the intact hemisphere in monkey B. In the same monkey, there was also a decreased spike-field coherence in beta between spikes from the inactivated LIP and LFP signal from the intact LIP, suggesting deficits in functional connectivity from inactivated to intact hemisphere during movement preparation. From the intact hemisphere to inactivated hemisphere, results were not as consistent across the two monkeys. Nevertheless, there were also synchronization alterations in the theta, alpha and beta range, suggesting deficits in functional connectivity also from the intact to the inactivated hemisphere.

Around saccades, we found no or little effect after dorsal pulvinar inactivation. Unlike what we described in the LFP analysis, results of spike-field synchronization measures do not suggest alterations in saccades-related processes.

4.4.5 Inactivation effect on field-field synchronization within and between hemispheres

4.4.5.1 Field-field pairwise phase consistency within LIP in the inactivated hemisphere

We calculated field-field pairwise phase consistency between LFP sites within the inactivated hemisphere (4563 pairs in monkey L and 3289 in monkey B), in the pre- and post-injection block both in instructed (Figure 4.4.28) and in free-choice trials (Figure 4.4.29).

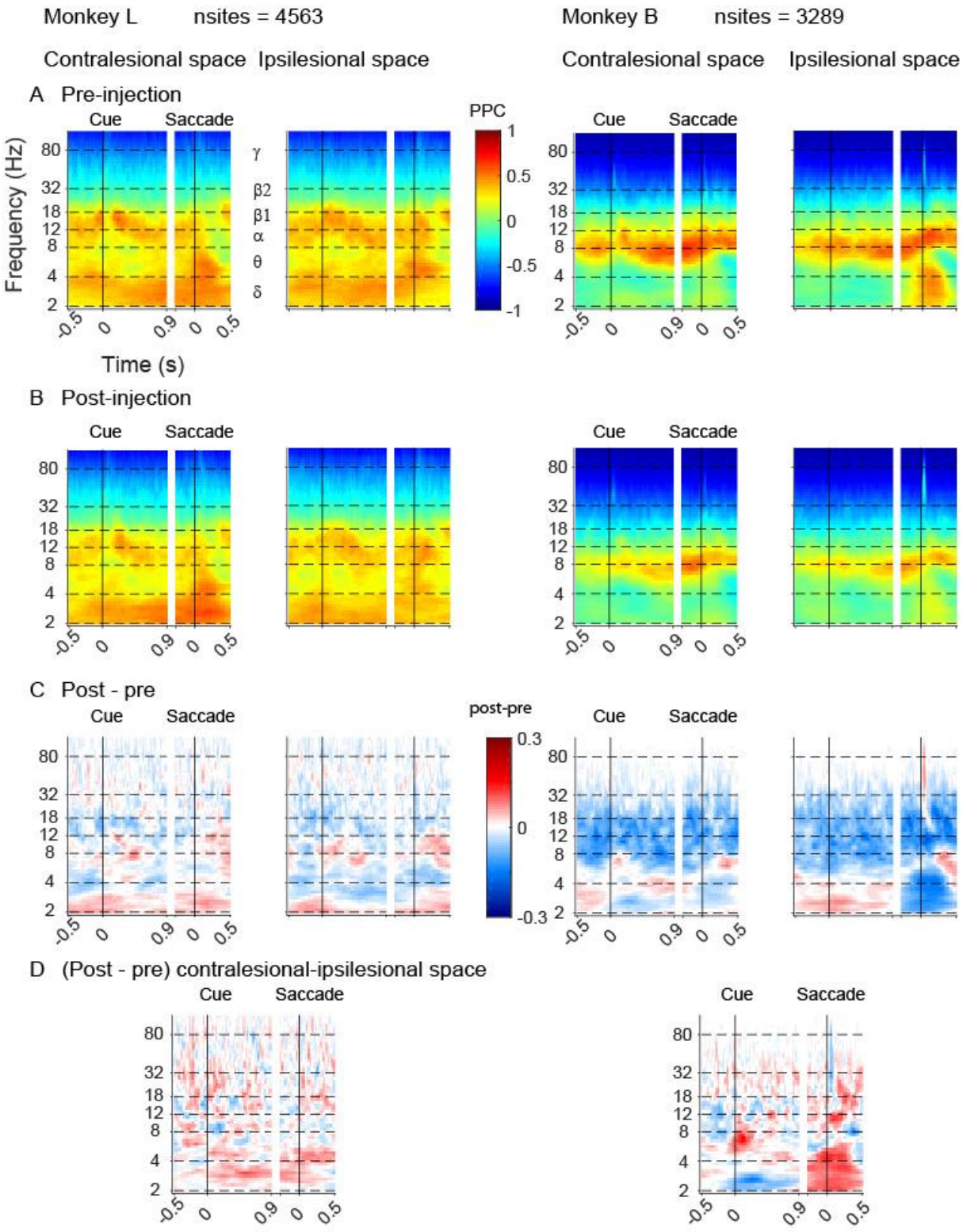

Figure 4.4.28 Field-field pairwise phase consistency within LIP in the inactivated hemisphere (instructed trials). **A** PPC values in the pre-injection block. **B** PPC values in the post-injection block. **C** Difference in PPC values between pre- and post-injection. Only significant bins are shown (paired t-test with Bonferroni correction). **D** Difference in PPC values between contralesional and ipsilesional of the difference between pre- and post-injection (C). Only significant bins are shown (paired t-test with Bonferroni correction).

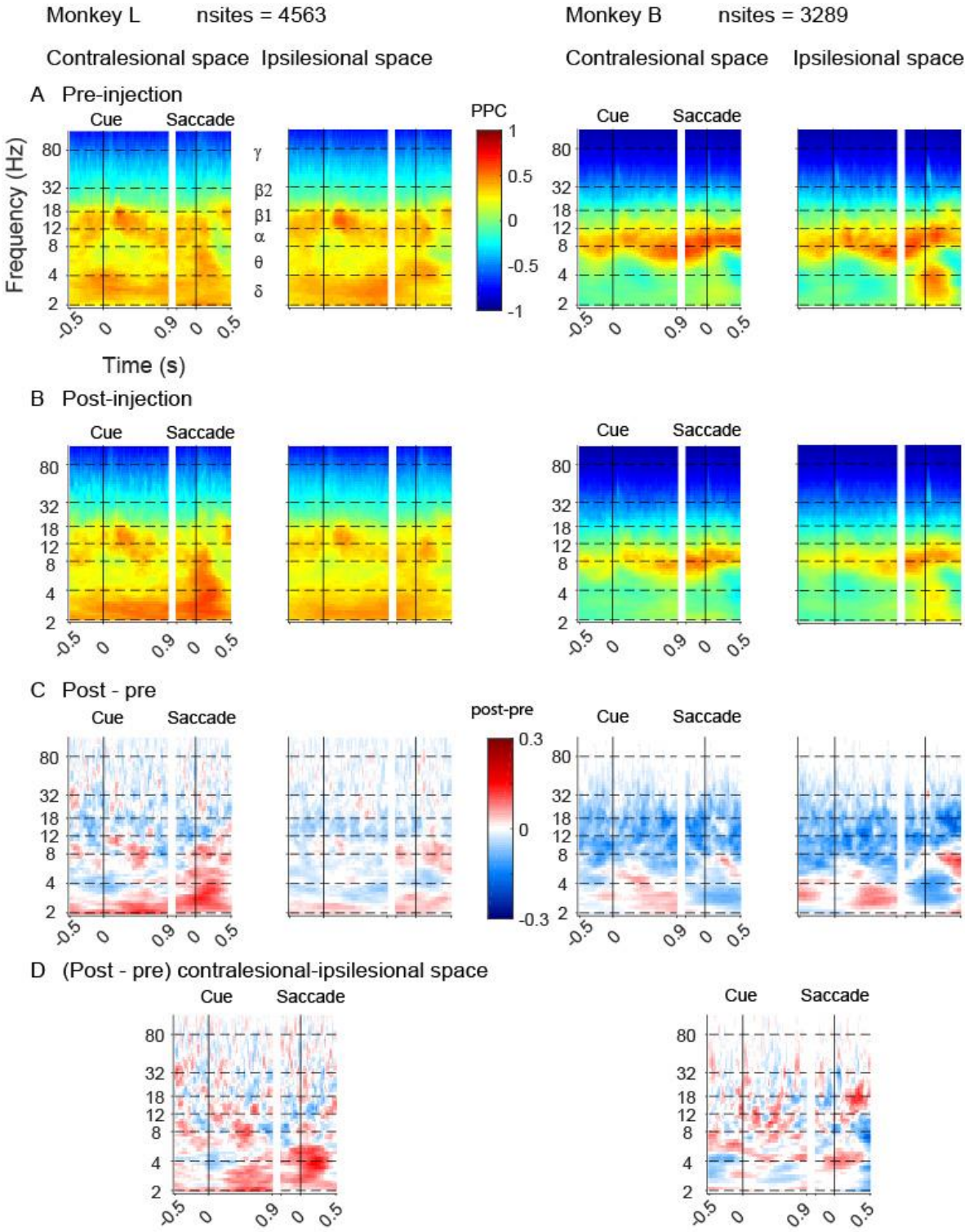

Figure 4.4.29 Field-field pairwise phase consistency within LIP in the inactivated hemisphere (free-choice trials). A PPC values in the pre-injection block. **B** PPC values in the post-injection block. **C** Difference in PPC values between pre- and post-injection. Only significant bins are shown (paired t-test with Bonferroni correction). **D** Difference in PPC values between contralesional and ipsilesional of the difference between pre- and post-injection (C). Only significant bins are shown (paired t-test with Bonferroni correction).

First of all, the LFP-LFP pairwise phase consistency profile was similar to what we described in the Chapter 3. Namely, there was strong synchronization in low-beta in monkey L and alpha in monkey B. Interestingly, the inactivated hemisphere in this experiment was often the right hemisphere (7/10 sessions) whereas in chapter 3, all sessions were recorded from the left hemisphere. Therefore, frequencies of interactions that might differ slightly between monkeys might be shared across both hemispheres within monkey. In monkey L, there was also strong synchronization in the delta and theta range.

After dorsal pulvinar inactivation, we observed a decreased synchronization in low-beta and alpha in both monkeys in both instructed and free-choice trials, suggesting alterations in local functional connectivity. However, there was no differences in the inactivation effect between instructed contralesional and ipsilesional saccades as well as between contralesional and ipsilesional choices. Also, the decreased synchronization was observed throughout the entire trial. These results suggest that the synchronization alteration described in this frequency range were not space specific but rather a global effect of the dorsal pulvinar inactivation.

In the theta range, there was mostly a decreased synchronization throughout the trial in both monkeys and in both instructed in free-choice trials. Like in alpha/low-beta, there was no clear space specificity and it suggests a global decrease in theta synchronization after inactivation.

The field-field synchronization in the delta range was differentially altered in the two monkeys. In monkey L, there was an increased synchronization throughout the trial. Interestingly, it was stronger for instructed saccades or for contralesional choices, particularly during the delay period and around saccades. In monkey B, we observed inconsistent effect during the delay period between instructed and free-choice trials. Indeed, the pairwise phase consistency was decreased before instructed contralesional saccades whereas it was increased before instructed ipsilesional saccades and free-choices trials, independently of the upcoming choice. It was also decreased around saccades, more strongly when the direction was towards the ipsilesional hemifield. This result is in contrast with what we observed in monkey L.

4.4.5.2 Field-field pairwise phase consistency within LIP in the intact hemisphere

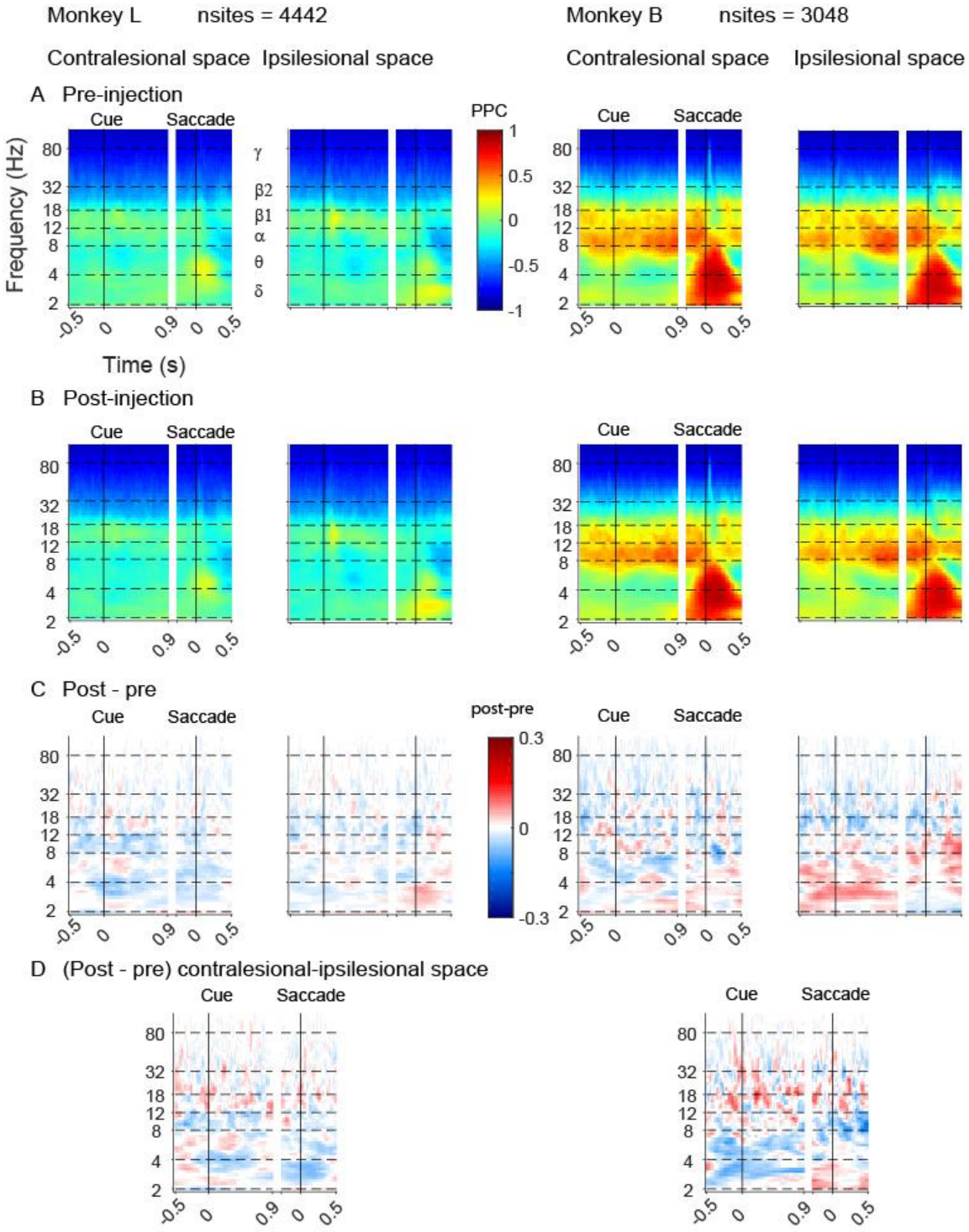

Figure 4.4.30 Field-field pairwise phase consistency within LIP in the intact hemisphere (instructed trials). A PPC values in the pre-injection block. **B** PPC values in the post-injection block. **C** Difference in PPC values between pre- and post-injection. Only significant bins are shown (paired t-test with Bonferroni correction). **D** Difference in PPC values between contralesional and ipsilesional of the difference between pre- and post-injection (C). Only significant bins are shown (paired t-test with Bonferroni correction).

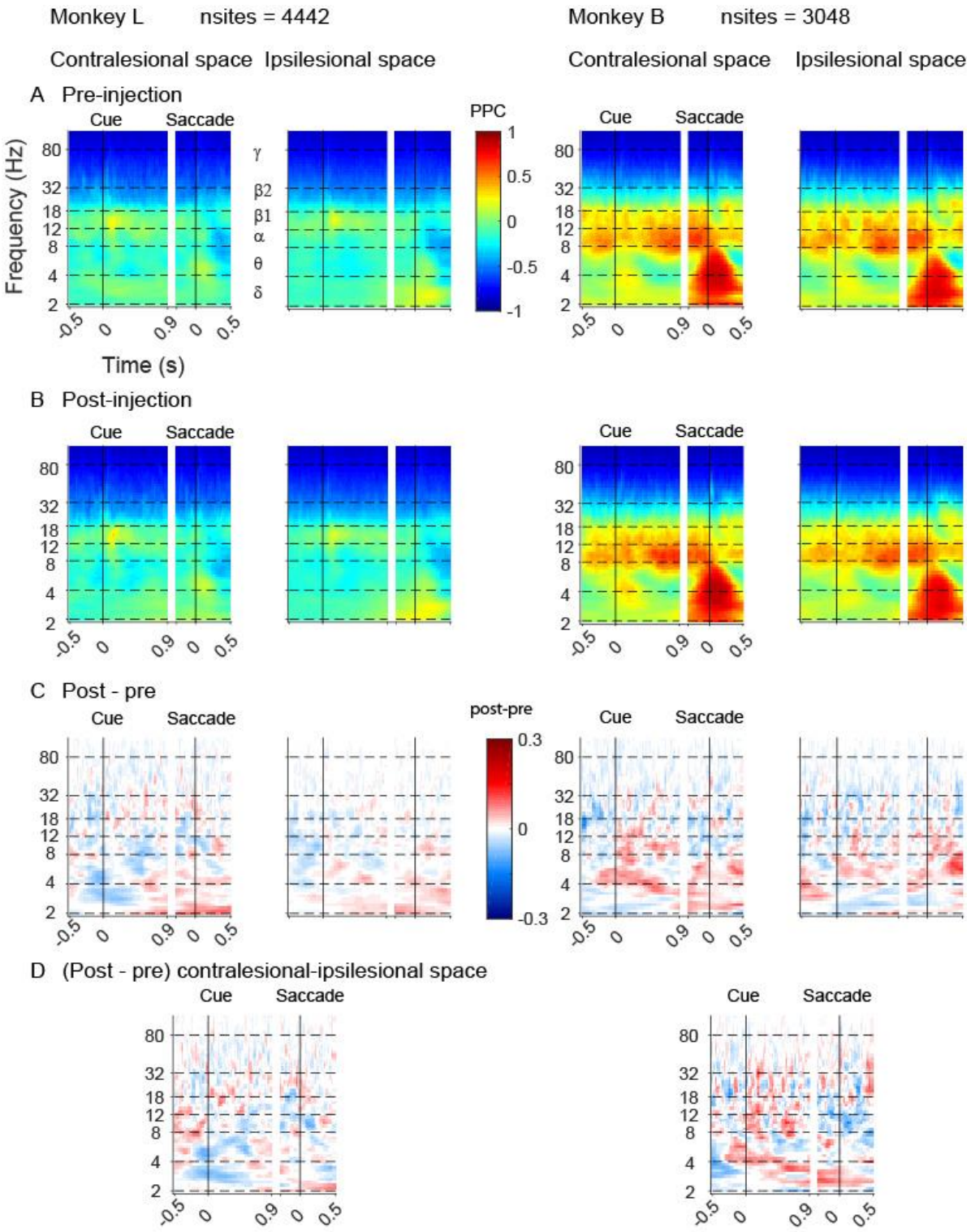

Figure 4.4.31 Field-field pairwise phase consistency within LIP in the intact hemisphere (free-choice trials). A PPC values in the pre-injection block. **B** PPC values in the post-injection block. **C** Difference in PPC values between pre- and post-injection. Only significant bins are shown (paired t-test with Bonferroni correction). **D** Difference in PPC values between contralesional and ipsilesional of the difference between pre- and post-injection (C). Only significant bins are shown (paired t-test with Bonferroni correction).

We calculated field-field pairwise phase consistency between LFP sites within the intact hemisphere (4442 pairs in monkey L and 3048 in monkey B), in the pre- and post-injection block both in instructed (Figure 4.4.30) and in free-choice trials (Figure 4.4.31).

In the intact hemisphere, like in the opposite hemisphere, there was on going oscillations in low-beta in monkey L and in alpha in monkey B, bringing additional evidence on shared frequencies of oscillations between the two hemispheres within monkey, despite differences across monkeys. After inactivation, we did not observe consistent increase or decrease in pairwise phase consistency in respective frequency range. This result suggests that the upregulation of activity observed on LFP time-frequency spectrogram (gamma range) and spiking activity was not due to or induced by changes in on going local synchronization.

In the theta range, we observed in monkey L a decreased pairwise phase consistency after contralesional target presentation, in instructed trials and before contralesional choices. In contrast, there was an increased synchronization in monkey B after instructed ipsilesional target presentation and before contralesional choices. Inconsistencies between monkeys in that frequency range question the functional significance of local theta oscillations during the processing of visual stimuli. Around saccades, we observed in this frequency range inconsistent results, both within and across monkeys. In monkey L, there was a decreased pairwise phase consistency in instructed trials but it was increased in free-choice trials. In monkey B, there were no clear changes in instructed trials but an increase in free-choice trials.

4.4.5.3 LIP field-field pairwise phase consistency between the two hemispheres

We calculated field-field pairwise phase consistency between LFP sites from the inactivated and the intact hemisphere (9301 pairs in monkey L and 6170 in monkey B), in the pre- and post-injection block both in instructed (Figure 4.4.32) and in free-choice trials (Figure 4.4.33).

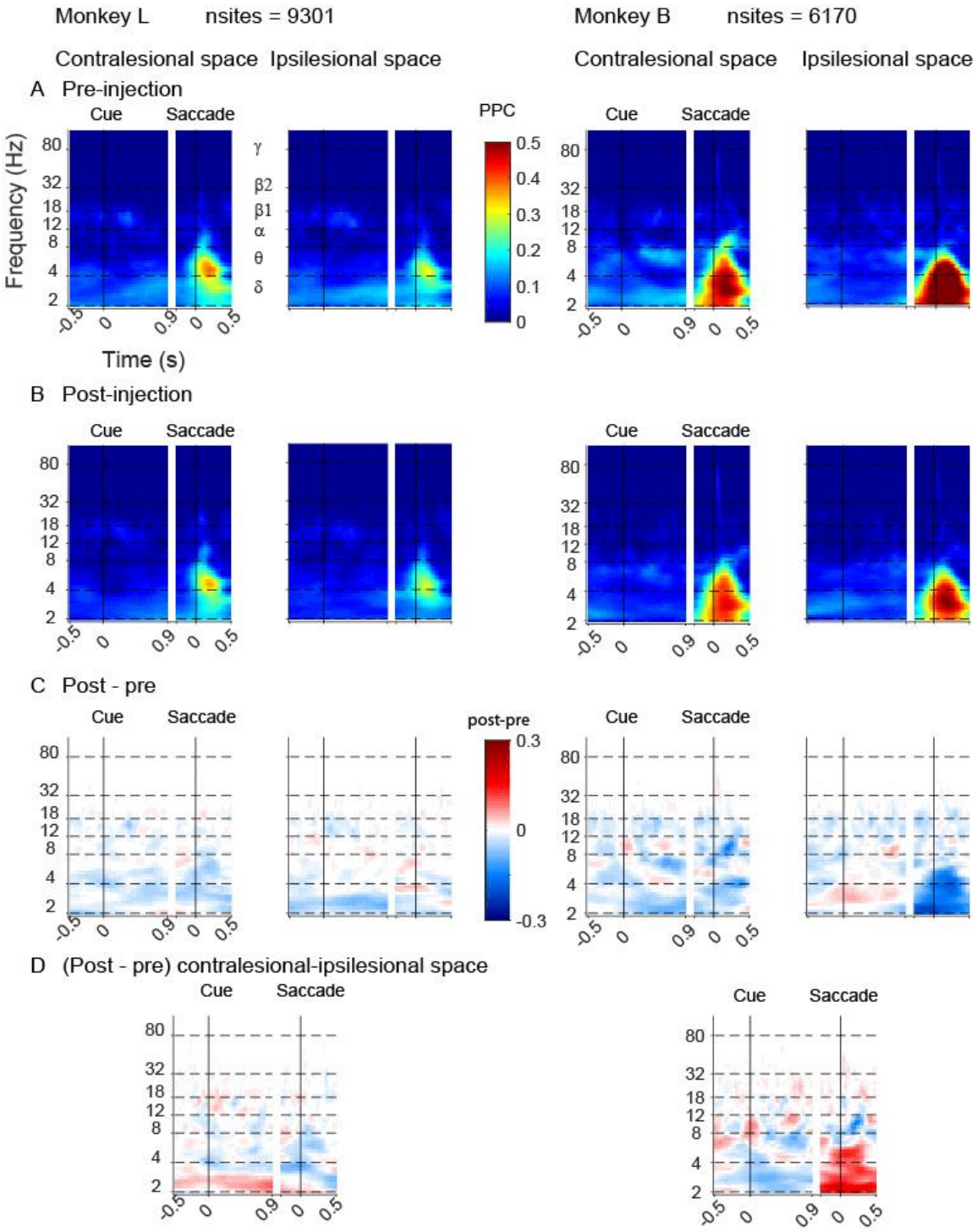

Figure 4.4.32 Field-field pairwise phase consistency between LIPs (instructed trials). A PPC values in the pre-injection block. **B** PPC values in the post-injection block. **C** Difference in PPC values between pre- and post-injection. Only significant bins are shown (paired t-test with Bonferroni correction). **D** Difference in PPC values between contralesional and ipsilesional of the difference between pre- and post-injection (C). Only significant bins are shown (paired t-test with Bonferroni correction).

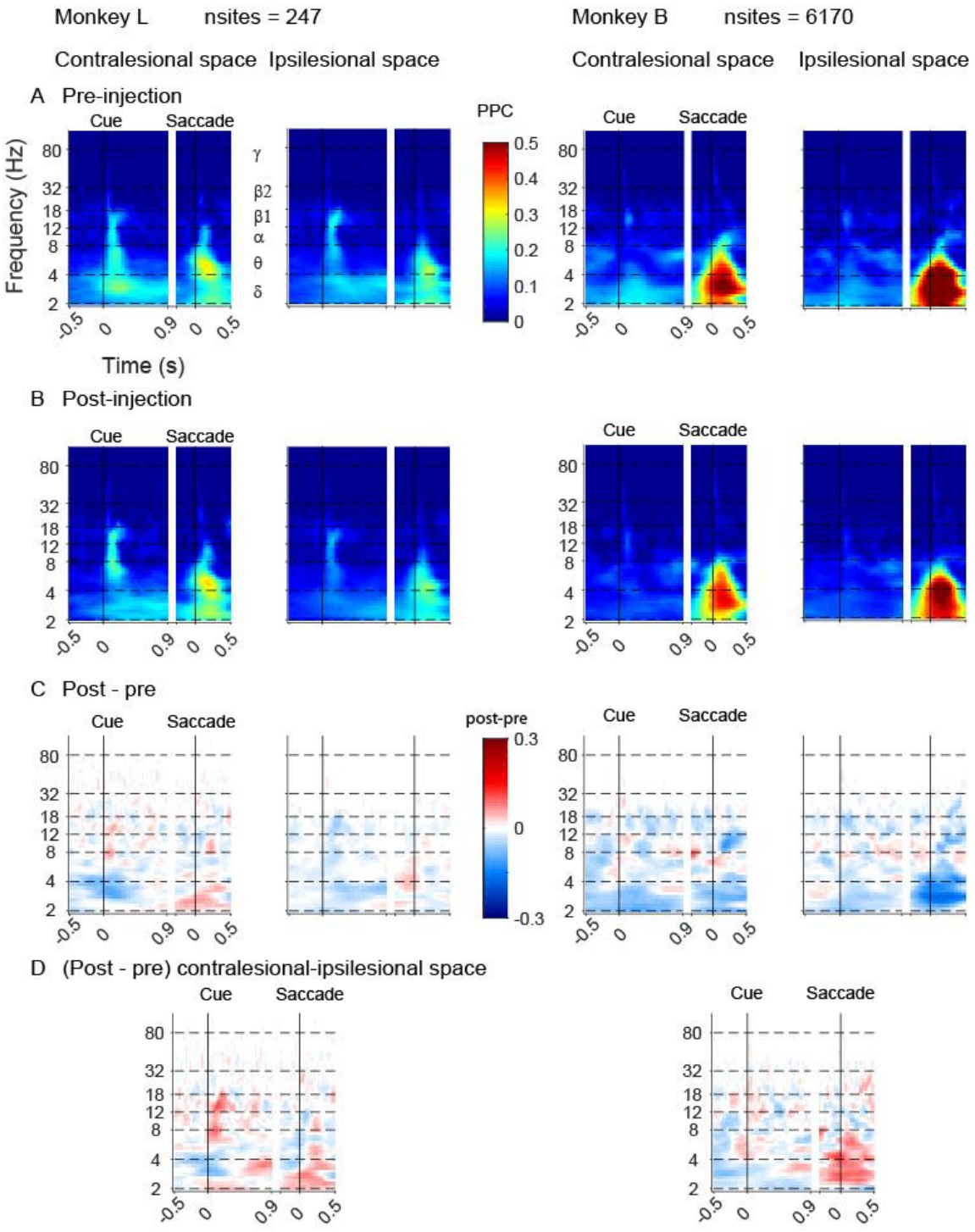

Figure 4.4.33 Field-field pairwise phase consistency between LIPs (free-choice trials). A PPC values in the pre-injection block. **B** PPC values in the post-injection block. **C** Difference in PPC values between pre- and post-injection. Only significant bins are shown (paired t-test with Bonferroni correction). **D** Difference in PPC values between contralesional and ipsilesional of the difference between pre- and post-injection (C). Only significant bins are shown (paired t-test with Bonferroni correction).

Between the two hemispheres, we found synchronization in similar frequency range, from delta to low-beta, in both monkeys. Interestingly, on visual inspection, there was stronger interactions between the two hemispheres upon presentation of two targets in opposite hemifield as compare with single instructed target.

After dorsal pulvinar inactivation, we found weaker pairwise phase consistency. Upon target presentation, there was a decreased synchronization in delta/theta. Interestingly, the decrease was stronger for instructed target in the contralesional hemifield or before contralesional choices. In addition, we found in monkey L inter-hemispheric synchronization in the alpha range during free-choice trials that was decreased before upcoming ipsilesional choices.

During the delay, the synchronization was also decreased in low-beta, particularly in monkey B. This decrease was independent of the target position, indicating global alterations of interactions in this frequency range during movement preparation.

The strongest interactions between the two hemispheres was in the post-saccadic epoch in the delta/theta range in both monkeys. After inactivation, there was different effect in both monkeys. In monkey L, there was a decreased synchronization around instructed contralesional saccades. Surprisingly, in the same monkey, the synchronization was increased in free-choice trials when the upcoming choice was towards the contralesional hemifield. In monkey B, we found a decreased synchronization around saccades. This effect was stronger around ipsilesional instructed saccades and ipsilesional choices.

Together, results indicate decreased functional connectivity between the two hemispheres after unilateral dorsal pulvinar inactivation. In addition, we found stronger alterations during visual processing when at least one target was located in the contralesional hemifield. During movement preparation, there was no space-specific alterations. Finally, we found inconsistent results around the saccades, when interactions between hemispheres were the strongest.

4.5 Discussion

4.5.1 Behavioral deficits after unilateral dorsal pulvinar inactivation

Dorsal pulvinar inactivation led to a decreased probability of selecting contralesional targets during free-choice saccade task, confirming previous results (Wilke et al., 2010, 2013). Such pulvinar inactivation-induced choice bias was also seen using reaches, both in monkey perturbation studies and human patient studies (Wilke et al., 2010, 2018), confirming the involvement of the dorsal pulvinar in decision-making and movement planning of both arms and saccades movements. The lack of saccadic reaction time alterations is in agreement with a previous study using delayed-saccade task (Wilke et al., 2010) whereas increased saccadic reaction time was reported for contralesional saccades when using memory saccade task (Wilke et al., 2013). Therefore, it is possible dorsal pulvinar inactivation only leads to deficits in saccades intention when no visual stimulus is present during movement preparation. Finally, the ability to perform the task was not altered, suggesting that the choice bias was not a consequence of purely motor deficits.

4.5.2 Altered neuronal activity in area LIP in the inactivated hemisphere

The spiking activity at the population level in area LIP of the inactivated hemisphere was not dramatically altered, despite modulation at the single-neuron level. Nevertheless, we did observe a slightly decreased visual response to contralateral instructed target presentation in one monkey. In the same monkey, it was also decreased during delay in delay enhanced subpopulation. This result is consistent with a recent unpublished fMRI study (Wilke, Kagan and Andersen, in preparation) showing a decreased activity during contralesional trials after pulvinar inactivation. Consistently, the spike-field synchronization was decreased in low frequencies upon contralesional target presentation, However, visual responses to instructed targets in both hemifields were slightly increased in the second monkey. During free-choice trials, the normalized activity was decreased in response to targets presentation in one monkey and decreased during pre-saccadic epoch before ipsilesional choices in both monkeys. Pulvinar inactivation also altered the spatial tuning in both monkeys with a decreased contralesional tuning to instructed targets and decreased spatial-tuning during free-choices. Together, data suggests deficits in contralesional representation of visual stimuli. In an attentional task, inactivation of ventral pulvinar led to an increased basal firing rate and decreased visual response in area V4 (Zhou et al., 2016a). On the other hand, dorsolateral pulvinar inactivation did not alter spiking activity in

area LIP during passive viewing (Eradath et al., 2021). Together, the causal role of dorsal pulvinar on LIP spiking activity remains to be further investigated in different conditions and tasks. Neuronal oscillations were also altered after dorsal pulvinar inactivation. First, there was an increased power in low frequencies. This result suggests a decreased 'alert state' in the inactivated hemisphere (Foxe and Snyder, 2011; Brüers and VanRullen, 2018) and is consistent with the idea that the pulvinar plays a role in maintaining cortical alertness as well as results from ventral pulvinar inactivation on V4 oscillations (Zhou et al., 2016). Oscillations in beta were decreased throughout the entire trial. In addition, when normalizing each block to its own baseline (fixation hold), we observe an increased beta power during the delay period, and more strongly before contralesional saccades, suggesting deficits in modulating beta oscillations between period of fixations and movement preparation. Consistently, Field-field analysis revealed a decreased synchronization within LIP in the beta range throughout the trial. In addition, the spike-field synchronization in the beta range was decreased before ipsilesional saccades and increased before contralesional saccades suggesting a facilitation of movement planning towards to the ipsilesional hemifield and deficits towards the contralesional hemifield. Altogether, dorsal pulvinar inactivation altered neuronal activity in LIP of the same hemisphere in different ways. As global alterations, it decreased the cortical alertness and local synchronization throughout the trial. The synchronization alteration is in line with idea that the pulvinar plays a crucial role in regulating coherent activity in the parietal cortex (Saalmann et al., 2012; Fiebelkorn et al., 2019). As a more specific effect, dorsal pulvinar inactivation also induced deficits in the contralesional representation of visual stimuli and subsequent movement planning and is consistent with recent unpublished fMRI study in our lab (Wilke, Kagan and Andersen, in preparation).

4.5.3 Upregulation of LIP activity in the intact hemisphere

Recording in both hemispheres after unilateral dorsal pulvinar inactivation allowed us to assess the indirect consequences on neuronal activity in area LIP within the intact hemisphere. For the first time, we could assess the consequences of pulvinar inactivation on neuronal activity in the opposite hemisphere. There was a basal increase of firing rates which was consistent with a global increase in gamma oscillations. In addition, normalized neuronal oscillations were decreased in low frequencies, suggesting higher cortical alertness. The upregulation of local processing in the intact hemisphere suggest a disinhibition from the inactivated hemisphere in the context of push-pull interactions. On top of this global increase, we observed in some neurons task-specific changes, leading to an increased ipsilesional preference during instructed trials whereas in free-choice trials, the spatial tuning in free-choice trials was decreased, both for

contralesional and ipsilesional choices. The spike-field synchronization was reduced in low frequencies upon instructed contralesional target presentation, but not during free-choice trials. This result suggests a deficit in the processing of contralesional visual stimuli, even in the intact hemisphere and might partially explain the increased ipsilesional tuning during instructed trials. In the beta range, the synchronization was decreased during movement preparation towards the ipsilesional hemifield, suggesting a facilitation of ipsilesional saccades planning. However, there was inconsistent results in both monkeys before contralesional saccades and there were no alterations in local field-field synchronization. Overall, the activity in the intact was upregulated as result of inactivation. The global increase of activity suggests push-pull interactions between the two hemispheres during target selection and planning. As compared to the effect in the inactivated hemisphere, space-specific were not as pronounced. Nevertheless, there were indications in favor of an increased ipsilesional tuning together with a deficit in the processing of visual stimuli in the contralesional hemifield.

4.5.4 Functional connectivity alterations between the two hemispheres after unilateral dorsal pulvinar inactivation

The spike-field synchronization after instructed contralesional target presentation was decreased between the two hemispheres. The synchronization from the intact to inactivated hemisphere was also decreased during free-choice trials but not from the inactivated to the intact hemisphere. Field-field synchronization was also decreased upon target presentation in the theta range, both in instructed and free-choice trials, more strongly when a target was located in the contralesional hemifield. Therefore, the functional connectivity between the two hemispheres was decreased during the processing of visual stimuli, particularly when this latter one was located in the contralesional hemifield. During the delay period, we only found interactions in the beta range in monkey B. Interestingly, it was decreased during free-choice and instructed contralesional trials from the intact to the inactivated hemisphere. In the same monkey, there was beta synchronization from the inactivated to the intact hemisphere only in instructed trials. Nevertheless, it was also decreased after inactivation. Consistently, field-field synchronization in the beta range was decreased in this monkey. In addition, we found lower synchronization in low frequencies in both monkeys. Together, data indicates a decreased functional connectivity between the two hemispheres during movement preparation. It remains unclear if the dorsal pulvinar plays a role in the transmission of information across hemispheres. Recent data from dorsal pulvinar microstimulation in combination with fMRI showed activation in several cortical areas in the opposite hemisphere, but not in area LIP (Kagan et al., 2021). Therefore, altered

inter-hemispheric connectivity could result from indirect consequences rather than direct implication.

4.5.5 Conclusions and future directions

In this study we confirmed the effect of unilateral dorsal pulvinar inactivation on oculomotor decision-making with a bias towards the ipsilesional hemifield. In the inactivated hemisphere, we showed that it led to both global and space-specific deficits. First, there was a decreased alert cortical state, confirming a role for the pulvinar in maintaining cortical alertness (Foxe and Snyder, 2011; Brüers and VanRullen, 2018). Then, the local synchronization decreased throughout the entire trial. The synchronization alteration is in line with idea that the pulvinar plays a crucial role for coherent activity in the parietal cortex (Saalmann et al., 2012; Fiebelkorn et al., 2019). As a more specific effect, dorsal pulvinar inactivation also induced deficits in the contralesional representation of visual stimuli and subsequent movement planning and is consistent with recent fMRI study in our lab (Wilke, Kagan and Andersen, in preparation). In the intact hemisphere, there was a global upregulation of neuronal activity, suggesting a disinhibition as a result of push-pull interactions between the two hemispheres during target selection. In addition, there were indications in favor of an increased ipsilesional tuning as well as a deficit in the processing of visual stimuli in the contralesional hemifield. Finally, we showed that interactions between the two hemispheres were reduced after inactivation throughout the trial and that during the processing of visual stimuli, it was altered more strongly when the target was located in the contralesional hemifield. This space-specific alteration might partially explain the deficit of contralesional stimuli processing in the intact hemisphere.

For the first time, we revealed a constellation of neuronal alterations during visually-guided saccades and decision-making in the parietal cortex after unilateral dorsal pulvinar inactivation. This study also shed light on push-pull interactions between the two hemispheres during target selection in the context of free choices as well as the role of pulvinar in modulating the transmission of information across hemispheres. Altogether, it appears that unilateral dorsal pulvinar inactivation led to choice bias The dorsal pulvinar has been hypothesized to play an important role in the transmission of information between cortical areas within the same hemisphere (Grieve et al., 2000; Fiebelkorn et al., 2019). It would therefore be interesting to investigate for instance the effect of dorsal pulvinar inactivation on the transmission of information between area LIP and FEF.

5 General discussion

The overall aim of this thesis was to use visually-guided saccade tasks with different levels of spatial choice, in combination with electrophysiological recordings and MRI-targeted pharmacological manipulation of the pulvinar, to get a better understanding of the role of pulvinar-parietal circuitry in decision-making and visually-guided behaviors. In the first experiment, I utilized simultaneous multielectrode electrophysiological recordings in the two regions, the dorsal pulvinar (dPul) and LIP. This allowed to characterize similarities and differences in the neuronal tuning properties between the two regions, and to assess the functional connectivity between the dorsal pulvinar and LIP while monkeys performed instructed and free-choice delayed saccade movements, at the level of spike-LFP and LFP-LFP measures. In the second experiment, I investigated the causal role of the dorsal pulvinar in oculomotor task performance and underlying modulation of the neuronal activity in area LIP, as well as interhemispheric cortico-cortical interactions. To do so, I recorded electrophysiological activity in both LIPs before and after reversible unilateral dorsal pulvinar inactivation. In the following, I am summarizing the main findings of both experiments, the relationship between them, discuss the limitations, and place these results, open questions and future perspectives within a more general framework related to understanding thalamo-cortical mechanisms of distributed processing.

5.1 Summary of results

We first showed the flexibility of functional interactions between the dorsal pulvinar and LIP with ongoing oscillations and transient shifts upon visual processing and around saccade execution. In addition, a stronger connectivity during free-choice trials led to higher probability to select contralateral targets. Then, we showed that unilateral dorsal pulvinar inactivation led to an ipsilesional choice bias, a decreased ‘alert state’, an altered contralesional representation of visual stimuli as well as neuronal synchronization in area LIP in the same hemisphere. On the contrary, there was an upregulated neuronal activity in the opposite hemisphere. Finally, we found a decreased inter-hemispheric functional connectivity. Altogether, this study shed light on a crucial role for pulvinar-parietal interactions in maintaining cortical alertness, the representation of contralateral visual stimuli and subsequent movement selection and planning. More generally scheme, it highlighted the importance of thalamo-cortical loops in shaping the neuronal activity locally and across homotopic regions, as opposed to only relaying information across cortical areas within a cortical “hierarchy”. Finally, our results suggest push-pull interactions between the two hemispheres during spatial selection and oculomotor preparation.

5.2 Potential mechanisms leading to altered activity in LIP

In the first study, we described ongoing pulvinar-parietal interactions (in alpha/beta range) during fixation and movement preparation with a transient interruption and shift towards lower frequencies (theta) upon target presentation and around saccades, reflecting the transient increase in low frequency oscillations within the two regions. In addition, we reported stronger functional connectivity in theta between the two regions after bilateral target presentation when the upcoming choice was toward the contralateral hemifield. We also showed that the partial disruption of these interactions led to deficits in the contralesional representation of stimuli that were the target of an upcoming saccade. Recently, Fiebelkorn and colleagues (Fiebelkorn et al., 2019) suggested that theta oscillations in the medial pulvinar and LIP mediate the allocation of attention. In a similar way, pulvinar-parietal functional connectivity in low frequencies might play a role in representing the saliency of a visual stimuli located in the contralesional hemifield, that might drive the consequent target selection. Since the processing of visual stimuli might disrupt prospective movement planning and the fixation during the delay period, ongoing alpha/beta connectivity between the two regions might play a role of functional inhibition on the processing of potentially distracting visual stimuli. The presence of a neuronal population showing suppressed activity without spatial tuning in the dorsal pulvinar and the alterations of beta oscillations in LIP after inactivation are in line with this hypothesis. An experiment with not only single or double target presented continuously, but a presentation of sequential stimuli, some acting as distractors and some that might override the original spatial goal, might provide more substantiate evidence for the role of dPul and pulvinar-parietal interactions in flexible target selection.

5.3 Limitations

In the early stages of our attempt to investigate the role of the pulvinar-parietal circuitry in oculomotor behaviors, we decided to use a rather simple delayed visually-guided saccade task, which already allowed us to make significant progress. However, due to the apparent complexity of thalamo-cortical interactions and their implications in a wide range of cognitive functions, the use of more sophisticated behavioral tasks, using different type of sensory-based features in different categorical contexts will be necessary to get a better understanding of higher order nuclei role in distributed cortical processing.

Despite the lack of anatomical evidences from MRI images, recording from LIP between monkeys as well as between hemispheres may have targeted different functional subdivision. Indeed, in

monkey L (in the right hemisphere in the inactivation experiment), the neuronal profile, in spiking activity, LFP power, and synchronization suggested that we targeted more visual functional subdivisions of area LIP as compared to monkey B, in which we observe more motor preparation related activity. Also, our recordings in the dorsal pulvinar were limited to a few 'sections' and it is likely that we might observe some slight differences in the neuronal activity by recording in more anterior, posterior, lateral or medial location. The systematic characterization of these potential differences would help to better unravel the functional organization of the pulvinar. In a similar way, inactivating different regions of the dorsal pulvinar might lead to slightly different effect on the neuronal activity within area LIP.

It is important to note that the effect of dorsal pulvinar inactivation on cortical neuronal activity might be substantially different depending on the cortical layer. In the present study, the angle of penetration together with the fact that LIP lies within the parietal sulcus, it was not possible to discern between cortical layers, neither from an anatomical estimation nor from analysis of electrophysiological signals such as current source density. In addition, we pulled in our analysis of the spiking activity different cell types e.g excitatory pyramidal cells and inhibitory interneurons since it was not possible to differentiate between them, despite an attempt to look at different features within average waveforms. However, it is possible that the effect of dorsal pulvinar inactivation on spiking activity might depend on the cell type. Finally, the effect of inactivation most likely also depend on the nature of the connectivity between a recorded neurons and the dorsal pulvinar. Assessing this connectivity before dorsal pulvinar inactivation, by using electrodes allowing both recording and fluid injection, was one of our goal at the beginning of this work. Unfortunately, due to the combination of technical challenges and the lack of time, we were not able to fulfill that goal.

In addition to these specific limitations pertaining to our work, there are currently unresolved methodologies issues that hamper the progress in dissecting the intricate thalamo-cortical circuitry, in the primate studies. Unlike the very revealing work in rodents, where advanced optogenetic tools and large-scale neuronal recording using e.g. Neuropixels are readily available, we currently are only at the threshold of getting reliably-working tools that would allow systematic dissection of cell-type / pathway-specific connectivity, as well as driving vs modulatory influences (Kirchgessner et al., 2021).

5.4 Conclusions and future directions

Higher order thalamic nuclei such as the pulvinar, receiving their driving inputs mostly from the cortex and projecting back to it, have challenged the classical view of the thalamus as being a sensory relay from the periphery to the cortex, which came from primary order nuclei such as the lateral geniculate nucleus which relays visual information from the retina to the cortex. Until then, the contribution of the thalamus to information processing in the cortex has been largely neglected. This novel view, with a transthalamic cortico-cortical route, opened the door for challenging our understanding of distributed processing in the cortex. Based on its extensive connectivity with a variety of cortical areas and the fact that it receives inputs via branching axons which also project to subcortical motor centers, the thalamus has been proposed to relay efference copies from one cortical area to another up in the hierarchy (Sherman, 2017). However, what would be the advantage of having a parallel route through the thalamus in addition to direct cortico-cortical projections? First, it is yet to be proven that all cortico-cortical projections have a parallel transthalamic route and vice versa. Then it is possible that the transthalamic route influences the efficiency of direct cortico-cortical transmission by regulating the neuronal oscillations and synchronization in the source and/or target area (Kohn et al., 2020). Recent studies on the role of pulvinar in spatial attention brought evidences supporting this idea (Saalmann et al., 2012; Saalmann, 2014; Fiebelkorn et al., 2019). However, it is important to note that these two hypotheses are not mutually exclusive and that the nature of the pathways might depend on the cognitive context and/or pathways (e.g. feedforward vs feedback). Nevertheless, thalamus nuclei which receive cortical inputs do not only project to a target area but also back to the source area. Therefore, our view of higher order nuclei role in cortical processing has to be updated again. Based on its connectivity, the pulvinar does not only have the possibility to modulate the transmission of information across cortical areas but also within area. Therefore, it likely plays a role in the local processing of information (Nakajima and Halassa, 2017) and this was the main focus of this thesis in which we highlighted the role of pulvinar-parietal circuitry in shaping local neuronal activity, oscillations and synchronization. The understanding of the higher order nuclei contribution to distributed cortical processing supporting advanced cognitive functions is only at glimpse and it might dramatically change our view of cognitive functions.

6 References

Acuna C, Cudeiro J, Gonzalez F, Alonso JM, Perez R (1990) Lateral-posterior and pulvinar reaching cells--comparison with parietal area 5a: a study in behaving Macaca nemestrina monkeys. Exp Brain Res 82:158–166.

Arcaro MJ, Pinsk MA, Chen J, Kastner S (2018) Organizing principles of pulvino-cortical functional coupling in humans. Nature Communications 9:5382.

Arcaro MJ, Pinsk MA, Kastner S (2015) The Anatomical and Functional Organization of the Human Visual Pulvinar. J Neurosci 35:9848–9871.

Arend I, Machado L, Ward R, McGrath M, Ro T, Rafal RD (2008) The role of the human pulvinar in visual attention and action: evidence from temporal-order judgment, saccade decision, and antisaccade tasks. Prog Brain Res 171:475–483.

Balan PF, Gottlieb J (2009) Functional significance of nonspatial information in monkey lateral intraparietal area. The Journal of neuroscience : the official journal of the Society for Neuroscience 29:8166–8176.

Barash S, Bracewell RM, Fogassi L, Gnadt JW, Andersen RA (1991) Saccade-related activity in the lateral intraparietal area. II. Spatial properties. J Neurophysiol 66:1109–1124.

Bender DB (1981) Retinotopic organization of macaque pulvinar. J Neurophysiol 46:672–693.

Bender DB, Youakim M (2001) Effect of attentive fixation in macaque thalamus and cortex. J Neurophysiol 85:219–234.

Benevento LA, Port JD (1995) Single neurons with both form/color differential responses and saccade-related responses in the nonretinotopic pulvinar of the behaving macaque monkey. Vis Neurosci 12:523–544.

Berman RA (2005) Dynamic Circuitry for Updating Spatial Representations. I. Behavioral Evidence for Interhemispheric Transfer in the Split-Brain Macaque. Journal of Neurophysiology 94:3228–3248.

Bisley JW, Goldberg ME (2010) Attention, intention, and priority in the parietal lobe. Annu Rev Neurosci 33:1–21.

Blatt M, Wiseman S, Domany E (1996) Superparamagnetic Clustering of Data. Phys Rev Lett 76:3251–3254.

Bruce CJ, Goldberg ME, Bushnell MC, Stanton GB (1985) Primate frontal eye fields. II. Physiological and anatomical correlates of electrically evoked eye movements. J Neurophysiol 54:714–734.

Brüers S, VanRullen R (2018) Alpha Power Modulates Perception Independently of Endogenous Factors. Frontiers in Neuroscience 12 Available at: https://www.frontiersin.org/article/10.3389/fnins.2018.00279 [Accessed June 8, 2022].

Buzsáki G, Anastassiou CA, Koch C (2012) The origin of extracellular fields and currents — EEG, ECoG, LFP and spikes. Nature Reviews Neuroscience 13:407–420.

Christopoulos VN, Bonaiuto J, Kagan I, Andersen RA (2015) Inactivation of Parietal Reach Region Affects Reaching But Not Saccade Choices in Internally Guided Decisions. J Neurosci 35:11719–11728.

Christopoulos VN, Kagan I, Andersen RA (2018) Lateral intraparietal area (LIP) is largely effector-specific in free-choice decisions. Sci Rep 8:8611.

Cortes N, de Souza BOF, Casanova C (2020) Pulvinar Modulates Synchrony across Visual Cortical Areas. Vision 4:22.

Creem S, Proffitt D (2001) Creem, S. H. & Proffitt, D. R. Grasping objects by their handles: a necessary interaction between cognition and action. J. Exp. Psychol. Hum. Percept. Perform. 27, 218-228. Journal of experimental psychology Human perception and performance 27:218–228.

Cudeiro J, Gonzalez F, Perez R, Alonso JM, Acuna C (1989) Does the pulvinar-LP complex contribute to motor programming? Brain Res 484:367–370.

Dean HL, Hagan MA, Pesaran B (2012) Only Coherent Spiking in Posterior Parietal Cortex Coordinates Looking and Reaching. Neuron 73:829–841.

Dominguez-Vargas A-U, Schneider L, Wilke M, Kagan I (2017) Electrical Microstimulation of the Pulvinar Biases Saccade Choices and Reaction Times in a Time-Dependent Manner. The Journal of Neuroscience 37:2234–2257.

Eradath MK, Pinsk MA, Kastner S (2021) A causal role for the pulvinar in coordinating task-independent cortico–cortical interactions. Journal of Comparative Neurology 529:3772–3784.

Fiebelkorn IC, Pinsk MA, Kastner S (2019) The mediodorsal pulvinar coordinates the macaque fronto-parietal network during rhythmic spatial attention. Nat Commun 10:215.

Foxe J, Snyder A (2011) The Role of Alpha-Band Brain Oscillations as a Sensory Suppression Mechanism during Selective Attention. Frontiers in Psychology 2 Available at: https://www.frontiersin.org/article/10.3389/fpsyg.2011.00154 [Accessed June 8, 2022].

Fries P (2015) Rhythms For Cognition: Communication Through Coherence. Neuron 88:220–235.

Gandhi NJ, Katnani HA (2011) Motor Functions of the Superior Colliculus. Annu Rev Neurosci 34:205–231.

Gnadt JW, Andersen RA (1988) Memory related motor planning activity in posterior parietal cortex of macaque. Experimental Brain Research 70:216–220.

Grieve KL, Acuña C, Cudeiro J (2000) The primate pulvinar nuclei: vision and action. Trends in Neurosciences 23:35–39.

Guillery RW (1995) Anatomical evidence concerning the role of the thalamus in corticocortical communication: a brief review. J Anat 187 (Pt 3):583–592.

Gutierrez C, Cola MG, Seltzer B, Cusick C (2000) Neurochemical and connectional organization of the dorsal pulvinar complex in monkeys. Journal of Comparative Neurology 419:61–86.

Hardy SG, Lynch JC (1992) The spatial distribution of pulvinar neurons that project to two subregions of the inferior parietal lobule in the macaque. Cereb Cortex 2:217–230.

Hawellek DJ, Wong YT, Pesaran B (2016) Temporal coding of reward-guided choice in the posterior parietal cortex. Proceedings of the National Academy of Sciences 113:13492–13497.

Hordacre B, Goldsworthy MR (2018) Commentary: Cooperation Not Competition: Bihemispheric tDCS and fMRI Show Role for Ipsilateral Hemisphere in Motor Learning. Frontiers in Human Neuroscience 12 Available at: https://www.frontiersin.org/article/10.3389/fnhum.2018.00097 [Accessed May 6, 2022].

Huk AC, Shadlen MN (2005) Neural activity in macaque parietal cortex reflects temporal integration of visual motion signals during perceptual decision making. J Neurosci 25:10420–10436.

Kaas JH, Baldwin MKL (2019) The Evolution of the Pulvinar Complex in Primates and Its Role in the Dorsal and Ventral Streams of Cortical Processing. Vision (Basel) 4:E3.

Kaas JH, Lyon DC (2007) Pulvinar contributions to the dorsal and ventral streams of visual processing in primates. Brain Research Reviews 55:285–296.

Kagan I, Gibson L, Spanou E, Wilke M (2021) Effective connectivity and spatial selectivity-dependent fMRI changes elicited by microstimulation of pulvinar and LIP. NeuroImage 240:118283.

Kagan I, Iyer A, Lindner A, Andersen RA (2010) Space representation for eye movements is more contralateral in monkeys than in humans. Proc Natl Acad Sci U S A 107:7933–7938.

Katz LN, Yates JL, Pillow JW, Huk AC (2016) Dissociated functional significance of decision-related activity in the primate dorsal stream. Nature 535:285–288.

Kirchgessner MA, Franklin AD, Callaway EM (2021) Distinct “driving” versus “modulatory” influences of different visual corticothalamic pathways. Current Biology 31:5121-5137.e7.

Kohn A, Jasper AI, Semedo JD, Gokcen E, Machens CK, Yu BM (2020) Principles of Corticocortical Communication: Proposed Schemes and Design Considerations. Trends in Neurosciences 43:725–737.

Kraskov A, Dancause N, Quallo MM, Shepherd S, Lemon RN (2009) Corticospinal neurons in macaque ventral premotor cortex with mirror properties: a potential mechanism for action suppression? Neuron 64:922–930.

Kusunoki M, Gottlieb J, Goldberg ME (2000) The lateral intraparietal area as a salience map: the representation of abrupt onset, stimulus motion, and task relevance. Vision Research 40:1459–1468.

Mathers LH, Rapisardi SC (1973) Visual and somatosensory receptive fields of neurons in the squirrel monkey pulvinar. Brain Res 64:65–83.

May PJ (2006) The mammalian superior colliculus: laminar structure and connections. Prog Brain Res 151:321–378.

Mazzoni P, Bracewell RM, Barash S, Andersen RA (1996) Motor intention activity in the macaque's lateral intraparietal area. I. Dissociation of motor plan from sensory memory. J Neurophysiol 76:1439–1456.

Michaels JA, Dann B, Scherberger H (2016) Neural Population Dynamics during Reaching Are Better Explained by a Dynamical System than Representational Tuning. PLoS Comput Biol 12:e1005175.

Mirpour K, Bisley JW (2016) Remapping, Spatial Stability, and Temporal Continuity: From the Pre-Saccadic to Postsaccadic Representation of Visual Space in LIP. Cereb Cortex 26:3183–3195.

Mishkin M, Ungerleider LG, Macko KA (1983) Object vision and spatial vision: two cortical pathways. Trends in Neurosciences 6:414–417.

Nakajima M, Halassa MM (2017) Thalamic control of functional cortical connectivity. Current Opinion in Neurobiology 44:127–131.

Oostenveld R, Fries P, Maris E, Schoffelen J-M (2011) FieldTrip: Open source software for advanced analysis of MEG, EEG, and invasive electrophysiological data. Comput Intell Neurosci 2011:156869.

Paul LK, Brown WS, Adolphs R, Tyszka JM, Richards LJ, Mukherjee P, Sherr EH (2007) Agenesis of the corpus callosum: genetic, developmental and functional aspects of connectivity. Nat Rev Neurosci 8:287–299.

Pesaran B (2009) Uncovering the mysterious origins of local field potentials. Neuron 61:1–2.

Pesaran B (2010) Neural correlations, decisions, and actions. Curr Opin Neurobiol 20:166–171.

Pesaran B, Nelson MJ, Andersen RA (2008) Free choice activates a decision circuit between frontal and parietal cortex. Nature 453:406–409.

Petersen SE, Robinson DL, Keys W (1985) Pulvinar nuclei of the behaving rhesus monkey: visual responses and their modulation. J Neurophysiol 54:867–886.

Petersen SE, Robinson DL, Morris JD (1987) Contributions of the pulvinar to visual spatial attention. Neuropsychologia 25:97–105.

Pierrot-Deseilligny Ch, Ploner CJ, Müri RM, Gaymard B, Rivaud-Péchoux S (2002) Effects of Cortical Lesions on Saccadic. Annals of the New York Academy of Sciences 956:216–229.

Platt ML, Glimcher PW (1999) Neural correlates of decision variables in parietal cortex. Nature 400:233–238.

Purushothaman G, Marion R, Li K, Casagrande VA (2012) Gating and control of primary visual cortex by pulvinar. Nature neuroscience 15:905–912.

Quiroga RQ, Nadasdy Z, Ben-Shaul Y (2004) Unsupervised spike detection and sorting with wavelets and superparamagnetic clustering. Neural Comput 16:1661–1687.

Rafal R, McGrath M, Machado L, Hindle J (2004) Effects of lesions of the human posterior thalamus on ocular fixation during voluntary and visually triggered saccades. J Neurol Neurosurg Psychiatry 75:1602–1606.

Redinbaugh MJ, Phillips JM, Kambi NA, Mohanta S, Andryk S, Dooley GL, Afrasiabi M, Raz A, Saalmann YB (2020) Thalamus Modulates Consciousness via Layer-Specific Control of Cortex. Neuron 106:66-75.e12.

Robinson DL, McClurkin JW, Kertzman C (1990) Orbital position and eye movement influences on visual responses in the pulvinar nuclei of the behaving macaque. Exp Brain Res 82:235–246.

Robinson DL, Petersen SE, Keys W (1986) Saccade-related and visual activities in the pulvinar nuclei of the behaving rhesus monkey. Exp Brain Res 62:625–634.

Roitman JD, Shadlen MN (2002) Response of neurons in the lateral intraparietal area during a combined visual discrimination reaction time task. J Neurosci 22:9475–9489.

Romanski LM, Giguere M, Bates JF, Goldman-Rakic PS (1997) Topographic organization of medial pulvinar connections with the prefrontal cortex in the rhesus monkey. The Journal of comparative neurology 379:313–332.

Rorie AE, Gao J, McClelland JL, Newsome WT (2010) Integration of sensory and reward information during perceptual decision-making in lateral intraparietal cortex (LIP) of the macaque monkey. PLoS One 5:e9308.

Saalmann YB (2014) Intralaminar and medial thalamic influence on cortical synchrony, information transmission and cognition. Frontiers in Systems Neuroscience 8 Available at: http://journal.frontiersin.org/article/10.3389/fnsys.2014.00083/abstract [Accessed September 26, 2015].

Saalmann YB, Kastner S (2011) Cognitive and perceptual functions of the visual thalamus. Neuron 71:209–223.

Saalmann YB, Pinsk MA, Wang L, Li X, Kastner S (2012) The pulvinar regulates information transmission between cortical areas based on attention demands. Science 337:753–756.

Schneider L, Dominguez-Vargas A-U, Gibson L, Kagan I, Wilke M (2020) Eye position signals in the dorsal pulvinar during fixation and goal-directed saccades. Journal of Neurophysiology 123:367–391.

Schneider L, Dominguez-Vargas A-U, Gibson L, Wilke M, Kagan I (2021) Visual, delay and oculomotor timing and tuning in macaque dorsal pulvinar during instructed and free choice memory saccades. bioRxiv 2021.12.21.473504 Available at: https://www.biorxiv.org/content/10.1101/2021.12.21.473504v1 [Accessed December 29, 2021].

Shen K, Mišić B, Cipollini BN, Bezgin G, Buschkuehl M, Hutchison RM, Jaeggi SM, Kross E, Peltier SJ, Everling S, Jonides J, McIntosh AR, Berman MG (2015) Stable long-range interhemispheric coordination is supported by direct anatomical projections. Proc Natl Acad Sci U S A 112:6473–6478.

Sherman SM (2007) The thalamus is more than just a relay. Current Opinion in Neurobiology 17:417–422.

Sherman SM (2017) Functioning of Circuits Connecting Thalamus and Cortex. In: Comprehensive Physiology, pp 713–739. John Wiley & Sons, Ltd. Available at: https://onlinelibrary.wiley.com/doi/abs/10.1002/cphy.c160032 [Accessed October 13, 2022].

Shumikhina S, Molotchnikoff S (1999) Pulvinar participates in synchronizing neural assemblies in the visual cortex, in cats. Neuroscience Letters 272:135–139.

Snyder LH, Batista AP, Andersen RA (1997) Coding of intention in the posterior parietal cortex. Nature 386:167-70.

Soares JGM, Diogo ACM, Fiorani M, Souza APB, Gattass R (2004) Effects of inactivation of the lateral pulvinar on response properties of second visual area cells in Cebus monkeys. Clin Exp Pharmacol Physiol 31:580–590.

Suárez R, Gobius I, Richards LJ (2014) Evolution and development of interhemispheric connections in the vertebrate forebrain. Front Hum Neurosci 8:497.

Tasserie J, Uhrig L, Sitt JD, Manasova D, Dupont M, Dehaene S, Jarraya B (2022) Deep brain stimulation of the thalamus restores signatures of consciousness in a nonhuman primate model. Science Advances 8:eabl5547.

Van der Stigchel S, Arend I, van Koningsbruggen MG, Rafal RD (2010) Oculomotor integration in patients with a pulvinar lesion. Neuropsychologia 48:3497–3504.

Verstynen T, Diedrichsen J, Albert N, Aparicio P, Ivry RB (2005) Ipsilateral motor cortex activity during unimanual hand movements relates to task complexity. J Neurophysiol 93:1209–1222.

Vinck M, van Wingerden M, Womelsdorf T, Fries P, Pennartz CMA (2010) The pairwise phase consistency: A bias-free measure of rhythmic neuronal synchronization. NeuroImage 51:112–122.

Wardak C, Olivier E, Duhamel J-R (2002) Saccadic Target Selection Deficits after Lateral Intraparietal Area Inactivation in Monkeys. J Neurosci 22:9877–9884.

Wilke M, Kagan I, Andersen RA (2012) Functional imaging reveals rapid reorganization of cortical activity after parietal inactivation in monkeys. Proceedings of the National Academy of Sciences of the United States of America 109:8274–8279.

Wilke M, Kagan I, Andersen RA (2013) Effects of Pulvinar Inactivation on Spatial Decision-making between Equal and Asymmetric Reward Options. Journal of Cognitive Neuroscience 25:1270–1283.

Wilke M, Schneider L, Dominguez-Vargas A-U, Schmidt-Samoa C, Miloserdov K, Nazzal A, Dechent P, Cabral-Calderin Y, Scherberger H, Kagan I, Bähr M (2018) Reach and grasp deficits following damage to the dorsal pulvinar. Cortex 99:135–149.

Wilke M, Turchi J, Smith K, Mishkin M, Leopold DA (2010) Pulvinar Inactivation Disrupts Selection of Movement Plans. Journal of Neuroscience 30:8650–8659.

Zhou H, Schafer RJ, Desimone R (2016a) Pulvinar-Cortex Interactions in Vision and Attention. Neuron 89:209–220.

Zhou Y, Liu Y, Lu H, Wu S, Zhang M (2016b) Neuronal representation of saccadic error in macaque posterior parietal cortex. eLife Available at: https://elifesciences.org/articles/10912 [Accessed February 20, 2019].

Acknowledgements

First of all, I would like to thank Dr. Igor Kagan and Prof. Dr. Melanie Wilke for their supervision, which has shaped and refined my scientific thinking, and for their support throughout the thesis.

I thank my third thesis committee member Prof. Hansjörg Scherberger for insightful comments and discussions.

I thank Prof. Dr. Alexander Gail, Prof. Dr. Andrea Antal, and Prof. Dr. Michael Wibral for participating in my doctoral examination board

I would like to give a special thanks to Danial Arabali, Lukas Schneider and Daniela Lazzarini, who became dear friends, for their amazing help and support along the way.

I also would like to thank all members from the Cognitive Neuroscience Lab for helpful and entertaining discussion at many occasions.

I thank all the caretakers, technical assistants and vets without whom this work would not have been possible.

I thank Sarath Ravindran Marina Slashcheva, Burno Carniatto, Jaya Sathiyamani and Margaret Young who contributed to this project as lab rotation or master students.

I also thank Pietro Amerio, Vladislav Kozyrev and Ryo Sagawa, for being amazing office mates.

I thank all my family and close friends for their unconditional support, and particularly my wife, Kasumi Kawanishi, who made all of this possible.

Last but not least, I thank our son, Naotaro, who brings us joy every day and was kind enough to not disturb our nights too much during this last year.

7 Appendix

7.1 The poster presented at the Society for Neuroscience meeting (SfN) 2018

Bihemispheric effects of dorsal pulvinar inactivation on saccade and reach representations in parietal cortex

Mathieu Pachoud[1], Danial Arabali[1], Lukas Schneider[1], Melanie Wilke[1,2], Igor Kagan[1]

[1] Decision and Awareness Group, Cognitive Neuroscience Laboratory, German Primate Center, Göttingen, Germany
[2] Department of Cognitive Neurology, University Medicine, Göttingen, Germany

222.09 / FF17

Decision and Awareness Group
German Primate Center

UNIVERSITÄTSMEDIZIN GÖTTINGEN UMG

DPZ

Introduction and aims

Evolutionary history and anatomical connectivity of the thalamic dorsal pulvinar suggest its involvement in visuomotor processing and coordination of eye and hand movements [1-4]. The causal perturbation and lesion studies support this notion [5-8]. The neuronal signature and functional significance of pulvinar contribution to sensorimotor regions in the parietal cortex are however poorly understood.

In this study, we performed unilateral reversible pharmacological inactivation of the dorsal pulvinar (medial pulvinar and dorsomedial portion of lateral pulvinar) by injecting the GABA-A agonist THIP, and recorded in parietal areas MIP and LIP while a monkey did delayed visually-guided reach and saccade tasks.

The **main aim** was to find out if changes in parietal space and hand tuning might underlie previously observed inactivation-induced behavioral deficits.

Methods

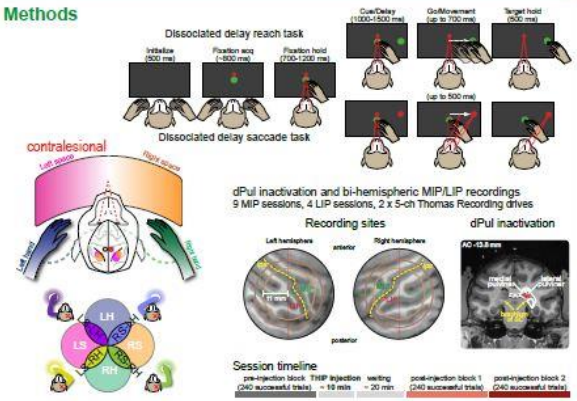

Mainly contralesional deficits after dorsal pulvinar inactivation

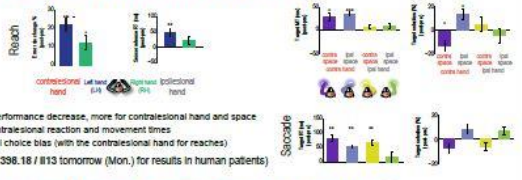

- General performance decrease, more for contralesional hand and space
- Slower contralesional reaction and movement times
- Ipsilesional choice bias (with the contralesional hand for reaches)

(see poster **398.18 / II13** tomorrow (Mon.) for results in human patients)

Effects of dPul inactivation on MIP and LIP spiking activity: example units

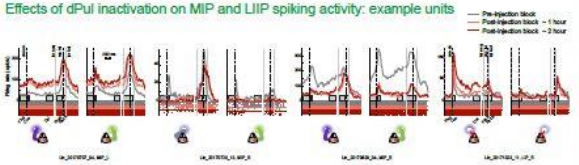

MIP: Differentialy altered spiking activity in both hemispheres

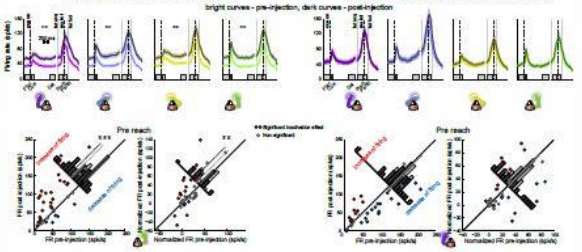

- 87% show effect of inactivation, 82% of those - interaction with epoch
- Mostly increased firing due to baseline shift AND epoch-specific effects
- In both hemispheres, inactivation-induced effects go beyond baseline shift
- 81% show effect of inactivation, 87% of those - interaction with epoch
- Roughly equal proportion of increased and decreased firing rates

MIP: Increased ipsilesional tuning in both hemispheres

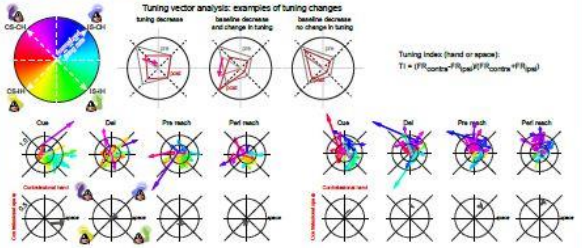

- Increased ipsilesional space tuning in cue, delay, and reach
- Increased ipsilesional hand tuning in the pre reach and reach
- Increased ipsilesional space tuning in pre reach and reach
- Strong contralateral hand tuning persists after inactivation

MIP: Mainly opposite effects on Local Field Potential in the two hemispheres

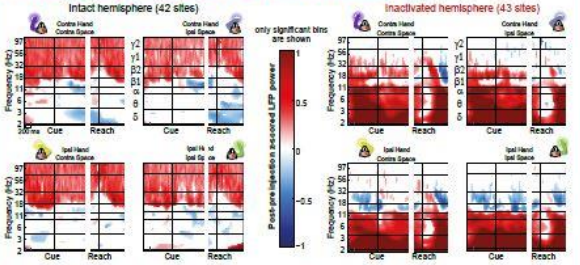

- Increased power in high frequencies
- Decreased power in β/α frequencies for contralesional hand
- Increased power in low frequencies
- Increased power in high β frequencies for contralesional hand

LIP: Mainly hemifield-specific changes, no baseline effect

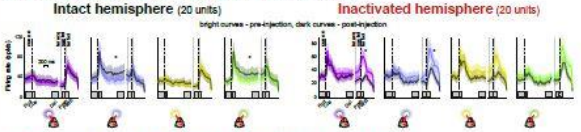

LIP: Increased ipsilesional tuning, mainly in the intact hemisphere

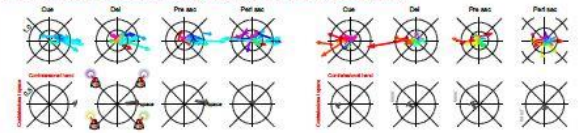

- 80% show effect of inactivation, 69% of those - interaction with epoch
- No overall baseline shift, increased ipsilesional delay activity
- Increased ipsilesional space tuning in cue, delay and pre saccade
- 85% show effect of inactivation, 75% of those - interaction with epoch
- Suppressed mainly contralesional saccade / post-saccade response

LIP: Opposite effects in two hemispheres, ipsilesional increase in the intact hemisphere

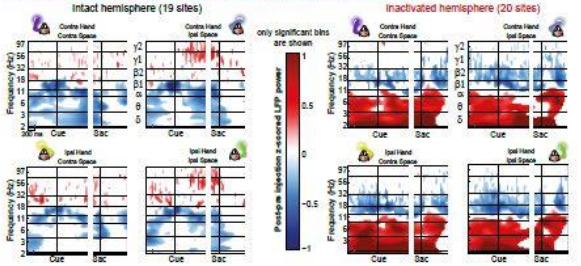

Conclusions

- Dorsal pulvinar inactivation decreased overall performance and caused mainly contralesional hand/space behavioral deficits.
- The inactivation had strong but divergent effects on parietal activity in both hemispheres, due to **baseline changes** and/or **epoch-specific** effects:
  In the inactivated hemisphere neurons showed **both increase and decrease** of firing.
  In the intact hemisphere, MIP but not LIP showed stronger **post-injection enhancement** than suppression, consistent with LFP power increase in high frequencies.
- MIP tuning in both hemispheres shifted towards **ipsilesional space/hand**. The two hemispheres however showed an opposite effect on the contralesional hand β/α power.
  Only intact LIP showed enhanced **ipsilesional space** firing and tuning, in line with ipsilesional enhancement of γ LFP power.
- LFP results are consistent with the notion that the pulvinar helps maintaining **"alert cortical state"** [9], at least in the same hemisphere. **But the removal of pulvinar drive also leads to space- and hand-specific alterations and activity up-regulation in the opposite hemisphere, influencing the competition between contralesional and ipsilesional representations that might underlie contralesional behavioral deficits.**

References:
[1] Kaas JH, Lyon DC. Pulvinar contributions to the dorsal and ventral streams of visual processing in primates. Brain Res Rev 2007;55:285-96.
[2] Sherman SM, Guillery RW. The role of the thalamus in the flow of information to the cortex. Philos Trans R Soc Lond B Biol Sci 2002;357:1695-708.
[3] Arcaro MJ, Pinsk MA, Kastner S. The Anatomical and Functional Organization of the Human Visual Pulvinar. J Neurosci 2015;35:9848-71.
[4] Mundinano IC, Kwan DM, Kwan WC, Wilcox D, Tso L, Hosmann-Ludlow J, et al. Transient visual pathway critical for normal development of primate grasping behavior. PNAS 2019;201717016.
[5] Wilke M, Kagan I, Andersen RA. Effects of Pulvinar Inactivation on Spatial Decision-making between Equal and Asymmetric Reward Options. J Cog Neurosci 2012;24:1270-83.
[6] Wilke M, Turchi J, Smith K, Mishkin M, Leopold DA. Pulvinar Inactivation Disrupts Selection of Movement Plans. J Neurosci 2010;30:8650-9.
[7] Domínguez-Vargas A-U, Schneider L, Wilke M, Kagan I. Electrical Microstimulation of the Pulvinar Biases Saccade Choices and Reaction Times in a Time-Dependent Manner. J Neurosci 2017;37:2234-57.
[8] Wilke M, Schneider L, Domínguez-Vargas A-U, Schmidt-Samoa C, Iakovenko K, Nazzal A, et al. Reach and grasp deficits following damage to the dorsal pulvinar. Cortex 2018;98:135-49.
[9] Zhou H, Schafer RJ, Desimone R. Pulvinar-Cortex Interactions in Vision and Attention. Neuron 2016;89:209-20.

Igor Kagan ikagan@dpz.eu http://dpz.eu/idag

Supported by the Schilling Stiftung Foundation, CNMPB "Primate platform", DFG